UNCLASSIFIED

AD NUMBER
AD893427
LIMITATION CHANGES

TO:

Approved for public release; distribution is unlimited.

FROM:

Distribution authorized to U.S. Gov't. agencies only; Test and Evaluation; JUL 1971. Other requests shall be referred to Air Force Flight Dynamics Laboratory, AFFDL/FY, Wright-Patterson AFB, OH 45433.

AUTHORITY

AFFDL ltr, 6 Nov 1973

THIS PAGE IS UNCLASSIFIED

AFFDL-TR-71-107

AD 893427

ACOUSTIC FATIGUE OF AIRCRAFT
STRUCTURAL COMPONENT ASSEMBLIES

FRED F. RUDDER, JR.

LOCKHEED-GEORGIA COMPANY

TECHNICAL REPORT AFFDL-TR-71-107

FEBRUARY 1972

D D C

RECEIVED

APR 18 1972

A

AIR FORCE FLIGHT DYNAMICS LABORATORY
AIR FORCE SYSTEMS COMMAND
WRIGHT-PATTERSON AIR FORCE BASE, OHIO

193

NOTICE

When Government drawings, specifications, or other data are used for any purpose other than in connection with a definitely related Government procurement operation, the United States Government thereby incurs no responsibility nor any obligation whatsoever; and the fact that the government may have formulated, furnished, or in any way supplied the said drawings, specifications, or other data, is not to be regarded by implication or otherwise as in any manner licensing the holder or any other person or corporation, or conveying any rights or permission to manufacture, use, or sell any patented invention that may in any way be related thereto.

Copies of this report should not be returned unless return is required by security considerations, contractual obligations, or notice on a specific document.

ACOUSTIC FATIGUE OF AIRCRAFT
STRUCTURAL COMPONENT ASSEMBLIES

FRED F. RUDDER, JR.

LOCKHEED-GEORGIA COMPANY

Details of illustrations in
this document may be better
studied on microfiche

FOREWORD

This technical report has been reviewed and is approved.

WALTER J. MYKYTOW
Asst. for Research and Technology
Vehicle Dynamics Division
Air Force Flight Dynamics Laboratory

ABSTRACT

Analytical results for estimating natural frequencies and stress response for conventional stiffened flat panels, two-sided box structure, wedge structure, and unstiffened cylindrical panels are presented. Acoustic fatigue tests of 12 stiffened flat panel and six box structure designs, two specimens for each design, were used to develop design equations for estimating acoustic fatigue resistance of skin, stringer, and rib structure. Computer programs are presented for estimating frequencies of stiffened flat panels, box structure, and wedge structure. Nomographs are presented for skin design and curved panel stress response.

TABLE OF CONTENTS

LIST OF FIGURES

LIST OF FIGURES (Cont'd)

LIST OF FIGURES (Cont'd)

LIST OF FIGURES (Cont'd)

LIST OF TABLES

LIST OF SYMBOLS

A	amplitude ratio Figure 3; aspect ratio of curved panel, b/a, Figure 12; area
a	length of a rectangular panel in the x-direction
b	length of a rectangular panel in the y-direction
C_x, C_y, C_z	distances defined by Figure 2
C_{ij}	defined by Table I
D	flexural rigidity of a thin uniform plate, $Et^3/12(1-\nu^2)$
E	Young's modulus of elasticity; denotes shear center of a thin-walled open-section beam
e	denotes the location of the shear center
$F_{mn}(b,a)$	defined by Equation 14
f	denotes frequency in Hertz.
G	shear modulus of elasticity (see Equation 60 for other use in Section II.F)
$G_p(\omega)$	spectral density of acoustic pressure at frequency ω
I*	defined by Equations 34 and 67
I_{xx}, I_{xz}, I_{zz}	second area moments of a cross-section shape with respect to a centroidal (x,z) axis system
I_{yy}, I_{yz}, I_{zz}	second area moments of a cross-section shape with respect to a centroidal (y,z) axis system
I_{px}, I_{py}	defined by Equation 8
I_m	defined by Equation 54 and Table IV
J	St. Venant's torsion constant for a thin-walled open-section beam (see Appendix I)
K_r	modal stiffness of the rth mode
k_m, k_n	defined by Equation 60
k_{xi}, k_{yi}	defined by Equation 24b
M_o	defined by Equation 34
M_r	modal mass of the rth mode

N_c	cycles to failure
$P_{mn}(t)$	generalized force for the $(m,n)^{th}$ mode
$p(x,y,t)$	time-dependent pressure
p	mode number for z-direction, Section II.D.2
p	internal pressure for a cylindrical panel, Section II.F.1
q	mode number for z-direction, Section II.D.3
q_o	magnitude of a uniform pressure distribution
R	radius of a cylindrical panel
R_{mn}	defined by Equation 28
S	defined by Figure 10
$S_p(f)$	spectral density of acoustic pressure, Section V.B.2
S_x, S_y, S_z	distances defined by Figure 2
T	kinetic energy
t	thickness of a plate or time (no confusion should arise)
U	potential energy or amplitude of a displacement function in the x-direction (no confusion should arise)
$u(y,z)$	displacement function in the x-direction
$V(0,y)$	defined by Equation 32
$\bar{V}$	defined by Equation 33
$v(x,z)$	displacement function in the y-direction
W	amplitude of displacement function in the z-direction
$w(x,y)$	displacement function in the z-direction
x,y,z	denotes a right-hand rectangular Cartesian coordinate system
α	defined by Figure 10
Γ_e	warping constant for a thin-walled open-section beam with the pole taken at the shear center
Γ_x^*, Γ_y^*	defined by Equation 7

LIST OF SYMBOLS (Cont'd)

γ	mass per unit volume
γ_i	bending moment factors defined in Section II.D.4
δ_i	bending moment factors defined in Section II.D.4
$\bar{\varepsilon}$	overall rms strain, μ in/in
ζ_r	viscous damping ratio for the rth mode
η_r	solid damping ratio for the rth mode
Θ_{ij}	twist amplitude defined by Equation 18 and Table II
ν	Poisson's ratio
π	3.14159
ρ	mass per unit area
σ	stress
$\bar{\sigma}$	overall rms stress, ksi
$\bar{\sigma}_c$	stress calculated using theory (see Equations 65 and 66)
$\bar{\sigma}_e$	stress calculated using theory and empirical data (see Equations 65 and 66)
φ	sector angle of a cylindrical panel (see Figure 12)
$\varphi_r(x)$	the rth mode of vibration
ω	radian frequency
ω_r	radian frequency of the rth mode
ω_c	radian frequency of a curved panel
ω_∞	radian frequency of a flat panel

Note on Subscripts

The use of subscripts to denote mode numbers, components of structure, and types of structure is rather free. In each instance, the context of the usage should be clear.

I - INTRODUCTION

Previous investigations directed toward eliminating or reducing acoustic fatigue effects from intense noise on flight vehicle structure have established design criteria and nomographs. The original development program was conducted by McGowan (ASD-TDR-63-820, 1963). Nomographs were empirically derived from acoustic fatigue tests of certain popular structural designs. The fatigue tests were conducted generally using discrete frequency excitation, and the resulting fatigue data were converted to 'random fatigue data' through the use of Mile's single degree-of-freedom theory and the Miner-Palmgren cumulative damage rule. These nomographs have been helpful in designing acoustic-fatigue-resistant structure for present-day and near-future aircraft.

For high-performance aircraft, lightweight, acoustic-fatigue-resistant structure is essential. To meet these critical demands for weight reduction and increased resistance to acoustic fatigue, McGowan's work was refined by Ballentine (AFFDL-TR-67-156, 1968) with the objective of removing conservatism and extending the range of application of the existing design methods. Ballentine conducted additional acoustic fatigue tests using random noise excitation. The structural configurations considered by Ballentine consisted of flat stiffened panels and flat honeycomb sandwich panels.

McGowan's original work concerning acoustic fatigue resistance of internal airframe structure (stringers, ribs, and frames) has proved, in practice, to be conservative from a weight standpoint. Ballentine based the design of his stiffened panel specimens on McGowan's design techniques. Of the sixty stiffened panel specimens tested by Ballentine, no failure of the internal structure was observed. Hence, an exploratory program to define more accurately the acoustic fatigue resistance of internal structure was required in order to remove the weight penalty incurred by using available design techniques.

Ballentine's work was the first step in the acoustic fatigue refinement program. The research study described here is a continuation of this refinement program. A description of the analytical investigation is presented in Section II; the experimental program is described in Section III; Section IV presents the correlation of test data and analytical results; and the development of design equations and nomographs is presented in Section V. Appendices are included that describe the data collection and reduction system, detailed specimen mode shapes, and computer programs for calculating frequencies and mode shapes of stiffened flat panel structure, two-sided structure, and wedge structure.

II - ANALYTICAL

A. Introduction

The main emphasis of this program was to provide experimental data for the acoustic fatigue resistance of internal airframe structure. The analytical effort was conducted to suggest the significant parameters and mathematical expressions governing orthogonally stiffened flat panels, box structure (typical of flaps), wedge structure (typical of control surfaces), and simple cylindrical panels. The structural configurations considered analytically were selected based upon the experimental specimen designs. In order to develop simple expressions suitable for design application, several approximations have been made in formulating the analytical models. These approximations allow the development of design equations for estimating the significant parameters in a form suitable for design studies.

B. General Theory

1. Response of Linear Single-Degree-of-Freedom Oscillator to Random Acoustic Excitation

In Reference 1, Clarkson presents a summary of the general theory of response of a linear oscillator to random acoustic excitation. The basic assumptions in the development are that only one mode is predominant in the frequency range of interest, that the excitation spectrum changes slowly with frequency near the predominant mode, and that the excitation pressure is completely in phase over the portion of structure of interest. For these assumptions, the mean square displacement response for the rth mode at the point $\bar{x}$ on the structure is given by the equation

$$\overline{w^2(\bar{x})} = \frac{\pi}{2\omega_r^3 \eta_r} \frac{\varphi_r^2(\bar{x})}{M_r^2} \left[\int_A \varphi_r(x)dA \right]^2 G_p(\omega_r) \tag{1}$$

In terms of the static displacement $W_o(\bar{x})$ due to a uniform pressure of unit magnitude, the mean square displacement can be written as

$$\overline{w^2(\bar{x})} = \frac{\pi}{2\eta_r} \omega_r G_p(\omega_r) W_o^2(\bar{x}) \tag{2}$$

where

$$W_o(\bar{x}) = \frac{\varphi_r(\bar{x})}{\omega_r^2 M_r} \int_A \varphi_r(x)dA$$

For a linear single-degree-of-freedom system, Miles has shown in Reference 2 that the mean square stress at the point of interest can be expressed as

2

$$\overline{\sigma^2(\bar{x})} = \frac{\pi}{4\zeta_r} f_r G_p(f_r) \sigma_o^2(\bar{x}) \tag{3}$$

where the viscous damping ratio, ζ_r, and the response frequency, f_r (Hz), for the rth mode have been introduced. The term σ_o is the dimensionless stress at the point of interest due to a uniform static pressure of unit magnitude. The emphasis of the analytical program is to develop expressions for the natural frequency, f_r, of the rth structural mode and the dimensionless stress, σ_o, as indicated in Equation 3.

2. Frequency Analysis

Single mode response of a structure can be estimated using the Rayleigh method provided that reasonably accurate mode shapes are used in the analysis. For the structural configurations considered, the Rayleigh energy method has been used exclusively. The main emphasis was to develop suitable mode functions for the structure. Letting W_r denote the amplitude of the rth mode of the structure, the kinetic energy and the potential energy can be expressed as

$$T = \frac{1}{2} M_r \dot{W}_r^2 \qquad\qquad U = \frac{1}{2} K_r W_r^2 \tag{4}$$

where M_r is the modal mass.

K_r is the modal stiffness.

For simple harmonic motion, the kinetic energy can be expressed in terms of the radian frequency, ω_r, as

$$T = \frac{1}{2} \omega_r^2 M_r W_r^2 \tag{5}$$

Equating the maximum values of the kinetic and potential energy one obtains for simple harmonic motion the expression

$$\omega_r = \sqrt{(K_r/M_r)} \tag{6}$$

The definitions in Equations 4 and 6 will be used to estimate the natural frequency, $f_r = \omega_r/2\pi$, for the structure and mode under consideration. Expressions for the dimensionless stress, σ_o, will be developed subsequently for each structure considered.

C. Flat Stiffened Panels

The structural configuration under consideration is illustrated in Figure 1. The nine-bay panel is typical of configurations adopted for acoustic fatigue testing. The portion of the structure of interest is the center bay denoted by the coordinate w_{22} in Figure 1 and the supporting structure surrounding the center bay. The dynamic characteristics of such

3
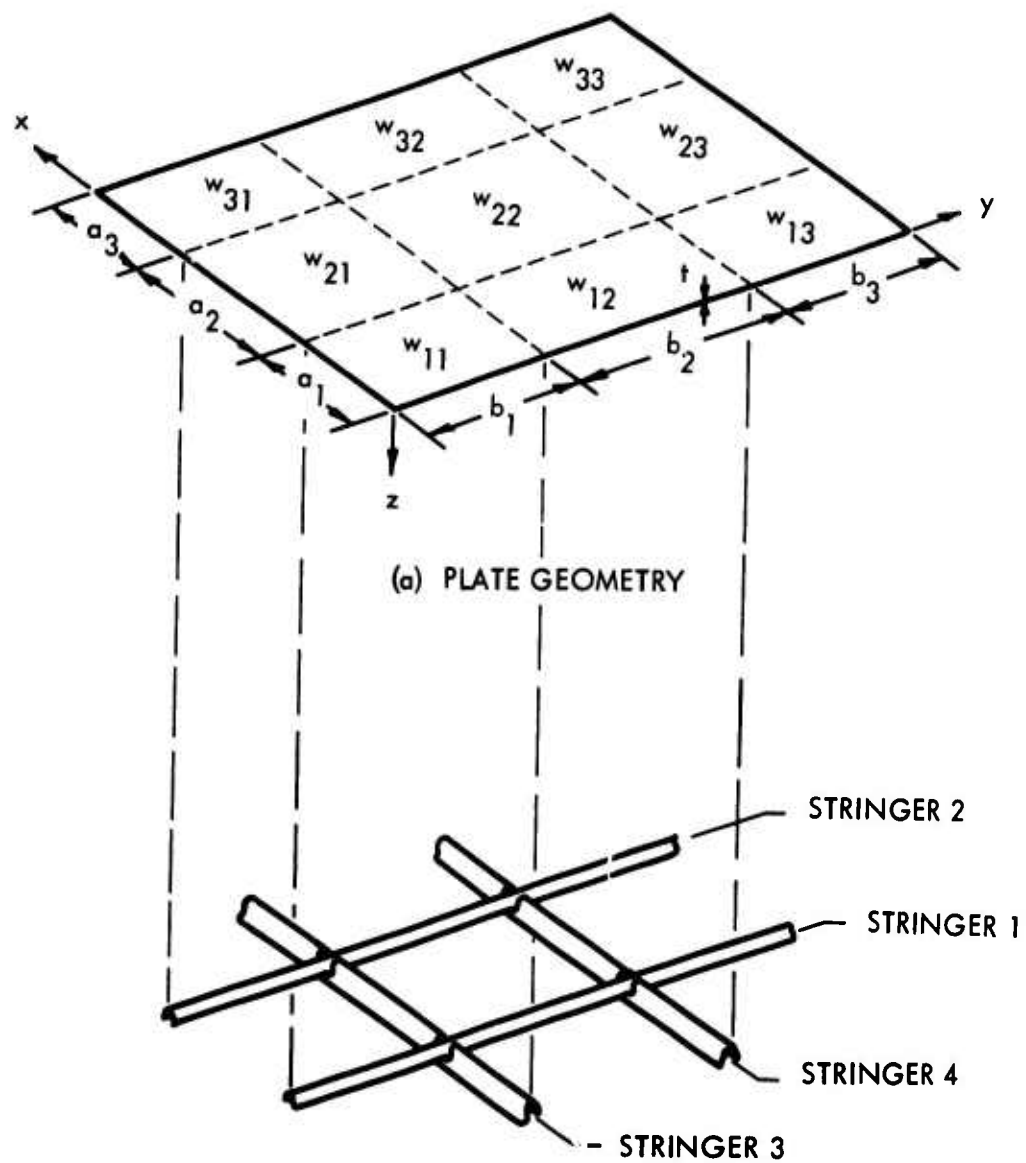
(a) PLATE GEOMETRY

(b) SUBSTRUCTURE GEOMETRY AND NOMENCLATURE

FIGURE 1. NINE-BAY FLAT STIFFENED PANEL

structure are extremely complex. Analytically, several methods of analysis have been applied to such structure. The finite element approach has attracted much attention (References 3, 4, and 5); however, this approach is not very suitable for rapid design application, since extensive computer facilities are required. Clarkson has pointed out that an elementary approach can provide estimates at least within the scatter of fatigue data (Reference 1).

1. Supporting Structure

The common stiffening members used in aircraft construction can be broadly classified as thin-walled open-section beams. The difference between this type of structure and the elementary beam usually encountered in practice is that warping of the cross-section normal to its plane must be considered in addition to the axial strains introduced in the elementary bending theory. The discussion here shall focus on the torsional restraint offered by such stiffeners, since this is the basic mode of deformation. Strictly speaking, the bending and torsion motion of such structure are coupled, but for the stiffeners considered here, the bending stiffness is several orders of magnitude greater than the torsional rigidity. Vlasov, Reference 6, and Oden, Reference 7, give very complete developments for the analysis of thin-walled open-section beams.

Figure 2 illustrates the stiffener geometry under consideration. The attach point is taken as the point at which the stiffener is connected to the panel. It is assumed that the stiffener is free only to rotate about the attach point so that it is necessary to present expressions for the warping constant and polar moment of inertia referenced to the axis system at the attach point. It can be shown that (References 6 and 7) the effective warping constants Γ_x^* and Γ_y^* are given by the expressions (see Figure 2)

$$\Gamma_x^* = \Gamma_e + S_z^2 I_{zz} - 2 S_y S_z I_{yz} + S_x^2 I_{yy} \tag{7a}$$

for stiffeners parallel to the x-axis and

$$\Gamma_y^* = \Gamma_e + S_z^2 I_{zz} - 2 S_x S_z I_{xz} + S_x^2 I_{xx} \tag{7b}$$

for stiffeners parallel to the y-axis.

The polar moment of inertia, referenced to rotations about the attach point, are

$$I_{px} = I_{yy} + I_{zz} + (C_y^2 + C_z^2) A \tag{8a}$$

$$I_{py} = I_{xx} + I_{zz} + (C_x^2 + C_z^2) A \tag{8b}$$

These expressions will be used subsequently for developing expressions for the potential and the kinetic energy for the frequency analysis of the stiffened panel.

5
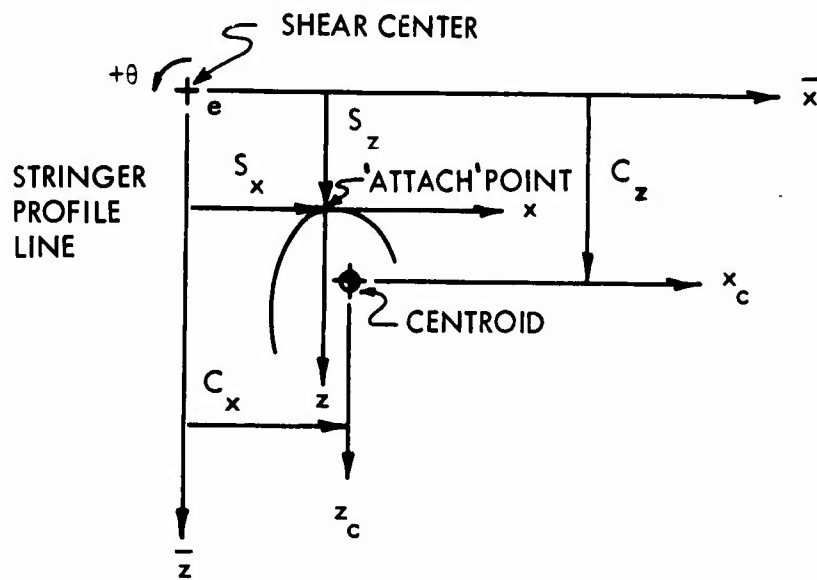
(a) STRINGER NOMENCLATURE - STRINGERS PARALLEL TO Y-AXIS
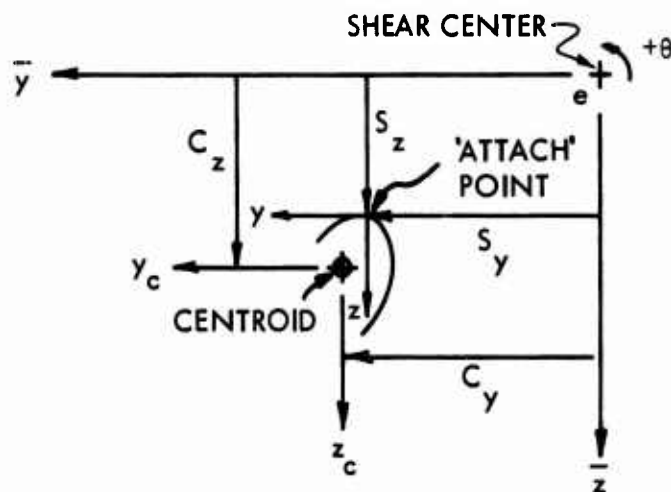
(b) STRINGER NOMENCLATURE - STRINGERS PARALLEL TO X-AXIS

FIGURE 2. STIFFENER CROSS-SECTION GEOMETRY AND NOMENCLATURE

6

2. Frequency Analysis

The development here assumes that the cover sheet is supported at the stiffener attach line so that the only motion of the structure consists of transverse displacement of each panel bay and rotation about the stiffener attach line. Adjacent panel bays are constrained so that slope continuity across the stiffener attach line is preserved. Energy methods are used to obtain expressions for the modal stiffness, modal mass, and the generalized force.

2.1 Cover Sheet - For the rectangular panel illustrated in Figure 1, the transverse displacement function for a bay with dimensions a_i and b_j is denoted by $w_{ij}(x,y)$ where (x,y) denotes a local axis system for each panel bay. The cover sheet is assumed to be of constant thickness and uniform material properties.

Assuming a mode for each panel bay of the form

$$w_{ij}(x,y) = C_{ij} \sin\left(\frac{m\pi x}{a_i}\right) \sin\left(\frac{n\pi y}{b_i}\right) \tag{9}$$

it is seen that there are nine amplitude parameters, C_{ij}, to be determined. For bay motion described by Equation 9 there are eight independent slope continuity conditions across the stiffener attach line between adjacent bays. Selecting the center bay amplitude as the reference amplitude, the parameters, C_{ij}, given in Equation 9 are expressed in terms of the center bay amplitude as indicated in Table I. The center bay motion is given as

$$w_{22}(x,y) = \sin\left(\frac{m\pi x}{a_2}\right) \sin\left(\frac{n\pi y}{b_2}\right) {}_2W_{mn} \tag{10}$$

TABLE I

VALUES OF $C_{ij}/{}_2W_{mn}$ FOR A NINE BAY STIFFENED PANEL

i =	1	2	3
j = 1	$(-1)^{m+n}(a_1 b_1/a_2 b_2)$	$(-1)^n(b_1/b_2)$	$(-1)^{m+n}(a_1 b_1/a_2 b_2)$
j = 2	$(-1)^m(a_1/a_2)$	1	$(-1)^m(a_1/a_2)$
j = 3	$(-1)^{m+n}(a_1 b_1/a_2 b_2)$	$(-1)^n(b_1/b_2)$	$(-1)^{m+n}(a_1 b_1/a_2 b_2)$

For a thin rectangular plate of dimensions a x b undergoing bending deformations, the expression for the kinetic energy is

$$T = \frac{1}{2}\gamma t \int_0^a \int_0^b \dot{w}^2(x,y)dydx \tag{11}$$

7

an￼ ￼he potential energy is

$$U = \frac{1}{2}D \int_0^a \int_0^b \left[w^2_{,xx} + w^2_{,yy} + 2\nu w_{,xx} w_{,yy} + 2(1-\nu)w^2_{,xy} \right] dy\, dx \qquad (12)$$

For a simply supported plate with dimensions a x b vibrating in the $(m,n)^{th}$ mode, the expressions for the kinetic and potential energy become

$$T = \frac{1}{8} \gamma t\, ab\, \dot{W}^2_{mn} \qquad (13)$$

$$U = \frac{1}{8} \frac{\pi^4 D}{ab} m^2 n^2 F_{mn}(b,a)\, W^2_{mn} \qquad (14)$$

where

$$F_{mn}(b,a) = \left[\left(\frac{m}{n}\right)\left(\frac{b}{a}\right) + \left(\frac{n}{m}\right)\left(\frac{a}{b}\right) \right]^2$$

and the mode shape is given by

$$w(x,y) = \sin\left(\frac{m\pi x}{a}\right) \sin\left(\frac{n\pi y}{b}\right) W_{mn} \qquad (15)$$

Substituting the mode functions given by Equation 9 with amplitudes given in Table I into Equations 13 and 14 and summing the terms from each bay, one obtains the expression for the kinetic energy of the cover sheet as

$$T_1 = \frac{1}{8} \gamma t (a_2 + 2a_1)(b_2 + 2b_1)\, _2\dot{W}^2_{mn} \qquad (16)$$

and the potential energy as

$$U_p = \frac{1}{8} \frac{\pi^9 D}{a_2 b_2} m^2 n^2 \{ F_{mn}(b_2,a_2) + 2(b_1/b_2) F_{mn}(b_1,a_2) + 2(a_1/a_2) F_{mn}(b_2,a_1)$$

$$+ 4(a_1/a_2)(b_1/b_2) F_{mn}(b_1,a_1) \}\, _2W^2_{mn} \qquad (17)$$

Equations 16 and 17 will be used to formulate the modal mass and stiffness of the structure.

2.2 Supporting Structure - The substructure geometry and nomenclature are illustrated in Figure 1. Figure 2 illustrates the cross-section geometry for the stiffeners indicating the relative location of the shear center, attach point, and centroid for the stringers parallel to both the x-axis and the y-axis. The stiffener rotation is defined as

8

$$\theta_{ij}(x) = \sin\left(\frac{m\pi x}{a_i}\right)\Theta_{ij} \tag{18a}$$

$$\theta_{ij}(y) = \sin\left(\frac{n\pi y}{b_i}\right)\Theta_{ij} \tag{18b}$$

where i is the stiffener number and j is the bay index number.

Assuming that each stiffener is uniform along its length, the kinetic energy for stiffeners parallel to the x-axis is

$$T_{si} = \frac{1}{2}(\gamma\, I_{px})_i \sum_{j=1}^{3} \int_0^{a_i} \dot{\theta}_{ij}^2(x)\, dx \qquad i = 3,4 \tag{19a}$$

and for stiffeners parallel to the y-axis

$$T_{si} = \frac{1}{2}(\gamma\, I_{py})_i \sum_{j=1}^{3} \int_0^{b_i} \dot{\theta}_{ij}^2(y)\, dy \qquad i = 1,2 \tag{19b}$$

where I_{px} and I_{py} are given by Equation 8.

The potential energy of stiffeners parallel to the x-axis is given by

$$U_{si} = \frac{1}{2}\sum_{j=1}^{3}\left\{ (E\Gamma_x^*)_i \int_0^{a_i} \theta_{ij}''^2(x)dx + (GJ_x)_i \int_0^{a_i} \theta_{ij}'^2(x)dx \right\} \tag{20a}$$

and for the stiffeners parallel to the y-axis

$$U_{si} = \frac{1}{2}\sum_{j=1}^{3}\left\{ (E\Gamma_y^*)_i \int_0^{b_i} \theta_{ij}''^2(y)dy + (GJ_y)_i \int_0^{b_i} \theta_{ij}'^2(y)dy \right\} \tag{20b}$$

where Γ_x^* and Γ_y^* are given by Equation 7.

The stringer twist amplitudes, Θ_{ij}, normalized to the center bay plate amplitude, $_2W_{mn}$, are given in Table II.

9

TABLE II

VALUES OF $\Theta_{ij}/{_2}W_{mn}$

	j = 1	2	3
i = 1	$(-1)^n m\pi b_1/a_2 b_2$	$m\pi/a_2$	$(-1)^n m\pi b_1/a_2 b_2$
i = 2	$(-1)^{m+n} m\pi b_1/a_2 b_2$	$(-1)^m m\pi/a_2$	$(-1)^{m+n} m\pi b_1/a_2 b_2$
i = 3	$(-1)^m n\pi a_1/a_2 b_2$	$n\pi/b_2$	$(-1)^m n\pi a_1/a_2 b_2$
i = 4	$(-1)^{m+n} n\pi a_1/a_2 b_2$	$(-1)^n n\pi/b_2$	$(-1)^{m+n} n\pi a_1/a_2 b_2$

Substituting Equation 18a into Equations 19a and 20a and Equation 18b into Equations 19b and 20b, performing the integrations, and substituting the amplitude coefficients given in Table II, the expressions for the kinetic and potential energy become

$$T_{si} = \frac{\pi^2}{4}(\gamma I_{px})_i \frac{n^2}{b_2^2}\left(\frac{a_2}{b_2}\right)\left[1 + 2\left(\frac{a_1}{a_2}\right)^3\right] {_2}\dot{W}_{mn}^2 \qquad i = 3,4 \quad (21a)$$

$$U_{si} = \frac{\pi^6}{4}\frac{(E\Gamma_x^*)_i}{a_2^3 b_2^2} m^4 n^2\left[1 + k_{xi2}^2 + 2\left(\frac{a_2}{a_1}\right)\left(1 + k_{xi1}^2\right)\right] {_2}W_{mn}^2 \qquad i = 3,4 \quad (21b)$$

for stringers parallel to the x-axis, and

$$T_{si} = \frac{\pi^2}{4}(\gamma I_{py})_i \frac{m^2}{a_2}\left(\frac{b_2}{a_2}\right)\left[1 + 2\left(\frac{b_1}{b_2}\right)^3\right] {_2}\dot{W}_{mn}^2 \qquad i = 1,2 \quad (22a)$$

$$U_{si} = \frac{\pi^6}{4}\frac{(E\Gamma_y^*)_i}{a_2^2 b_2^3} m^2 n^4\left[1 + k_{yi2}^2 + 2\left(\frac{b_2}{b_1}\right)\left(1 + k_{yi1}^2\right)\right] {_2}W_{mn}^2 \qquad i = 1,2 \quad (22b)$$

for stringers parallel to the y-axis
where $k_{yij}^2 = (GJ_y/E\Gamma_y^*)_i (b_i/n\pi)^2$; $k_{xij}^2 = (GJ_x/E\Gamma_x^*)_i (a_i/m\pi)^2$.

For simplicity, it will be assumed that the stiffeners parallel to the x-axis are identical and that the stiffeners parallel to the y-axis are identical. Then Equations 21a and 21b become

$$T_{sx} = \frac{\pi^2}{4} (\gamma\, I_{px}) \frac{n^2}{b_2}\left(\frac{a_2}{b_2}\right)\left[1 + 2\left(\frac{a_1}{a_2}\right)^3\right] {}_2\dot{W}_{mn}^2 \tag{23a}$$

$$U_{sx} = \frac{\pi^6}{4} \frac{(E\Gamma_x^*)}{a_2^3 b_2^2} m^4 n^2 \left[1 + k_{x2}^2 + 2\left(\frac{a_2}{a_1}\right)\left(1 + k_{x1}^2\right)\right] {}_2W_{mn}^2 \tag{23b}$$

and Equations 22a and 22b become

$$T_{sy} = \frac{\pi^2}{4} (\gamma\, I_{py}) \frac{m^2}{a_2}\left(\frac{b_2}{a_2}\right)\left[1 + 2\left(\frac{b_1}{b_2}\right)^3\right] {}_2W_{mn}^2 \tag{24a}$$

$$U_{sy} = \frac{\pi^6}{4} \frac{(E\Gamma_y^*)}{a_2^2 b_2^3} m^2 n^4 \left[1 + k_{y2}^2 + 2\left(\frac{b_2}{b_1}\right)\left(1 + k_{y1}^2\right)\right] {}_2W_{mn}^2 \tag{24b}$$

where $k_{xi}^2 = (GJ/E\Gamma^*)_x (a_i/m\pi)^2$; $k_{yi}^2 = (GJ/E\Gamma^*)_y (b_i/n\pi)^2$.

2.3 Modal Stiffness and Modal Mass

2.3 Modal Stiffness and Modal Mass – With reference to Equations 4 and 5, the modal stiffness and modal mass for the (m,n)th mode of the structure are obtained by summing the contributions of each component. From Equations 16 and 17 and Equations 21 and 22 the expression for the modal stiffness is

$$\begin{aligned}
K_{mn} = \frac{\pi^4}{4} \frac{D}{a_2 b_2} m^2 n^2 \Bigg\{&\left[F_{mn}(b_2, a_2) + 2\left(\frac{a_1}{a_2}\right) F_{mn}(b_2, a_1)\right.\\
&\left. + 2\left(\frac{b_1}{b_2}\right) F_{mn}(b_1, a_2) + 4\left(\frac{a_1}{a_2}\right)\left(\frac{b_1}{b_2}\right) F_{mn}(b_1, a_1)\right]\\
&+ 4\pi^2 n^2 \frac{(E\Gamma_y^*)}{D a_2 b_2^2}\left[1 + k_{y2}^2 + 2\left(\frac{b_2}{b_1}\right)\left(1 + k_{y1}^2\right)\right]\\
&+ 4\pi^2 m^2 \frac{(E\Gamma_x^*)}{D a_2^2 b_2}\left[1 + k_{x2}^2 + 2\left(\frac{a_2}{a_1}\right)\left(1 + k_{x1}^2\right)\right]\Bigg\}
\end{aligned} \tag{25}$$

The expression for the modal mass is

$$M_{mn} = \frac{1}{4}\left\{\gamma t(a_2 + 2a_1)(b_2 + 2b_1) + 4\pi^2(\gamma I_{px})\frac{n^2}{b_2}\left(\frac{a_2}{b_2}\right)\left[1 + 2\left(\frac{a_1}{a_2}\right)^3\right]\right.$$

$$\left. + 4\pi^2(\gamma I_{py})\frac{m^2}{a_2}\left(\frac{b_2}{a_2}\right)\left[1 + 2\left(\frac{b_1}{b_2}\right)^3\right]\right\} \tag{26}$$

The frequency for the $(m,n)^{th}$ mode is given by

$$f_{mn} = \frac{1}{2\pi}\sqrt{(K_{mn}/M_{mn})}$$

2.4 Generalized Force - For a time-dependent pressure distributed over the surface of the panel, the expression for the generalized force is

$$P_{mn}(t) = \int_A p(x,y,t)\, w(x,y)\, dA \tag{27}$$

Assuming that the pressure is uniformly distributed over the surface of the structure, substituting the mode functions for each bay and integrating over the surface of the structure, the expression for the generalized force is

$$P_{mn}(t) = \frac{a_2 b_2}{\pi^2 mn}\left[(-1)^m - 1\right]\left[(-1)^n - 1\right]R_{mn}\, P_o(t) \tag{28}$$

where $R_{mn} = 1 + 2(-1)^n\left(\frac{b_1}{b_2}\right)^2 + 2(-1)^m\left(\frac{a_1}{a_2}\right)^2 + 4(-1)^{m+n}\left(\frac{a_1}{a_2}\right)^2\left(\frac{b_1}{b_2}\right)^2$

3. Stiffener Response to Uniform Static Pressure

For a simply supported panel loaded by a uniform pressure, q_o, the pressure can be resolved into a Fourier series as

$$P_o = \sum\sum\frac{16q_o}{\pi^2 mn}\sin\left(\frac{m\pi x}{2}\right)\sin\left(\frac{n\pi y}{b}\right) \tag{29}$$

For a displacement function of the form

$$w(x,y) = \sin\left(\frac{m\pi x}{a}\right)\sin\left(\frac{n\pi y}{b}\right)W_{mn} \tag{30}$$

the static response of the panel to the load q_o in the $(m,n)^{th}$ mode is

12

$$W_{mn} = \frac{16 q_o a^2 b^2}{\pi^6 m^3 n^3 D F_{mn}(b,a)} \qquad (31)$$

The stress response to the static loading must consider stresses in the cover sheet and stresses in the supporting ribs. Ballentine's design method for establishing skin thicknesses of acoustically loaded panels (Figure 73, Reference 8) is sufficiently accurate so that additional effort on this aspect of the problem is not required for stiffened panels.

The stress response of the substructure is of primary interest. The static loading of the panel is assumed to be transferred to the stiffener by a shear force. The intensity of the load transmitted can be estimated from thin plate theory by computing the shear loading along the edge of the panel. For a panel deforming as given in Equation 30, the distributed shear loading along the edge $x = 0$ is given by the expression

$$V(0,y) = \frac{16 q_o b \left[F_{mn}^{1/2}(b,a) + (1 - \nu)\left(\frac{n}{m}\right)\left(\frac{a}{b}\right) \right]}{\pi^3 mn^2 F_{mn}(b,a)} \sin\left(\frac{n\pi y}{b}\right) \qquad (32)$$

for a uniform loading q_o. The resultant of this shear loading is obtained by integrating Equation (32) over the length of the edge and subtracting the two corner reactions of the plate (Reference 9, pp. 105, 107). The resultant shear load is given as

$$\overline{V} = \frac{16 q_o b^2 [(-1)^n - 1]}{\pi^4 mn^3 F_{mn}^{1/2}(b,a)} \qquad (33)$$

Considering the stringer to be clamped on both ends (for bending) and loaded by a uniform load of intensity $\overline{V}/b$, the bending moment at the support has magnitude (setting $q_o = 1$)

$$M_o = \frac{4b^3 [(-1)^n - 1]}{3\pi^4 mn^3 F_{mn}^{1/2}(b,a)} \qquad (34)$$

The bending stress in the flange of the stiffener is given in Reference 7, p. 193, as

$$\sigma_o = \frac{I_{zz} M_o h}{2(I_{xx} I_{zz} - I_{xz}^2)} = \frac{M_o h}{2I^*} \qquad (35)$$

where h = height of the stiffener cross-section.

The area moments of inertia given in Equation 35 are referenced to the centroidal axes. Expressions for the area moments, St. Venant's torsion constant, and the warping constant

13

are given in Appendix I for constant thickness zee, channel, and hat cross-section shapes.

D. Box Structure

The broad definition of a box type structure is taken to be two parallel plates stiffened by deep shear ribs. Such structure can be taken as a model for flap, fin, or pylon type structure encountered on modern aircraft. The box structure shall be classified by the number of cells formed by the intersecting cover sheets and ribs. Two configurations shall be considered for the frequency analysis: three cell and nine cell box structures. These structures are illustrated in Figure 3. The three cell configuration has been investigated by Clarkson and Abrahamson, Reference 10, and by Sen Gupta and Mead, Reference 11. The presentation here follows that of Reference 10 although the development was independent.

1. Derivation of Mode Shapes

The detailed derivation of the mode shapes for the Rayleigh frequency analysis of the three cell box structure is presented in this section. Consider the structure illustrated in Figure 3a with the coordinate nomenclature for each component. The mode functions for each component are taken as (local x-y coordinates are implied for each component):

$$_1w_1(x,y) = \sin\left(\frac{i\pi x}{a}\right) \sin\left(\frac{k\pi y}{b_1}\right) {}_1W_1$$

$$_1w_2(x,y) = \sin\left(\frac{i\pi x}{a}\right) \sin\left(\frac{\ell\pi y}{b_2}\right) {}_1W_2$$

$$_1w_3(x,y) = \sin\left(\frac{i\pi x}{a}\right) \sin\left(\frac{m\pi y}{b_3}\right) {}_1W_3$$

$$v_1(x,z) = \sin\left(\frac{i\pi x}{a}\right) \sin\left(\frac{n\pi z}{h}\right) V_1$$

$$v_2(x,z) = \sin\left(\frac{i\pi x}{a}\right) \sin\left(\frac{p\pi z}{h}\right) V_2 \tag{36}$$

$$_2w_1(x,y) = \sin\left(\frac{i\pi x}{a}\right) \sin\left(\frac{q\pi y}{b_1}\right) {}_2W_1$$

$$_2w_2(x,y) = \sin\left(\frac{i\pi x}{a}\right) \sin\left(\frac{r\pi y}{b_2}\right) {}_2W_2$$

$$_2w_3(x,y) = \sin\left(\frac{i\pi x}{a}\right) \sin\left(\frac{s\pi y}{b_3}\right) {}_2W_3$$

where i, k, ℓ, m, n, p, q, r, and s are integer mode numbers.

14
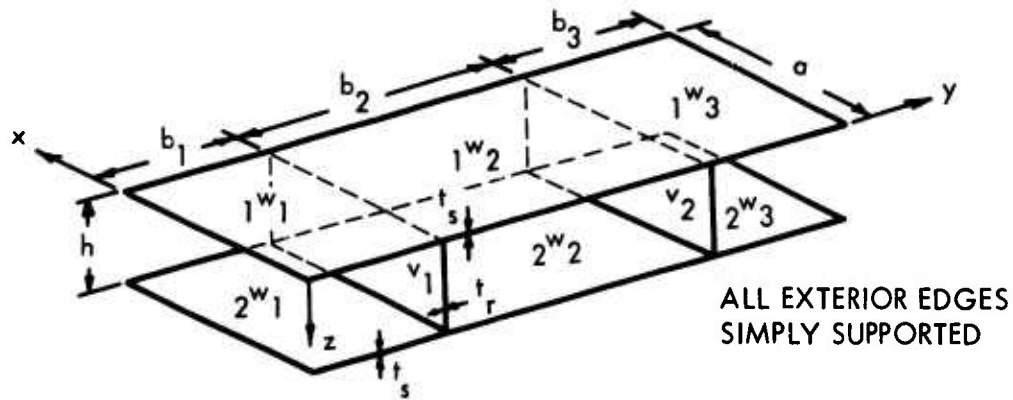
(a) THREE CELL CONFIGURATION
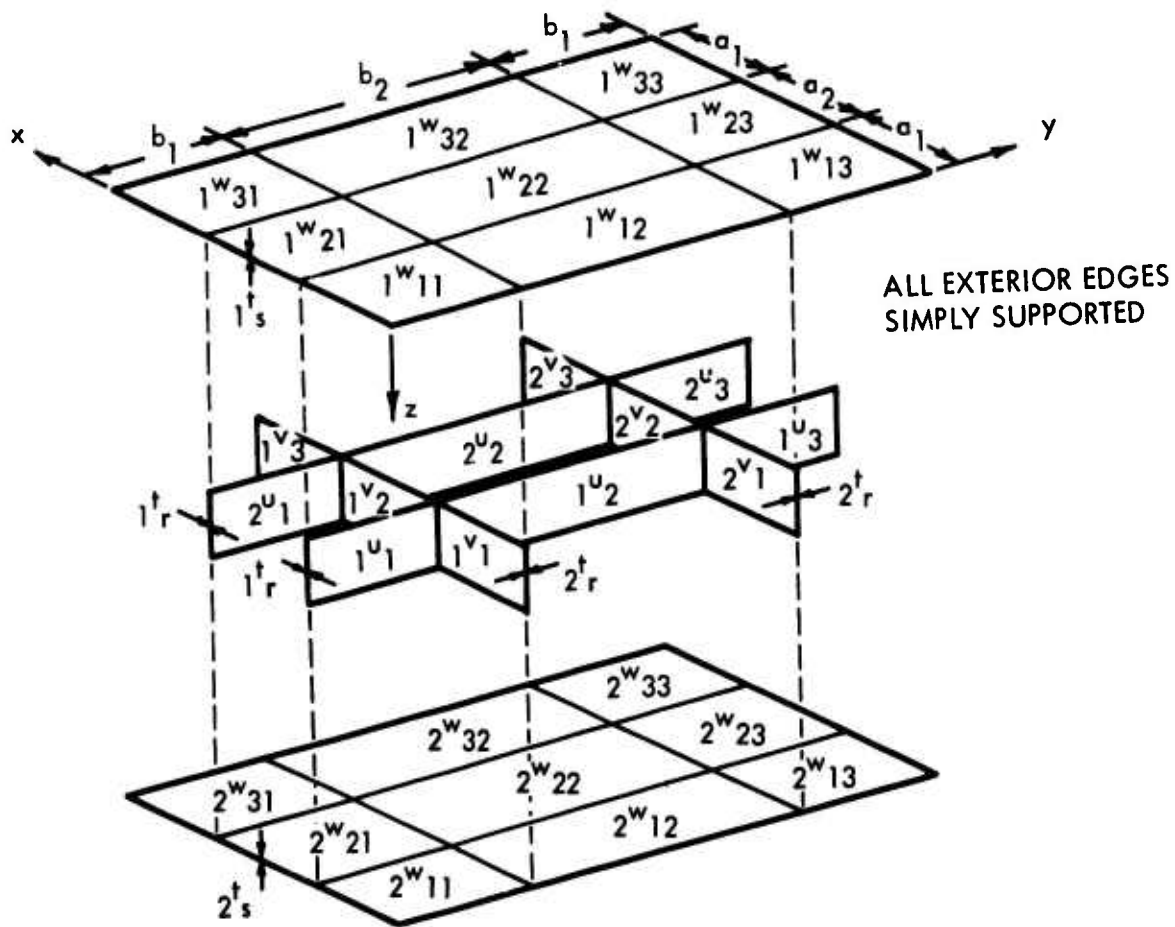
(b) NINE CELL CONFIGURATION (EXPLODED)

FIGURE 3. BOX STRUCTURE CONFIGURATIONS

Assuming that each joint is allowed only to rotate and that all components intersecting at a joint have the same slope (zero shear condition), one obtains the constraint conditions:

$$_1w_{1,y}(b_1) + v_{1,z}(0) = 0 \qquad _1w_{2,y}(b_1) + v_{2,z}(0) = 0$$

$$_1w_{2,y}(0) + v_{1,z}(0) = 0 \qquad _1w_{3,y}(0) + v_{2,z}(0) = 0$$

$$_2w_{1,y}(b_1) + v_{1,z}(h) = 0 \qquad _2w_{2,y}(b_1) + v_{2,z}(h) = 0 \qquad (37)$$

$$_2w_{2,y}(0) + v_{1,z}(h) = 0 \qquad _2w_{3,y}(0) + v_{2,z}(h) = 0$$

The eight homogeneous equations given above have a non-zero solution (i.e., the amplitudes $_1W_1$, $_1W_2$, etc., are non-zero) only if the determinant of the coefficient matrix vanishes. Substituting from Equation 36 into Equations 37 and evaluating the determinant of the coefficient matrix, one obtains the condition on the mode numbers that $(-1)^{n+r} = (-1)^{\ell+p}$ for the determinant to vanish. That is, the mode numbers, n, r, ℓ, and p must be selected such that $(n+r)$ and $(\ell+p)$ are either both odd or both even ($n=1$, $r=1$, $\ell=2$, $p=1$ would not be a valid mode number set, for example).

The above derivation is too general to be of design value and has been presented only to illustrate the general technique for establishing valid modes for the Rayleigh energy analysis.

2. Three Cell Box Structure

The derivation of expressions for the modal stiffness and modal mass is rather straight-forward once the mode shapes for the structure are established. For design purposes, it will be assumed that the rib spacing is uniform ($b_1 = b_2 = b_3 = b$ in Figure 3a), that the material properties of the cover sheets and ribs are identical and that the only modes considered are described by the set (p,m,r) for the (x,y,z) coordinate directions.

For the above assumptions, one makes the following substitution for mode number s as given in Equation 36

$$i = p; \quad k = \ell = q = r = s = m; \quad n = p = r .$$

With this assignment the determinant of the coefficient matrix vanishes identically. Expressing the eigenvector of component amplitudes in terms of the amplitude $_1W_2$ (center bay of the cover sheet in the plane $(x,y,0)$), one obtains:

$$_1W_1 = (-1)^m\, _1W_2 \qquad\qquad _2W_1 = (-1)^{m+r}\, _1W_2$$

$$_1W_3 = (-1)^m\, _1W_2 \qquad\qquad _2W_2 = (-1)^r\, _1W_2 \qquad (38)$$

$$V_1 = -\left(\frac{h}{b}\right)\left(\frac{m}{r}\right)\, _1W_2 \qquad\qquad _2W_3 = (-1)^{m+r}\, _1W_2$$

16

$$V_2 = (-1)^{m+1} \left(\frac{h}{b}\right) \left(\frac{m}{r}\right) {}_1W_2 \qquad \qquad \text{(38 cont'd)}$$

Figure 4 illustrates six possible mode shapes for the structure for the indicated modes for a section through the structure in the plane $(a/2, y, z)$. Figures 4a, 4b, 4c illustrate the fact that for fundamental modes in the cover sheet $(p = m = 1)$ all rib modes $(r = 1, 2, 3 \ldots)$ can be excited. Also, if r is odd, the two cover sheets are out-of-phase and, if r is even, the cover sheets are in-phase. Since the excitation pressures are on the cover sheets and the generalized force will be maximum for the fundamental mode in the cover sheet, it should be possible to excite any rib mode. This effect has been observed experimentally.

2.1 Frequency Analysis - The kinetic energy and potential energy expressions are obtained by substituting the mode shapes for each component (as defined by Equations 36 and 38) into Equations 11 and 12. The expression for the modal stiffness is

$$K_{pmr} = \frac{\pi^4}{ab} D_s p^2 m^2 \left\{ 3F_{pm}(a,b) + \left(\frac{h}{b}\right)\left(\frac{t_r}{t_s}\right)^3 F_{rp}(a,h) \right\}$$

(39)

and for the modal mass

$$M_{pmr} = \rho_s ab \left\{ 3 + \left(\frac{h}{b}\right)^3 \left(\frac{t_r}{t_s}\right)\left(\frac{m}{r}\right)^2 \right\}$$

where it has been assumed that $b_1 = b_2 = b_3 = b$.

The frequency of the $(p,m,r)^{th}$ mode is

$$f_{pmr} = \frac{1}{2\pi}\sqrt{(K_{pmr}/M_{pmr})}, \ Hz$$

2.2 Generalized Force - The expression for the generalized force for the three-cell box structure will be derived assuming uniform pressures of different intensities over the two cover sheets. Denoting the pressure on the upper cover sheet, $(x,y,0)$ plane, as $p_1(t)$ and the pressures on the lower cover sheet, (x,y,h) plane, as $p_2(t)$ and assuming that the pressure is positive if directed toward the interior of the structure, the expression for the generalized force is

$$P_{pmr}(t) = p_1(t) \sum_{i=1}^{3} \int_0^a \int_0^b {}_1w_i(x,y)dydx + p_2(t) \sum_{i=1}^{3} \int_0^a \int_0^b {}_2w_i(x,y)dydx \qquad (40)$$

Substituting for the modes shapes ${}_1w_i(x,y)$ and ${}_2w_i(x,y)$ and noting the relations given by Equations 36 and 38, one obtains

$$P_{pmr}(t) = \frac{ab}{\pi^2 mn} \left[p_1(t) - (-1)^r p_2(t) \right]\left[1 - 2(-1)^m \right]\left[(-1)^m - 1 \right]\left[(-1)^p - 1 \right] \qquad (41)$$

17
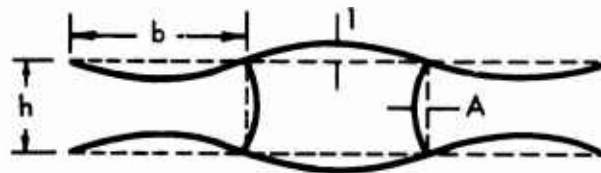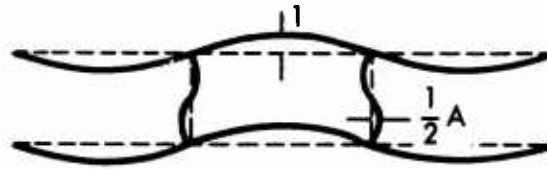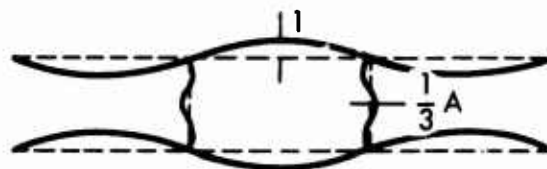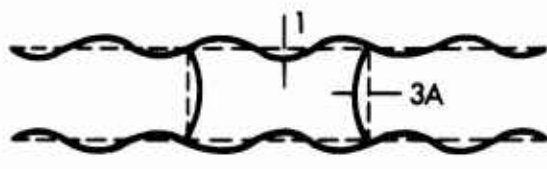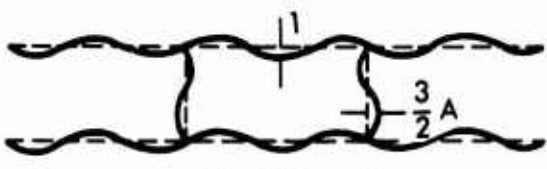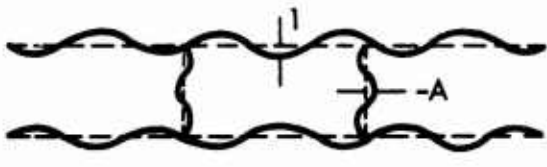
FIGURE 4   MODE SHAPES FOR A THREE CELL BOX STRUCTURE

Equation 41 clearly illustrates that only modes for p and m odd will be excited, as would be expected.

3. Nine Cell Box Structure

The configuration of the nine cell box structure is illustrated in Figure 3b. This configuration was adopted for the experimental program described subsequently. The displacement functions for each component are denoted in Figure 3b where cover sheet displacement is given by the functions $_1w_{ij}$ and $_2w_{ij}$ (positive in the positive z direction) and rib displacement functions $_1u_i$, $_2u_i$ and $_1v_i$, $_2v_i$ (positive in the positive x and y directions, respectively). As described for the three cell box structure, the application of a zero shear condition at each joint of a rib and cover sheet allows one to describe a mode in terms of a mode number set and a single amplitude. Also, the analysis presented here assumes that a mode is described by the mode numbers (m,n,q) so that the assumed modes for each component have the form

$$_kw_{ij}(x,y) = \sin\left(\frac{m\pi x}{a_i}\right) \sin\left(\frac{n\pi y}{b_i}\right) {_kW_{ij}}$$

$$_ku_i(y,z) = \sin\left(\frac{n\pi y}{b_i}\right) \sin\left(\frac{q\pi z}{h}\right) {_kU_i} \tag{42}$$

$$_kv_i(x,z) = \sin\left(\frac{m\pi x}{a_i}\right) \sin\left(\frac{q\pi z}{h}\right) {_kV_i}$$

for the kth component of the cover sheet or rib. Selecting the center bay of the upper cover sheet as the arbitrary amplitude, $_1W_{22}$, the amplitudes of the components in terms of the mode number and geometry are given as:

$$_1W_{12} = {_1W_{31}} = {_1W_{13}} = {_1W_{33}} = (-1)^{m+n} (a_1/a_2)(b_1/b_2) {_1W_{mnq}}$$

$$_1W_{21} = {_1W_{23}} = (-1)^n (b_1/b_2) {_1W_{mnq}} \tag{43a}$$

$$_1W_{12} = {_1W_{32}} = (-1)^m (a_1/a_2) {_1W_{mnq}}$$

for the upper cover sheet amplitudes;

$$_1U_1 = {_1U_3} = -(-1)^n (h/a_2)(b_1/b_2) {_1W_{mnq}}$$

$$_1U_2 = -(h/a_2)(m/q) {_1W_{mnq}} \tag{43b}$$

$$_2U_i = (-1)^n {_1U_i}$$

19

$$_1V_1 = {_1}V_3 = - (-1)^m (h/b_2)(a_1/a_2) \, {_1}W_{mnq}$$

$$_1V_2 = - (h/b_2)(n/q) \, {_1}Wmnq \tag{43c}$$

$$_2V_i = (-1)^n \, {_1}V_i$$

for the rib amplitudes; and

$$_2W_{ij} = (-1)^q \, {_1}W_{ij} \tag{43d}$$

for the lower cover sheet amplitudes and $_1W_{mnq} = {_1}W_{22}$.

3.1 Frequency Analysis – For the frequency analysis, it will be assumed that the material properties of all components are identical and that the thickness of the components are as illustrated in Figure 3b. The modal stiffness and modal mass for the $(m,n,q)^{th}$ mode are obtained by substituting the component mode shape as given in Equation 42 with amplitudes given by Equations 43 into Equations 11 and 12 and summing for all components. Neglecting the detailed algebra, the expression for the modal mass is given by

$$M_{mnq} = {_1}\rho_s \, a_2 b_2 \left\{ (1 + {_2}t_s/{_1}t_s)M_s + 2 \left(\frac{{_1}t_r}{{_2}t_r}\right)\left(\frac{h}{b_2}\right)^3 \left(\frac{n}{q}\right)^2 M_r \right\} \tag{44}$$

where $_1\rho_s = \gamma_1 t_s$

$$M_s = 1 + 2(a_1/a_2)^3 + 2(b_1/b_2)^3 + 4(a_1/a_2)^3 (b_1/b_2)^3$$

$$M_r = 1 + 2(a_1/a_2) + \left(\frac{{_2}t_r}{{_1}t_r}\right)\left(\frac{b_2}{a_2}\right)^3 \left(\frac{m}{n}\right)^2 [1 + 2(b_1/b_2)]$$

The expression for the modal stiffness is given as

$$K_{mnq} = \frac{\pi^4 \, {_1}D_s}{a_2 b_2} m^2 n^2 \left\{ \left[1 + \left(\frac{{_2}t_s}{{_1}t_s}\right)^3 \right] K_s + 2 \left(\frac{{_1}t_r}{{_1}t_s}\right)^3 K_r \right\} \tag{45}$$

where $_1D_s = E \, {_1}t_s^3/12(1 - \nu^2)$

$$K_s = F_{mn}(b_2, a_2) + 2[(a_1/a_2)F_{mn}(b_2, a_1) + (b_1/b_2)F_{mn}(b_1, a_2)$$
$$+ 2(a_1/a_2)(b_1/b_2)F_{mn}(b_1, a_1)]$$

20

$$K_r = (h/b_2) [F_{mq}(h, a_2) + 2(a_1/a_2 F_{mq}(h, a_1))]$$

$$+ (h/a_2)(_2t_r/_1t_r)^3 [F_{nq}(h, b_2) + 2(b_1/b_2)F_{nq}(h, b_1)]$$

The frequency of the $(m, n, q)^{th}$ mode is given by the expression

$$f_{mnq} = \frac{1}{2\pi} \sqrt{(K_{mnq}/M_{mnq})}, \text{ Hz}$$

3.2 Generalized Force - The relationship for the generalized force for the nine-cell box structure is obtained in a manner identical to that described for the three cell box structure. Assuming that a pressure is positive if it is directed towards the interior of the structure and denoting the pressure on the upper surface as $p_1(t)$ ((x,y,0)-plane) and on the lower surface as $p_2(t)$ ((x,y,h)-plane), the generalized force for the $(m,n,q)^{th}$ mode is

$$P_{mnq}(t) = \frac{a_2 b_2}{\pi^2 mn} (p_1(t) - (-1)^q p_2(t))\Gamma_{mn} \tag{46}$$

where $\Gamma_{mn} = [(-1)^m - 1][(-1)^n - 1] R_{mn}$

R_{mn} is defined in Equation 28.

Equation 46 clearly illustrates that only modes for m and n odd will be excited, as would be expected.

4. Stress Response

As indicated by Equation 3, the stress response of the skin and ribs for box structure due to a uniform static pressure of unit magnitude is required to estimate the mean square or R.M.S. stress response of the structure. The approach taken here is dependent upon the flexibility of box-type structure as described in Reference 1 and is essentially different from the approach taken by Ballentine, Reference 8. The approximate method for computing stresses in continuous slabs as described by Timoshenko (Reference 9, pp. 236-245) is presented here -- modified to account for the rib supporting the cover sheet. This modification was first described by Clarkson, Reference 1.

Timonshenko's approximate method relies upon the synthesis of elementary solutions for uniformly loaded thin rectangular plates to obtain estimates of stresses in continuous slabs. The basic procedure is to divide the bays of the structure into components such that boundaries between adjacent bays are considered to be clamped. Considering the planform of the cover sheet for three cell and nine-cell box structure as illustrated in Figure 3, the bays of structure are taken with the boundary conditions as illustrated in Figure 5. Timoshenko presents tabulated data for estimating the bending moments at the panel center and the center of a clamped edge for uniformly loaded plates with various boundary conditions. At a point on the boundary between two plates, the resultant bending moment is approximated by the average value of the component bending moments. As illustrated in

21
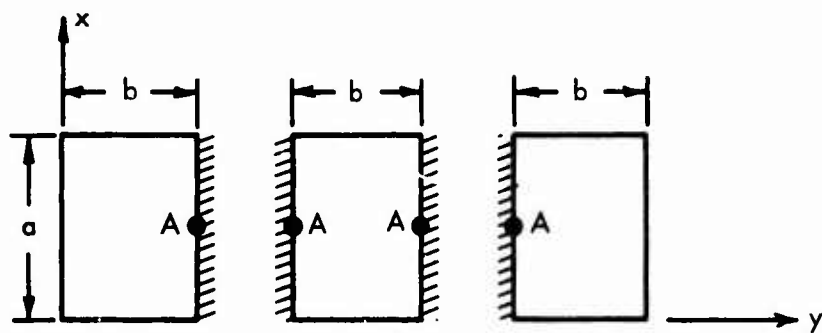
a) BOUNDARY CONDITIONS FOR THREE CELL BOX STRUCTURE
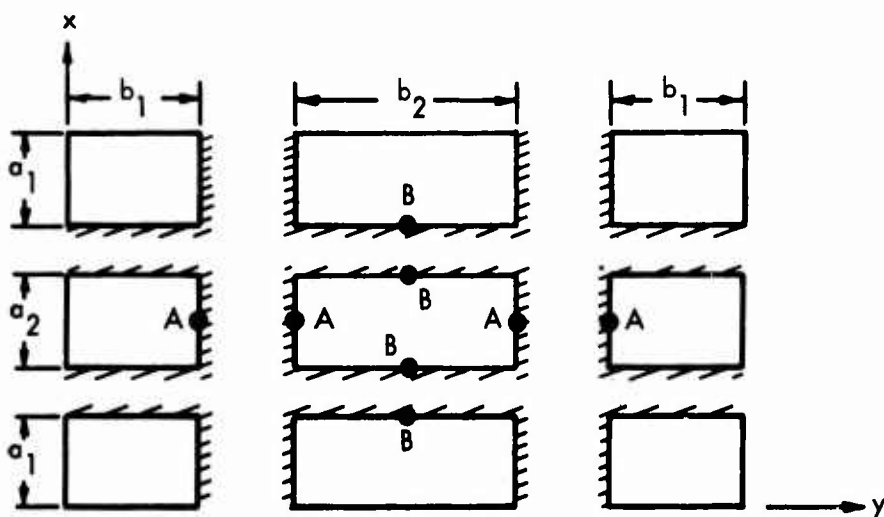
b) BOUNDARY CONDITIONS FOR NINE CELL BOX STRUCTURE

——————— SUPPORTED EDGE

⟋⟋⟋⟋ CLAMPED EDGE

FIGURE 5   COMPONENT BOUNDARY CONDITIONS: BOX STRUCTURE
STRESS CALCULATION

22

Figure 5, four different sets of boundary conditions are to be considered. Case 1 represents a rectangular plate with three edges supported and one edge clamped. Case 2 represents a rectangular plate with two opposite edges supported and two opposite edges clamped. Case 3 represents a rectangular plate with one edge supported and three edges clamped. Finally, Case 4 represents a rectangular plate with all edges clamped. The bending moments at the center of a clamped edge for a rectangular plate with dimensions a x b uniformly loaded by a pressure of magnitude q_o is given by Timoshenko as:

Case 1 $\qquad \bar{M}_y = \delta_2 \, q_o \, \ell^2 \qquad$ at $(x,y) = (a/2, 0)$

Case 2 $\qquad \bar{M}_y = \delta_3 \, q_o \, \ell^2 \qquad$ at $(x,y) = (a/2, 0)$ & $(a/2, b)$

Case 3 $\qquad \bar{M}_x = \gamma_5 \, q_o \, \ell^2 \qquad$ at $(x,y) = (0, b/2)$ & $(a, b/2)$

$\qquad\qquad\quad \bar{M}_y = \delta_5 \, q_o \, \ell^2 \qquad$ at $(x,y) = (a/2, 0)$

Case 4 $\qquad \bar{M}_x = \gamma_6 \, q_o \, \ell^2 \qquad$ at $(x,y) = (0, b/2)$ & $(a, b/2)$

$\qquad\qquad\quad \bar{M}_y = \delta_6 \, q_o \, \ell^2 \qquad$ at $(x,y) = (a/2, 0)$ & $(a/2, b)$

where ℓ is the smaller of the dimensions a and b and the subscripts on the γ's and δ's (the bending moment factors) follow Timoshenko's notation. Plotted values of the bending moment factors versus panel aspect ratio b/a are present in Figures 6, 7, and 8. For more accurate values of the bending moment factor, the referenced tabulated values can be used. The asymptotic values for the bending moment factors are listed in Table III.

TABLE III

ASYMPTOTIC VALUES OF THE BENDING MOMENT FACTORS

b/a	δ_2	δ_3	γ_5	δ_5	γ_6	δ_6
0.0	.1250	.0833	-	-	.0571	.0833
∞	.1250	.1250	.0833	.0566	.0833	.0571

NOTE: All values for the bending moment factors as presented here are positive instead of negative as presented by Timoshenko.

The use of the plotted or referenced tabulated data for computing bending moments in the cover sheet or rib of the panel arrays shown in Figure 5 is best illustrated by an example.

Example: (a) Three Cell Box Structure – Considering the panel array illustrated in Figure 5a, the values for δ_2 and δ_3 are obtained for the particular value of panel aspect ratio, b/a (Figure 6) and the expression for the bending moment at

23
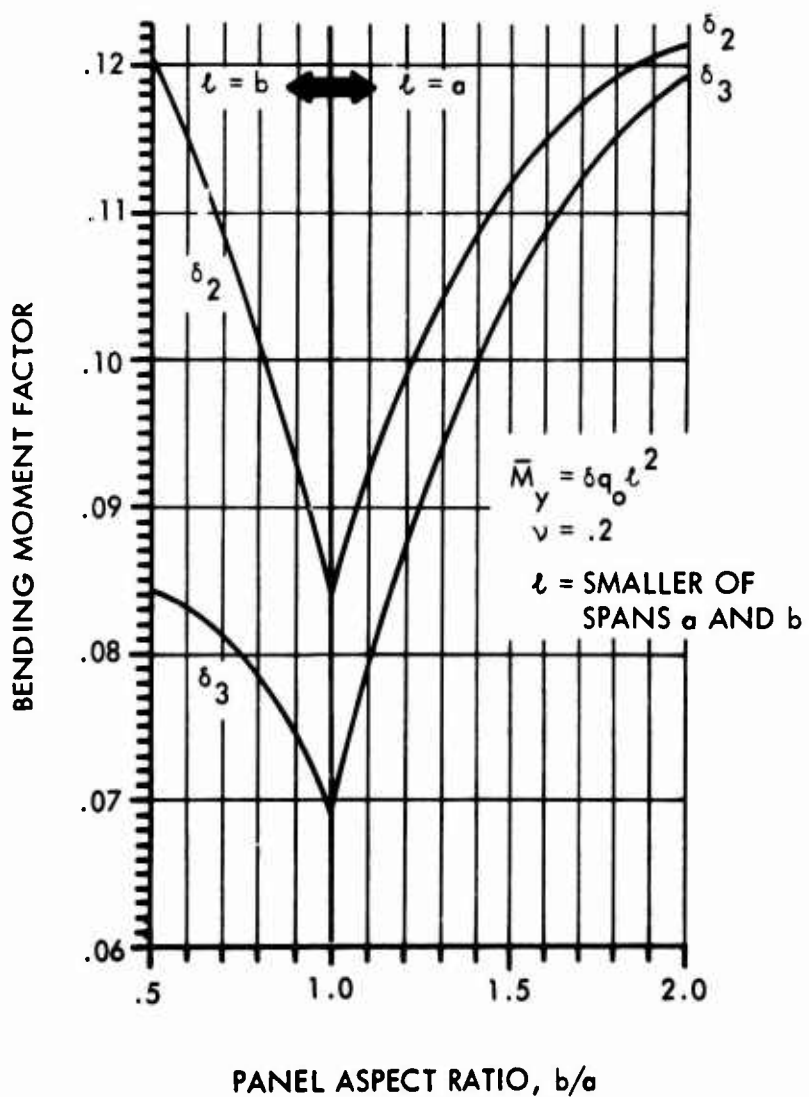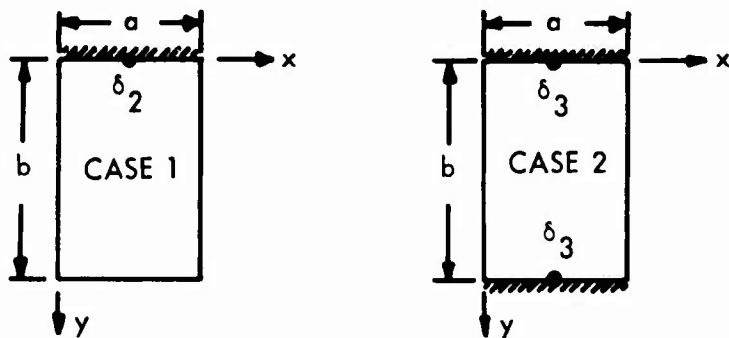
FIGURE 6   BENDING MOMENT FACTOR: CASES 1 & 2

24

The graph shows bending moment factor versus panel aspect ratio with the following annotations:

$\overline{M}_x = \gamma_5 q_0 \ell^2$

$\overline{M}_y = \delta_5 q_0 \ell^2$

$\nu = .2$

$\ell = $ SMALLER OF SPANS a AND b

$\ell = b$ $\ell = a$

Y-axis: BENDING MOMENT FACTOR (.05, .06, .07, .08, .09, .10, .11)

X-axis: PANEL ASPECT RATIO, b/a (.5, 1.0, 1.5, 2.0)
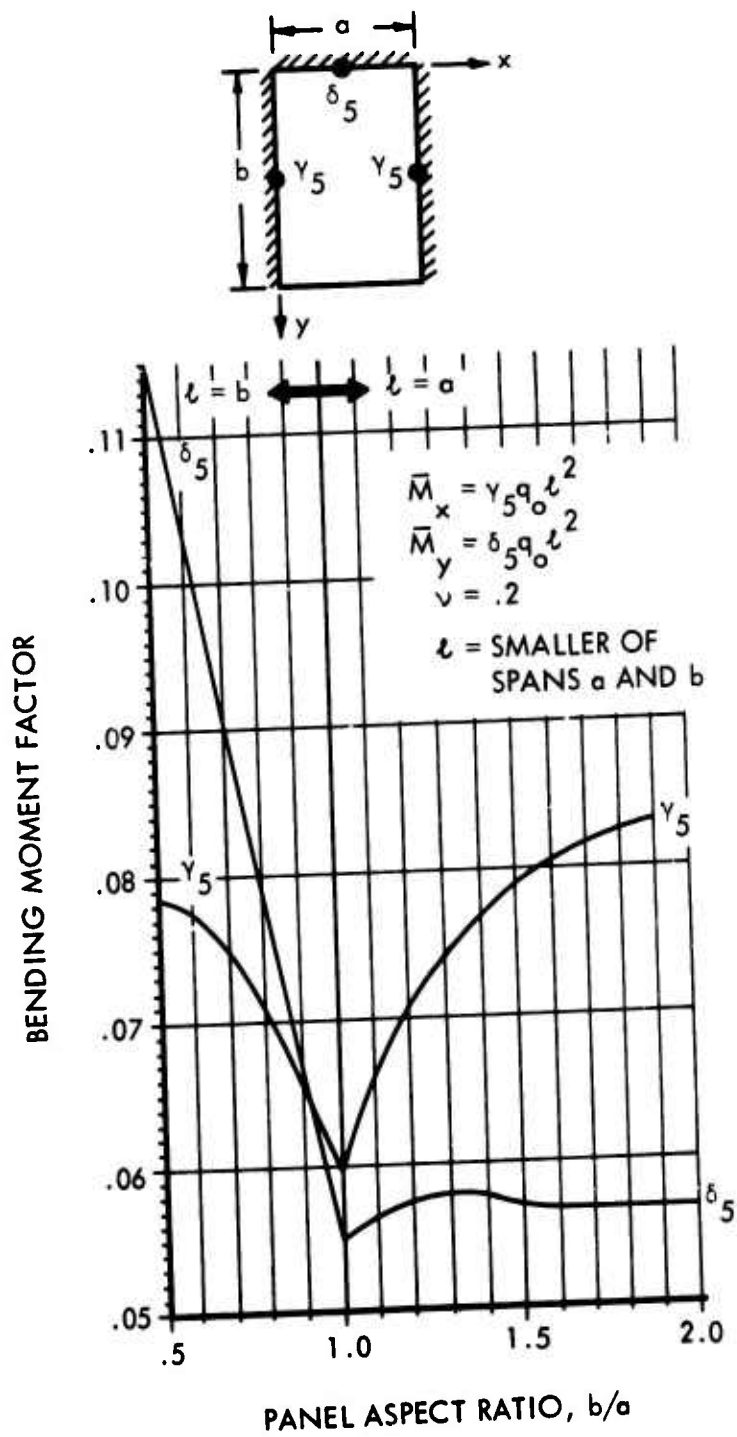
FIGURE 7 BENDING MOMENT FACTOR: CASE 3

25

$$\bar{M}_x = \gamma_6 q_o \ell^2 \qquad\qquad \bar{M}_y = \delta_6 q_o \ell^2$$
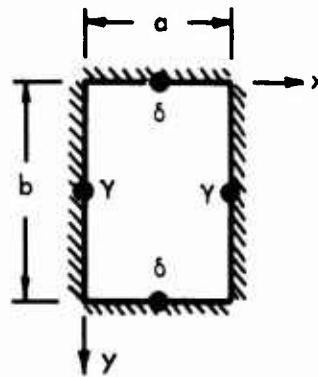
$\nu = .2 \qquad \ell = $ SMALLER OF SPANS a AND b
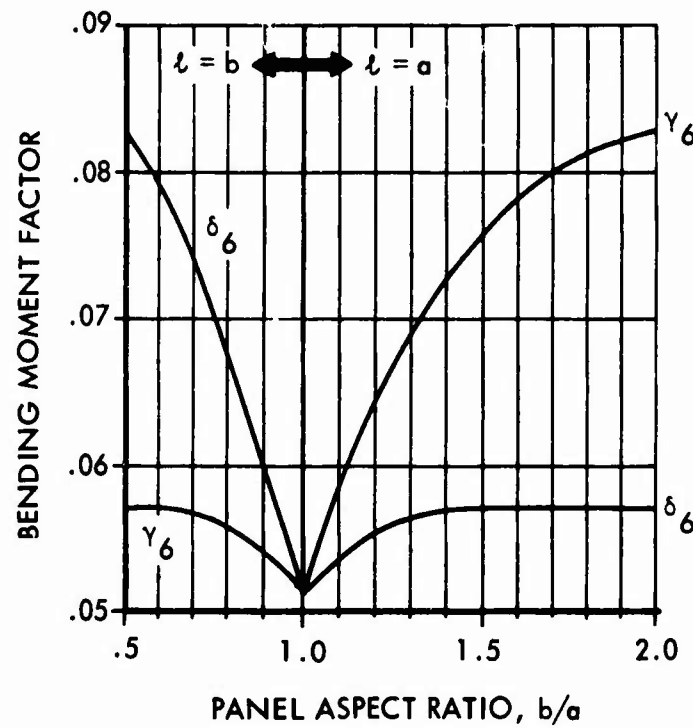
FIGURE 8   BENDING MOMENT FACTOR: CASE 4

point A (Figure 5a) is simply

$$\bar{M}_y = (\delta_2 + \delta_3) \, q_o \ell^2 / N \tag{47}$$

where ℓ is the smaller of the two dimensions a and b

  $N = 2$ for a stiffened panel array

  $N = 3$ for a box type structure, Ref. 1.

(b) Nine Cell Box Structure – Considering the panel array illustrated in Figure 5b, the value of δ_5 is obtained for the two panels with dimensions $a_2 \times b_1$ and $a_1 \times b_2$ and the values of γ_6 and δ_6 are obtained for the center bay so that for point A

$$\bar{M}_y = (\delta_5 \ell_1^2 + \delta_6 \ell_2^2) q_o / N \tag{48a}$$

and for point B

$$\bar{M}_x = (\delta_5 \ell_3^2 + \gamma_6 \ell_2^2) q_o / N \tag{48b}$$

where ℓ_1 is the smaller of the two dimensions a_2 and b_1

  ℓ_2 is the smaller of the two dimensions a_2 and b_2

  ℓ_3 is the smaller of the two dimensions a_1 and b_2

Stress is obtained from Equations 47 and 48 by use of the simple expression

$$\sigma = 6\bar{M}/t^2 \tag{49}$$

where t is the thickness of the cover sheet or rib.

E. Frequency Analysis of a Three Cell Wedge Structure

1. Basic Considerations

Wedge structure is typical of aircraft control surfaces such as ailerons, trailing edge of flaps, elevators and rudders. The presentation here is a very simplified approach to a complicated structural dynamics problem. The objective will be to obtain an estimate of the natural frequencies of such structure. Due to the very simple mode shape assumed for the rib in the radial direction, any attempt to obtain stress estimates would be of dubious value. However, the frequency estimates do seem reasonable.

2. Frequency Analysis

Consider the three cell wedge structure illustrated in Figure 9. For structural modes symmetric about the x-y plane, mode shapes for a component of the cover sheet are assumed to be of the form

27
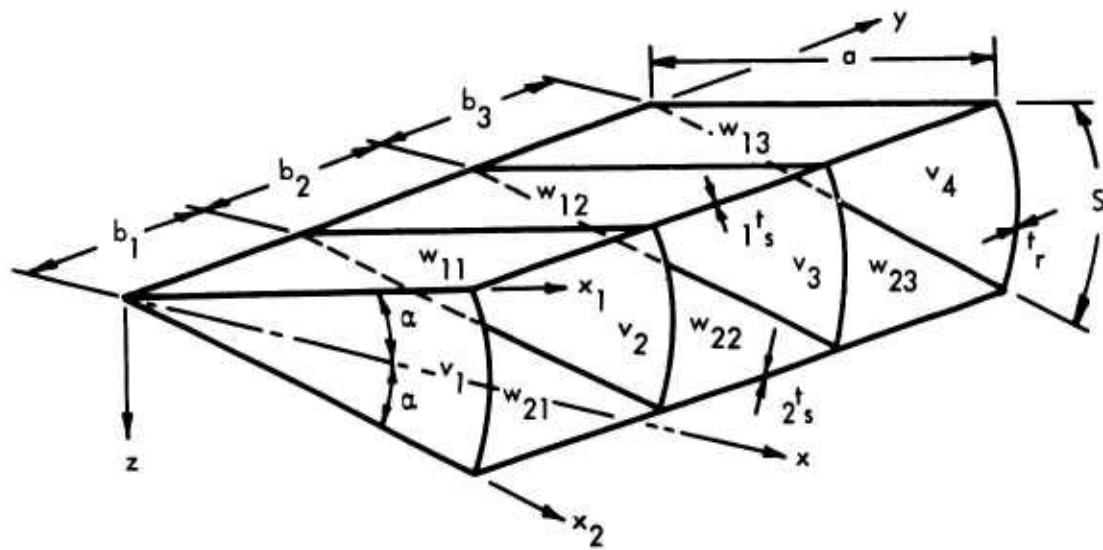
FIGURE 9   THREE CELL WEDGE STRUCTURE
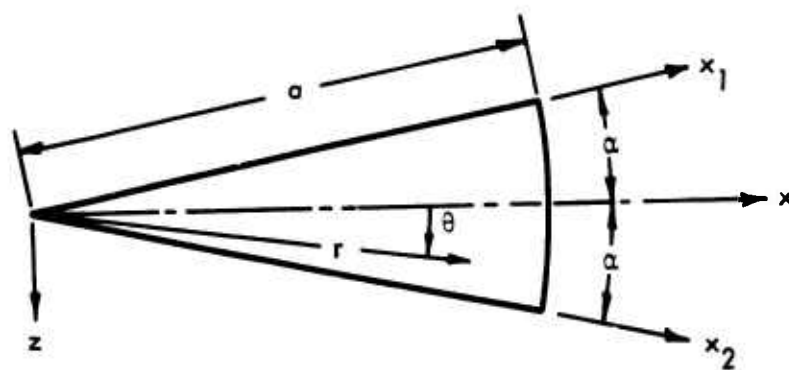
FIGURE 10   SECTOR PLATE COORDINATE SYSTEM

$$w_{ij}(x_i, y) = \sin\left(\frac{m\pi}{a} x_i\right) \sin\left(\frac{n\pi y}{b_i}\right) W_{ij} \qquad (50a)$$

$$v_k(r, \theta) = \sin\left(\frac{m\pi r}{a}\right) \cos\left(\frac{q\pi\theta}{2\alpha}\right) V_k \qquad (50b)$$

where $i = 1, 2$; $j = 1, 2, 3$; $k = 1, 2, 3, 4$; $q = 1, 3, 5, \ldots$ The mode functions w_{ij} represent displacements normal to the x_i-y plane and v_k represents the rib mode functions. For a zero shear condition at a joint of a rib and a cover sheet, one obtains the relations

$$\frac{1}{r}\frac{\partial v_k}{\partial \theta}\bigg|_{\theta=\alpha} + \frac{\partial w_{1j}}{\partial y}\bigg|_{y=0, b_i} = 0$$

$$\qquad (51)$$

$$\frac{1}{r}\frac{\partial v_k}{\partial \theta}\bigg|_{\theta=-\alpha} + \frac{\partial w_{2j}}{\partial y}\bigg|_{y=0, b_i} = 0$$

Substituting Equations 50 into 51, the rib amplitudes, V_k, are expressed in terms of the cover sheet amplitudes, W_{ij}, as

$$V_1 = 2\alpha (-1)^{(q+2n-1)/2} \left(\frac{n}{q}\right)\left(\frac{r}{b_2}\right) W_{12} = V_3$$

$$V_2 = 2\alpha (-1)^{(q-1)/2} \left(\frac{n}{q}\right)\left(\frac{r}{b_2}\right) W_{12} = V_4 \qquad (52)$$

$$W_{11} = (-1)^n \left(\frac{b_1}{b_2}\right) W_{12} = W_{13}$$

$$W_{2j} = -W_{1j}$$

where the amplitudes have been normalized to W_{12}.

The geometry of the sector plate is illustrated in Figure 10.

The expression for the potential energy of a sector plate (rib) is

$$U = \frac{1}{2} D \int_{-\alpha}^{\alpha} \int_0^a \left\{ \left(v_{,rr} + \frac{1}{r}v_{,r} + \frac{1}{r^2}v_{,\theta\theta}\right)^2 - 2(1-\nu)\frac{1}{r}v_{,rr}\left(v_{,r} + \frac{1}{r}v_{,\theta\theta}\right) \right.$$

$$\left. + 2(1-\nu)\left[\left(\frac{1}{r}v_{,\theta}\right)_{,r}\right]^2 \right\} r \, dr \, d\theta \qquad (53)$$

Substituting for the mode shapes given in Equation 50b, the expression for the potential energy becomes

$$U = \frac{1}{2} \frac{\alpha D}{a^2} \left(\frac{n}{q}\right)^2 \left(\frac{S}{b_2}\right)^2 \frac{(m\pi)^2}{2} \left\{ (m\pi)^2 + 15 + 8\nu + 4\left(\frac{q\pi}{2\alpha}\right)^2 \right.$$

$$\left. + 4\left[\left(\frac{q\pi}{2\alpha}\right)^2 - 1\right]^2 I_m \right\} W_{12}^2 \tag{54}$$

where $S = 2a\alpha$

$$I_m = \frac{2}{(m\pi)^2} \int_0^a \frac{1}{r} \sin^2\left(\frac{m\pi r}{a}\right) dr$$

The integral, I_m, can be evaluated in terms of an infinite series. Values of I_m for $m = 1, 2, 3, 4, 5$ are given in Table IV.

TABLE IV

VALUES OF THE INTEGRAL I_m

$m =$	1	2	3	4	5
$I_m =$	0.24699	0.07888	0.03958	0.02408	0.01632

The kinetic energy of a sector plate is given by the expression

$$T = \frac{1}{2} \gamma t_r \int_{-\alpha}^{\alpha} \int_0^a \dot{v}^2(r, \theta) \, r \, dr \, d\theta \tag{55}$$

Substituting for the mode shapes given in Equation 50b, the expression for the kinetic energy is

$$T = \frac{1}{2} \frac{\rho a b_2}{16} \left(\frac{n}{q}\right)^2 \left(\frac{S}{b_2}\right)^3 \left[1 - \frac{3}{(m\pi)^2}\right] \dot{W}_{12}^2 \tag{56}$$

The expressions for the kinetic energy and the potential energy of the flat rectangular cover sheets are obtained by substituting Equation 50a into Equations 11 and 12. For the normalized values of amplitude given in Equations 52, the expressions for the kinetic and potential energy are expressed in the form of Equation 39.

Assuming that the cover sheets and ribs are made of the same material and that the ribs all have the same thickness, the expressions for the modal stiffness and modal mass are

30

$$K_{mnq} = \frac{\pi^4 m^2 n^2}{4ab_2} {}_1D_s \left\{ \left(1 + \left(\frac{2t_s}{1t_s}\right)^3\right) \left[F_{mn}(b_2,a) + \left(\frac{b_2}{b_1}\right) F_{mn}(b_1,a) + \left(\frac{b_2}{b_3}\right) F_{mn}(b_3,a)\right] \right.$$

$$\left. + \left(\frac{t_r}{1t_s}\right)^3 \left(\frac{2\alpha}{q\pi}\right)^2 \left(\frac{S}{b_2}\right) \left[(m\pi)^2 + 15 + 8\nu + 4\left(\frac{q\pi}{2\alpha}\right)^2 + 4\left[\left(\frac{q\pi}{2\alpha}\right)^2 - 1\right]^2 I_m\right\} \qquad (57)$$

$$M_{mnq} = \frac{1}{4} \rho_1 ab_2 \left\{ \left(1 + \frac{2t_s}{1t_s}\right)\left[1 + \left(\frac{b_1}{b_2}\right) + \left(\frac{b_3}{b_2}\right)\right] + \frac{t_r}{1t_s} \left(\frac{n}{q}\right)^2 \left(\frac{S}{b_2}\right)^3 \left[1 - \frac{3}{(m\pi)^2}\right] \right\} \qquad (58)$$

where ${}_1D_s = E_1 t_s^3/12(1 - \nu^2)$

$\qquad S = 2\alpha a$

The frequency of the $(m,n,q)^{th}$ mode is given as

$$f_{mnq} = \frac{1}{2\pi} \sqrt{(K_{mnq}/M_{mnq})} \quad , \quad Hz.$$

Typical mode shapes for the rib modes $(1,1,1)$, $(2,1,1)$, and $(3,1,1)$ are illustrated in Figure 11.

F. Approximate Frequencies of Cylindrical Panels

1. Szechenyi's Approximate Formulae

Szechenyi, Reference 12, presents an approximation technique for estimating the natural frequencies of curved panels. Szechenyi's result has been checked against analytical and experimental data presented by Petyt, Reference 13, with good agreement. The following formulae are taken directly from Reference 12.

For either simply supported or clamped boundaries of the rectangular cylindrical shell illustrated in Figure 12, Szechenyi obtains the expression for the frequency of the $(m,n)^{th}$ mode as

$$f_{mn} = \frac{1}{2\pi} \sqrt{\frac{D}{M}} \left[(k_m^2 + k_n^2)^2 + \sigma_x \frac{tk_m^2}{D} + \sigma_y \frac{tk_n^2}{D} + \frac{12G}{t^2R^2}\right]^{1/2} \qquad (59)$$

where $D = Et^3/12(1 - \nu^2)$

$\qquad M = \gamma t$

$\qquad m =$ mode number in the longitudinal direction

$\qquad n =$ mode number in the circumferential direction

31
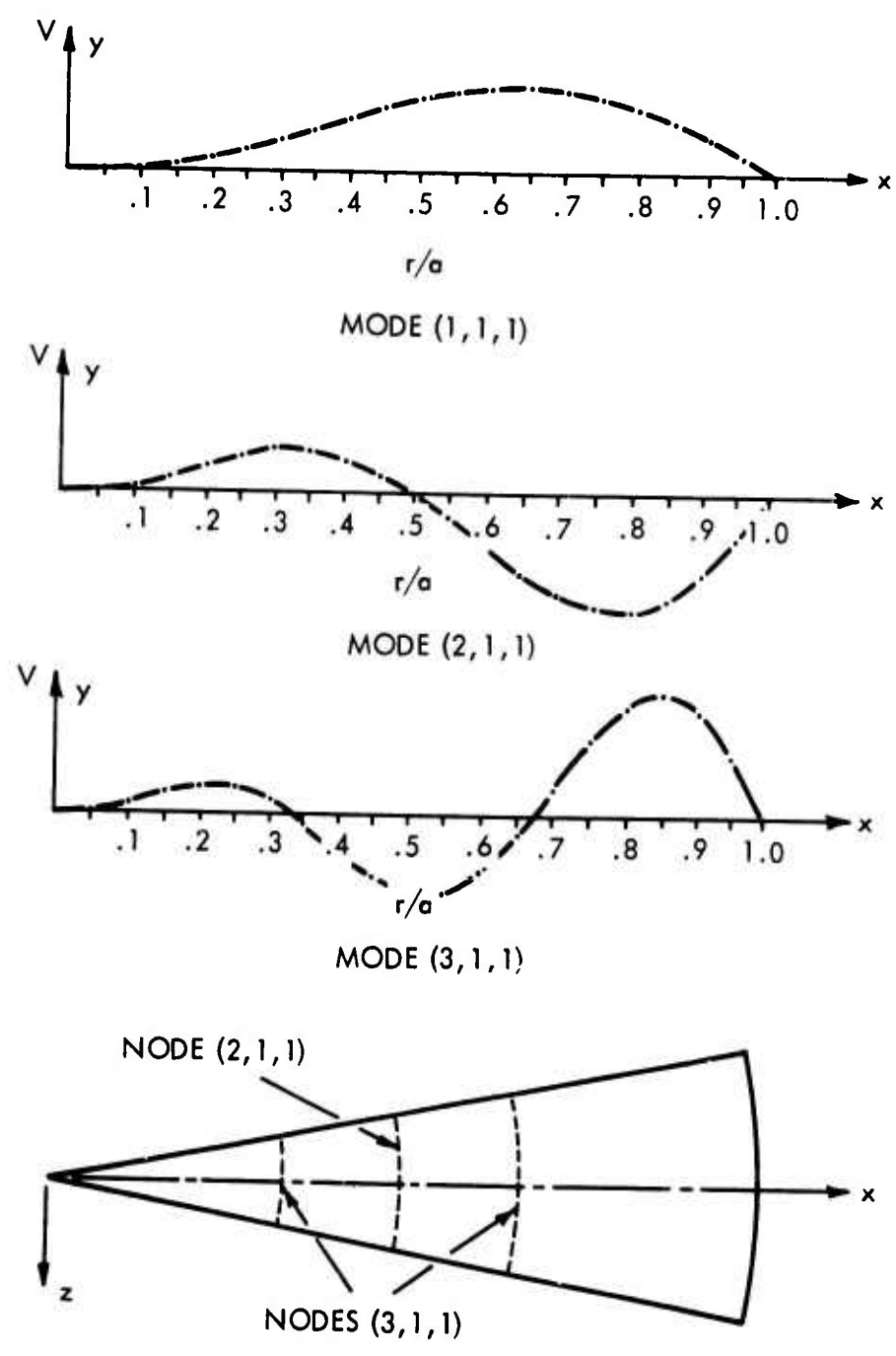
FIGURE 11   TYPICAL RIB MODE SHAPES FOR A WEDGE STRUCTURE
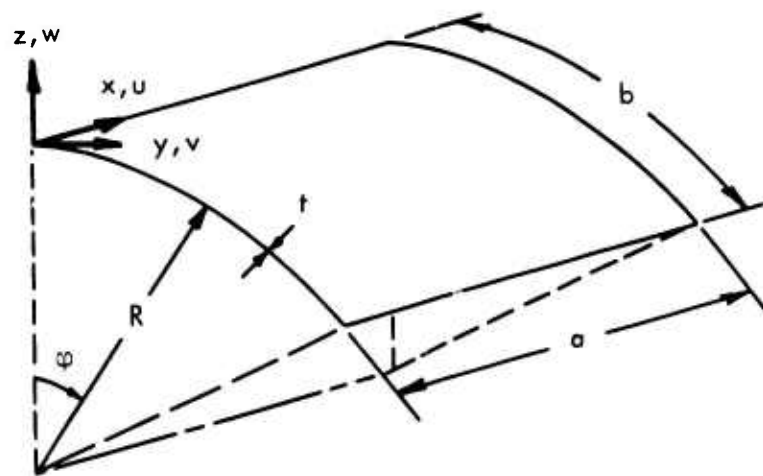
FIGURE 12   CYLINDRICALLY CURVED RECTANGULAR PANEL

σ_x = longitudinal panel edge stress

σ_y = 'hoop' stress

The terms k_m, k_n, and G depend upon the type of boundary conditions of the panel. For simply supported edges:

$$k_m = (m\pi/a)$$

$$k_n = (n\pi/b) \tag{60}$$

$$G = (1 - \nu^2)k_m^4/(k_m^2 + k_n^2)^2$$

For clamped edges:

$$k_m = m\pi/\zeta_m a$$

$$k_n = n\pi/\zeta_n b \tag{61a}$$

values of G are given in Figure 13 and values of ζ_m and ζ_n as a function of edge stress parameter are presented in Figure 14.

For zero edge stress,

$$\zeta_m \approx 1/(1 + .15/m)$$

$$\zeta_n \approx 1/(1 + .15/n) \tag{61b}$$

In terms of an internal pressure, p, the hoop stress is given by

$$\sigma_y = pR/t \tag{62}$$

2. Plumblee's Approximate Formulae

Plumblee, Reference 8, has developed expressions for the frequency ratio and bending stress ratio for a thin cylindrical panel compared to a flat panel. The boundary conditions are considered to be clamped. For the $(m,n)^{th}$ panel mode, the frequency ratio is given as

$$\frac{\omega_c}{\omega_\infty} = \left[1 + \frac{0.006\, b^3/tR}{A^4 + 0.61A^2 + 1} \right]^{1/2} \tag{63}$$

and the stress ratio for a point on the middle of the straight edge is given as

34
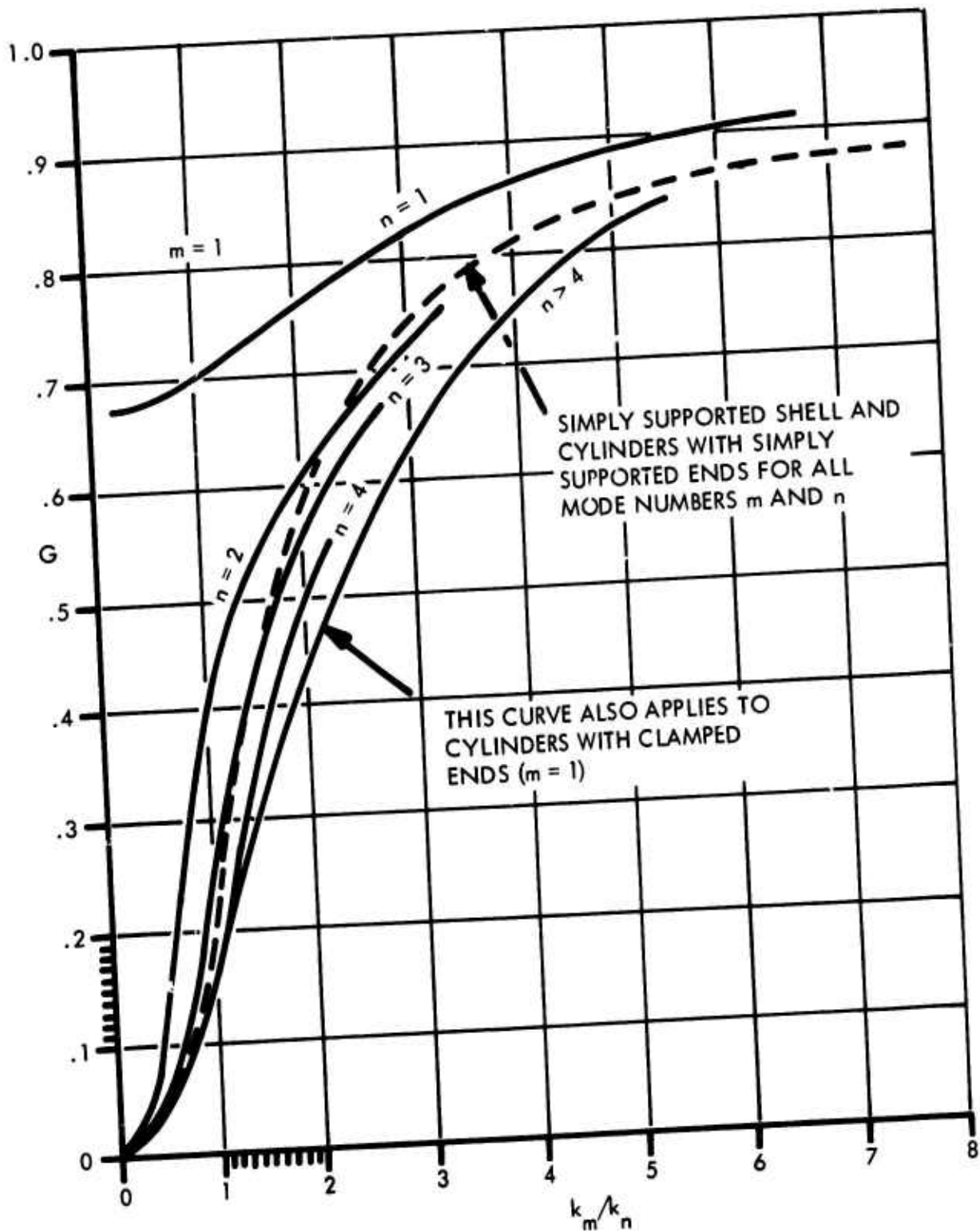
FIGURE 13   G FACTOR FOR m = 1

35
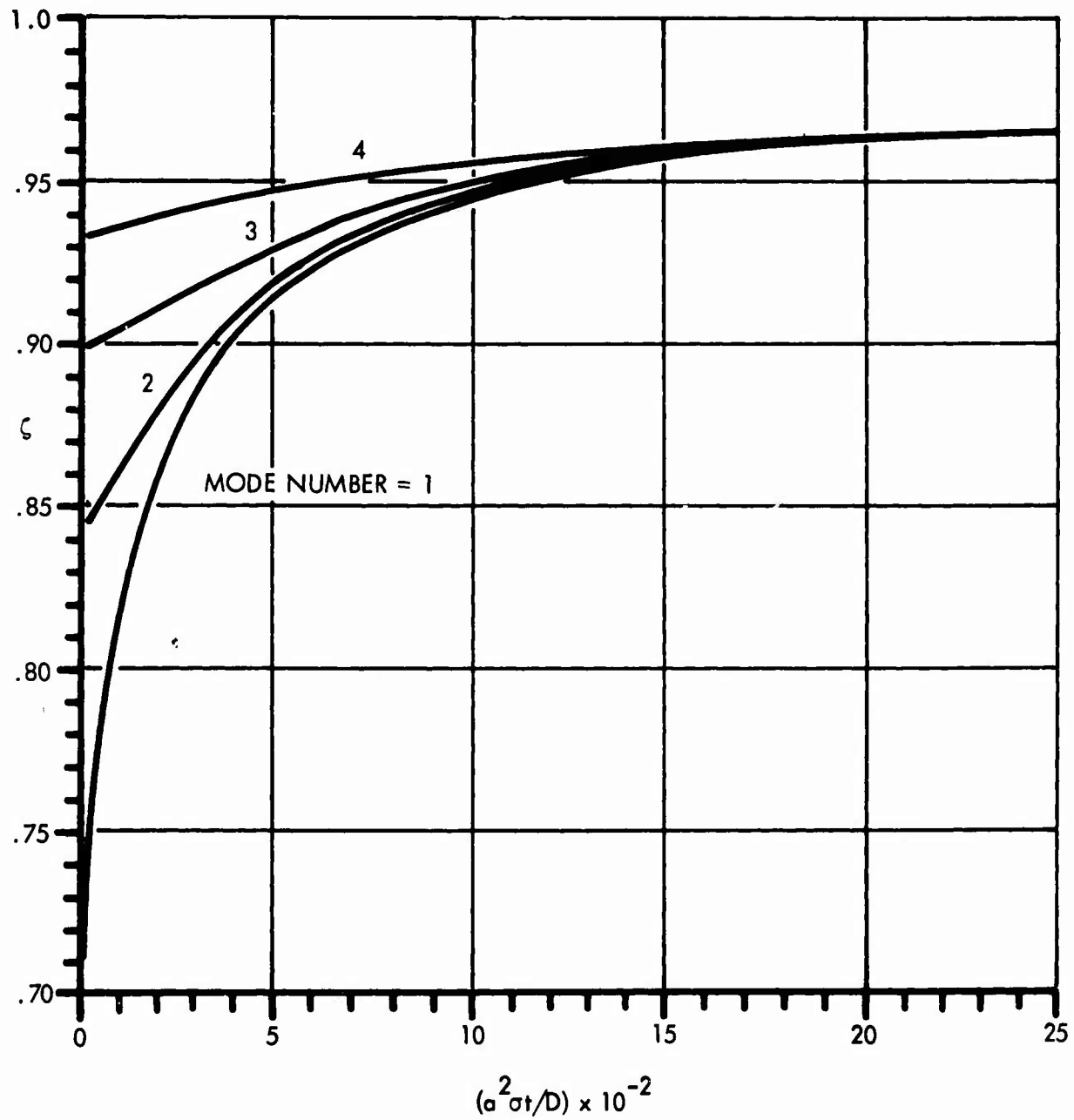
FIGURE 14   PLOT OF ζ VS. $a^2\sigma t/D$

$$\frac{\sigma_c}{\sigma_\infty} = \left[1 + \frac{0.006b^4/t^2R^2}{A^4 + 0.61A^2 + 1}\right]^{-3/4} \left[1 + 0.453\left(\frac{A^2 + 0.034}{A^4 + 9.62A^2 + 1}\right)\frac{b^2}{tR}\right] \qquad (64)$$

where A = b/a, the panel aspect ratio. The constants in the above equations have been determined empirically.

The Rayleigh-Ritz analysis used by Plumblee requires that restrictions must be placed upon the parameters appearing in Equations 63 and 64. These restrictions are $\varphi \leq 0.35$, $a/t \geq 100$, and $0.3 \leq A \leq 3.0$.

III - EXPERIMENTAL

A. Introduction

The objective of the experimental program was to establish more accurate methods for the design of acoustic fatigue resistant internal airframe structure. The analytical effort described in Section II was used as a guide for the specimen design and interpretation of the observed experimental results.

To accomplish the intent of the investigation, high-intensity, random-noise acoustic fatigue tests of 36 specimens were conducted. The specimen configurations consisted of 12 stiffened panel designs and 6 box specimen designs with 2 specimens of each design to check repeatability. The parameter range covered by the specimen designs was as follows:

(a) Stiffened panel specimens:

skin thickness	0.032 to 0.050 inch
rib thickness	0.025 to 0.040 inch
rib spacing	6.0 to 9.0 inches
aspect ratio	2.0 to 3.0
rib shape	zee, channel, and hat cross-section

(b) Box specimens:

skin thickness	0.040 to 0.063 inch
rib thickness	0.020 to 0.063 inch
rib spacing	7.0 to 10.0 inches
height	7.0 and 10.0 inches
panel aspect ratio	2.0 to 4.0

Due to the limited number of test specimens, the above parameter range was not completely covered. A description of the test specimens, test procedure, and test results is given in the following sections.

B. Test Specimen Design

The test specimen design was accomplished in two phases. For each phase, 6 stiffened panel and 3 box specimen designs were considered. The first group of specimens was designed using the applicable design nomographs of Reference 8. The second group was designed using the same nomograms and data from the first phase experimental program. Fastener edge distances and other design details were selected in accordance with accepted aircraft standards. Standard manufacturing techniques and processes were used in test

specimen fabrication. All ribs and stringers were formed from flat sheet material and heat treated as necessary. All heat treatment was checked against process standards. Quality control procedures were used at all times. The material of all parts for the test specimens described here was 7075-T6.

Each specimen was assembled using the test frame as a jig to insure a minimum of specimen prestress in the test configuration. The specimen fabrication sequence was such that the acoustic fatigue testing was continued without interruption.

1. Stiffened Panel Specimens

The configuration of the stiffened panel specimens is illustrated in Figure 15. The basic details of the structure are given in Table V. The stringer dash number given in Table V refers to the stringer detail dimensions given in Table VI. For all specimens, the stringers were parallel to the length of the specimen. The channel section rib details are also presented in Table VI. Figure 16 illustrates the overall specimen test configuration and the method used for mounting the specimens in the test fixture. Both the skin side and the rib-stringer side are illustrated. The specimen designation follows the numerical sequence established in Reference 8.

TABLE V

STIFFENED PANEL DESIGN DETAILS

Designation	Qty.	a	b	t_s	Rib	Stringer	Stringer shape
STR-31	2	6.0	12.0	0.040	-1*	-1*	zee
STR-32	2	6.0	18.0	0.040	-1	-1	zee
STR-33	2	6.0	12.0	0.040	-1	-2	channel
STR-34	2	6.0	18.0	0.040	-1	-2	channel
STR-35	2	6.0	12.0	0.040	-1	-3	hat
STR-36	2	6.0	18.0	0.040	-1	-3	hat
STR-37	2	9.0	18.0	0.040	-2	-4	zee
STR-38	2	9.0	18.0	0.040	-2	-5	channel
STR-39	2	6.0	18.0	0.050	-2	-4	zee
STR-40	2	9.0	18.0	0.032	-2	-1	zee
STR-41	2	6.0	12.0	0.032	-2	-6	zee
STR-42	2	6.0	12.0	0.032	-2	-7	channel

NOTE: All dimensions in inches.

*See Table VI.

39
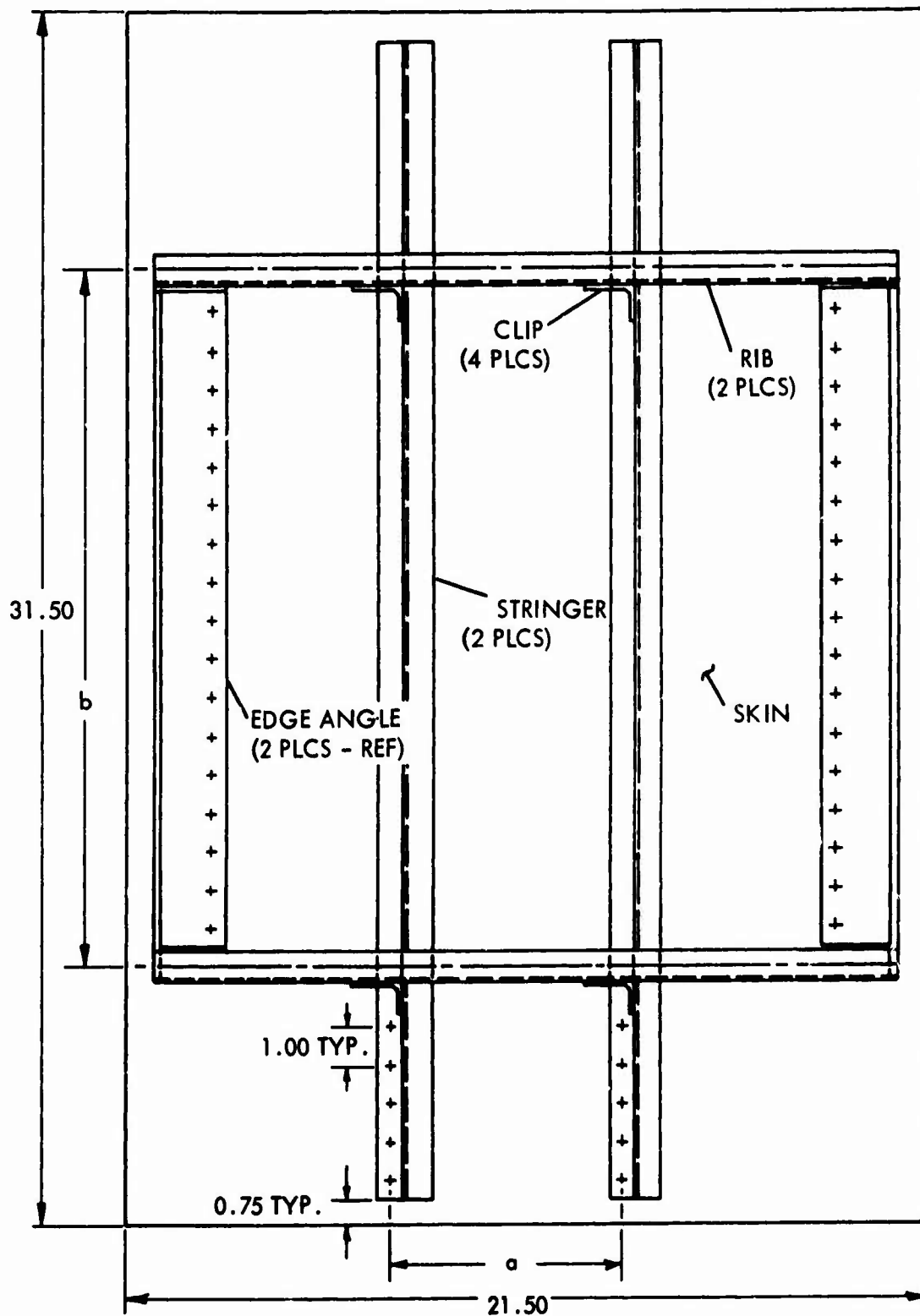
FIGURE 15 STIFFENED PANEL SPECIMEN CONFIGURATION
(EDGE FRAME OMITTED FOR CLARITY)

40
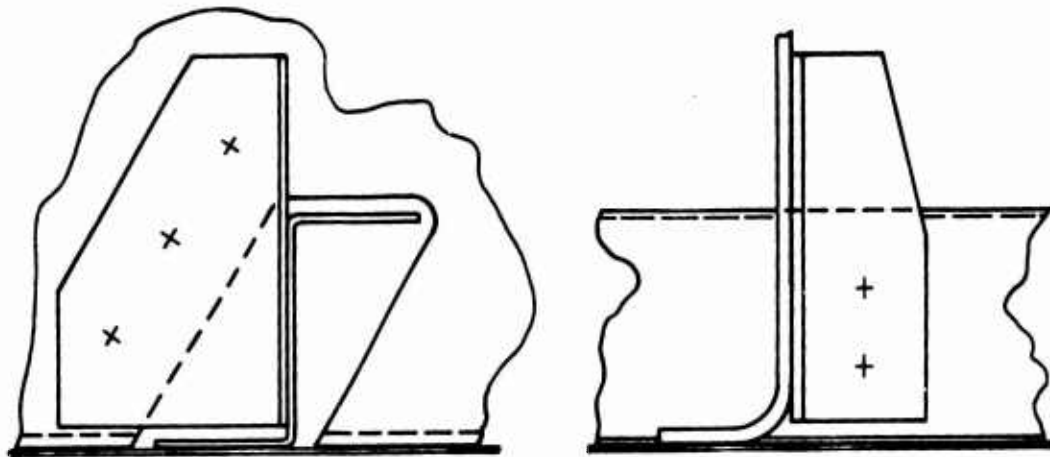
CLIP DETAIL: ZEE SECTION STRINGER
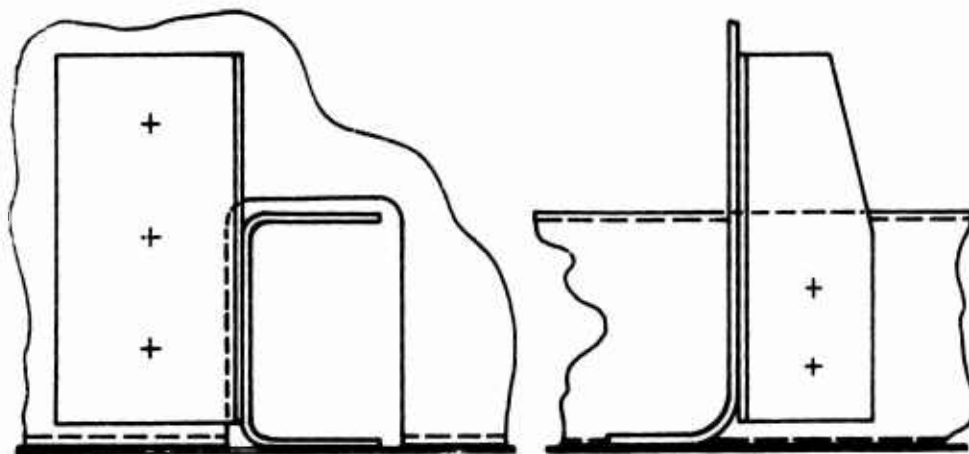
CLIP DETAIL: CHANNEL SECTION STRINGER
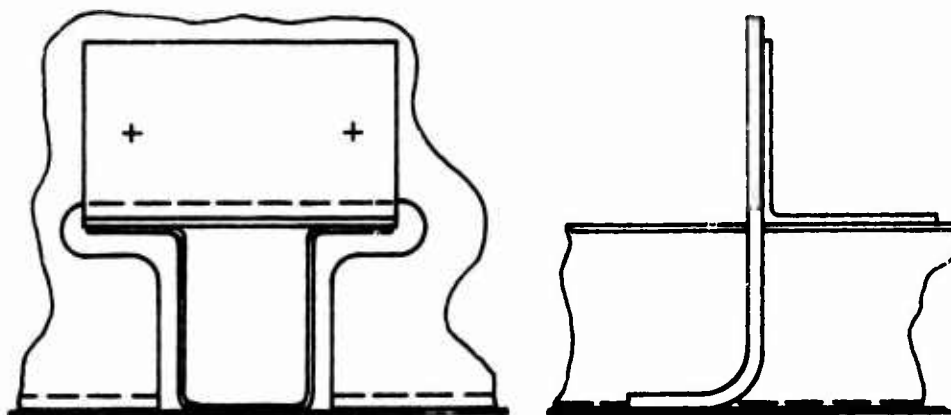
CLIP DETAIL: HAT SECTION STRINGER

FIGURE 15 STIFFENED PANEL SPECIMEN CONFIGURATION (CONCLUDED)

TABLE VI
STIFFENED PANEL STRINGER DESIGN DETAILS

Stringer	Shape	t_r	h	b_1	b_2	r
-1	zee	0.032	1.25	0.75	-	0.09
-2	channel	0.032	1.25	0.75	-	0.09
-3	hat	0.032	1.00	0.50	0.75	0.09
-4	zee	0.040	1.25	0.75	-	0.09
-5	channel	0.040	1.25	0.75	-	0.09
-6	zee	0.025	1.25	0.75	-	0.09
-7	channel	0.025	1.25	0.75	-	0.09

Rib	Shape	t_r	h	b_1	r
-1	channel	0.080	2.90	0.75	0.22
-2	channel	0.050	2.90	0.75	0.25

NOTE: All dimensions in inches
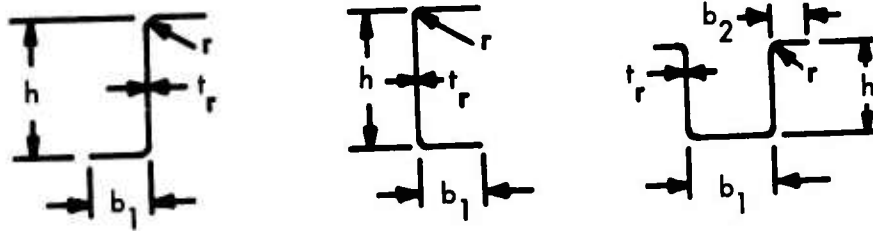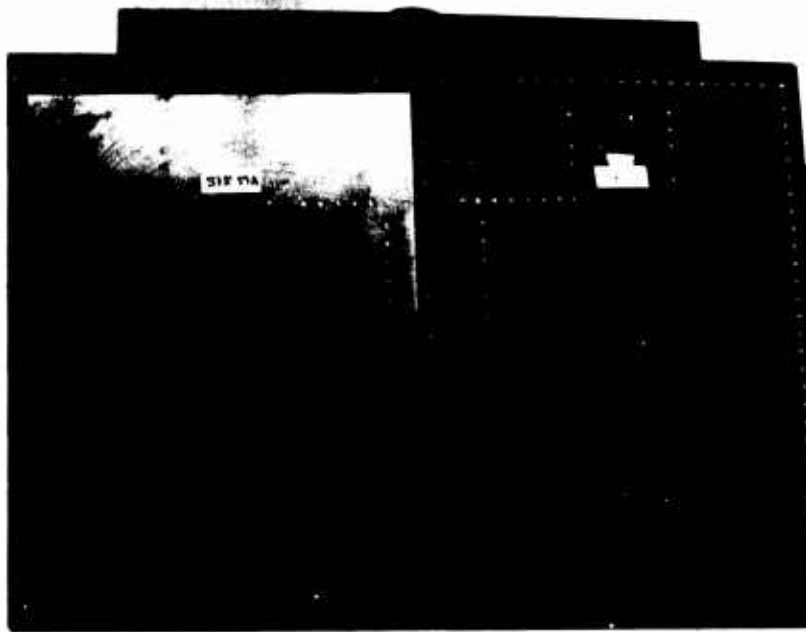
FIGURE 16 STIFFENED PANEL SPECIMEN MOUNTED IN TEST FIXTURE

2. Nine Cell Box Structure

The configuration of the box specimen structure is illustrated in Figure 17. The details of the structure are given in Table VII. For purpose of discussion, the internal structure shall be classified as either a frame or a rib. For all specimen designs, the frame was continuous across the width of the specimen. The ribs were divided into a center rib (test rib) and an end rib. The center rib and the end rib were attached to the frames with angle clips along the height of the specimen (dimension h). An angle clip was attached to the end of each frame and rib for attaching the specimen to the test fixture. The frames and the ribs were oriented so that the flanges faced the edge of the specimen. The test fixture, also used as an assembly jig, was designed to allow for variation of frame and rib spacing and specimen height. The cover sheets and ribs were firmly bolted to the test frame along all edges. This fixture design allowed visual inspection of all structure surfaces in the test configuration. Figure 18 illustrates the details of the test frame as viewed from the rear with test specimen BX6B installed.

C. General Test Procedure

The various tests were conducted using the following procedure:

1. Modal Frequency Studies

1.1 Stiffened Panel Specimens – The pair of stiffened panel specimens, mounted in the test frame as illustrated in Figure 16, were placed over an enclosure containing two electromechanical speakers as illustrated in Figure 19 with the stiffeners exposed for observation. Cork particles were sprinkled on the test specimen and a frequency sweep conducted. The Chladni patterns formed by the cork particles were observed and sketched. For the most predominant modes, accelerometer measurements were conducted to determine panel and stiffener motion.

1.2 Box Specimens – The modal frequency studies for the box specimens were conducted in a different manner than that described for the stiffened panel specimens. With the specimen mounted in the test frame as illustrated in Figure 18, two speaker enclosures were placed on either side of the specimen as illustrated in Figure 20. Accelerometers were placed on the center of each panel between the frames and the test rib. A frequency sweep was conducted and the accelerometer output recorded on an x-y plot. Three speaker phase conditions were used in this study. For purposes of discussion, the side of the structure to be exposed to random acoustic excitation will be called the front. The speaker excitation conditions used in the modal frequency studies were: one sided excitation speakers on the front side only; two sided excitation speakers on both sides, in phase and out-of-phase. Cork particles were sprinkled on the test ribs, and the Chladni patterns formed for each mode were sketched. Using accelerometers, the phase relations between the panel bays and the ribs were determined. The speaker excitation conditions ensured that all possible modes were excited. To determine the panel modes on the front surface of the structure, the specimen/test frame were placed with the front face up and a speaker enclosure placed at an angle to the specimen to allow visual observation of the specimen surface. Cork particles were sprinkled over the surface of the structure and Chladni
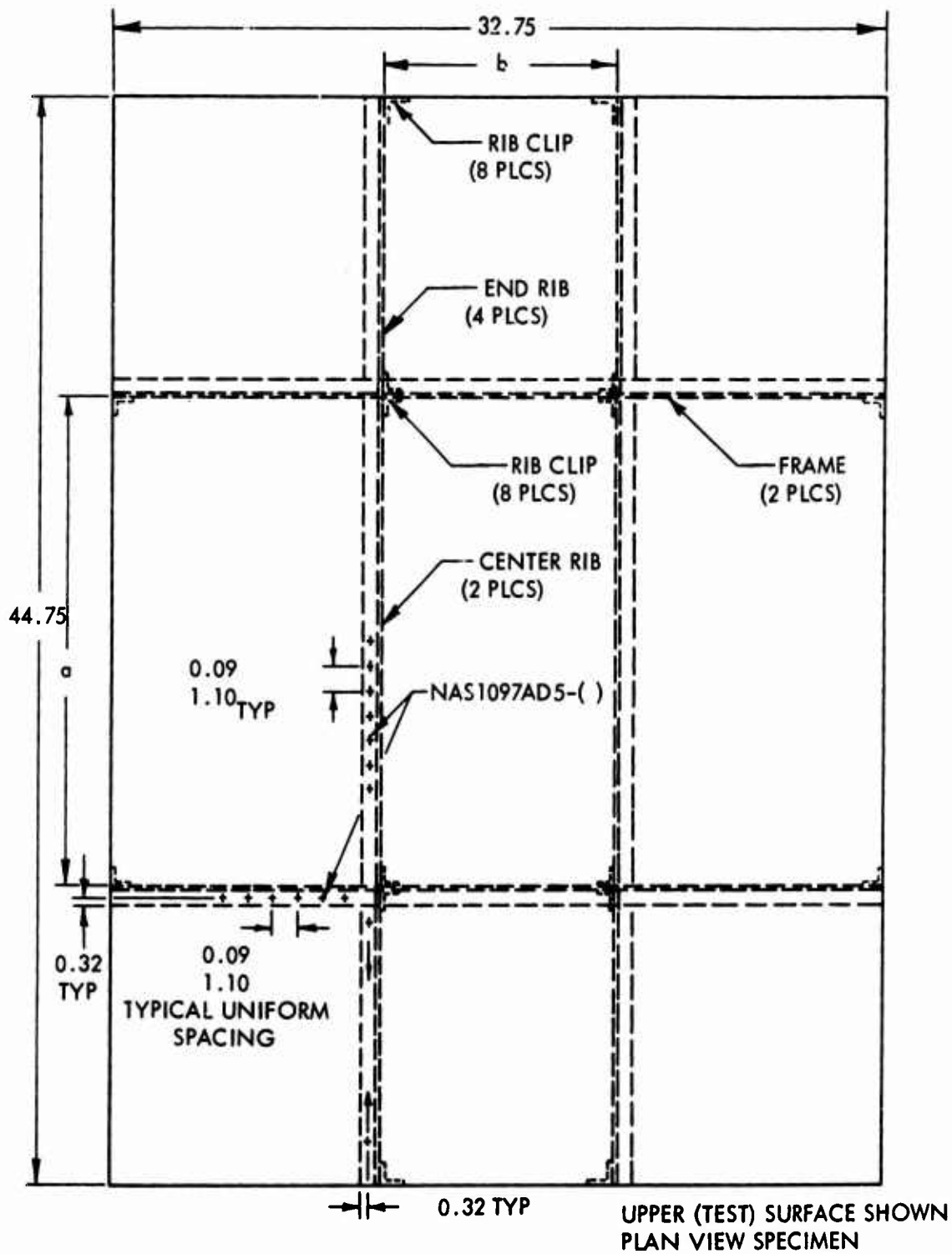
44

FIGURE 17 BOX SPECIMEN CONFIGURATION

45
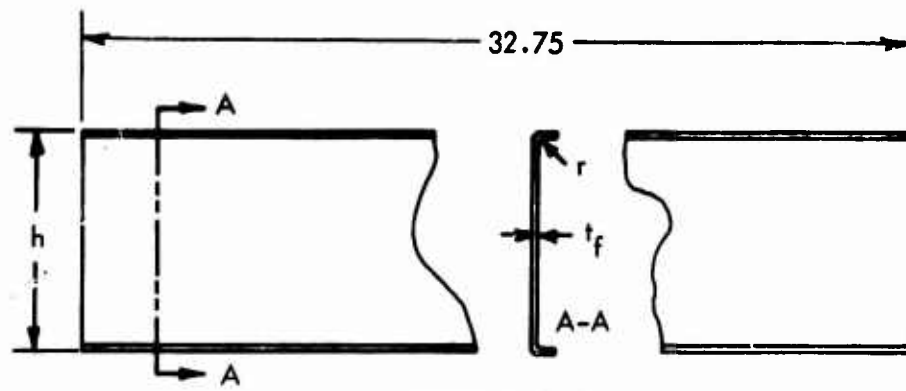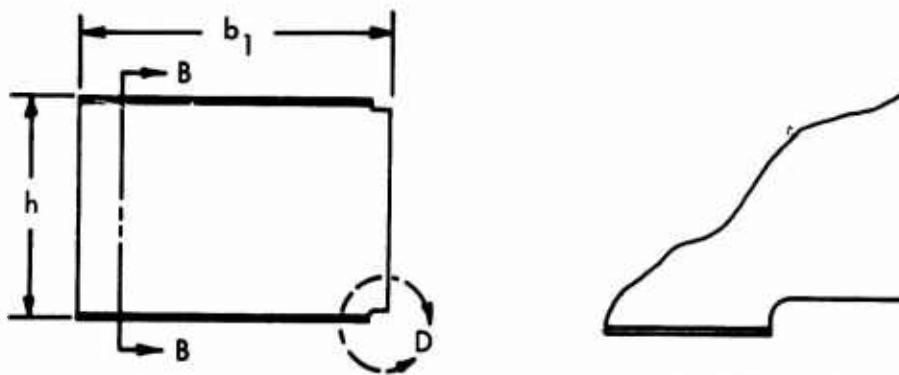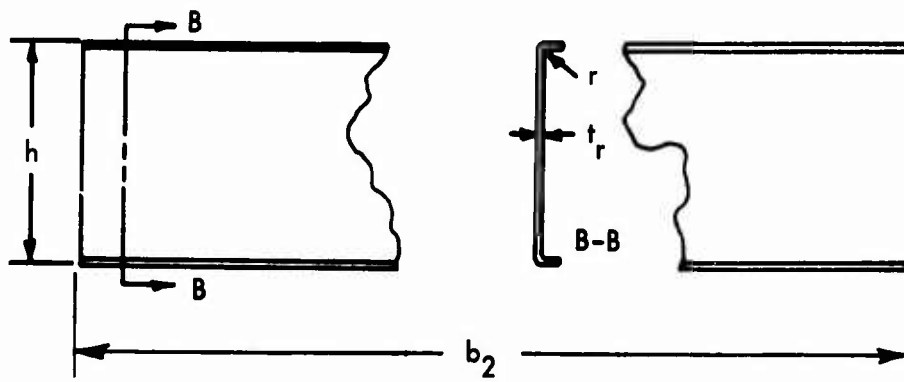
FIGURE 17 BOX SPECIMEN CONFIGURATION (CONCLUDED)

TABLE VII

BOX SPECIMEN DESIGN DETAILS

| Designation | Qty. | Cover Sheet | | | | Internal Structure | | | | |
| | | a | b | t_s | h | rib | | frame | | |
						t_r	r	t_f	r	
BX-1	2	10.0	20.0	0.063	10.0	0.063	0.16	0.080	0.22	
BX-2	2	8.0	24.0	0.050	10.0	0.063	0.16	0.080	0.22	
BX-3	2	7.0	28.0	0.040	10.0	0.050	0.12	0.080	0.22	
BX-4	2	10.0	20.0	0.063	10.0	0.032	0.16	0.040	0.22	
BX-5	2	8.0	24.0	0.040	10.0	0.020	0.12	0.040	0.22	
BX-6	2	8.0	24.0	0.040	7.0	0.020	0.12	0.040	0.22	

NOTE: All dimensions in inches.

FIGURE 18 BOX SPECIMEN MOUNTED IN TEST FiXTURE (REAR VIEW)
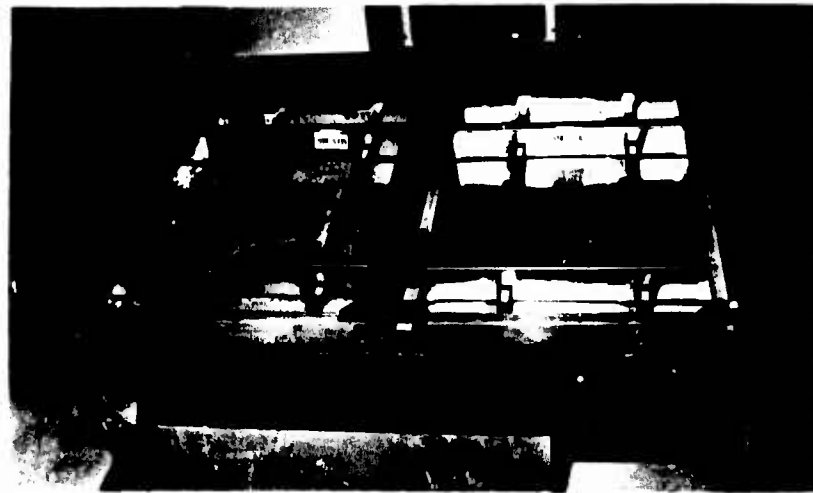
FIGURE 19 STIFFENED PANEL SPECIMEN MOUNTED FOP.
MODAL FREQUENCY STUDY

(a) SPECIMEN CONFIGURATION FOR TWO-SIDED EXCITATION
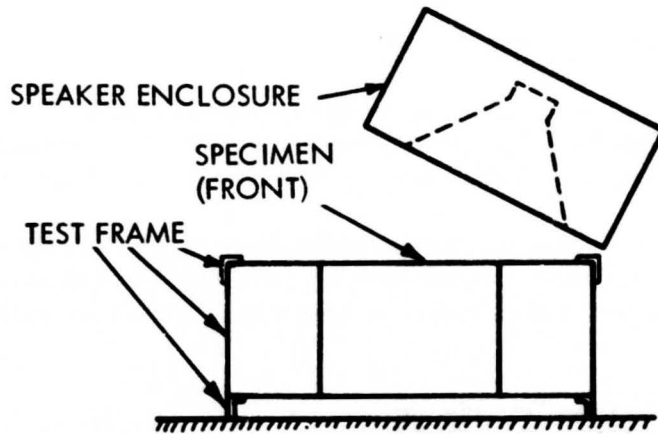
(b) SPECIMEN CONFIGURATION FOR OBSERVING FRONT
COVER SHEET MODES

FIGURE 20 BOX SPECIMEN MOUNTED FOR MODAL FREQUENCY STUDY

patterns for each predominant mode were sketched. With the response plots, phase information, and Chladni patterns, it was possible to define each responding mode.

2. Test Specimen Instrumentation

2.1 Stiffened Panel Specimens - After a thorough study of the test specimen response characteristics, strain gage locations were selected. Figure 21 shows typical uniaxial strain gage locations for the stiffened panel specimens.

2.2 Box Specimens - Uniaxial strain gage installation on the box specimens varied; however, typical installations for the front surface and ribs is indicated in Figure 22. For the speaker excitation conditions described in Section 1.2, frequency sweeps for selected strain gages were conducted with the strain gage response recorded on an x-y plot.

3. Damping Studies

Frequency sweeps using the electromechanical speakers previously described were conducted with the strain gage response displayed on an oscilloscope. At frequencies with predominant strain gage response, the excitation was suddenly chopped, and the decaying strain signal on the oscilloscope photographed. The decaying strain signals so obtained were used to determine the logarithmic decrement, δ, or the damping ratio, ζ, Reference 14. For the box specimens, only excitation on the front side was used for the damping studies.

4. High Intensity Sinusoidal Frequency Sweeps

The test specimens, instrumented as described in Section 2, were placed on the progressive wave test section of the high intensity acoustic fatigue facility at the Aerospace Sciences Research Laboratory. Typical installation details are described in Reference 8.

Grazing incidence sinusoidal frequency sweeps in the range of 50-1000 Hz were conducted at the selected specimen test level. Strains for all gages were recorded on x-y plots. The strain response was studied and used to shape the broad-band acoustical excitation for the fatigue tests.

5. Broad-Band Acoustical Noise Test Spectra

The test specimen/frame assembly was removed from the progressive wave test section and replaced by a one-inch thick plywood panel. The test sound pressure spectrum was then shaped out of the presence of the vibrating test specimen. The width of the excitation spectrum was at least three times the width of the strain response of the panel obtained during the high intensity sinusoidal sweeps. Spectrum shaping was required to concentrate the acoustical energy in the desired frequency range. The plywood panel was removed when the desired spectrum had been obtained.

6. Acoustic Fatigue Tests

The test specimen/frame assembly was re-installed in the progressive wave test section ready for fatigue testing to take place. Test specimen inspection was made in the following
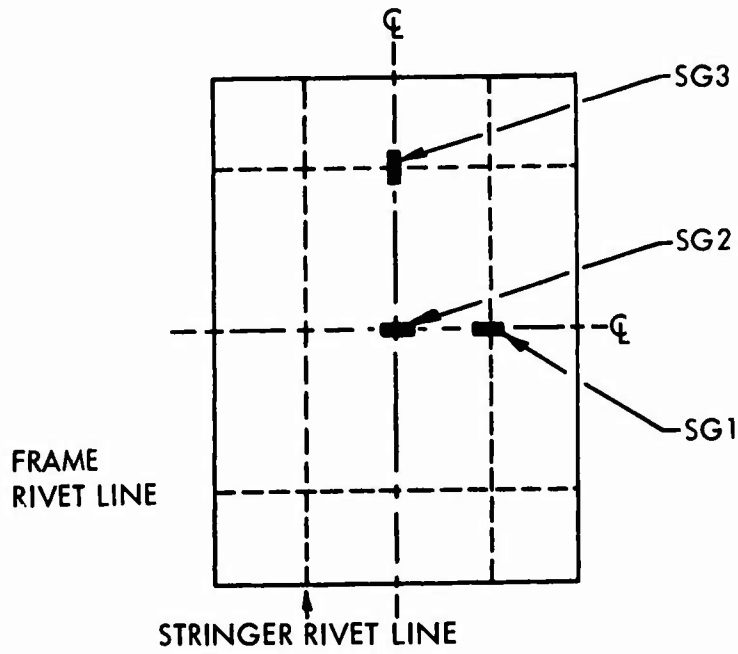
(a) STRAIN GAGE LOCATIONS FOR SKIN
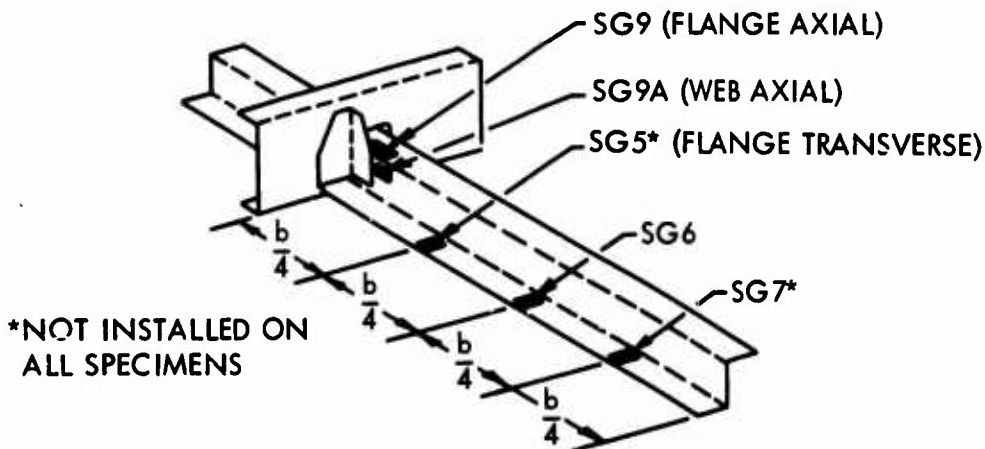
(b) STRAIN GAGE LOCATIONS FOR STRINGER

FIGURE 21 TYPICAL STRAIN GAGE LOCATIONS FOR
STIFFENED PANEL SPECIMEN

51
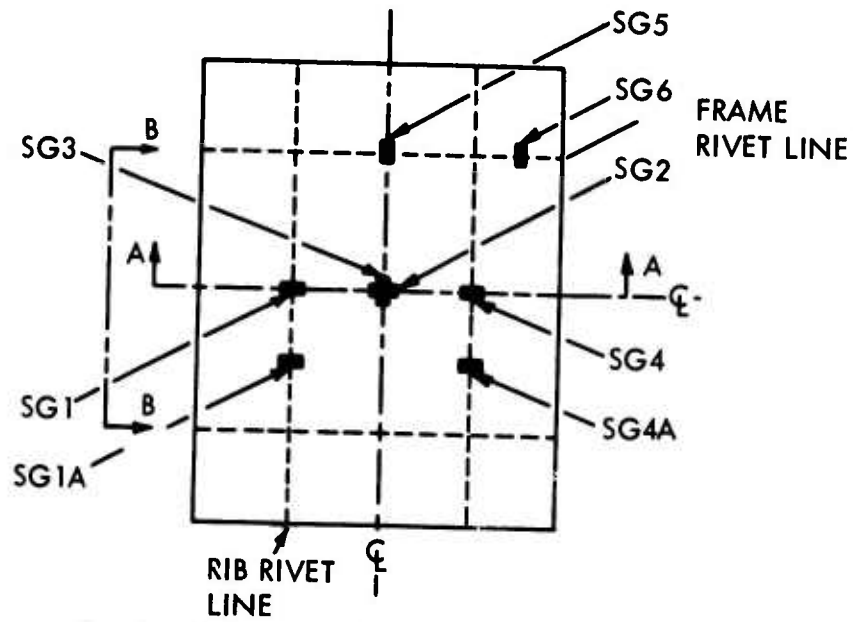
(a) STRAIN GAGE LOCATIONS FOR SKIN
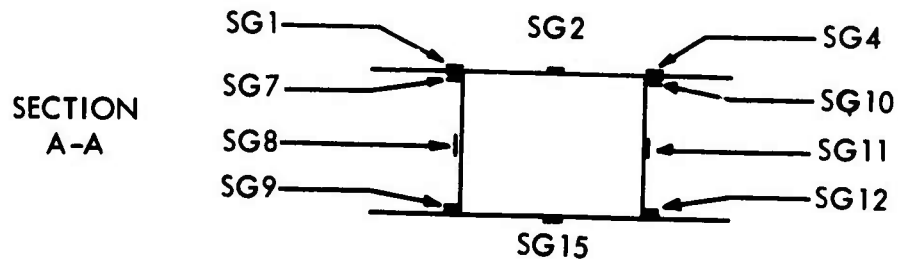
(b) STRAIN GAGE LOCATIONS FOR TEST RIB

FIGURE 22 TYPICAL STRAIN GAGE LOCATIONS FOR BOX SPECIMENS

sequence: every five minutes for the first hour; every fifteen minutes for the next two hours; every half hour for the next seven hours; and every hour until test termination.

When a fatigue failure was first observed, the time, location, and a brief description was recorded in a laboratory record book. The time of failure and crack length were marked on the specimen. Cracks were allowed to propagate until complete modes of failure had been observed. A complete description of the data recording and analysis systems used for mode studies and fatigue tests are presented in Appendix II.

D. Test Results

Results of the stiffened panel and box specimen experiments are presented in the following sections.

1. Stiffened Panel Test Results

Each stiffened panel design consisted of two specimens. Following the notation used by Ballentine, the specimen nomenclature is given by the panel design with the suffix A and B to denote the two specimens. For all fatigue tests, the stiffened panel specimens A and B were tested simultaneously.

1.1 Modal Frequency Studies - As discussed in Reference 5, the types of modes to be expected for nine bay panels would consist of various phase relations between adjacent bays for each mode number (m,n) of a panel. The Chladni patterns observed during the mode studies described in Section C.1.1 are presented in Appendix III. The similarity of the predominant modes for each panel design is apparent. The predominant mode for stiffener response was a fundamental mode for each panel bay between ribs with adjacent bays across the stringers out of phase. The predominant mode for skin response was adjacent bays across ribs out of phase (reversed bending). Since the ribs were much stiffer than the stringers, the strain response on the skin was generally maximum at the center of the short side of the center bay. This was to be expected due to the torsionally flexible stringers used in these experiments. A summary of the modal frequencies is given in Table VIII.

1.2 Damping Ratios - The decaying strain signals as described in Section III.C.3 were used to obtain average values for the damping ratio. An arithmetic average of the damping ratio for each design was obtained. Table IX is a listing of these average damping ratios as determined by the logarithmic decrement method. There were no significant differences between damping for the skin or the internal structure. Figure 23 presents a plot of damping ratio versus frequency for all responding strain gages and all specimens.

1.3 High Intensity Frequency Sweeps - Figures 24 and 25 are plots of strain response to high intensity sinusoidal excitation at the indicated sound pressure level. The frequency sweep plots are typical for the strain responses for all stiffened panel specimens at skin and stringer locations.

53

TABLE VIII

MODAL FREQUENCIES FOR STIFFENED PANELS*

(Low Intensity Sinusoidal Excitation)

Specimen	Frequency, Hz	Stringer Motion
STR-31A	160	Torsion
STR-31A	209,264	Bending-torsion
STR-31B	165	Torsion
STR-31B	213,262	Bending-torsion
STR-32A	166	Torsion
STR-32B	168	Torsion
STR-33A	194	Torsion
STR-33B	186	Torsion
STR-34A	159	Torsion
STR-34A	183	Bending-torsion
STR-34B	158	Torsion
STR-34B	170	Bending-torsion
STR-35A	205	Torsion
STR-35B	195	Torsion
STR-36A	166	Torsion
STR-36A	212	Bending-torsion
STR-36B	180	Torsion
STR-36B	217	Bending-torsion
STR-37A	75	Torsion
STR-37B	87	Torsion
STR-38A	96	Torsion
STR-38B	81	Torsion
STR-39A	177	Torsion
STR-39B	169	Torsion
STR-40A	52,92	Torsion
STR-40B	71	Torsion
STR-41A	123,164	Torsion
STR-41B	128,185	Torsion
STR-42A	180	Torsion
STR-42B	199	Torsion

*Only predominant frequencies are listed here, see Appendix III for Chladni patterns.

TABLE IX

AVERAGE DAMPING RATIOS FOR STIFFENED PANELS

Specimen	Average Damping Ratio, %
STR-31A	2.3
STR-31B	1.8
STR-32A	2.8
STR-32B	2.8
STR-33A	2.1
STR-33B	2.0
STR-34A	1.9
STR-34B	1.3
STR-35A	2.1
STR-35B	2.5
STR-36A	1.4
STR-36B	1.8
STR-37A	1.4
STR-37B	1.5
STR-38A	1.1
STR-38B	2.1
STR-39A	1.0
STR-39B	1.3
STR-40A	1.9
STR-40B	1.5
STR-41A	1.8
STR-41B	1.0
STR-42A	1.5
STR-42B	1.0

+ BOX SPECIMENS

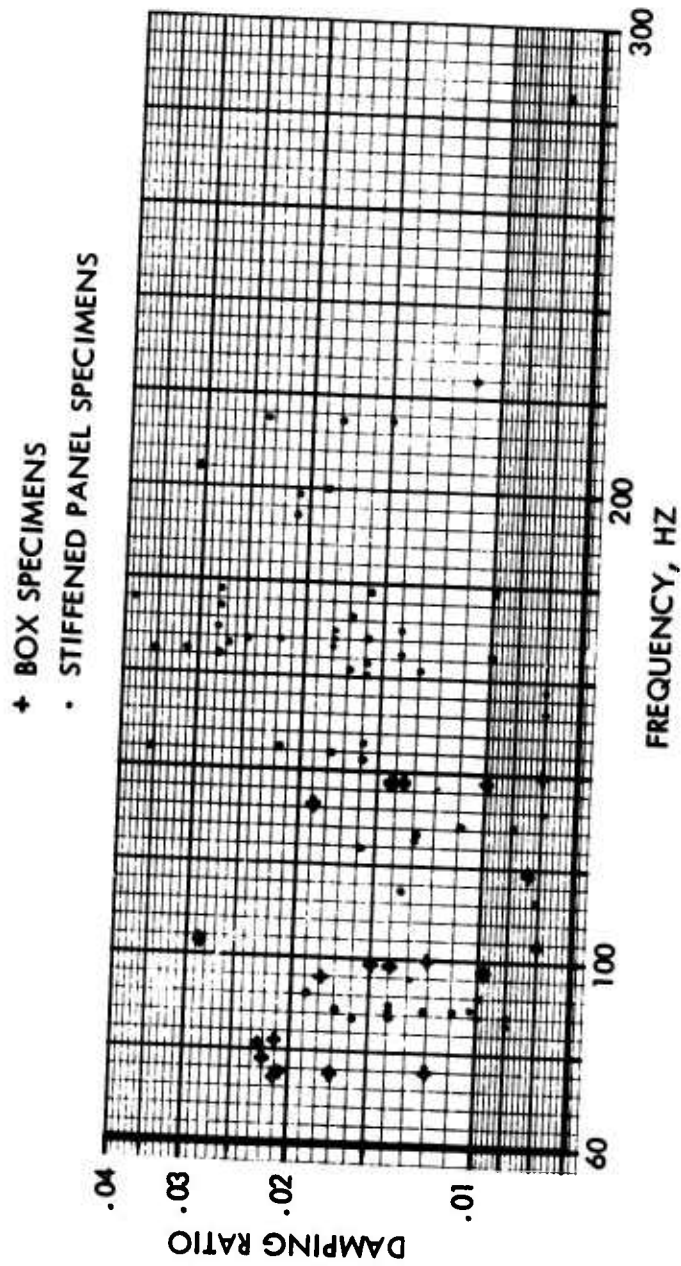• STIFFENED PANEL SPECIMENS

FIGURE 23 DAMPING RATIO VERSUS FREQUENCY

56
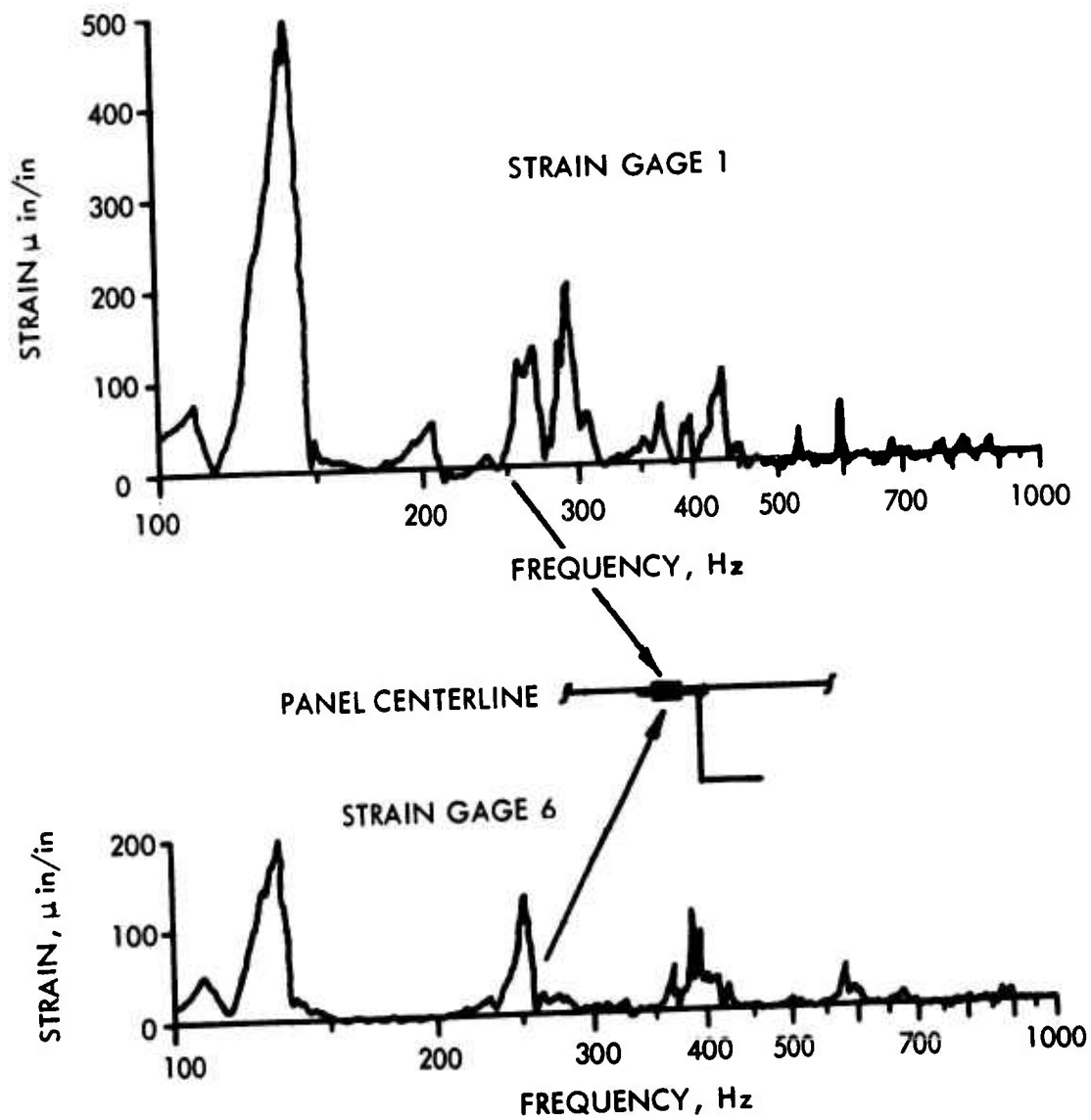
FIGURE 24   HIGH INTENSITY SINE SWEEP: STR 37A SKIN AND
STRINGER RESPONSE
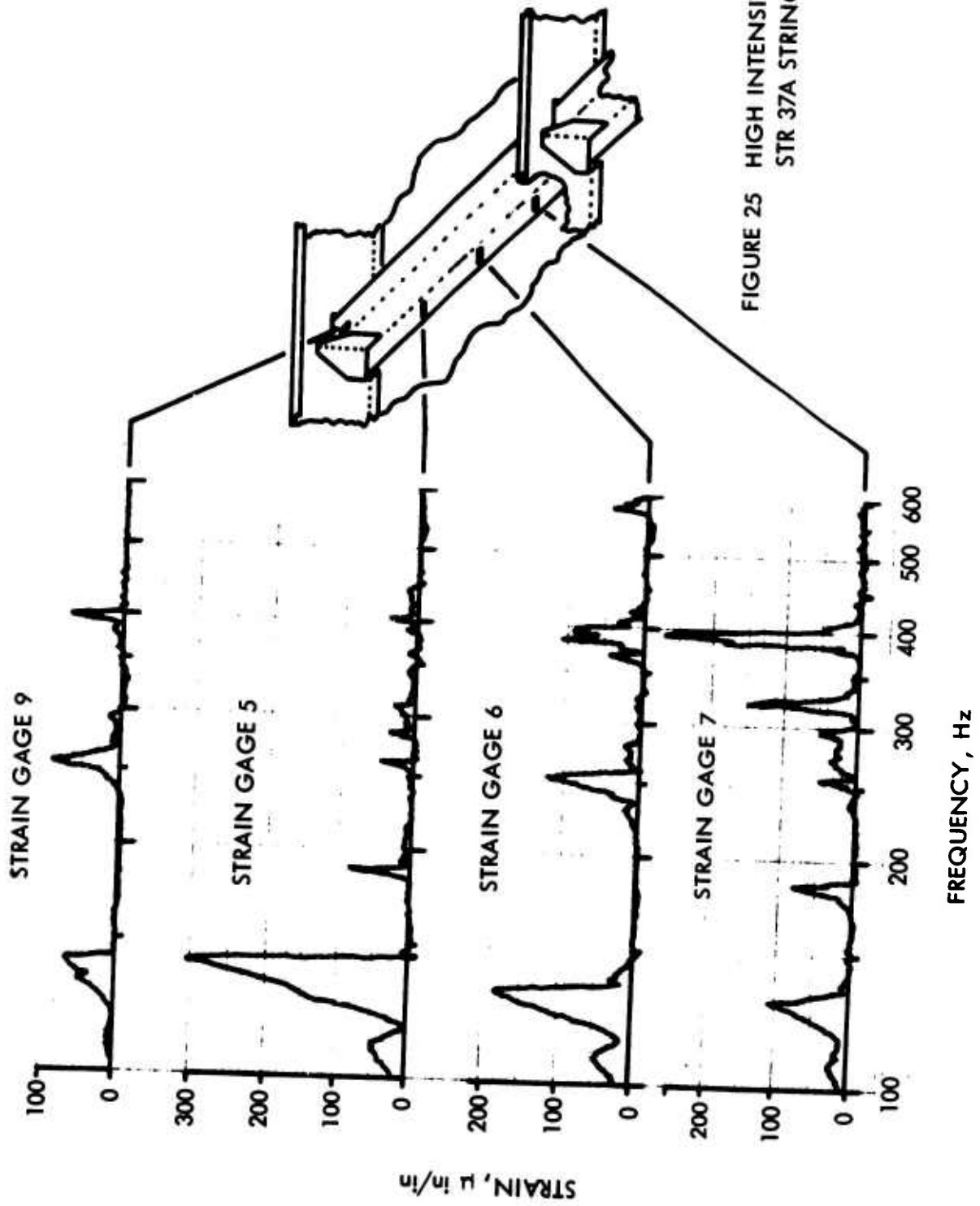
FIGURE 25   HIGH INTENSITY SINE SWEEP:
STR 37A STRINGER RESPONSE

58

1.4 Broad-Band Acoustical Noise Test Spectra – The acoustical noise test spectra were shaped such that the bandwidth of the excitation was at least three times the bandwidth of the test specimen sinusoidal response. If more than one mode was deemed significant, the test spectrum was shaped so as to include all responding modes. Figures 26 and 27 are typical broadband test spectra for the stiffened panel designs. All narrow band analyses for the broadband acoustical noise were accomplished using a 10Hz bandwidth filter. The test spectrum level was determined using the simple relation Spectrum Level = Sound Pressure Level - 10 log(Δf), dB, where Δf is the filter bandwidth. For Δf = 10, Spectrum Level = Sound Pressure Level - 10 dB. The test spectrum level is indicated in each figure.

1.5 Fatigue Tests – Twenty-four stiffened panel specimens, twelve designs with two replicates each, were exposed to broadband random acoustical excitation until one or more cracks developed in the skin or stringer. Table X is a summary of the test results.

Magnetic tape recordings were made of the signals from the strain gages positioned on the skin and the stringers. These strain data were analyzed using a narrow band filter (nominal 10 Hz) to determine the characteristics of the strain response to the acoustical excitation. Figures 28 through 35 are the narrow band analyses of typical single mode and multi-mode response.

In addition to the narrow band analysis, the recorded strain data was analyzed to determine the probability density of instantaneous strain. Figures 36 through 43 are typical results of these statistical analyses. For reference, a Gaussian distribution is plotted in each figure.

Figure 44 shows the relationship between overall nominal rms stress and the number of cycles to failure for the failure data. The number of cycles to failure was established from the number of zero crossings with negative slope (obtained as described in Appendix II) for each recorded strain signal and the time failure was observed. The regression line and 95% confidence limits given in Figure 44 were computed as described in Appendix II, Reference 8. The highest correlation coefficient for these data was obtained using failure data for strain gages located on the stiffener flange at the attach clip to the frame with the strain gage axis aligned with the stringer length. The regression line and confidence limits illustrated in Figure 44 are established for these data points only although all failure data is plotted.

2. Box Specimen Test Results

Due to the physical size of the box structure, these specimens were fatigue tested individually. The specimen nomenclature is given by the specimen design with the suffix A and B to denote the duplicate specimens.

2.1 Modal Frequency Studies – Mode shapes for each box specimen structure were determined as described in Section III.C.1. The experimentally observed modal frequencies are given in Table XI for each specimen. The notation for a specific mode is given by the mode numbers (m,n,q) as described in Section II. Figures 45 through 53 illustrate the
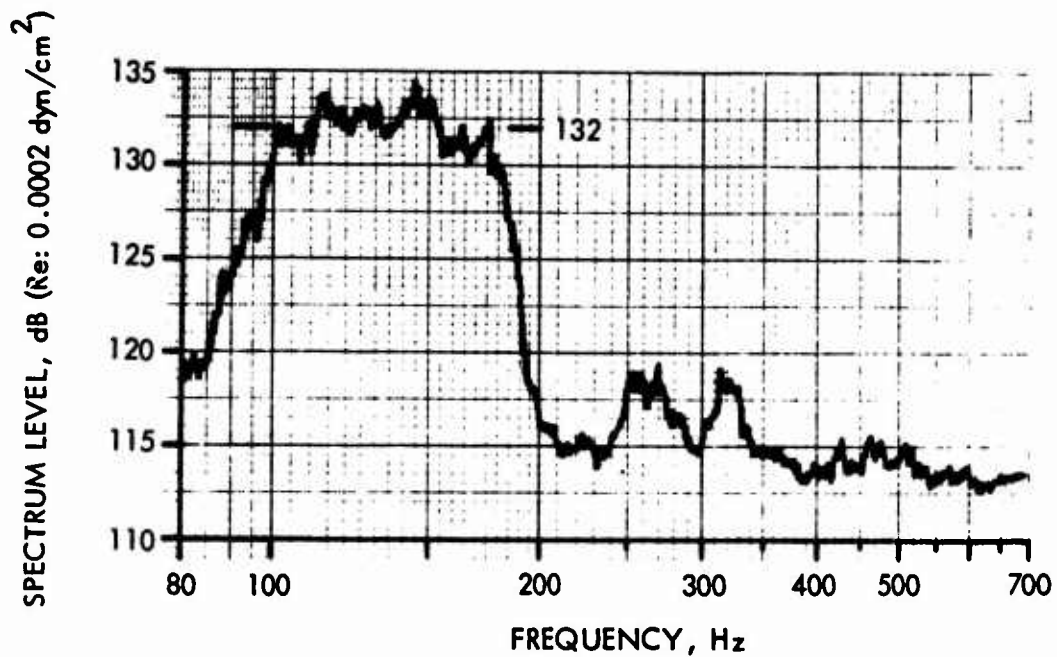
FIGURE 26   BROAD BAND TEST SPECTRUM: STR 37 A & B
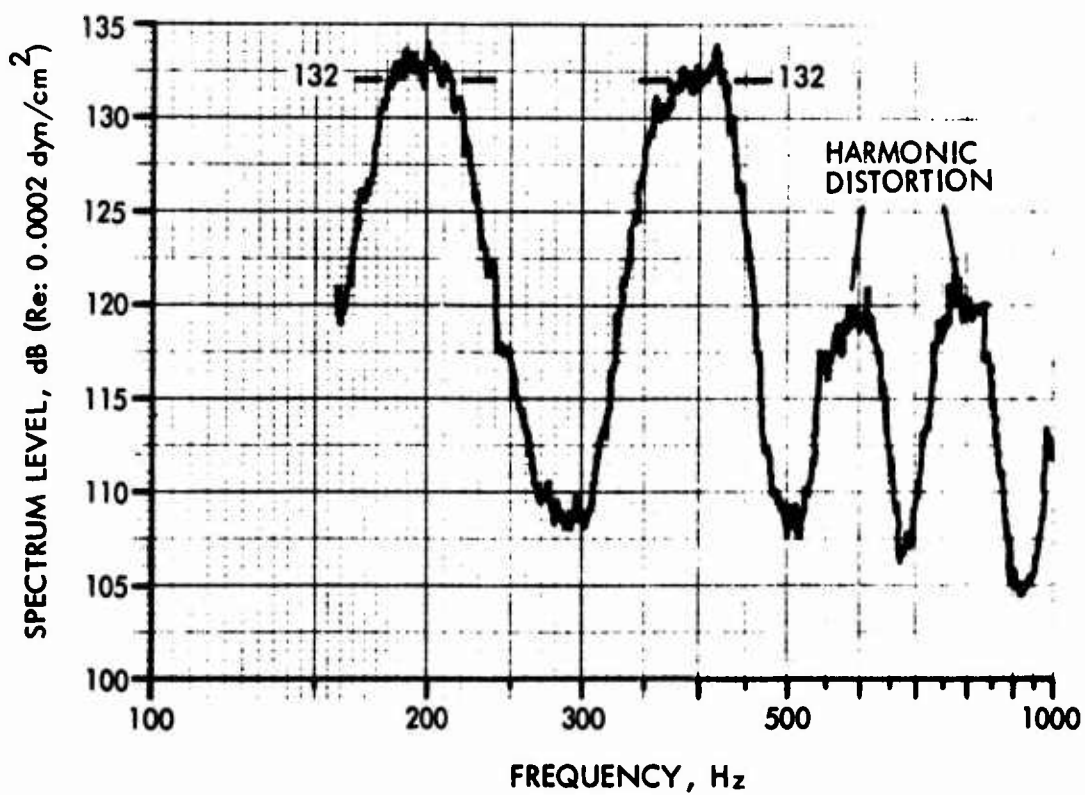
FIGURE 27   BROAD BAND TEST SPECTRUM: STR 39A & B
(MULTIMODE RESPONSE)

60

TABLE X

SUMMARY OF STIFFENED PANEL FATIGUE TESTS

Specimen	Test Spectrum Level, dB	Response Frequency Hz	$N_c \times 10^{-6}$	$\bar{\sigma}$ ksi	Remarks
STR-31A	124	160	2.2	5.2 (FT)*	
B	124	170	-	-	No failure at gage
STR-32A	124	180	5.5	2.0 (FT)	
A	124	180	6.8	3.2 (FT)	
A	124	180	5.2	4.2 (FA)	
A	124	180	5.1	2.0 (WA)	
B	124	170	-	-	No failure at gage
STR-33A	124	160,350	8.1	2.2 (FA)	
B	124	140,330	6.8	2.3 (FA)	
B	124	140,330	7.8	5.6 (FT)	
STR-34A	124	160,350	5.2	3.4 (WA)	
A	124	140,330	8.9	6.8 (FT)	
B	124		-	-	No failure at gage
STR-35A	124	240	-	-	No failure at gage
B	124	220	16.1	1.4 (FA)	
B	124	220	16.7	0.8 (FA)	
STR-36A	124	160	-	-	No failure at gage
B	124	185	8.3	2.8 (FA)	
B	124	185	7.0	3.6 (FA)	
STR-37A	132	145	4.2	1.6 (WA)	
B	132	140	1.4	1.2 (WA)	
B	132	140	2.2	2.3 (WA)	
STR-38A	128	175	2.2	5.2 (WA)	
A	128	175	0.7	3.5 (FA)	
A	128	175	1.03	4.9 (FA)	
B	128	140	2.5	4.2 (FA)	

TABLE X (Continued)

Specimen	Test Spectrum Level, dB	Response Frequency Hz	$N_c \times 10^{-6}$	$\bar{\sigma}$ ksi	Remarks
STR-39A	132	200,370	1.4	4.4 (WA)	
A	132	200,370	0.7	4.5 (WA)	
B	132	200,400	1.0	4.2 (WA)	
B	132	200,400	1.8	3.7 (WA)	
STR-40A	132	140,300	1.22	16.0 Skin @ Frame	
A	132	140,300	0.44	8.7 (FA)	
A	132	140,300	0.37	6.7 (FA)	
A	132	140,300	0.41	12.9 (FA)	
A	132	140,300	0.43	8.8 (FA)	
B	132	140,300	1.5	3.6 (FA)	
B	132	140,300	0.36	4.3 (FA)	
B	132	140,300	1.6	4.3 (FA)	
B	132	140,300	0.40	4.6 (FA)	
STR-41A	124	220	6.6	2.1 (FA)	
A	124	220	10.9	2.6 (FA)	
B	124	220	9.7	2.3 (FA)	
STR-42A	124	200-230	-	2.1 (FA)	No failure at gage
A	124	200-230	-	2.6 (FA)	No failure at gage
A	124	200-230	-	3.4 (FA)	No failure at gage
A	124	200-230	-	2.4 (FA)	No failure at gage
B	124	200-230	0.89	3.2 (FA)	
B	124	200-230	-	3.8 (FA)	No failure at gage
B	124	200-230	-	2.5 (FA)	No failure at gage
B	124	200-230	-	2.1 (FA)	No failure at gage

*(FT) – Flange transverse gage at stiffener center
 (FA) – Flange axial goge at clip
 (WA) – Web axial gage at clip

62
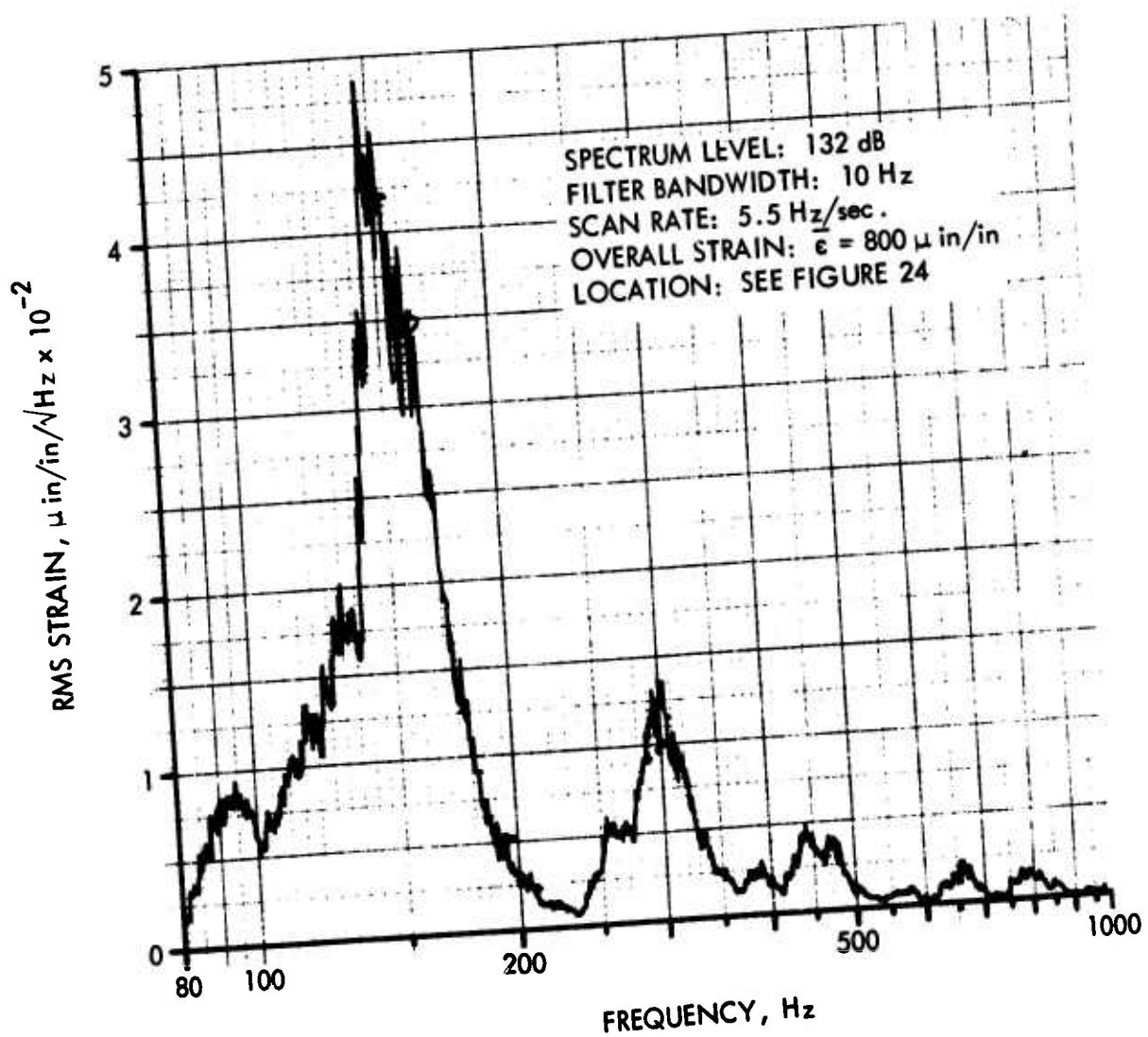
FIGURE 28   NARROW BAND ANALYSIS: STRAIN GAGE 1, STR-37A

SPECTRUM LEVEL: 132 dB
FILTER BANDWIDTH: 10 Hz
SCAN RATE: 5.5 Hz/sec
OVERALL STRAIN: $\bar{\epsilon}$ = 280 μ in/in
LOCATION: SEE FIGURE 25
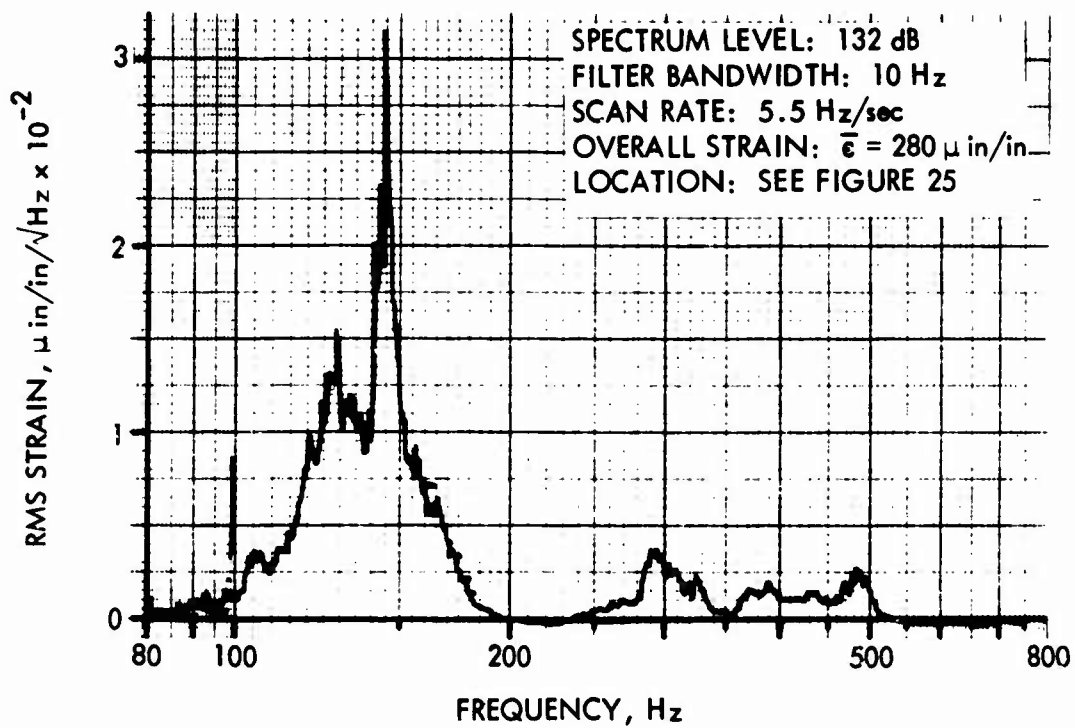
FIGURE 29 NARROW BAND ANALYSIS: STRAIN GAGE 9, STR-37A

SPECTRUM LEVEL: 132 dB
FILTER BANDWIDTH: 10 Hz
SCAN RATE: 5.5 Hz/sec
OVERALL STRAIN: $\bar{\epsilon}$ = 380 μ in/in
LOCATION: SEE FIGURE 25
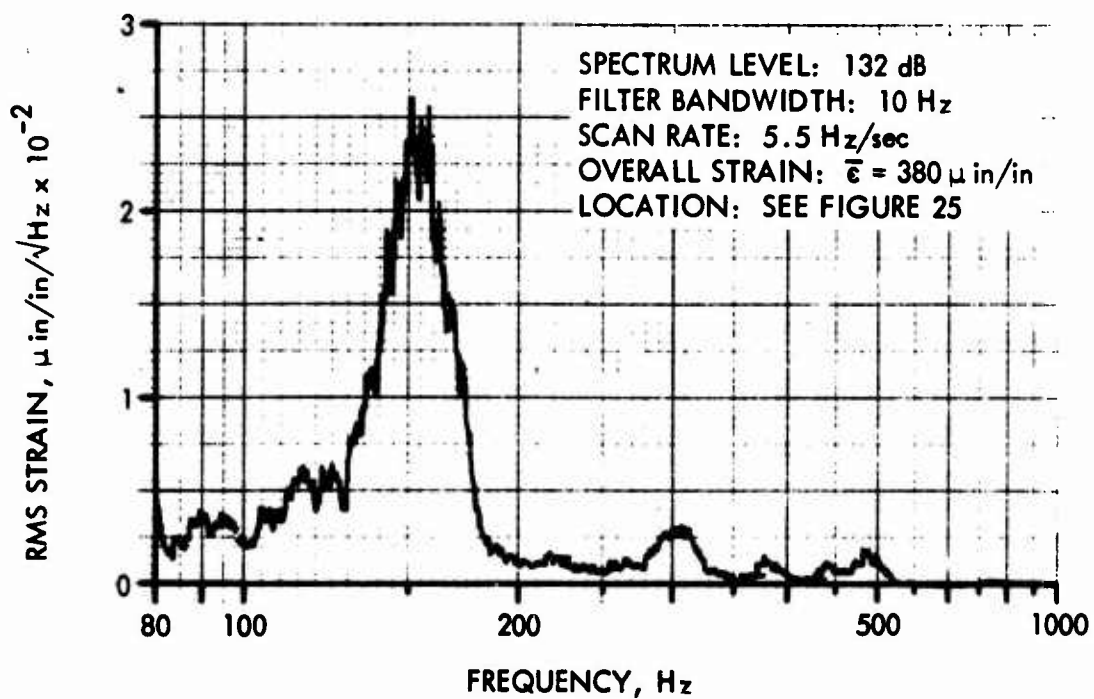
FIGURE 30 NARROW BAND ANALYSIS: STRAIN GAGE 5, STR-37A

64

SPECTRUM LEVEL: 132 dB
FILTER BANDWIDTH: 10 Hz
SCAN RATE: 5.5 Hz/sec
OVERALL STRAIN: $\bar{\epsilon}$ = 240 μ in/in
LOCATION: SEE FIGURES 24 & 25
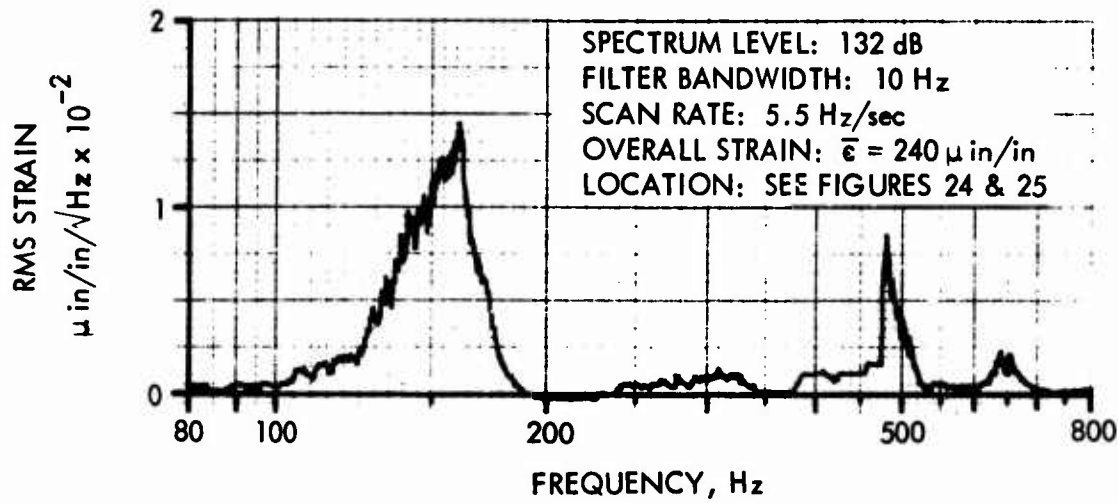
FIGURE 31 NARROW BAND ANALYSIS: STRAIN GAGE 6, STR-37A

SPECTRUM LEVEL: 132 dB
FILTER BANDWIDTH: 10 Hz
SCAN RATE: 5.5 Hz/sec
OVERALL STRAIN: $\bar{\epsilon}$ = 200 μ in/in
LOCATION: SEE FIGURE 25
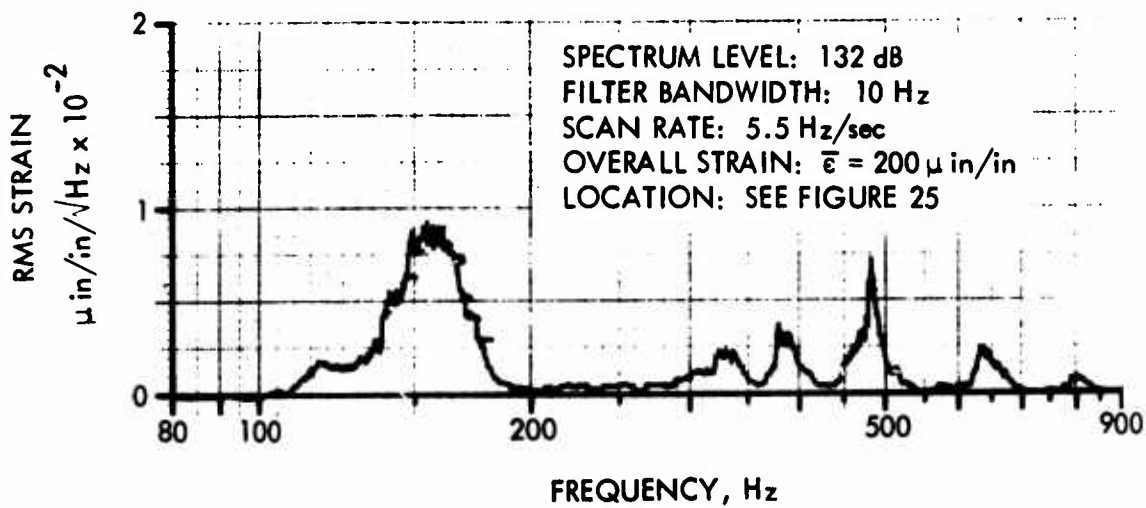
FIGURE 32 NARROW BAND ANALYSIS: STRAIN GAGE 7, STR-37A

65
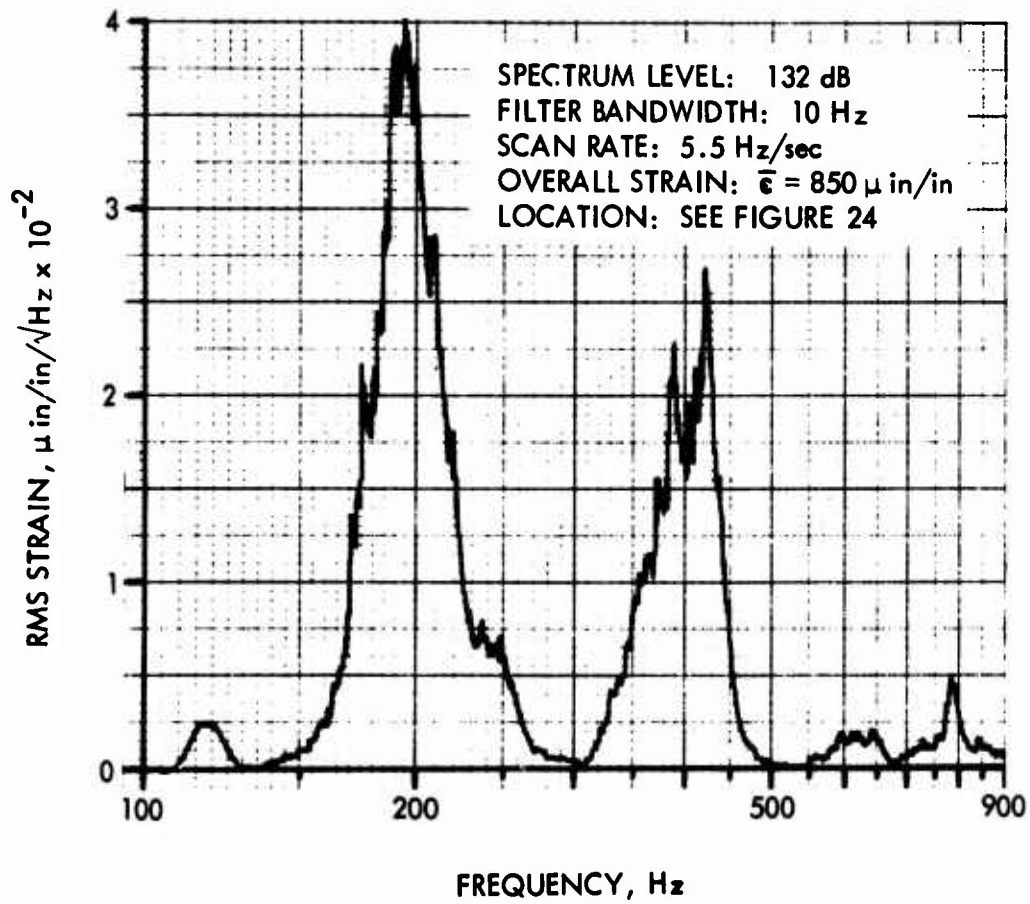
FIGURE 33 NARROW BAND ANALYSIS: STRAIN GAGE 1, STR-39A

SPECTRUM LEVEL: 132 dB
FILTER BANDWIDTH: 10 Hz
SCAN RATE: 5.5 Hz/sec
OVERALL STRAIN: $\bar{\epsilon}$ = 430 µ in/in
LOCATION: SEE FIGURE 21
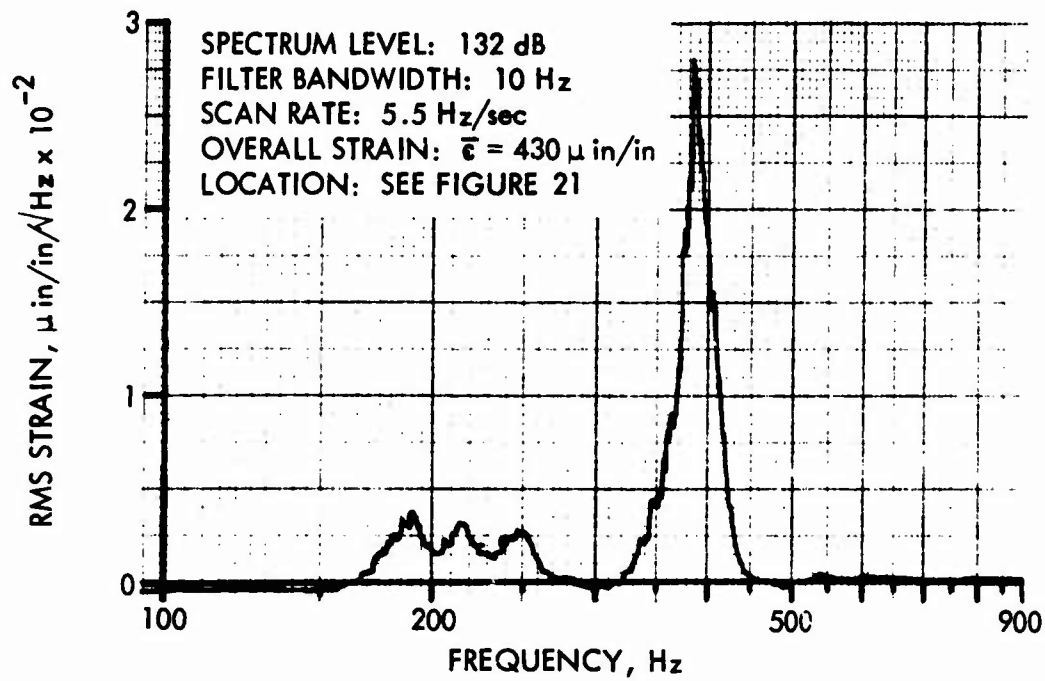
FIGURE 34   NARROW BAND ANALYSIS: STRAIN GAGE 9, STR-39A

SPECTRUM LEVEL: 132 dB
FILTER BANDWIDTH: 10 Hz
SCAN RATE: 5.5 Hz/sec
OVERALL STRAIN: $\bar{\epsilon}$ = 500µ in/in
LOCATION: SEE FIGURE 21
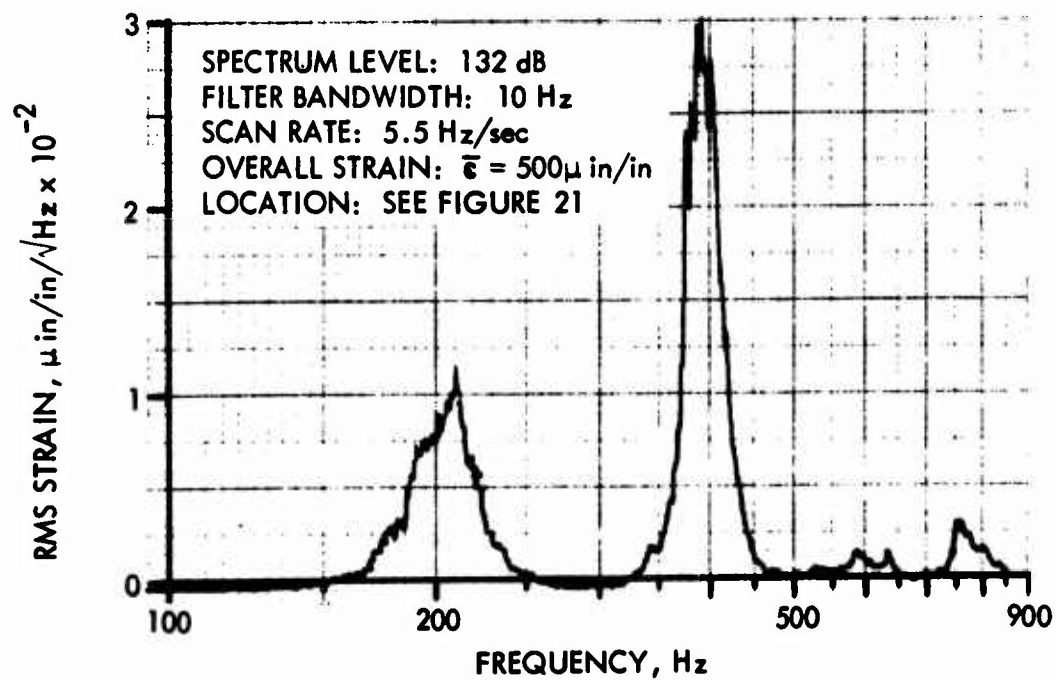
FIGURE 35 NARROW BAND ANALYSIS: STRAIN GAGE 6, STR-39A

67
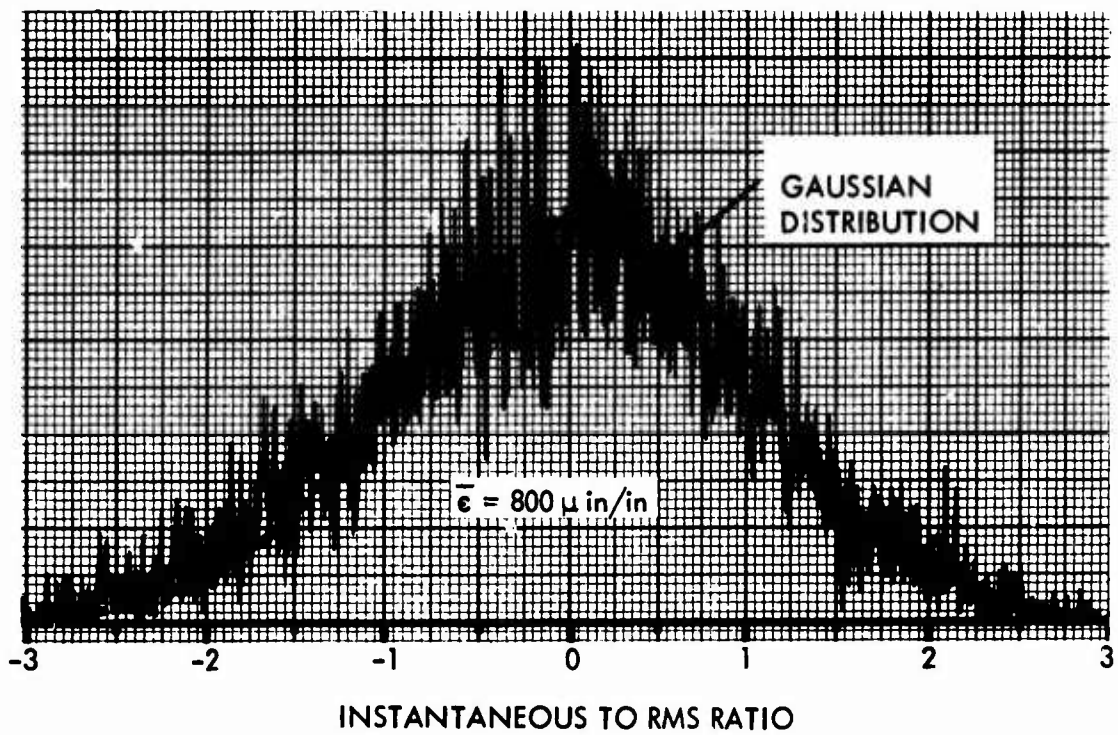
FIGURE 36 AMPLITUDE DISTRIBUTION OF STRAIN: STRAIN GAGE 1, STR-37A
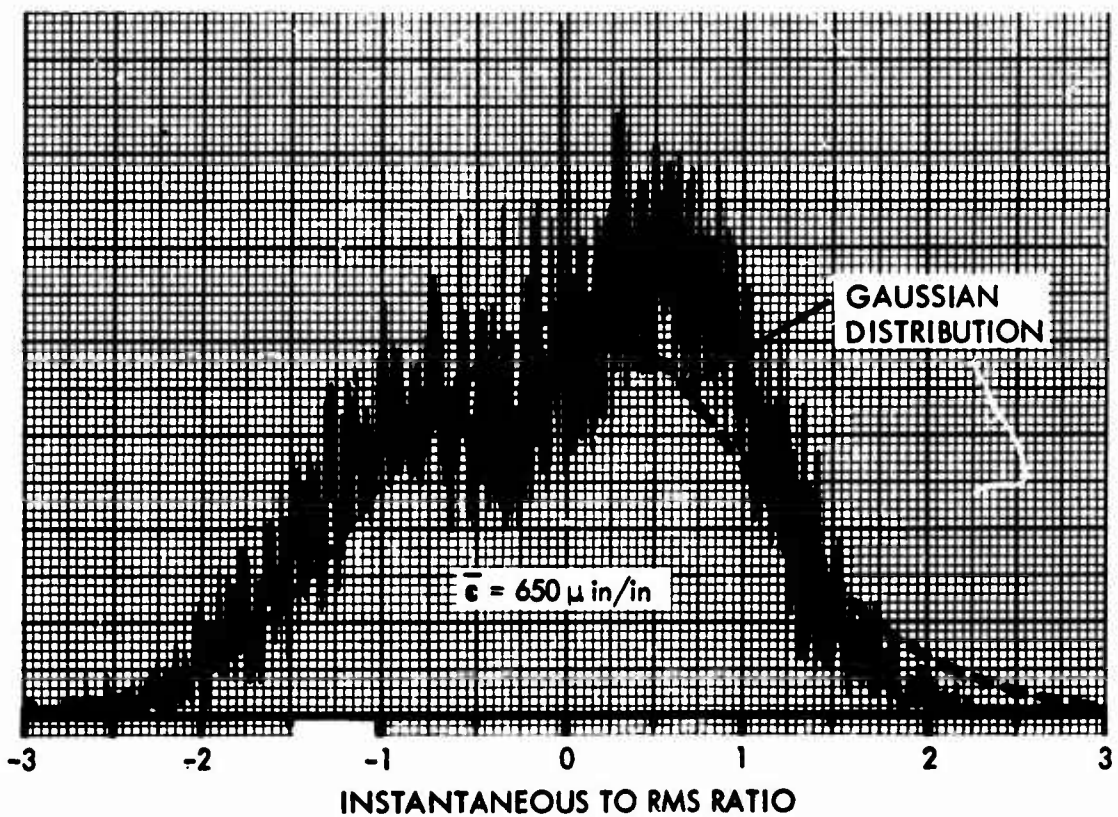
FIGURE 37 AMPLITUDE DISTRIBUTION OF STRAIN: STRAIN GAGE 2 (CENTER
OF CENTER BAY), STR-37A

68

GAUSSIAN
DISTRIBUTION

$\bar{\epsilon} = 240\,\mu in/in$

INSTANTANEOUS TO RMS RATIO
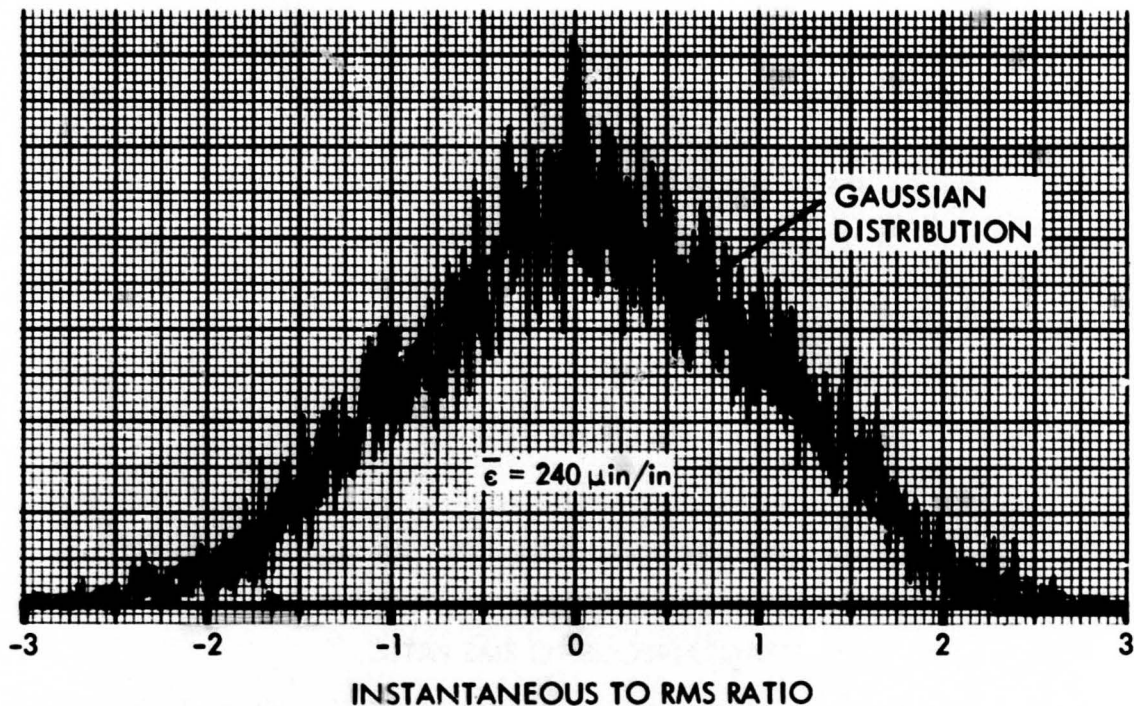
FIGURE 38 AMPLITUDE DISTRIBUTION OF STRAIN: STRAIN GAGE 6, STR-37A

GAUSSIAN
DISTRIBUTION

$\bar{\epsilon} = 150\,\mu in/in$

INSTANTANEOUS TO RMS RATIO
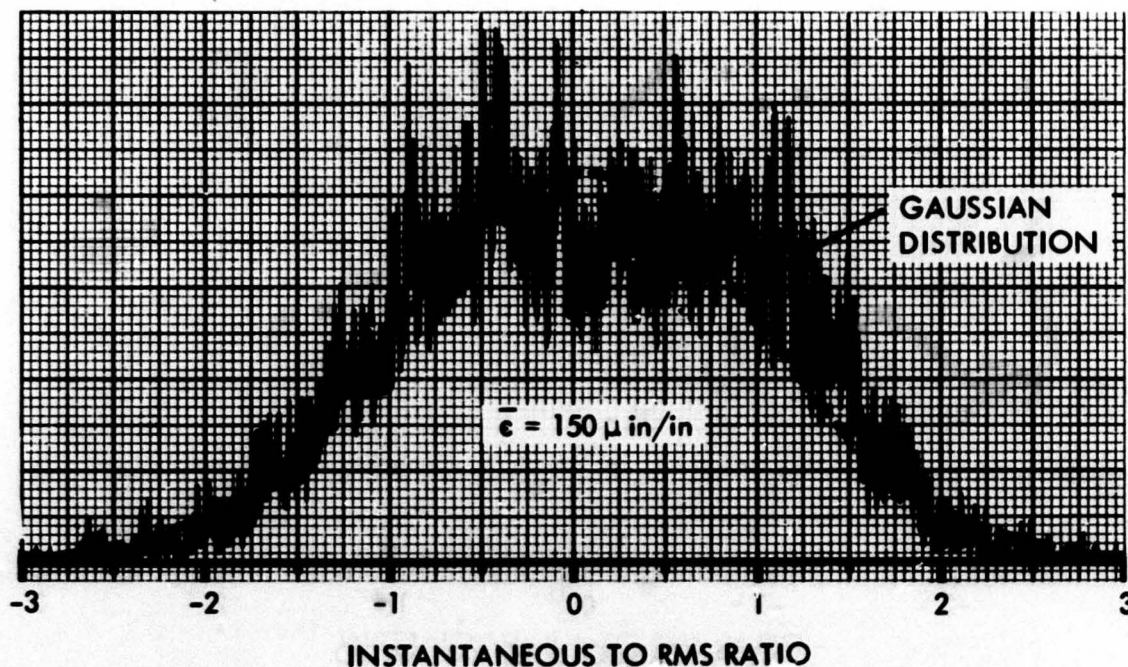
FIGURE 39 AMPLITUDE DISTRIBUTION OF STRAIN: STRAIN GAGE 9, STR-37A
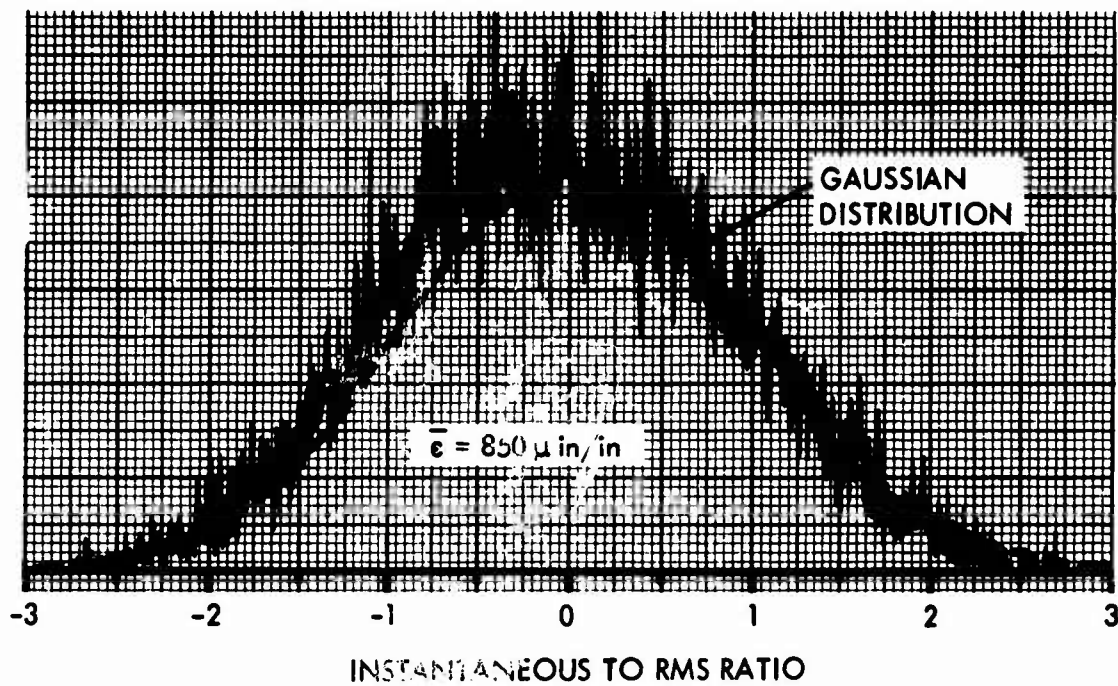
FIGURE 40 AMPLITUDE DISTRIBUTION OF STRAIN: STRAIN GAGE 1, STR-39A
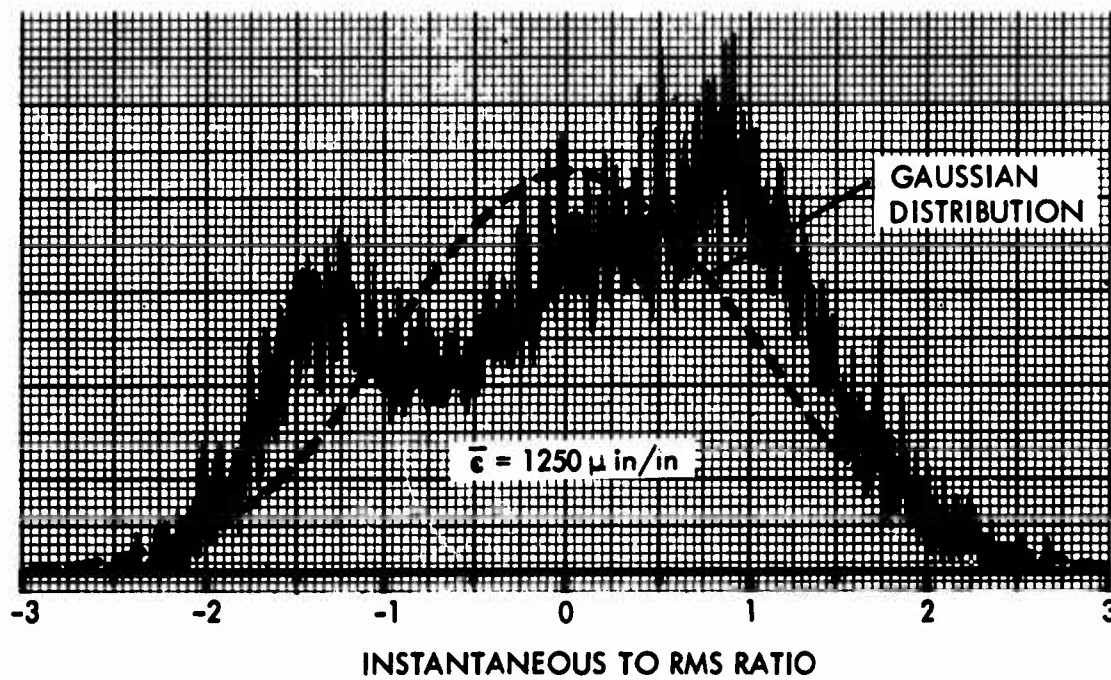
FIGURE 41 AMPLITUDE DISTRIBUTION OF STRAIN: STRAIN GAGE 3, STR-39B

70
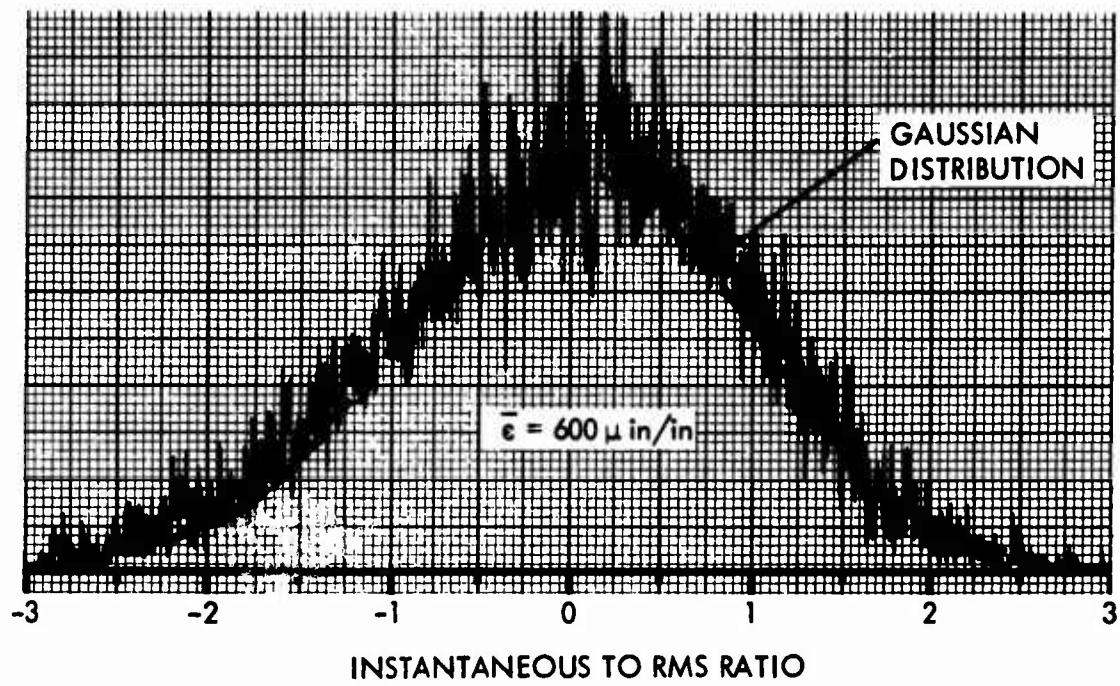
FIGURE 42 AMPLITUDE DISTRIBUTION OF STRAIN: STRAIN GAGE 6, STR-39A
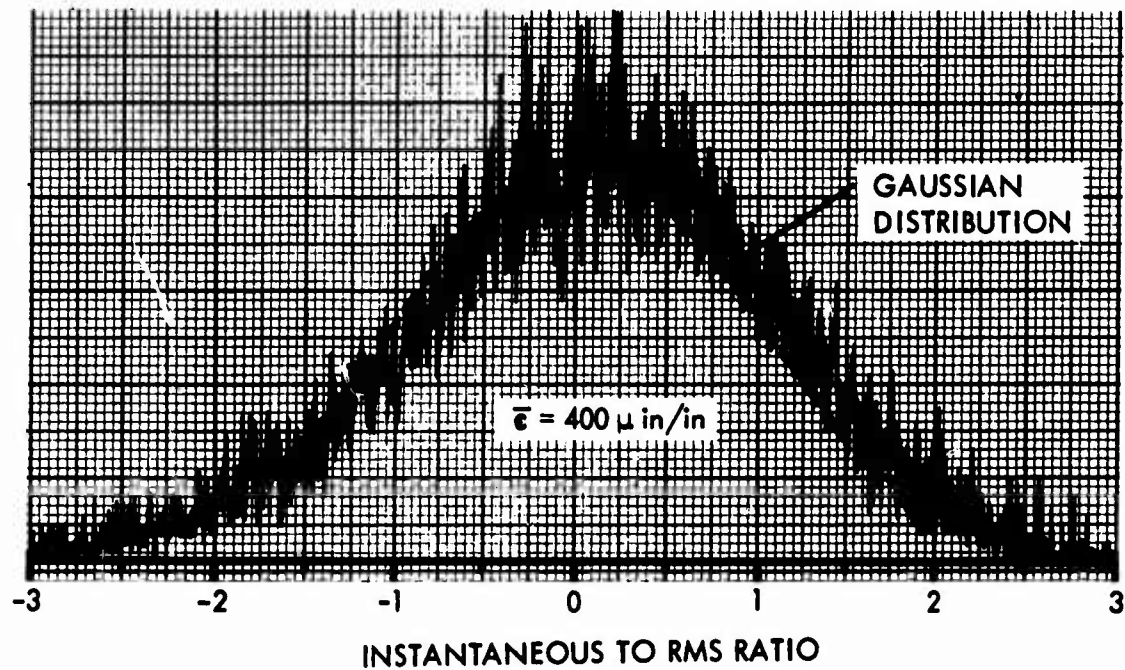
FIGURE 43 AMPLITUDE DISTRIBUTION OF STRAIN: STRAIN GAGE 9, STR-39A
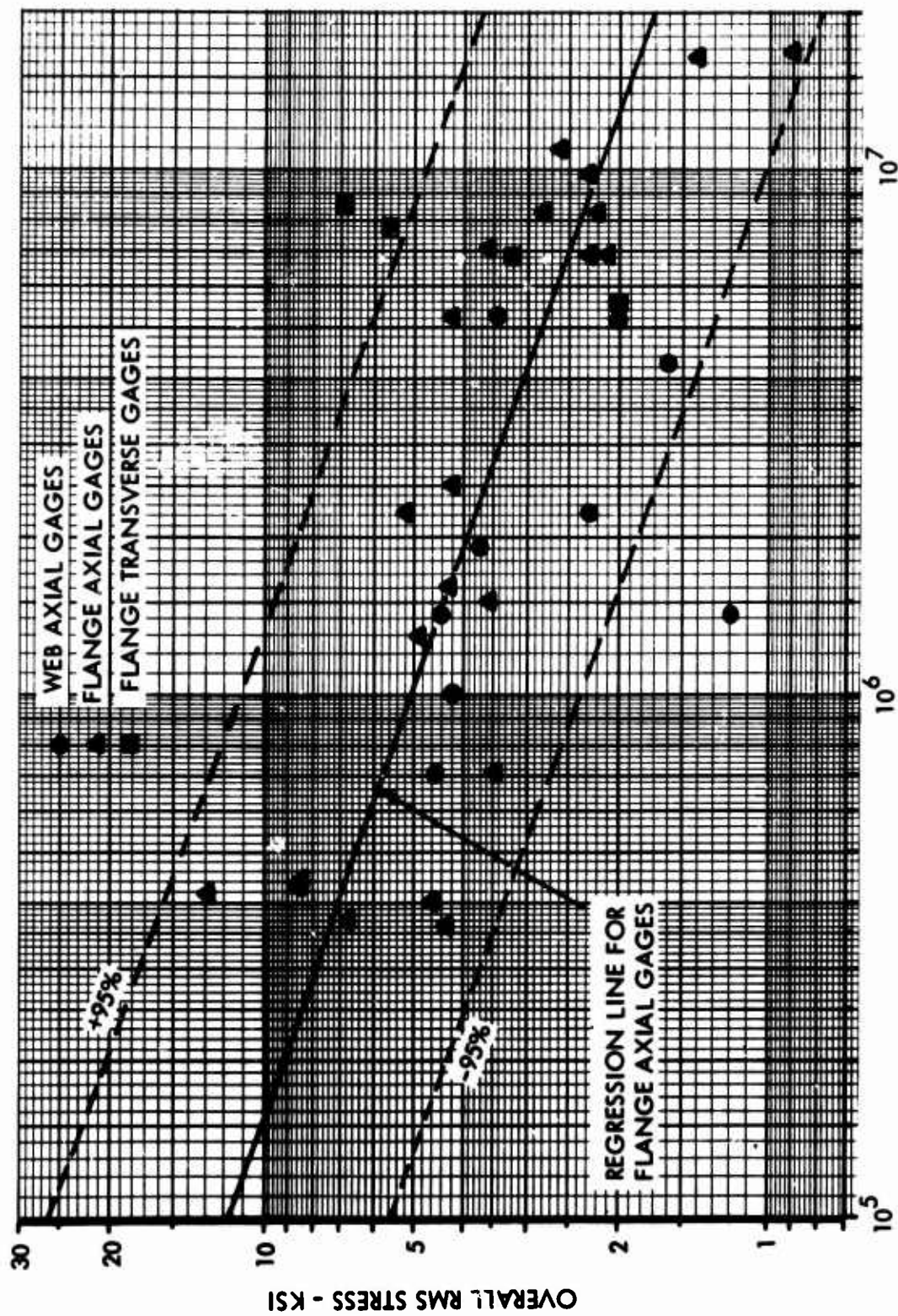
FIGURE 44 STIFFENED PANEL STRINGER FATIGUE CURVE

TABLE XI

MODAL FREQUENCIES FOR BOX SPECIMENS
(Low Intensity Sinusoidal Excitation)

Specimen	(1,1,1)	(1,2,1)	(1,3,1)	(1,3,2)
BX-1A	94	191	222	—
BX-1B	78	144	235	—
BX-2A	90	136	193	—
BX-2B	92	135	220	—
BX-3A	82	—	137	—
BX-3B	81	106	133	—
BX-4A	139	181	228	—
BX-4B	135	—	209	—
BX-5A	78	92	164	134
BX-5B	88	91	—	136
BX-6A	62	77	—	124
BX-6B	62	—	—	116
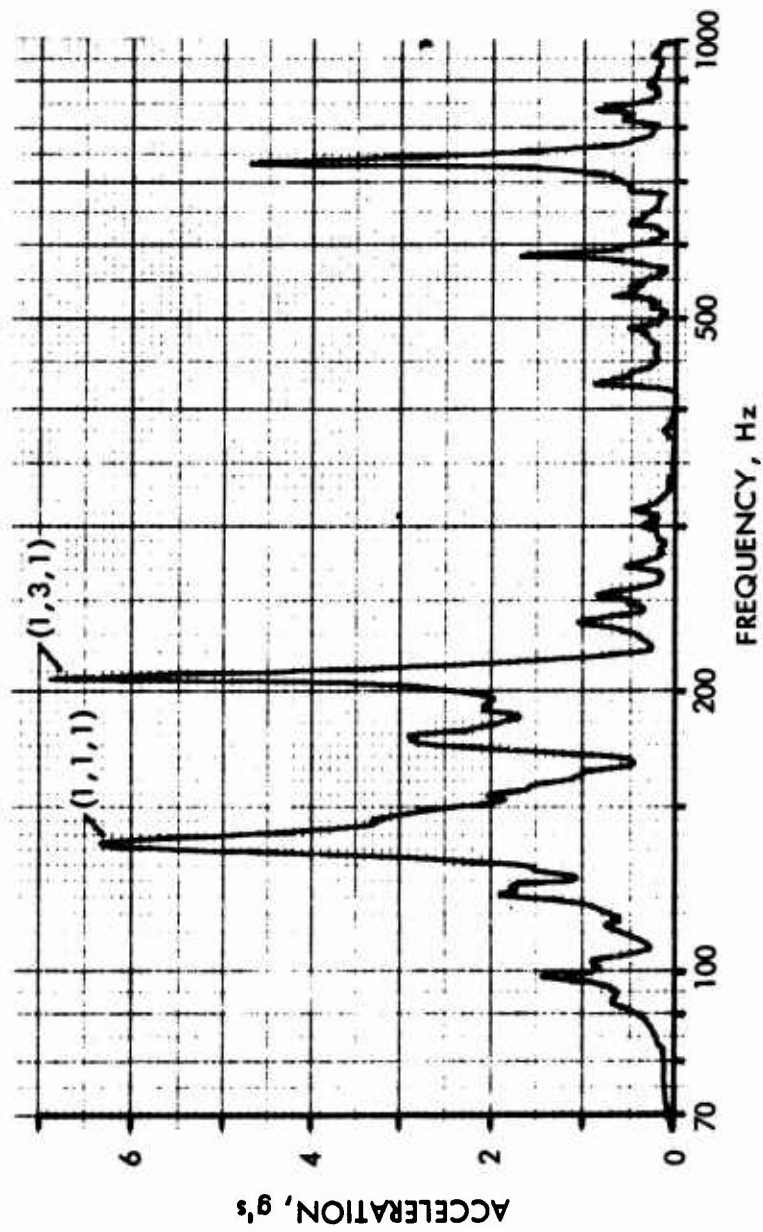
FIGURE 45   CENTER BAY RESPONSE, FRONT SIDE: EXCITATION ON FRONT SIDE, BX–4B

74
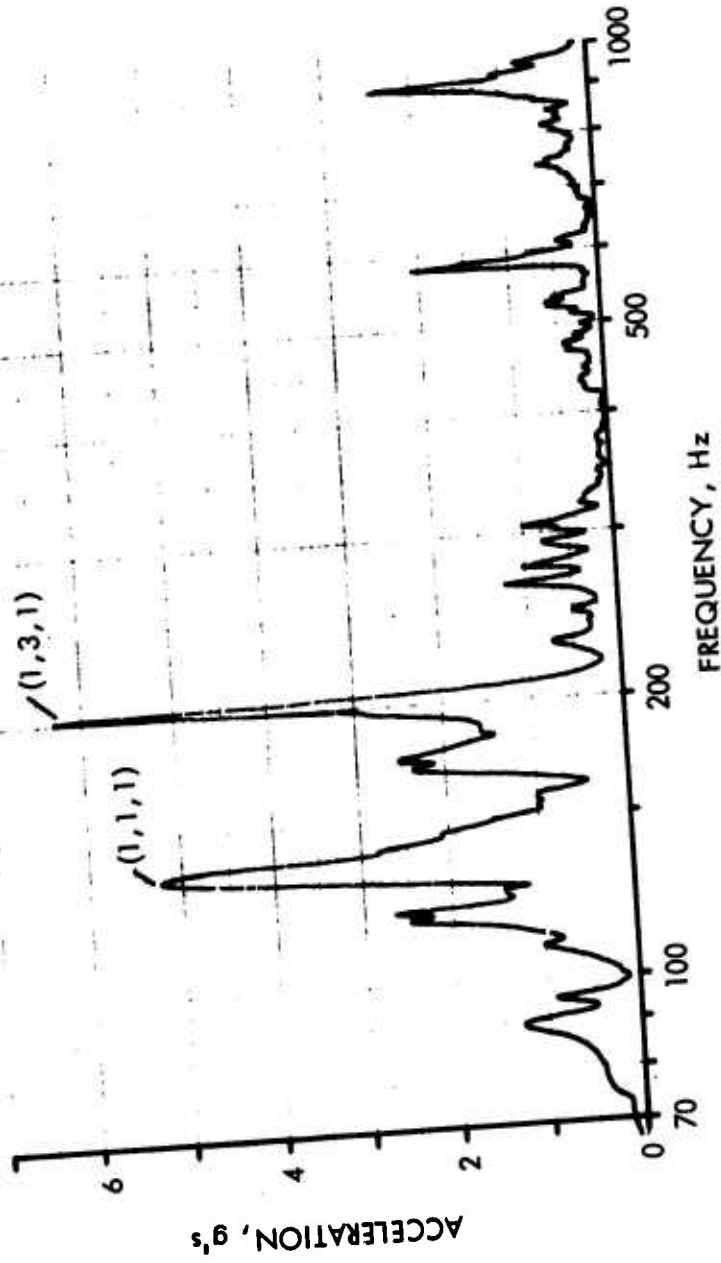
FIGURE 46 CENTER BAY RESPONSE, FRONT SIDE: IN PHASE EXCITATION
BOTH SIDE, BX4B

75
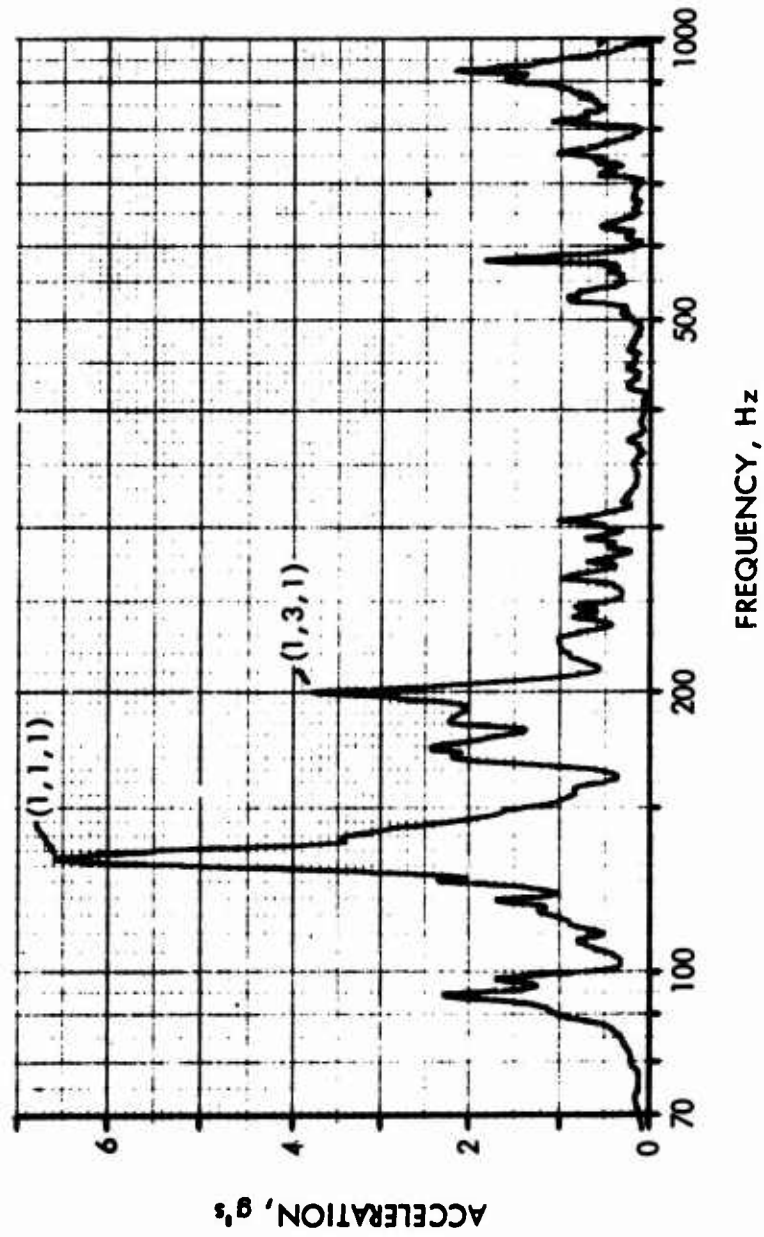
FIGURE 47 CENTER BAY RESPONSE, FRONT SIDE: OUT OF PHASE EXCITATION
BOTH SIDES, BX4B
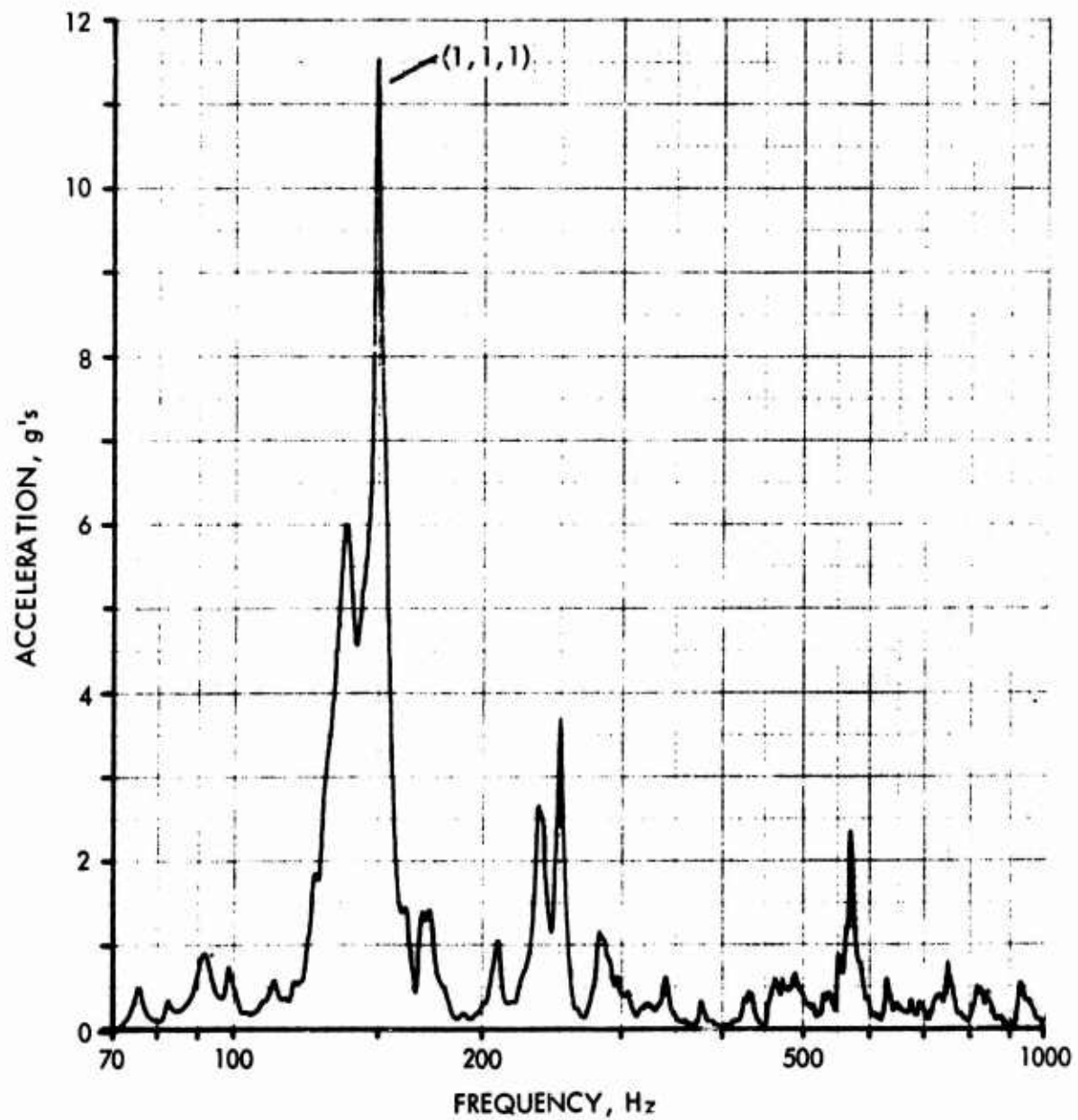
FIGURE 48 CENTER RIB RESPONSE: EXCITATION ON FRONT SIDE, BX4B
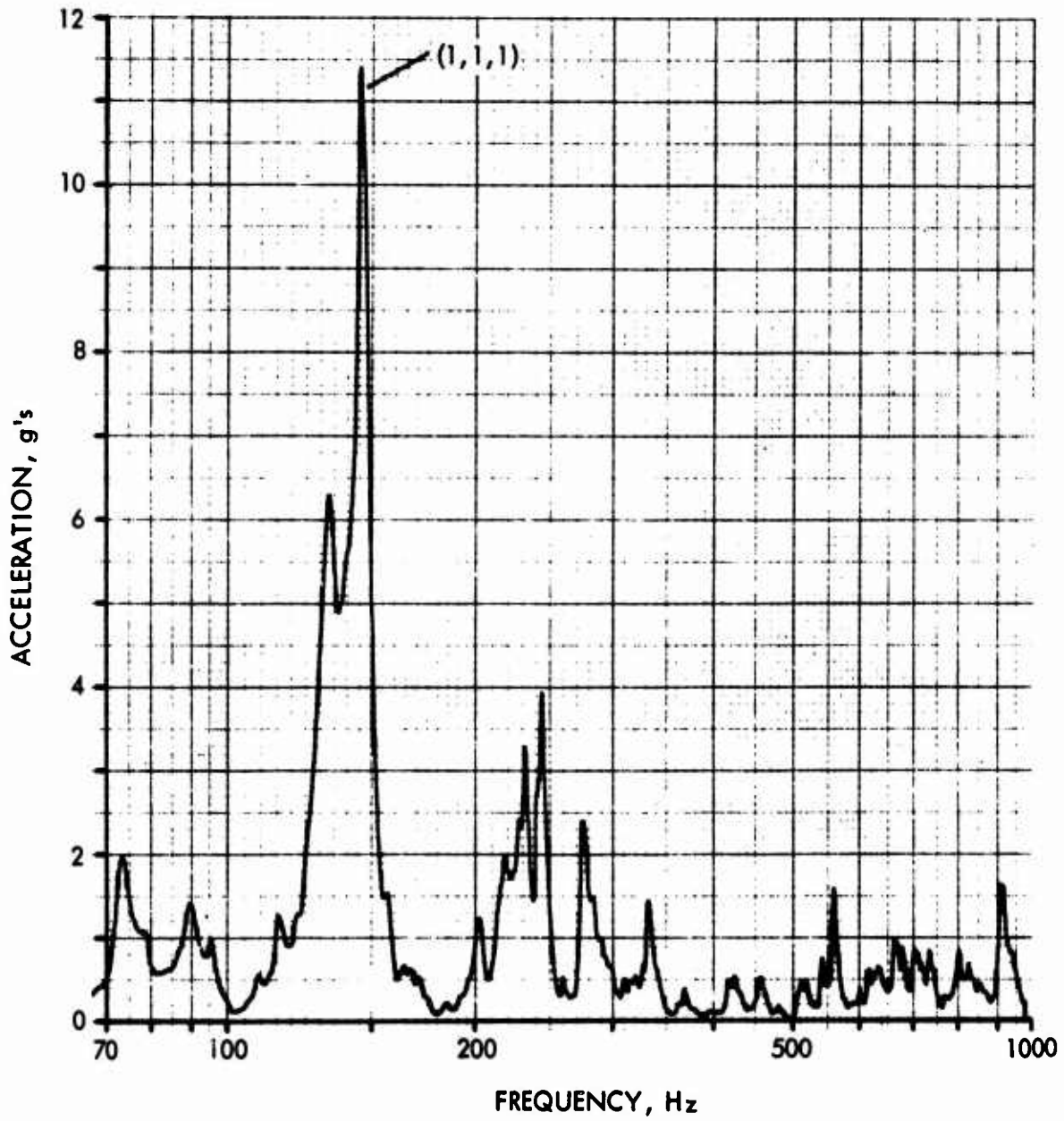
FIGURE 49 CENTER RIB RESPONSE: IN PHASE EXCITATION BOTH SIDES, BX4B
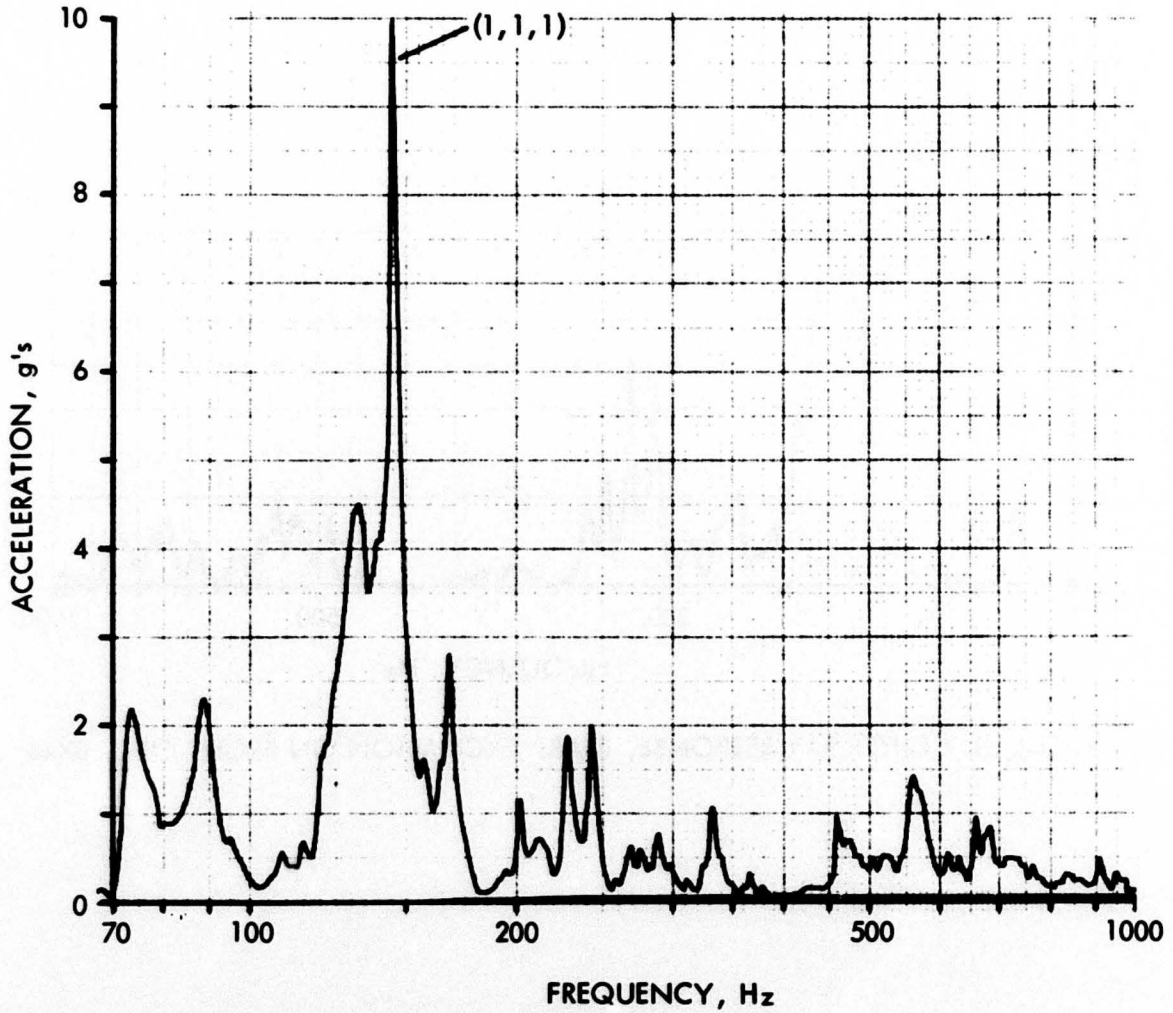
FIGURE 50 CENTER RIB RESPONSE: OUT OF PHASE EXCITATION BOTH SIDES, BX4B
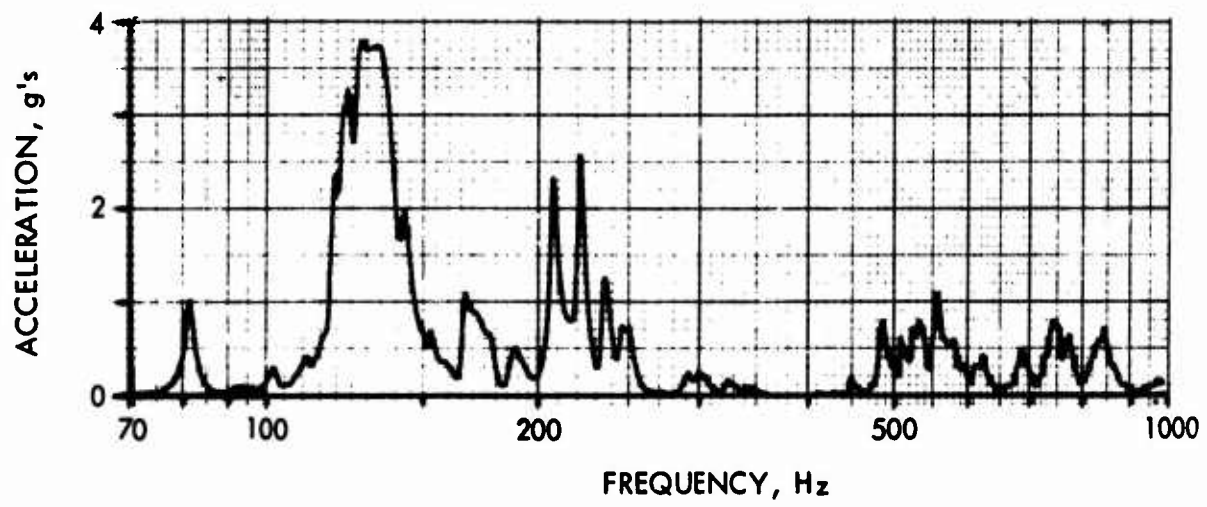
FIGURE 51 CENTER BAY RESPONSE, REAR: EXCITATION ON FRONT SIDE, BX4B
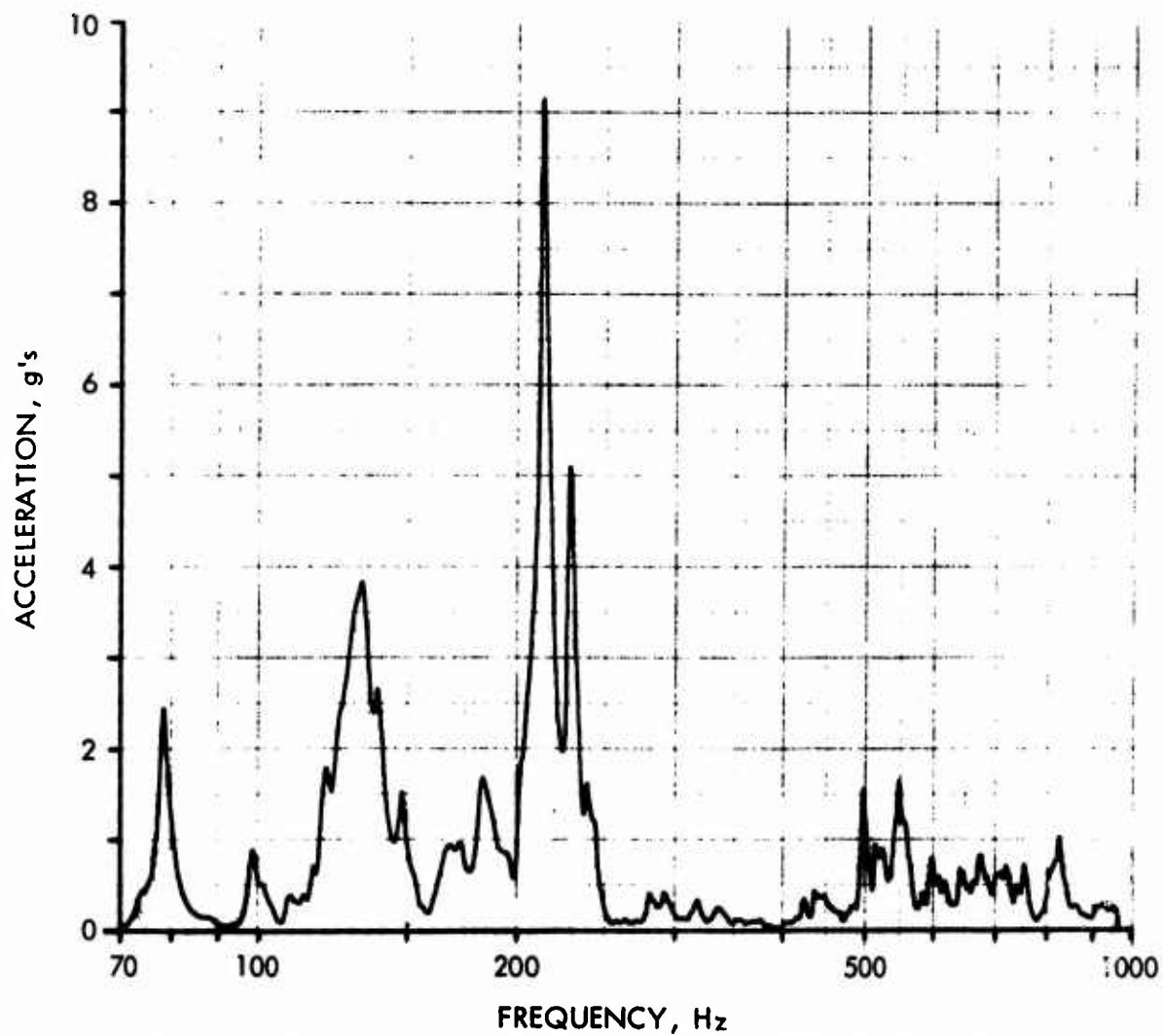
FIGURE 52 CENTER BAY RESPONSE, REAR: IN PHASE EXCITATION ON
BOTH SIDES, BX4B
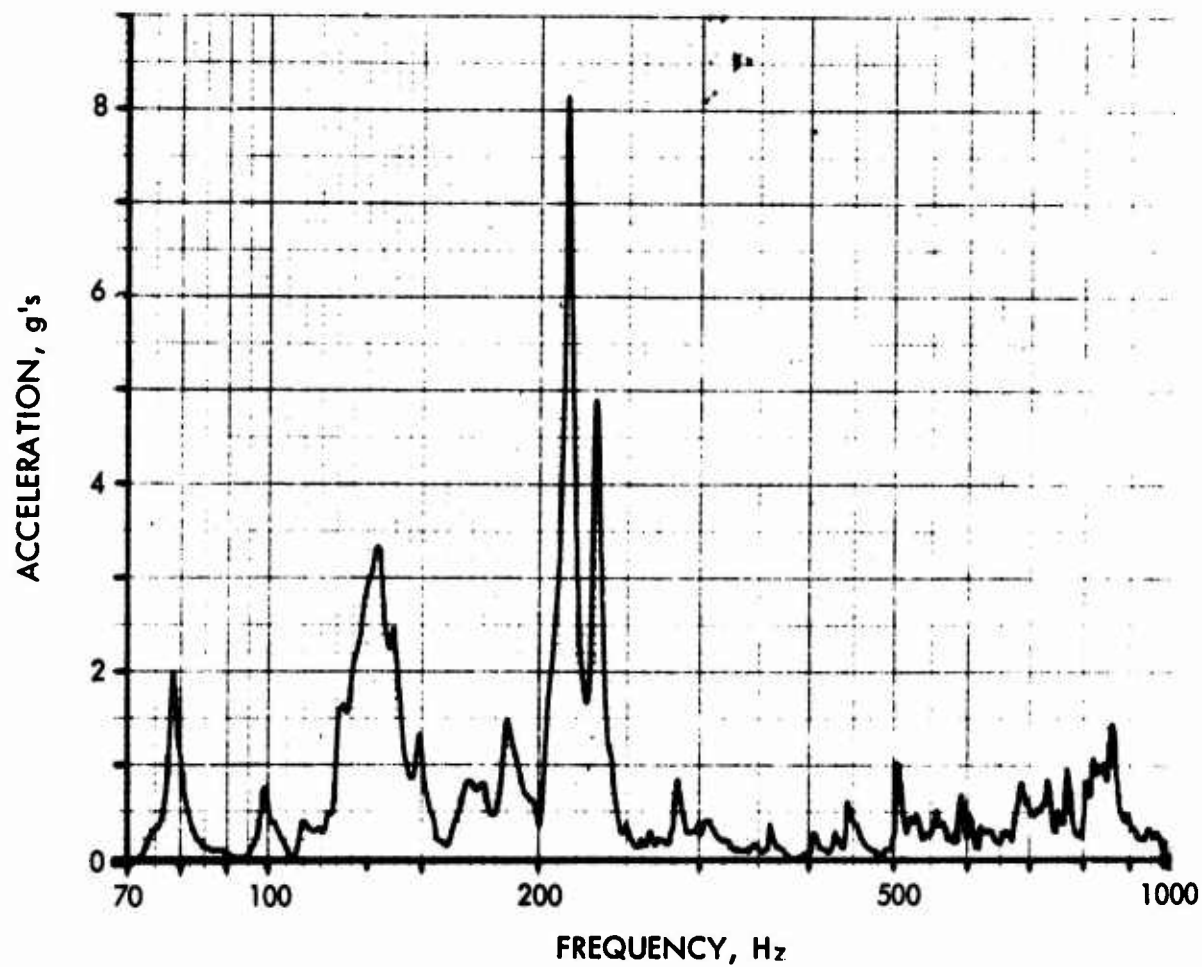
FIGURE 53 CENTER BAY RESPONSE, REAR: OUT OF PHASE EXCITATION
ON BOTH SIDES, BX4B

acceleration response of the front center panel bay, the center rib, and the rear center panel bay for the three excitation conditions of the low intensity sine sweeps. The accelerometer location was the center of the bay and rib. These results are typical of the low intensity sine sweeps conducted during the modal frequency studies.

2.2 Damping Ratios - The decaying strain signals as described in Section III.C.3 were used to obtain average values for the damping ratio. An arithmetic average for each design was obtained. Table XII is a listing of these average damping ratios as determined by the logarithmic decrement method. A plot of damping ratio versus frequency for the box specimens is given in Figure 23.

2.3 High Intensity Frequency Sweeps - Figures 54 through 57 are plots of strain response to high intensity sinusoidal excitation at the indicated sound pressure level. The strain gages illustrated are for specimen BX4B. Strain gage 1 is located across the rivet line at the middle of the long side of the center bay on the side exposed to acoustical excitation. Strain gage 7 is located across the rib flange directly under gage 1. Strain gage 8 is located in the center of the rib with the gage axis in the direction of the rib height. Strain gage 9 is located across the rib flange directly opposite to strain gage 7. These figures illustrate the discrete frequency strain response across the height of the structure with excitation on one side.

2.4 Broadband Acoustical Noise Test Spectra - The acoustical noise test spectra were shaped such that the bandwidth of the excitation was at least three times the bandwidth of the test specimen sinusoidal response. If more than one mode appeared to be significant, the test spectrum was shaped so as to include all responding modes. Figures 58 through 60 illustrate typical broadband test spectra for the box specimens. Figure 60 illustrates the test spectrum for specimen BX4B.

2.5 Fatigue Tests - Twelve box structure specimens, six designs with two replicates each, were exposed to broadband random acoustical excitation until one or more cracks developed in the skin or ribs. Table XIII is a summary of the test results.

Magnetic tape recordings were made of the signals from the strain gages positioned in the skin and the ribs. These strain data were analyzed using a narrow band filter (nominal 10 Hz) to determine the characteristics of the strain response to the acoustical excitation. Figures 61 through 64 are narrow band analyses of the strain response for strain gages 1, 7, 8, and 9 of specimen BX4B. (See Figures 54 through 57 for the high intensity sinusoidal response of these strain gages.)

In addition to the narrow band analysis, the recorded strain data were analyzed to determine the probability density of instantaneous strain. Figures 65 through 68 are plots of amplitude distribution for strain gages 1, 7, 8, and 9 of specimen BX4B. These results are typical of the statistical analyses. For reference, a Gaussian distribution is plotted on each figure.

Figure 69 shows the relationship between overall nominal rms stress and the number of cycles to failure for all failure data. The number of cycles to failure was established from the number of zero crossings with negative slope (obtained as described in Appendix II) for

TABLE XII

AVERAGE DAMPING RATIOS FOR BOX SPECIMENS

Specimen	Average Damping Ratio, %
BX-1A	1.7
BX-1B	2.5
BX-2A	2.2
BX-2B	2.0
BX-3A	2.4
BX-3B	2.2
BX-4A	1.3
BX-4B	1.4
BX-5A	2.2
BX-5B	3.0
BX-6A	1.5
BX-6B	2.0
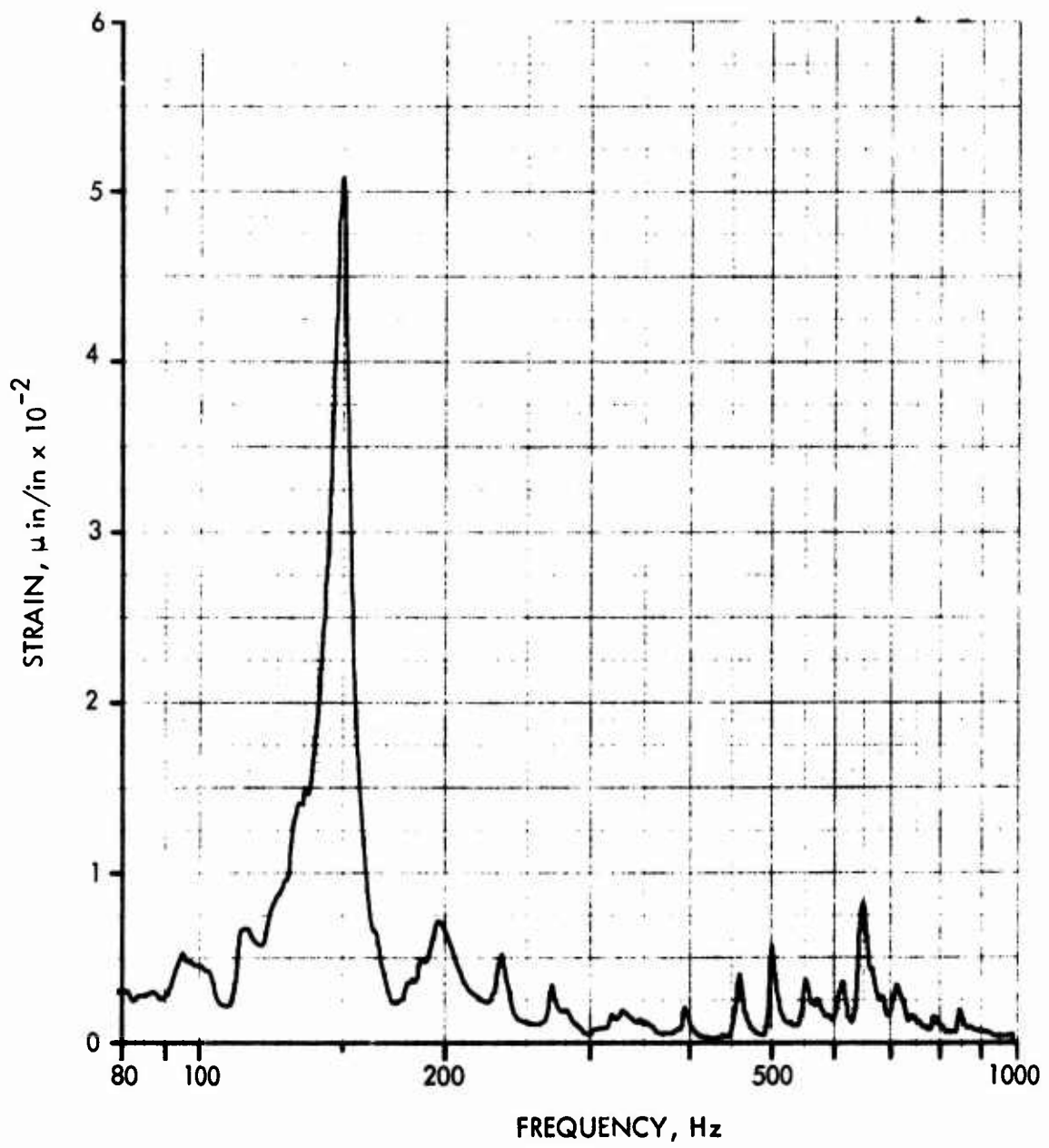
FIGURE 54 HIGH INTENSITY SINE SWEEP: STRAIN GAGE 1, BX-4B

85
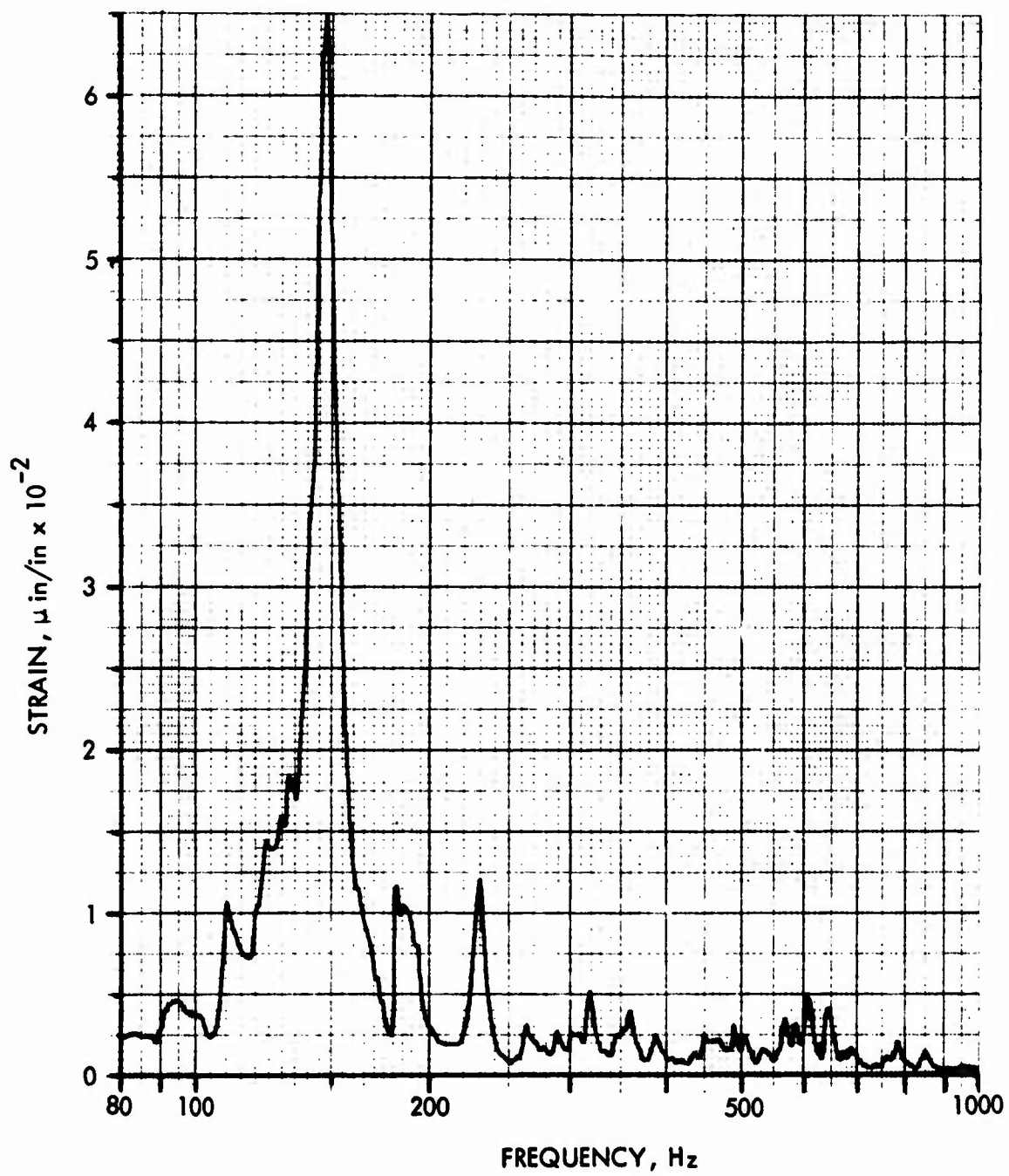
FIGURE 55 HIGH INTENSITY SINE SWEEP: STRAIN GAGE 7, BX-4B

86
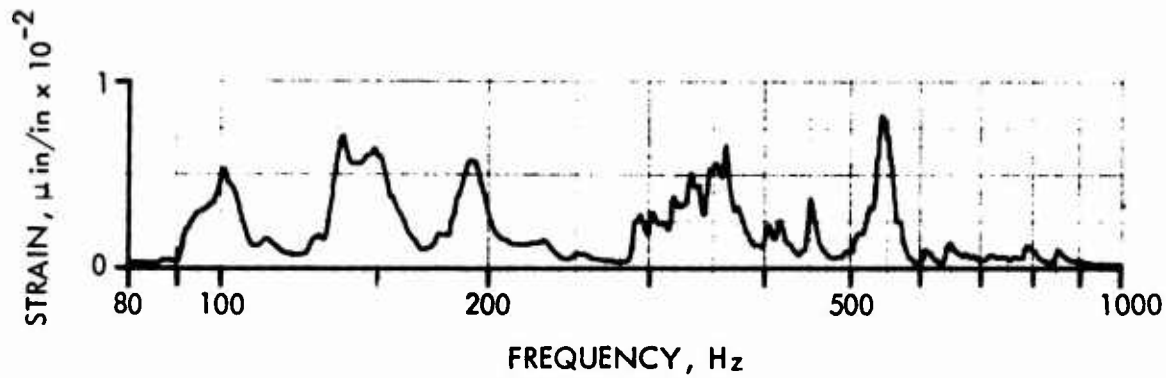
FIGURE 56 HIGH INTENSITY SINE SWEEP: STRAIN GAGE 8, BX-4B
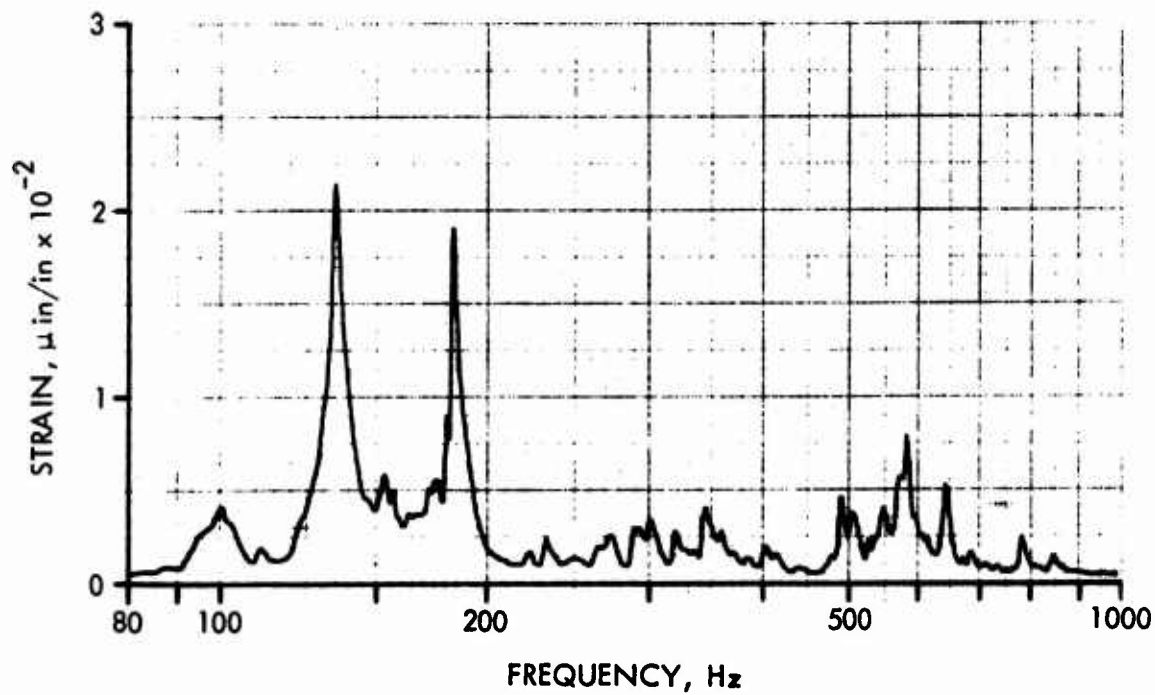
FIGURE 57 HIGH INTENSITY SINE SWEEP: STRAIN GAGE 9, BX-4B
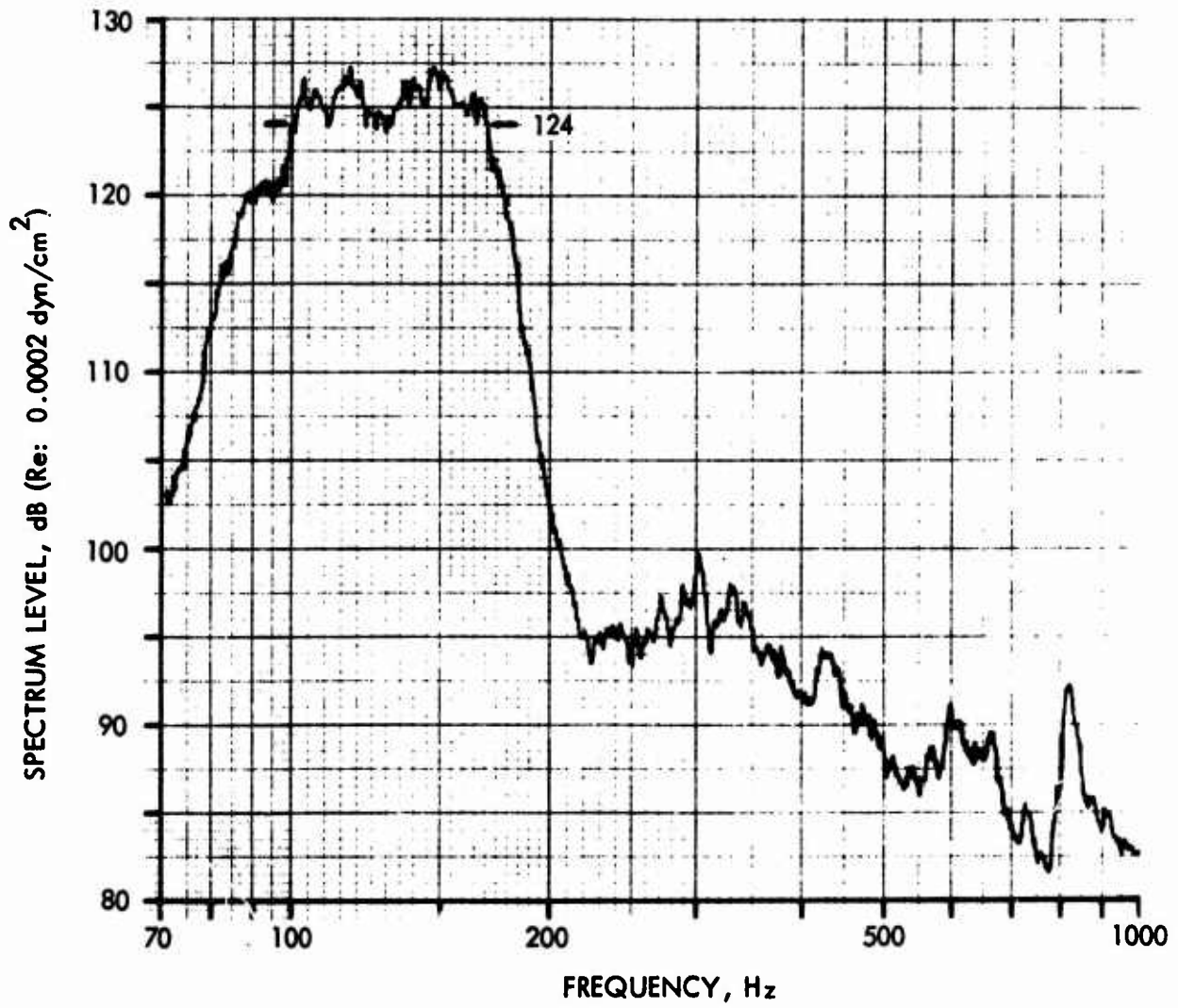
FIGURE 58 BROAD BAND TEST SPECTRUM, BX-1B
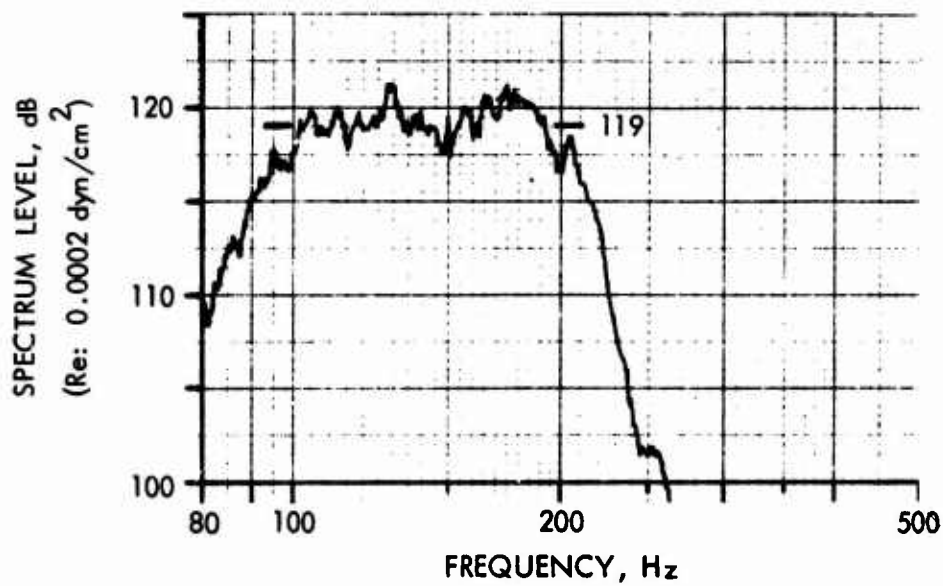
FIGURE 59 BROAD BAND TEST SPECTRUM, BX-3A
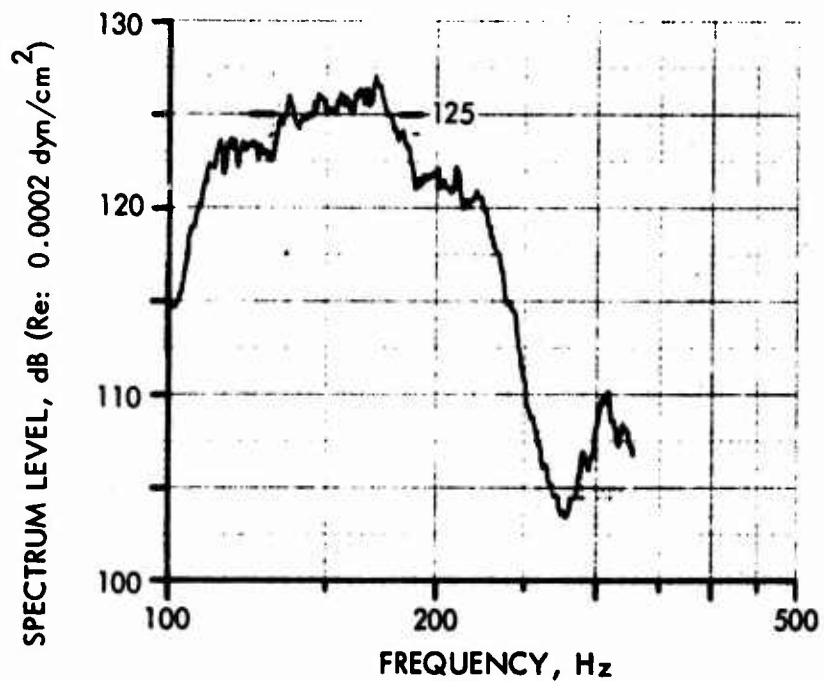
FIGURE 60 BROAD BAND TEST SPECTRUM, BX-4B

TABLE XIII

SUMMARY OF BOX SPECIMEN FATIGUE TESTS

Specimen	Test Spectrum Level dB	Response Frequency Hz	$N_c \times 10^{-6}$	$\bar{\sigma}$ ksi	Mode Responding
BX-1A	124	140-150*	6.2	6.0 (SF)*	(1,1,1)
BX-1A	124	140-150	6.3	6.8 (SF)	(1,1,1)
BX-1B	124	140-160	11.5	5.0 (SR)	(1,1,1)
BX-2A	121	140-180	9.25	5.2 (SF)	(1,1,1) & (1,3,1)
BX-2B	121	100-160	43.5	6.6 (SR)	(1,1,1) & (1,3,1)
BX-3A	119	130/160	No Failures	At Gages	(1,1,1) & (1,3,1)
BX-3B	119	115-145	No Failures	At Gages	(1,1,1) & (1,3,1)
BX-4A	124	140-160	4.3	6.6 (UF)	(1,1,1)
BX-4A	124	140-160	3.5	7.0 (UF)	(1,1,1)
BX-4A	124	140-160	4.2	7.2 (UF)	(1,1,1)
BX-4A	124	140-160	3.7	5.7 (UF)	(1,1,1)
BX-4B	125	150	0.68	13.9 (UF)	(1,1,1)
BX-4B	125	150	0.94	10.8 (UF)	(1,1,1)
BX-4B	125	150	1.22	10.3 (UF)	(1,1,1)
BX-4B	125	150	1.07	11.3 (UF)	(1,1,1)
BX-5A	124	83/175	0.22	22.2 (UF)	(1,1,1) & (1,3,2)
BX-5A	124	83/175	0.25	21.1 (UF)	(1,1,1) & (1,3,2)
BX-5A	124	83/175	0.25	18.6 (UF)	(1,1,1) & (1,3,2)
BX-5A	124	83/175	0.23	22.6 (UF)	(1,1,1) & (1,3,2)
BX-5B	125	90/135	0.25	24.8 (UF)	(1,1,1) & (1,3,2)
BX-5B	125	90/135	0.77	15.5 (LF)	(1,1,1) & (1,3,2)
BX-5B	125	90/135	0.28	21.6 (UF)	(1,1,1) & (1,3,2)
BX-5B	125	90/135	0.74	16.5 (LF)	(1,1,1) & (1,3,2)
BX-5B	125	90/135	0.27	17.6 (UF)	(1,1,1) & (1,3,2)
BX-5B	125	90/135	0.29	19.6 (UF)	(1,1,1) & (1,3,2)

90

TABLE XIII (Continued)

Specimen	Test Spectrum Level dB	Response Frequency Hz	$N_c \times 10^{-6}$	$\bar{\sigma}$ ksi	Mode Responding
BX-5B	125	90/135*	0.34	19.6 (UF)*	(1,1,1) & (1,3,2)
BX-5B	125	90/135	0.32	18.6 (UF)	(1,1,1) & (1,3,2)
BX-6A	124	90/135	0.47	15.5 (UF)	(1,1,1) & (1,3,1)
BX-6A	124	90/135	0.36	16.5 (UF)	(1,1,1) & (1,3,1)
BX-6A	124	90/135	0.55	13.9 (UF)	(1,1,1) & (1,3,1)
BX-6A	124	90/135	1.78	7.4 (LF)	(1,1,1) & (1,3,1)
BX-6A	124	90/135	2.50	9.8 (LF)	(1,1,1) & (1,3,1)
BX-6A	124	90/135	2.30	9.1 (LF)	(1,1,1) & (1,3,1)
BX-6A	124	90/135	0.84	11.3 (UF)	(1,1,1) & (1,3,1)
BX-6A	124	90/135	0.95	12.4 (UF)	(1,1,1) & (1,3,1)
BX-6A	124	90/135	1.14	11.9 (UF)	(1,1,1) & (1,3,1)
BX-6A	124	90/135	2.24	8.5 (LF)	(1,1,1) & (1,3,1)
BX-6A	124	90/135	2.10	7.0 (LF)	(1,1,1) & (1,3,1)
BX-6B	124	95/125	0.16	18.5 (UF)	(1,1,1) & (1,3,1)
BX-6B	124	95/125	0.34	13.9 (UF)	(1,1,1) & (1,3,1)
BX-6B	124	95/125	0.31	16.0 (UF)	(1,1,1) & (1,3,1)
BX-6B	124	95/125	0.79	16.5 (LF)	(1,1,1) & (1,3,1)
BX-6B	124	95/125	1.02	12.9 (LF)	(1,1,1) & (1,3,1)
BX-6B	124	95/125	0.89	13.4 (LF)	(1,1,1) & (1,3,1)
BX-6B	124	95/125	0.50	18.0 (UF)	(1,1,1) & (1,3,1)
BX-6B	124	95/125	0.58	16.0 (UF)	(1,1,1) & (1,3,1)
BX-6B	124	95/125	0.84	14.9 (UF)	(1,1,1) & (1,3,1)
BX-6B	124	95/125	0.50	20.6 (UF)	(1,1,1) & (1,3,1)
BX-6B	124	95/125	0.52	15.0 (LF)	(1,1,1) & (1,3,1)
BX-6B	124	95/125	1.07	10.8 (LF)	(1,1,1) & (1,3,1)

*Notes: 140-150 denotes a broad response in frequency range.

83/175 denotes a multimode response at indicated frequencies.

SF - strain gage on skin across frame
SR - strain gage on skin across rib
UF - strain gage on rib flange, excited surface
LF - strain gage on rib flange, unexcited surface

91

SPECTRUM LEVEL: 125 dB
FILTER BANDWIDTH: 10 Hz
SCAN RATE: 5.5 Hz/sec.
OVERALL STRAIN: $\bar{\varepsilon}$ = 840 μ in/in
LOCATION: See Figure 22
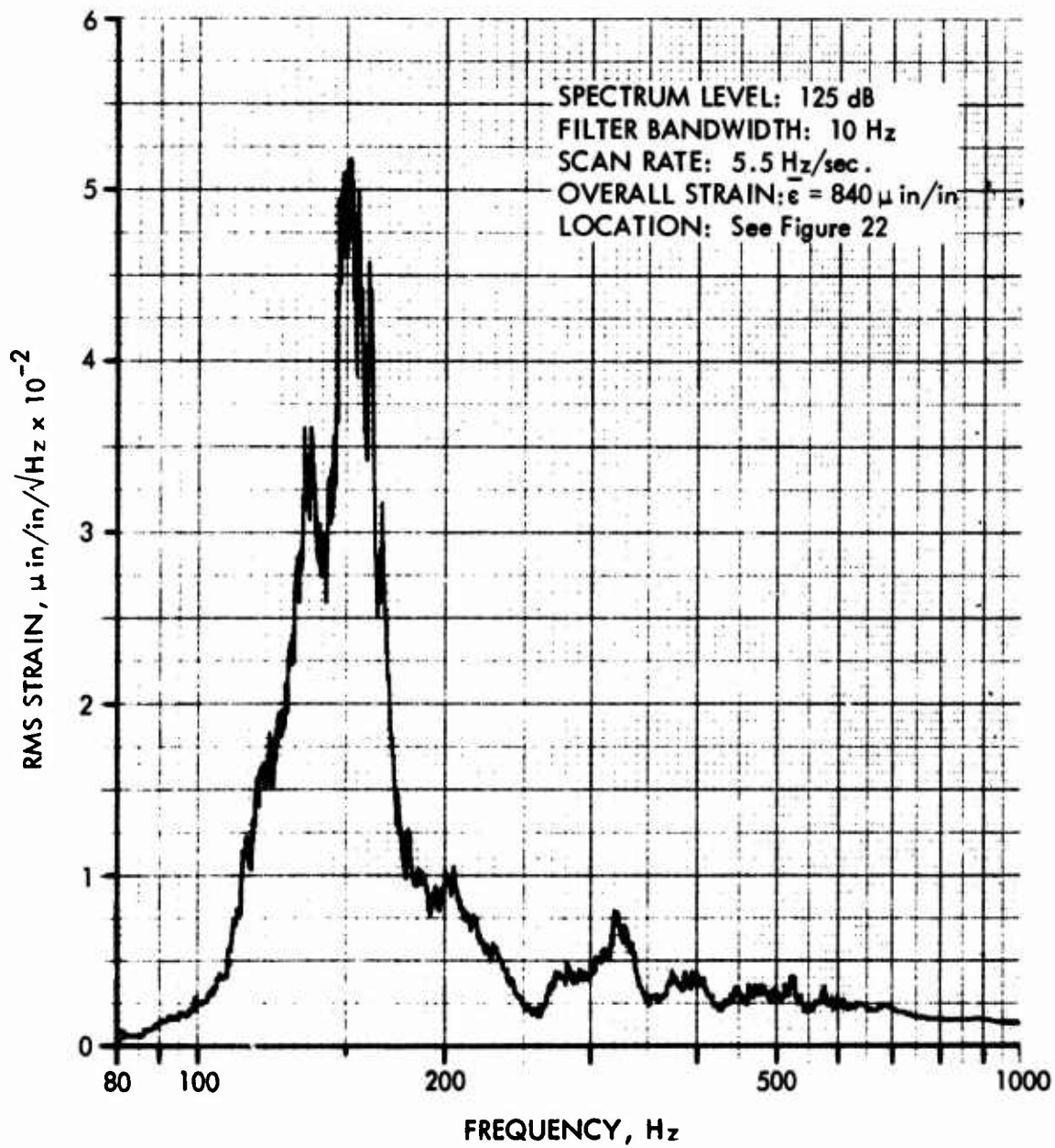
FIGURE 61 NARROW BAND STRAIN ANALYSIS: STRAIN GAGE 1, BX-4B
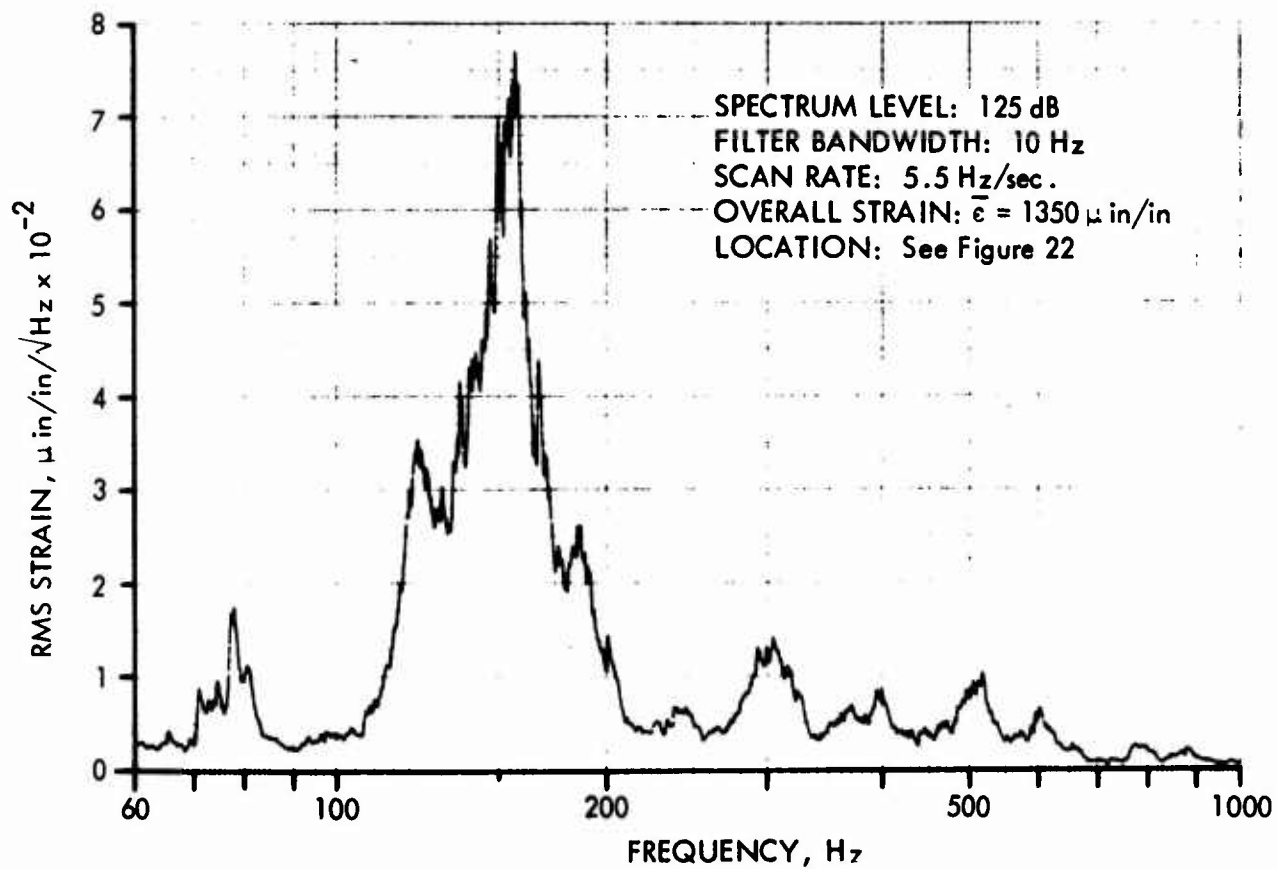
FIGURE 62 NARROW BAND STRAIN ANALYSIS: STRAIN GAGE 7, BX-4B
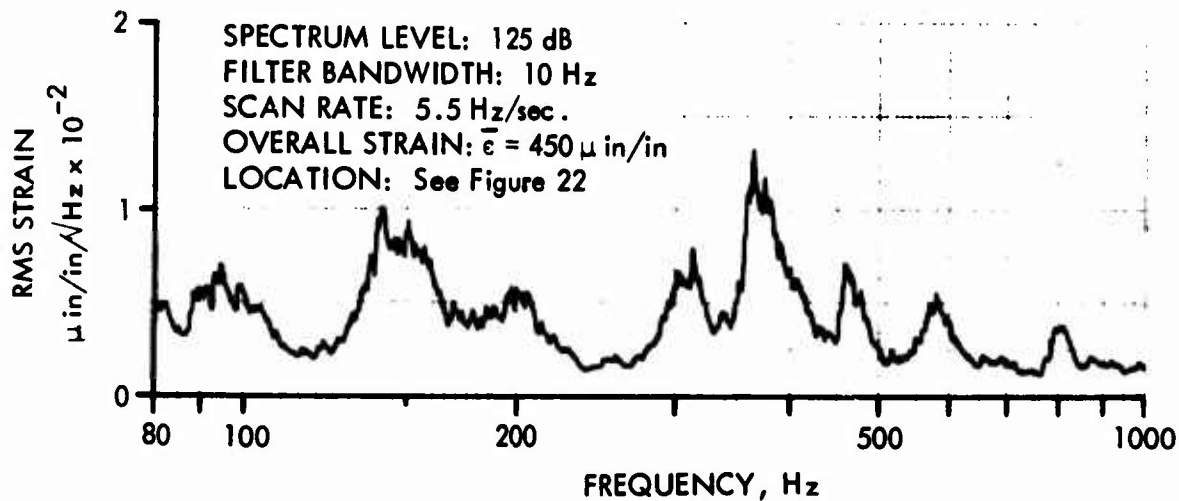
FIGURE 63 NARROW BAND STRAIN ANALYSIS: STRAIN GAGE 8, BX-4B
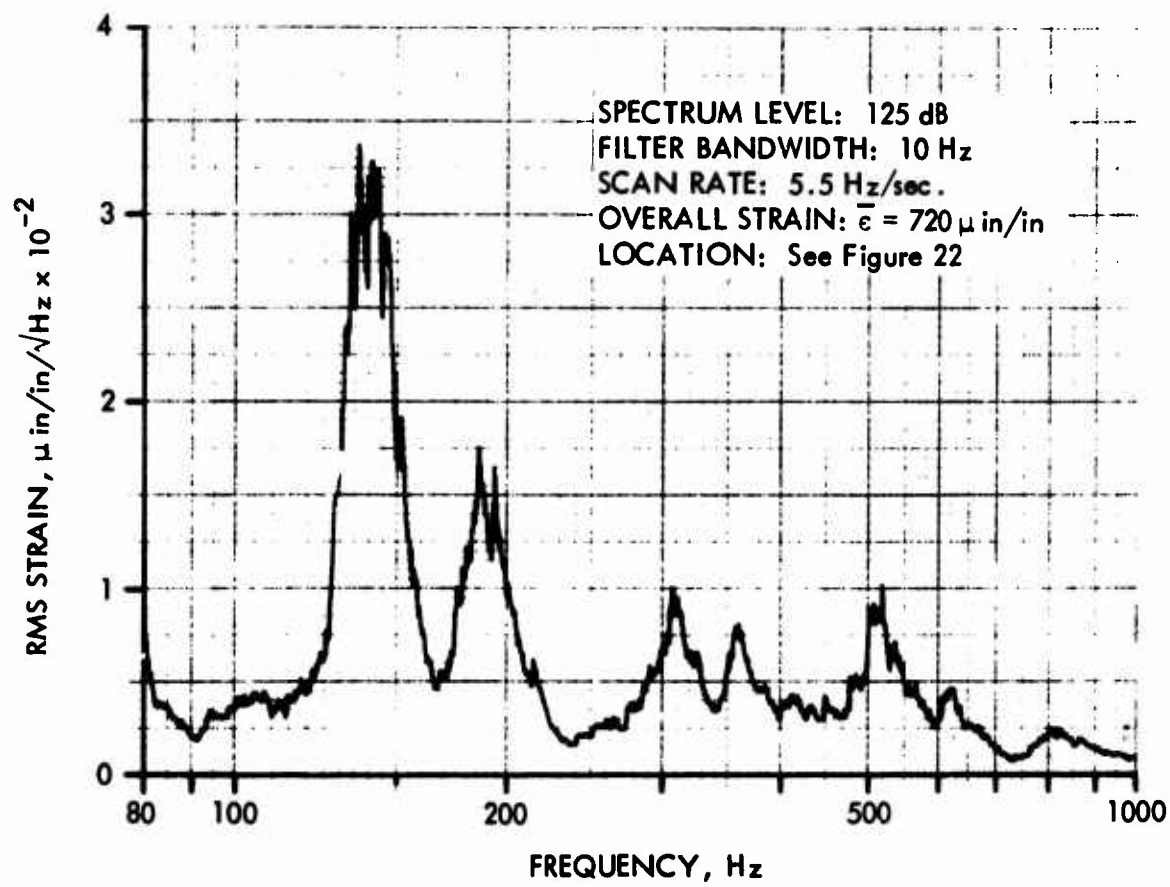
FIGURE 64 NARROW BAND STRAIN ANALYSIS: STRAIN GAGE 9, BX-4B

94
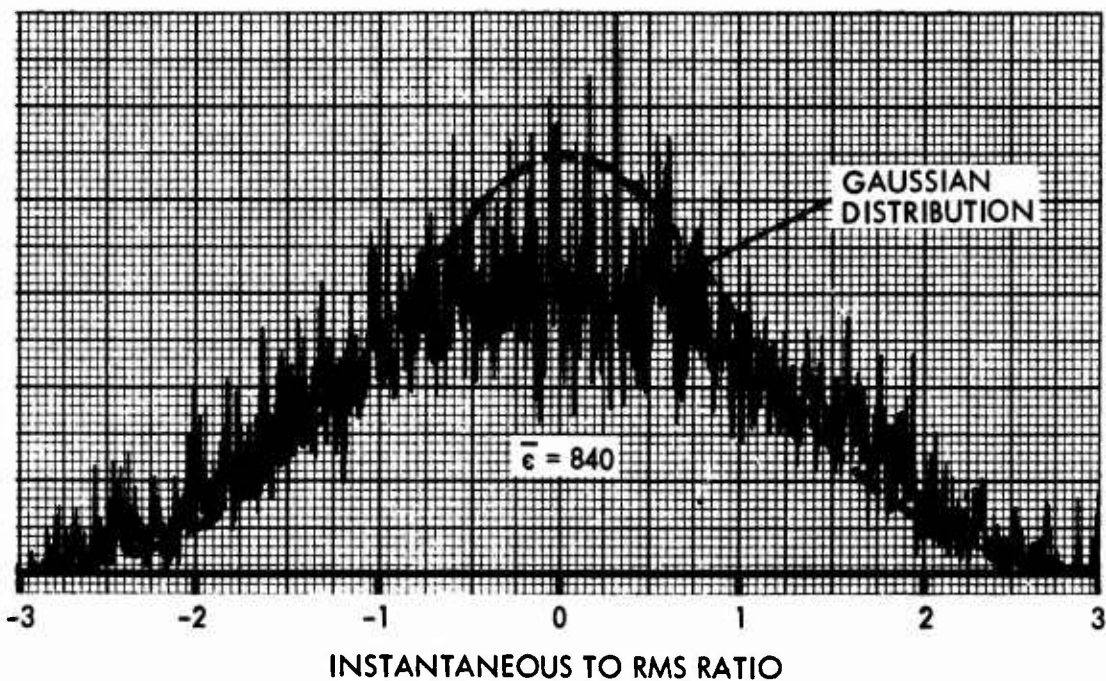
FIGURE 65 AMPLITUDE DISTRIBUTION OF STRAIN: STRAIN GAGE 1, BX-4B
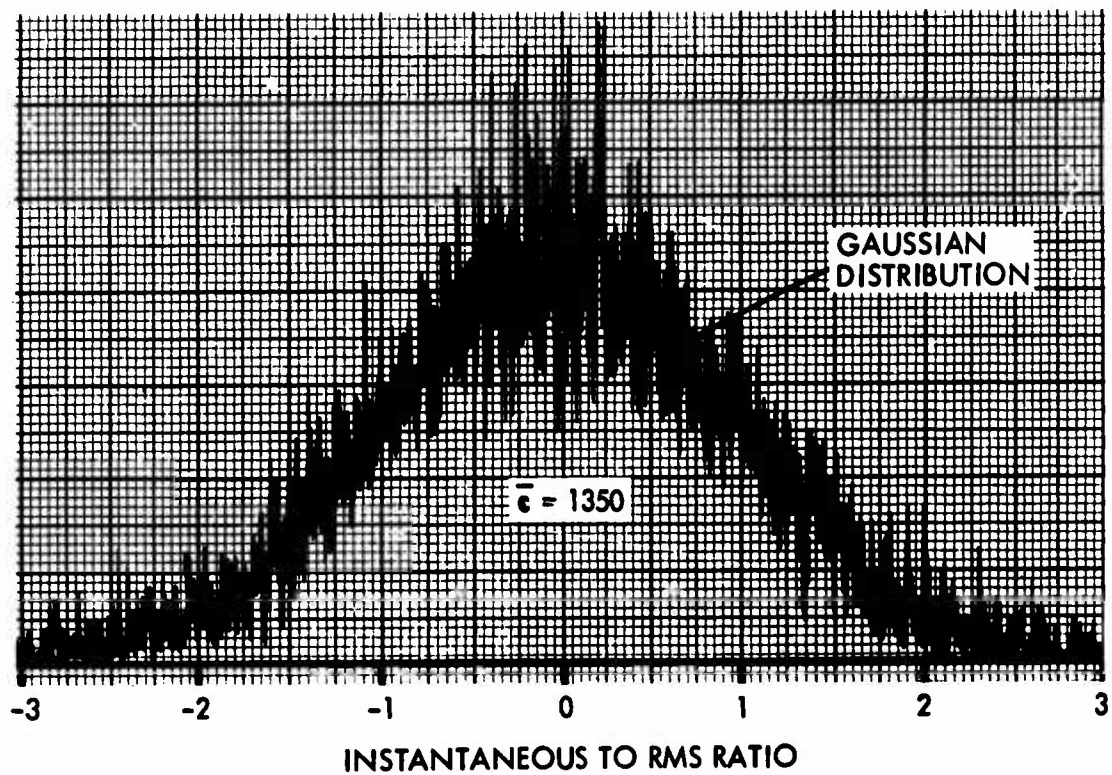
FIGURE 66 AMPLITUDE DISTRIBUTION OF STRAIN: STRAIN GAGE 7, BX-4B

95

GAUSSIAN DISTRIBUTION

$\overline{\epsilon} = 720$

INSTANTANEOUS TO RMS RATIO
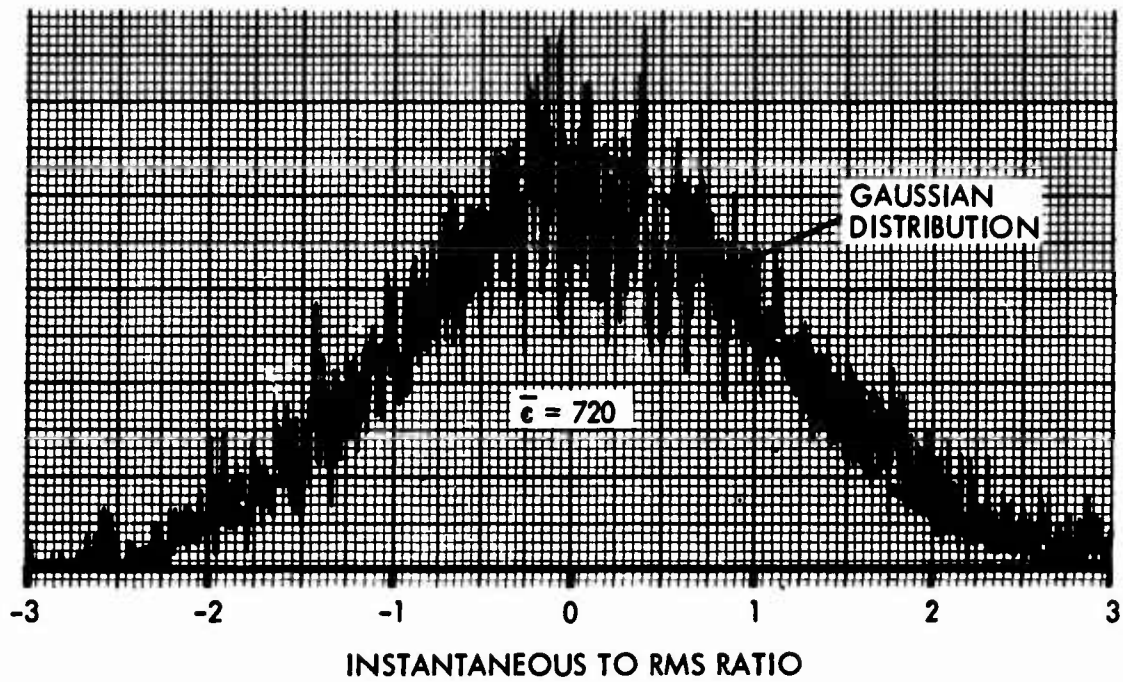
FIGURE 67 AMPLITUDE DISTRIBUTION OF STRAIN: STRAIN GAGE 9, BX-4B

GAUSSIAN DISTRIBUTION

$\overline{\epsilon} = 450$

INSTANTANEOUS TO RMS RATIO
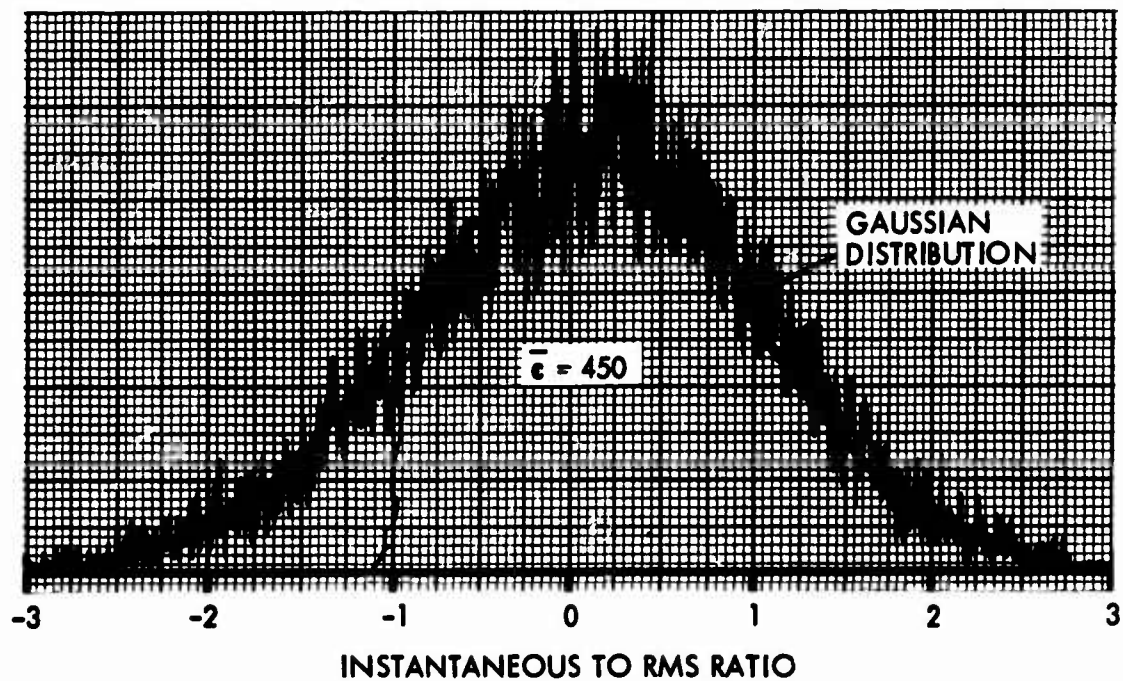
FIGURE 68 AMPLITUDE DISTRIBUTION OF STRAIN: STRAIN GAGE 8, BX-4B

96
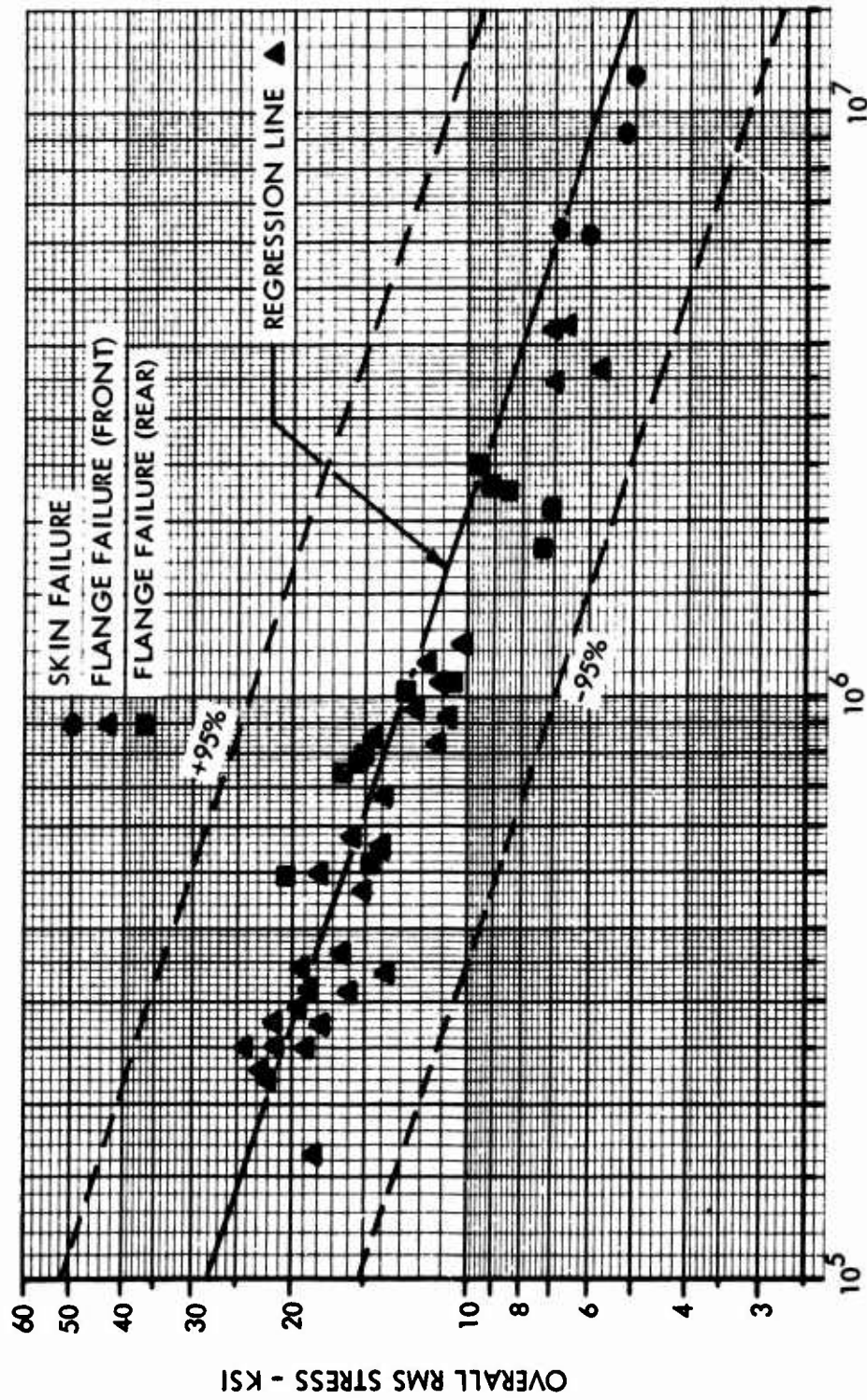
FIGURE 69 BOX SPECIMEN RIB FATIGUE CURVE

97

each recorded strain signal and the time failure was observed. The regression line and 95% confidence limits given in Figure 69 were computed as described in Appendix II, Reference 8. The highest correlation coefficient for these data was obtained by considering only failure data for strain gages located on the rib flange across the rivet line. The regression line and confidence limits illustrated in Figure 69 are established for these data only, although all failure data is plotted.

E.   Discussion of Test Results

1. Stiffened Panel Results

1.1 Modal Frequency Studies - For nine bay stiffened panels with the stringers much more flexible in bending and torsion than the ribs, it was expected that the center panel row between ribs (test area) would be the most responsive. This was, generally, the case. The predominant mode was a fundamental in each panel bay with adjacent bays out-of-phase (stringer torsion). The stringer bending mode (adjacent bays in phase) was observed as indicated in Table VIII; however, these modes were not so predominant as the stringer torsion modes. The reason for similar modes at different frequencies is due to the degree of coupling between adjacent bays influenced by the stringer bending – torsion characteristics. Acceleration measurements confirmed that the stringer deformation was basically a twist for all cross-section shapes considered.

A comparison of the frequencies determined in the mode study and the response frequencies determined from the high intensity size sweeps (Table X) show significant increases in modal frequency for the fatigue test configuration. This increase in frequency is attributed to temperature decrease (as much as 40°F) between the room in which the mode studies were conducted and the acoustic fatigue facility.

1.2 Frequency Sweeps - The high intensity sine sweeps were conducted to determine the specimen response in the fatigue test configuration. For all specimens the frequency range used to establish the excitation spectrum was based upon maximum strain response for strain gages located on the stringers. Strain gages on the skin generally had a similar frequency response as gages on the stringer (see Figure 24). However, if the mode study indicated that the panel bays across a frame exhibited appreciable out-of-phase response (reversed bending) a strain gage was located on the frame rivet line at the center of the span. These strain gages experienced a multi-mode response. High strain levels at the frame rivet line (short side of the center panel row) were experienced for both the fundamental mode of the center panel row and the mode for reversed bending of the skin across the frame.

1.3 Fatigue Tests - Two types of skin failure were commonly experienced during the fatigue testing of the stiffened panel specimens: the formation of fatigue cracks along a skin rivet line and fatigue failure of the fasteners (popped rivet heads). These types of failure occurred only along the frame rivet line for the specimens tested.

The failure experienced by design STR-31 influenced all subsequent panel designs. Figure 70 illustrates the fatigue failure mode of specimen STR-31A. For this design, the outer bays of the center panel row were of greater span than the center bay. The first observed failure occurred at the center of the rivet line on the short side (frame). The ends of the crack were drilled and a cold bonded metal patch was applied to the skin side. During subsequent testing, the cracks continued to propagate and the patch delaminated. The crack propagated very quickly along the edge of the panel and into the
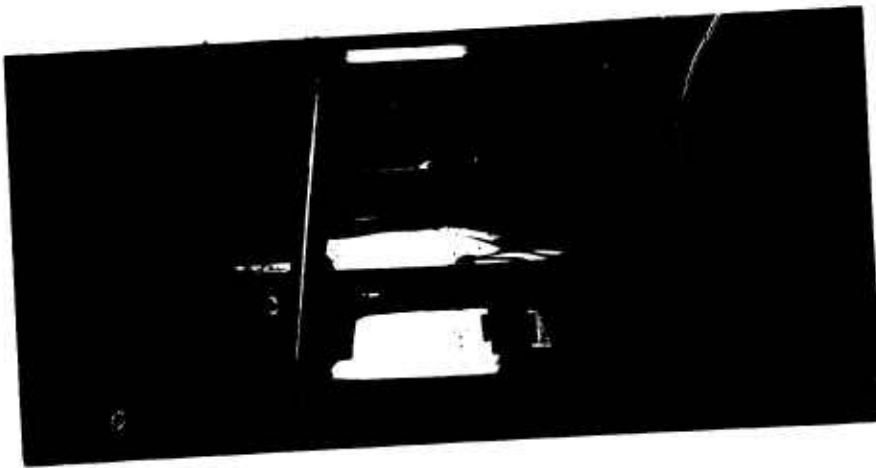
a) STIFFENER SIDE

b) SKIN SIDE

FIGURE 70 FATIGUE FAILURES FOR SPECIMEN STR-31A

center bay as illustrated. When the crack passed through the stringer, the flange failed as indicated in Figure 70. This failure was not considered to be valid since the failure did not originate in the center bay test area. To avoid this type of failure, it was decided that the center bay of the structure should be equal to or greater in area than the other bays. Since the total specimen size was determined by the test fixture, the center bay aspect ratio was a primary variable, and the nine bay configuration was desired, an angle brace was installed along the length of the outer bays of the center panel row. The brace comprised of an aluminum angle attached to the edge pan and riveted to the skin. This design change decreased the span of the outer bays so that the center panel bay had the greatest surface area. The brace is illustrated in Figure 15. It was installed on all designs except STR-37, -38, and -40 (see dimension 'a' Table V).

Two types of stringer failures were experienced for the specimens tested in this program: failure at the clip attachment to the frame and failure at the flange rivet line along the center of the stringer span. All designs tested experienced failures at the clip attachment to the frame. Only channel section stiffeners experienced fatigue failures at the mid-span of the flange rivet line. Figure 71 illustrates a typical clip attachment for zee section stringers: two rivets along the web height attaching the stringer to the clip. Channel section clip attachments were similar. The clip attachments for the hat section stiffeners used a right angle clip as illustrated in Figure 15.

Typical stiffener failures at the clip attachment are illustrated in Figure 72. Figure 72a is an overall view of the frame-stringer intersection from the skin side (skin removed) illustrating the failure mode. Typically, a crack would initiate at the rivet near the upper flange and propagate down the bend radius and across the upper flange. Figures 72b and 72c show closeup views of such failures for a channel section. The slight bow in the upper flange, as illustrated in Figure 72c, was apparently caused by local buckling of the flange after fatigue failure was complete. For this specimen, strain gages were installed on the web of the stringer aligned with the upper clip rivet. The strain gage axis is mounted parallel to the stringer axis on the side opposite to that illustrated (web axial gage (WA) - see Figure 21 and Table X). The center of the strain gage axis was approximately 0.5" in from the point at which the crack initiated. Figure 72d illustrates a typical stringer failure for a zee section for which the crack was allowed to propagate down the stringer web and flange rivet line. The strain gage installation at this failure was on the web axis between the rivet heads (overall rms stress 2.0 ksi). A strain gage mounted on the upper flange centered on the clip rivet line measured an overall rms stress of 4.0 ksi. Both of these strain gages were within 0.25" of the initial crack location. In Figure 72d, a portion of the flange has broken off (during testing) allowing the complete stringer failure to be viewed. Figures 71 and 72 illustrate the physical impossibility of locating a strain gage at the initial failure point; however, as indicated in Figure 44, the failure data for strain gages located on the flange and aligned with the stringer axis yielded the most significant data correlation. The measurement of the very steep strain gradients in the localized area of the stringer clip is a physically difficult problem that can only be resolved by additional testing.

The stringer flange failures at mid-span for the channel section are illustrated in Figure 73. This failure occurred independently of the failures illustrated in Figure 72a through 72c. Figure 73a is an overall view of the rib/frame assembly from the stiffener side (skin removed) and Figure 73b is a closeup view of the failure. In Figure 73b it is interesting to note that cracks initiated at the edge of the bucked rivet head rather than the rivet hole. The diagonal failure pattern is evidence of the complex strain field at this location on the stringer. The strain gage location is evident. It is believed that this type of failure was due to stiffener cross-section distortion in the plane of the stiffener cross-section. This type of failure was also observed on the flanges of the box-specimen structure.

100
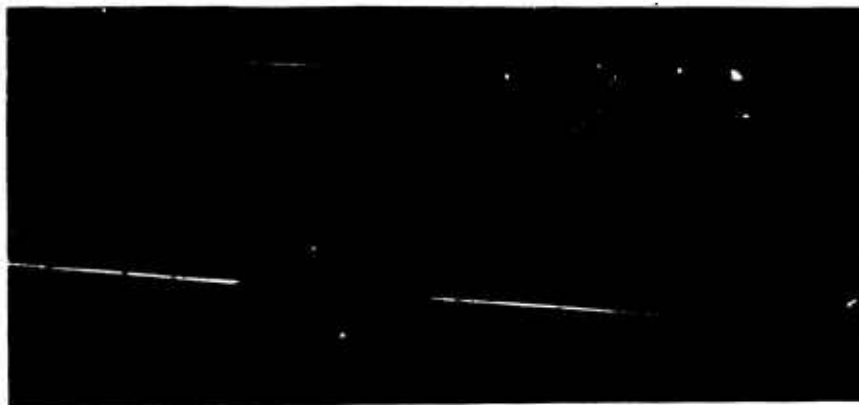
FIGURE 71 TYPICAL STRINGER CLIP ATTACHMENT
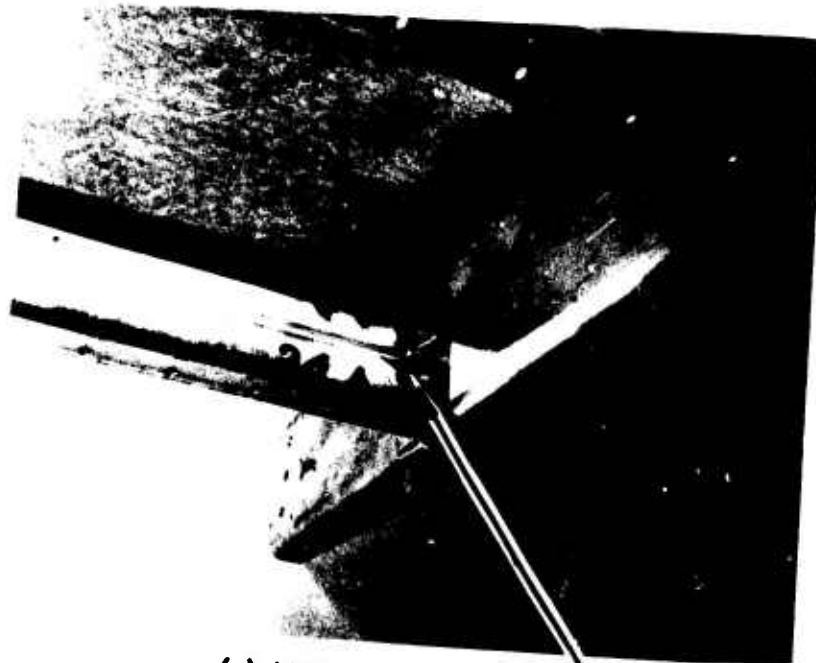
(a) VIEW FROM SKIN SIDE
(SKIN REMOVED)

(b) STRINGER BENT
TO EXPOSE CRACK
(OPPOSITE END)

(c) CLOSEUP VIEW OF FAILURE

FIGURE 72 TYPICAL STRINGER FAILURES AT CLIP
ATTACHMENTS

(d) FAILURE OF ZEE SECTION

(e) OVERALL SPECIMEN FAILURES

FIGURE 72 TYPICAL STRINGER FAILURES AT CLIP
ATTACHMENTS (CONCLUDED)

(a) OVERALL VIEW OF SPECIMEN
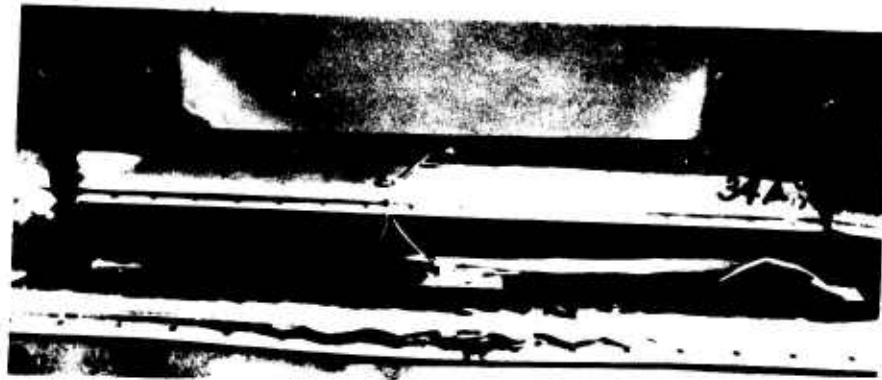
(b) CLOSEUP VIEW OF FLANGE FAILURE
(INDEPENDENT OF FAILURES AT CLIPS)

FIGURE 73 FLANGE FAILURE OF CHANNEL SECTION
STRINGER

Isolated stringer/frame clip fatigue failures were also observed during testing; however, these failures occurred after failure of the stringer. No fatigue failures of the ribs were recorded.

2. Box Specimen Structure

2.1 Modal Frequency Studies - The box specimen structure exhibited complex dynamic behavior. The analytical results described in Section II were an aid in the experimental investigation in that a uniform mode classification was developed. As indicated in Table XI, only a few modes could be excited and identified explicitly as coupled skin-rib modes. The degree of coupling between the skin and rib is proportional to the cube of the ratio of rib to skin thickness (see Equations 39 and 45). From Table VII, it can be seen that designs BX-1, -2, and -3 represent relatively thick ribs whereas designs BX-4, -5, and -6 represent relatively thin ribs (as compared to the skin thickness). Designs BX-1, -2, and -3 exhibited a higher degree of coupling between the skin and ribs than did designs BX-4, -5, and -6. The acceleration response of the cover sheet (front and rear) and ribs for designs BX-1, BX-2, and BX-3 was more highly coupled than that illustrated in Figures 45 through 53. Although the theory predicts that only odd number rib modes (across the structure height) would be excited by the out-of-phase condition (Equation 46), all modes were excited to some extent for all speaker conditions. The only significant difference in response was observed for the rear cover sheet with excitation on the front side. As would be expected, the rear surface response was significantly less (one half to one third) than that measured on the front cover sheet for one-sided excitation (see Figure 51).

2.2 Frequency Sweeps - For each specimen, high intensity sine sweeps were conducted to determine the specimen response in the fatigue test condition. For all specimens, the frequency range used to establish the excitation spectrum was based upon maximum strain response for strain gages located on the rib. For designs BX-1, -2, and -3 maximum rib strain response occurred at the center of the rib (strain gage 8, Figure 22). For designs BX-4, -5, and -6 maximum rib strain response occurred at the rib flange next to the front surface (exposed to excitation). Strain gages located across the frame rivet line exhibited very high response due to reversed bending of the skin across the frame (see Table VII). All strain gages exhibited predominant response in the frequency intervals listed in Table XIII. Comparing the modal frequencies listed in Table XI with the response frequencies given in Table XIII, the general increase in modal frequencies indicated is attributed to the temperature difference between the two rooms in which the tests were conducted as described for the stiffened panel specimens.

2.3 Fatigue Tests - For acoustic fatigue testing the box specimen structure was mounted in the test section side wall so that only one side (front) was exposed directly to the random noise. For all specimens skin failures were observed only on the front surface. Two types of skin failure were commonly experienced during the fatigue testing of box structure: the formation of fatigue cracks along a skin rivet line and fatigue failure of the fasteners (cracked and/or popped rivet heads). The skin failures occurred only for the designs BX-1, -2, and -3. Figure 74 illustrates typical skin failures for specimens BX-1A, BX-1B, BX-2A, and BX-3B. The location and extent of the skin failure is outlined for each specimen. No rib failures were observed for designs BX-1, -2, and -3.

Rib fatigue failures were observed for designs BX-4, BX-5, and BX-6. No skin fatigue failures for these designs were observed. The type of rib failure observed is illustrated in Figure 75 for specimen BX-5B. Figure 75a illustrates the complete specimen with the front skin removed. The fatigue failure of the ribs was complete along the entire rib length. Figure 75b is a closeup view of a center rib illustrating the failure of both rib

a) SKIN FAILURES: SPECIMEN BX-1A
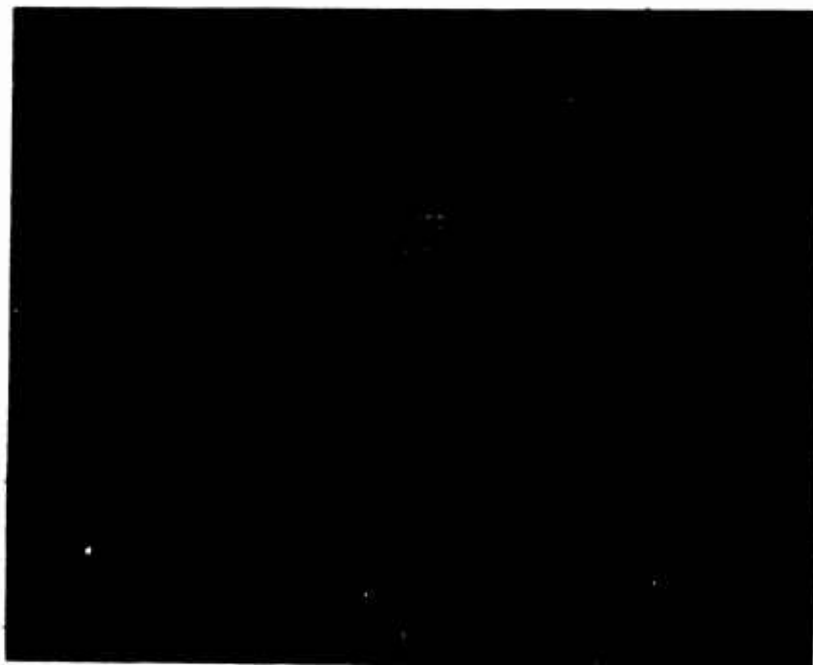
b) SKIN FAILURES: SPECIMEN BX-1B

FIGURE 74 TYPICAL SKIN FATIGUE FAILURES FOR
BOX STRUCTURE

c) SKIN FAILURES: SPECIMEN BX-2A
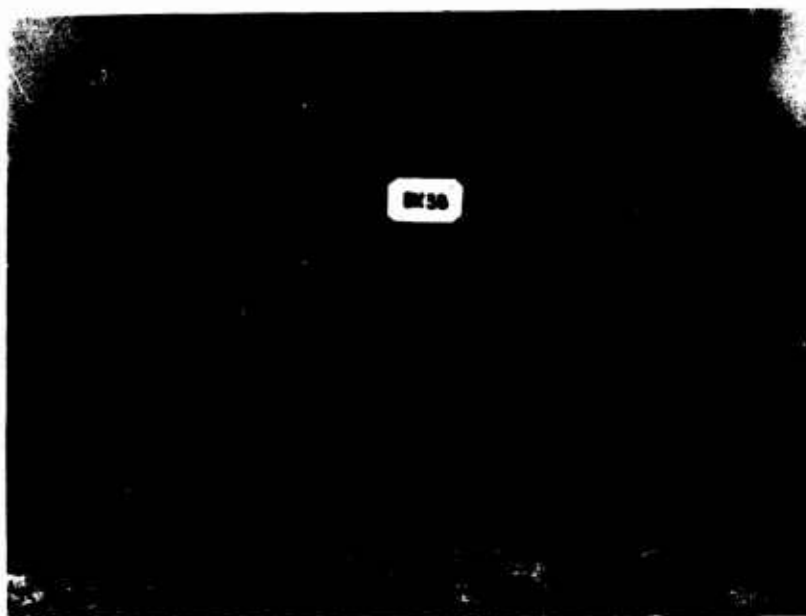
d) SKIN FAILURES: SPECIMEN BX-3B

FIGURE 74 TYPICAL SKIN FATIGUE FAILURES FOR
BOX STRUCTURE (CONCLUDED)
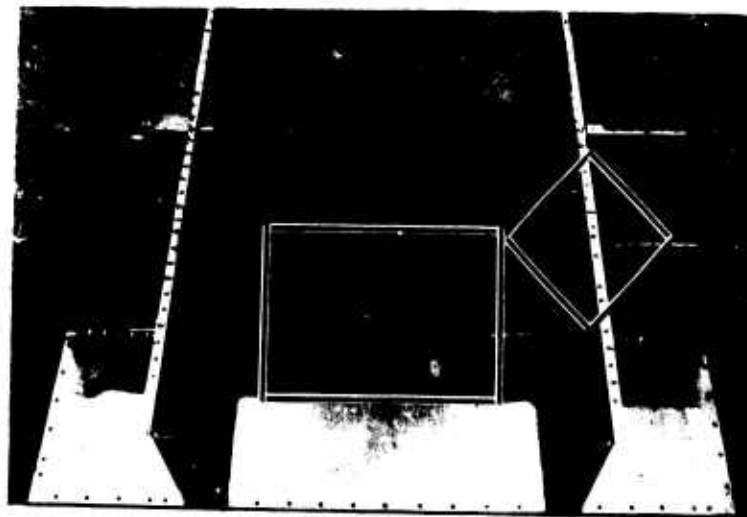
a) TYPICAL RIB FLANGE FAILURE: SPECIMEN BX-5B (SKIN REMOVED)
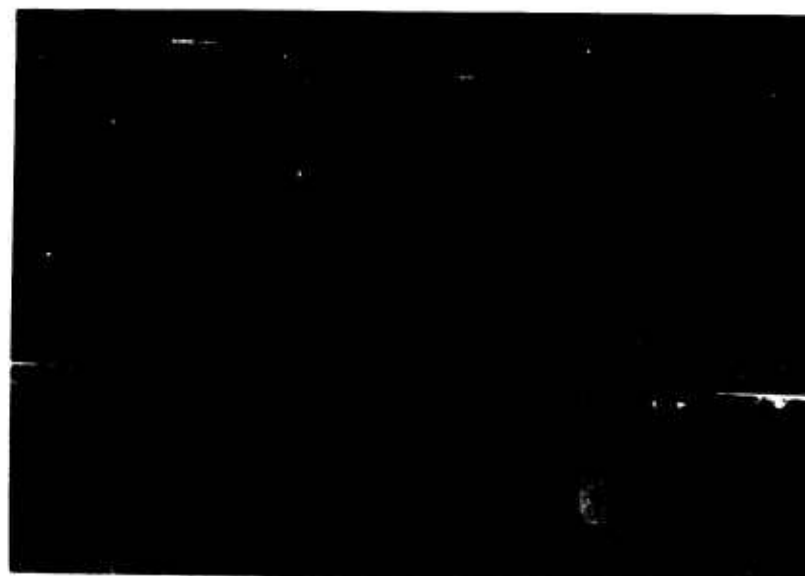
b) CENTER RIB ILLUSTRATING FLANGE FAILURE: SPECIMEN BX-5B

FIGURE 75 TYPICAL RIB FLANGE FATIGUE FAILURES: SPECIMEN BX-5B
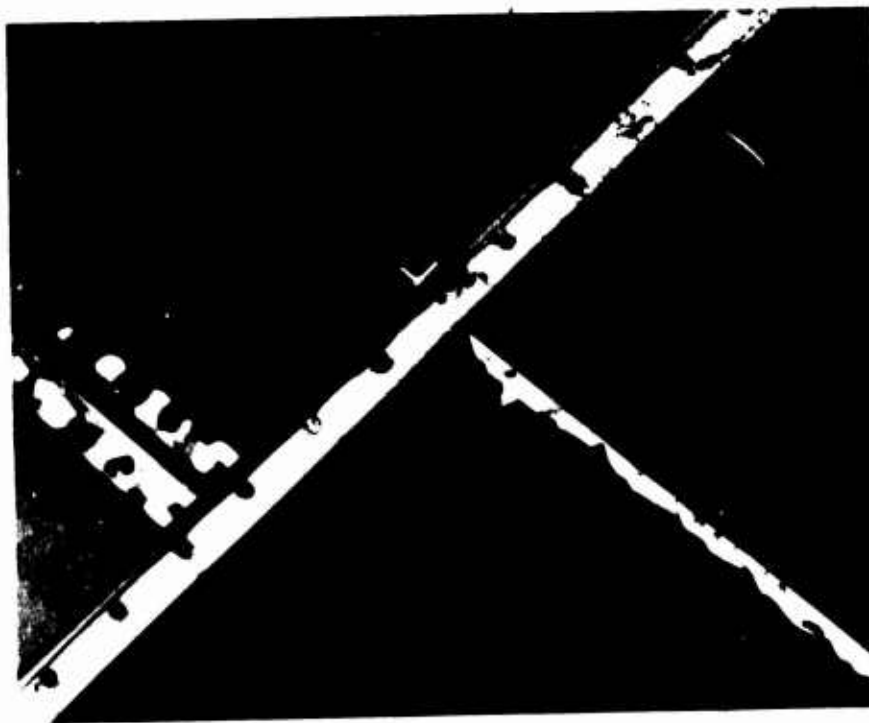
c) RIB/FRAME INTERSECTION: SPECIMEN BX-5B

FIGURE 75 TYPICAL RIB FLANGE FATIGUE FAILURES:
SPECIMEN BX-5B (CONCLUDED)

flanges. This failure is typical of designs BX-4, -5, and -6 in that rib flange fatigue was experienced on flanges next to the front and rear skins. Figure 75c is a closeup of the rib/frame intersection. No fatigue failures of the rib were observed at locations other than the flange and no frame fatigue failures were observed for all box specimen structure tested.

The obvious conclusion to be made from the box structure fatigue tests is the importance of designing the structure so that the rib and skin are highly coupled dynamically. This will be achieved by selecting rib and frame thickness identical to the skin thickness. To emphasize this point, Table XIV represents a summary of overall rms strain response for the box structure designs tested. It is seen that the strain response of designs BX-1, -2, and -3 is more uniformly distributed than for designs BX-4, -5, and -6.

TABLE XIV

OVERALL STRAIN DISTRIBUTION FOR BOX STRUCTURE
(See Figure 22)

Overall RMS Strain, Micro-inch/inch
Strain Gage Number

Specimen	1	2	4	7	10	8	11	9	12	15
BX-1A	580	550	—	480	500	500	500	—	—	—
BX-1B	900	610	530	—	—	—	515	—	—	—
BX-2A	495	—	530	—	—	—	—	—	—	—
BX-2B	595	560	600	—	—	490	500	—	—	—
BX-3A	420	505	500	500	470	—	430	475	—	—
BX-3B	480	495	490	—	—	140	—	—	—	490
BX-4A	520	360	580	640	680	240	350	220	320	110
BX-4B	840	600	750	1350	1050	450	400	720	800	500
BX-5A	—	700	1200	2150	2050	—	—	1800	1550	800
BX-5B	—	620	800	1200	1050	920	—	1500	1300	460
BX-6A	1150	520	520	1500	1100	—	700	720	580	460
BX-6B	1050	560	950	1800	1750	—	—	1600	2000	580

110

IV – TEST DATA CORRELATION

A. Introduction

The analysis presented in Section II suggests ways of correlating the test data presented in Section III for the stiffened panel stringer specimens and the nine-cell box structure specimens. The first mode response was in general the most predominant mode for each type of structure. For the stiffened panel specimens, stringer fatigue failures occurred at the clip attachment and skin fatigue failures occurred at the frame rivet line. Fatigue failures for box structure occurred at the frame and rib rivet lines for the skin and along the flange rivet line for the ribs. All skin fatigue failures for both types of structure fell within the 95% confidence limits established by Ballentine for aluminum plate fatigue failure (Reference 8, Figure 34, p. 91) indicating the validity of Ballentine's design nomograph (Reference 8, Figure 73, p. 151) for establishing skin thickness for the types of structure considered here.

The data correlation presented here is concerned with stringer fatigue failure at the clip attachment and flange fatigue failure for the deep plate-like ribs of the box structure. The approach taken for data correlation is somewhat different than that described by Ballentine in that overall rms stress is calculated using Equation 3 where the frequency and static stress estimate are calculated using the appropriate expressions from the analysis and the spectrum level of the excitation and damping values are taken from the experimental data. The resulting values of overall rms stress are then correlated with the measured overall rms stress (strain) to obtain an empirical expression for overall rms stress. This approach is open to question since scatter exists for the fatigue data (which is assumed to be error free for this correlation).

B. Stiffened Panel Stringer Fatigue Correlation

Average overall rms stress levels for the stringers were calculated using the experimental data presented in Table X. These values, denoted by $\overline{\sigma}_e$, are assumed to be error free. Values for the response frequency of the (1,1) mode (stringer-torsion) were calculated using Equations 25 and 26 and values for the stringer stress due to a uniform static pressure of unit magnitude were calculated using Equation 35 for each panel design. Using the experimental values for damping (Table IX) and rms sound pressure spectrum level (Table X), overall rms stress levels were calculated using Equation 3. These values, denoted by $\overline{\sigma}_c$, are assumed to be inaccurate due to discrepancies in estimating the frequency and static stress response. Table XV lists the two variables $\overline{\sigma}_c$ and $\overline{\sigma}_e$ for the various specimen designs. These data are plotted in Figure 76.

111
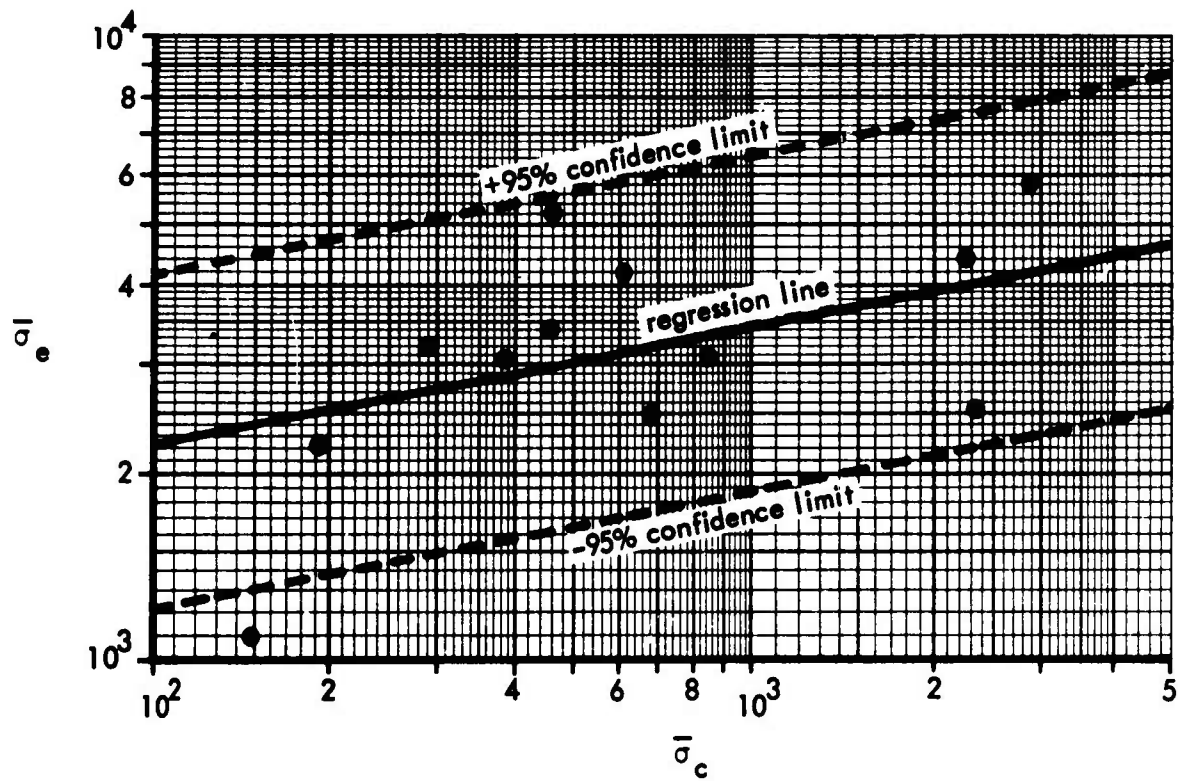
FIGURE 76 CALCULATED VERSUS MEASURED OVERALL RMS
STRESS: STIFFENED PANEL STRINGERS

TABLE XV

DATA FOR STRESS CORRELATION: STIFFENED PANEL STRINGERS

Specimen	$\overline{\sigma}_c \times 10^{-2}$	$\overline{\sigma}_e \times 10^{-2}$
STR-31	4.582	52.0
STR-32	8.420	31.0
STR-33	1.942	22.5
STR-34	4.597	34.0
STR-35	1.498	11.0
STR-36	3.820	32.0
STR-37	23.330	25.5
STR-38	6.050	42.0
STR-39	22.450	42.0
STR-40	28.440	58.0
STR-41	6.790	25.0
STR-42	2.900	32.0

From the data listed in Table XV, the correlation coefficient was established as 0.5754 for the twelve degrees-of-freedom. This level of data correlation is not very significant (one chance out of fifty that there is no correlation). The equation for the regression line is established as

$$\overline{\sigma}_e = 0.9 \, (\overline{\sigma}_c)^{1/5}, \text{ ksi} \tag{65}$$

The regression line and 95% confidence limits are presented in Figure 76.

C. Box Structure Flange Fatigue Correlation

Average overall rms stress levels for the rib flange were calculated using the experimental data presented in Table XIV. These values, denoted by $\overline{\sigma}_e$, are assumed to be error free. Values for the frequency of the (1,1,1) mode was calculated using Equations 44 and 45 and the static stress response to a uniform pressure of unit magnitude at the mid span of the flange was calculated using Equations 48b and 49. With these data, modal damping data (Table XII) and rms sound pressure spectrum level (Table XIII), the overall rms stress levels were calculated using Equation 3. These values, denoted by $\overline{\sigma}_c$, are assumed to be inaccurate due to discrepancies in estimating the frequency and static stress response. Table XVI lists the two variables $\overline{\sigma}_c$ and $\overline{\sigma}_e$ for the various specimen designs. These data are plotted in Figure 77.
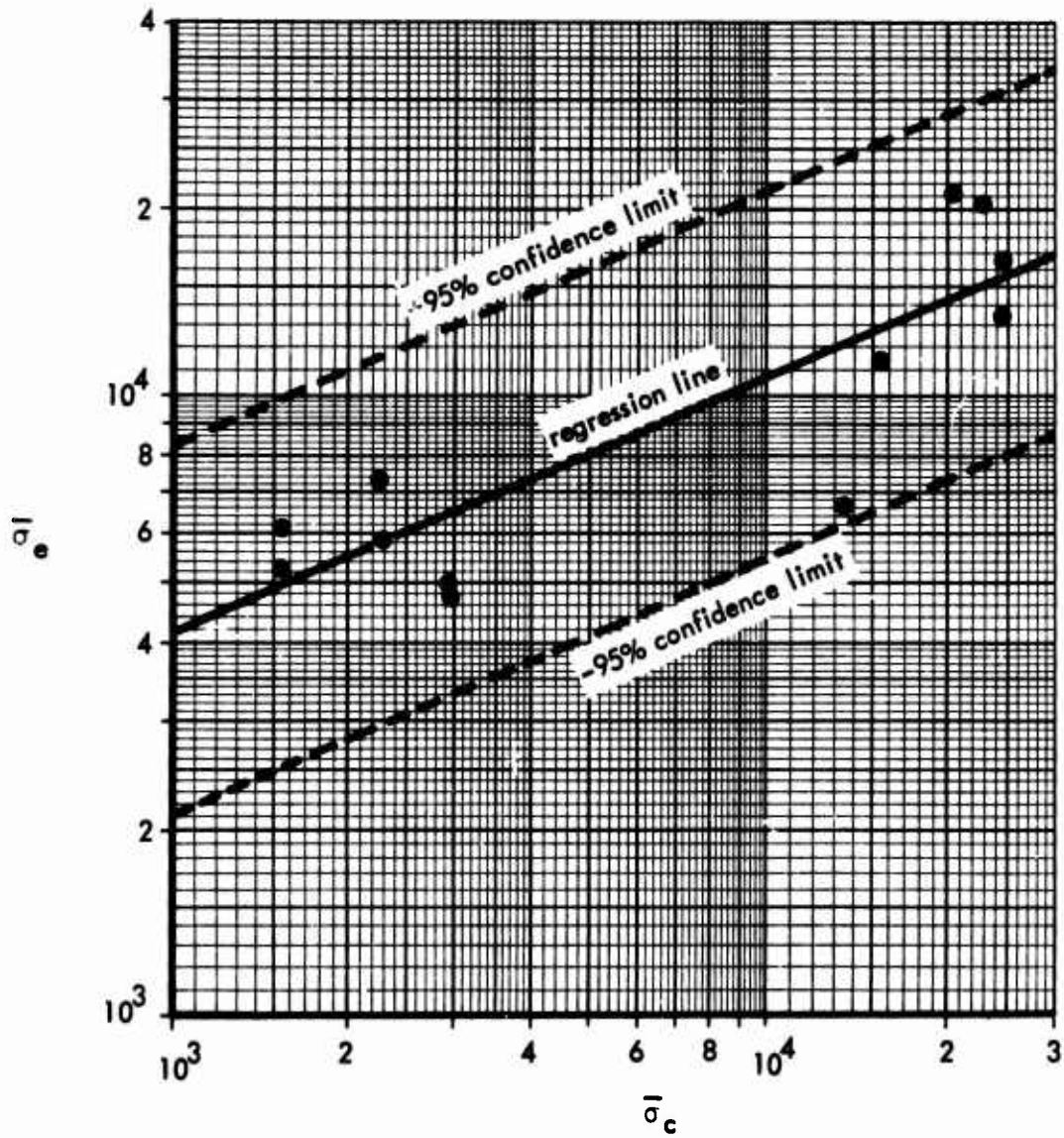
FIGURE 77   CALCULATED VERSUS MEASURED OVERALL RMS
STRESS: BOX STRUCTURE RIB FLANGES

114

TABLE XVI

DATA FOR STRESS CORRELATION: BOX STRUCTURE FLANGES
(FLANGES ON THE EXCITATION SIDE)

Specimen	$\bar{\sigma}_c \times 10^{-3}$	$\bar{\sigma}_e \times 10^{-3}$
BX-1A	2.2897	5.974
BX-1B	2.2897	7.365
BX-2A	1.5692	5.279
BX-2B	1.5692	6.154
BX-3A	2.8650	4.738
BX-3B	2.8650	5.996
BX-4A	13.5056	6.625
BX-4B	15.2012	11.580
BX-5A	20.2210	21.130
BX-5B	22.7599	20.300
BX-6A	24.8750	13.583
BX-6B	24.8750	16.840

From the data listed in Table XVI, the correlation coefficient was established as 0.862 for the twelve degrees-of-freedom. This level of correlation is significant (better than one chance out of one thousand that there is no data correlation). The equation for the regression line is established as

$$\bar{\sigma}_e = 0.245(\bar{\sigma}_c)^{.411}, \text{ ksi} \tag{66}$$

The regression line and 95% confidence limits are presented in Figure 77.

V - DEVELOPMENT OF DESIGN EQUATIONS AND NOMOGRAPHS

A. Introduction

The information required to produce a design nomograph for a specific type of structure is an analytical expression for the stress which is caused by the random acoustical excitation and the allowable fatigue stress and life relationship. The analytical expressions developed in Section II for frequency and stress at a point on the structure were modified empirically by the data correlation in Section IV.

To be useful and practical, a design nomograph also must be as free as possible of complexities, easy to use, and give an accurate representation of the test results from which it was derived. The expressions for estimating the natural frequency of the fundamental mode for the stiffened flat panel and box structure configuration are too complex to be presented in the form of a nomograph. Estimates for the modal stiffness and the modal mass can be readily obtained using the appropriate equations in Section II for any mode desired. For extensive parameter studies, computer programs have been developed, based upon the theory presented in Section II, for estimating the frequencies for stiffened flat panels, box structure, and a three-cell wedge structure. These computer programs and a description of the data input format are presented in Appendix IV.

B. Flat Stiffened Panels

1. Skin Design

The geometry and nomenclature for a bay of stiffened panel structure is presented in Figure 78. All skin failures were observed to fall within the confidence limits established by Ballentine for aluminum skin (Reference 8, Figure 73, p. 151). Ballentine's design nomograph is reproduced as Figure 79. An example problem is included.

2. Stringer Flange Stresses

The random acoustic pressures on the surface of a bay of stiffened panel structure are transferred to the supporting structure predominantly by a transverse shear loading. This loading causes the thin-walled open-section stiffeners to bend and twist. The stringer loading is reacted along the skin-stringer rivet line and the clip attachments of the frame and stringer. The stringer stress AT THE CLIP ATTACHMENT is estimated by the equation

$$\bar{\sigma}_c = \frac{\sqrt{(f_1/\zeta_1)} h b^3}{I^* [(b/a) + (a/b)]} S_p(f_1) \tag{67}$$

$$I^* = (I_{xx} I_{zz} - I_{xz}^2)/I_{zz}$$

for the fundamental mode, f_1, of the panel. The frequency of the fundamental mode, f_1, is obtained by using Equations 22 and 23 for $m = n = 1$. The damping ratio, ζ_1, can be estimated as 0.01 to 0.02 in the absence of experimental data.
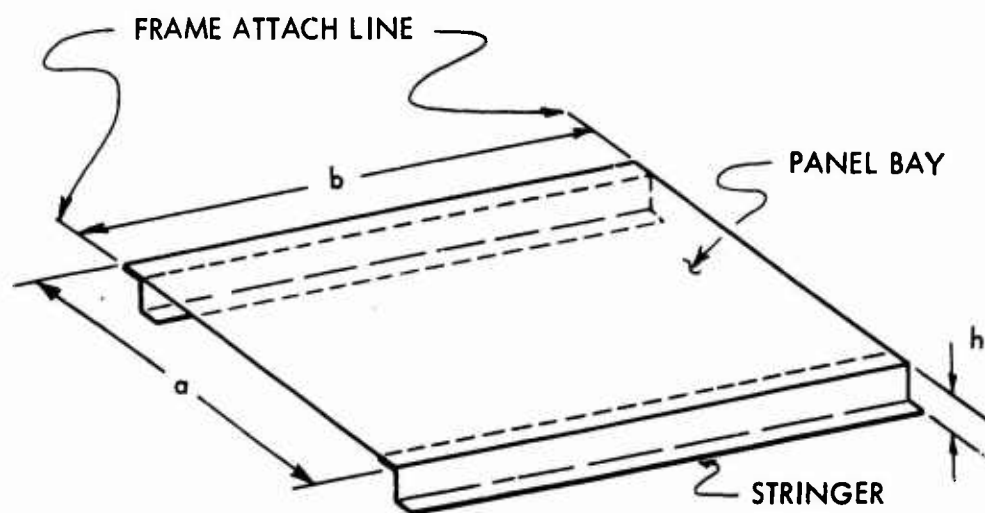
FIGURE 78 STIFFENED PANEL BAY AND STRINGER NOMENCLATURE

117

SPECTRUM LEVEL, db

120
124
128
132
136
140
144
148

DAMPING RATIO, ξ

.012
.032

STEPS OF .004

PANEL WIDTH, a, INCHES

10.0
9.0
8.0
7.0
6.0
5.0
4.0
3.0

SKIN THICKNESS, t

.100 .090
.080 .071
.064
.050
.040
.032
.025
.020

REFLECTING LINE

-95% CONFIDENCE LIMIT
-50% CONFIDENCE LIMIT
+50% CONFIDENCE LIMIT
+95% CONFIDENCE LIMIT

10^9
10^8
10^7
10^6

CYCLES TO FAILURE
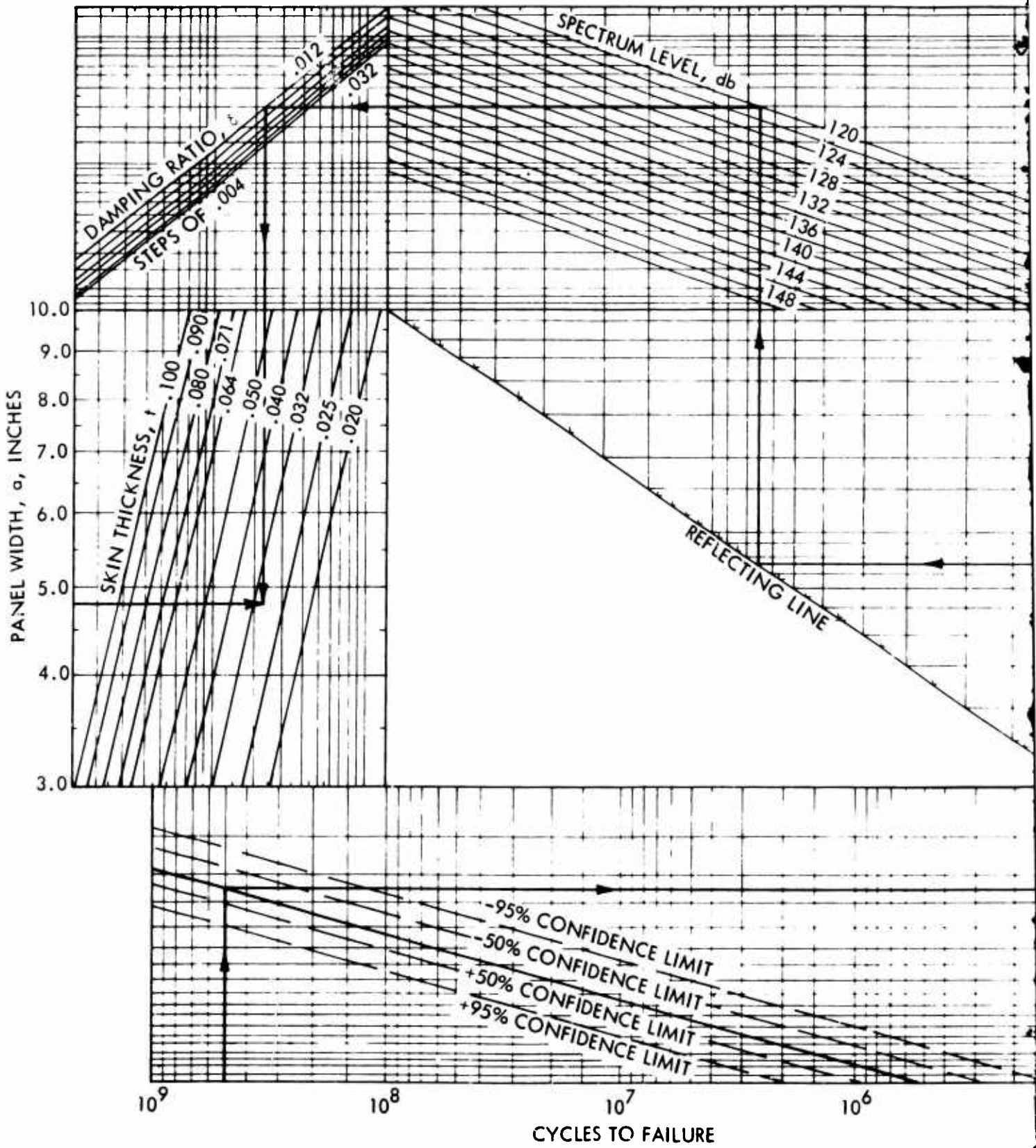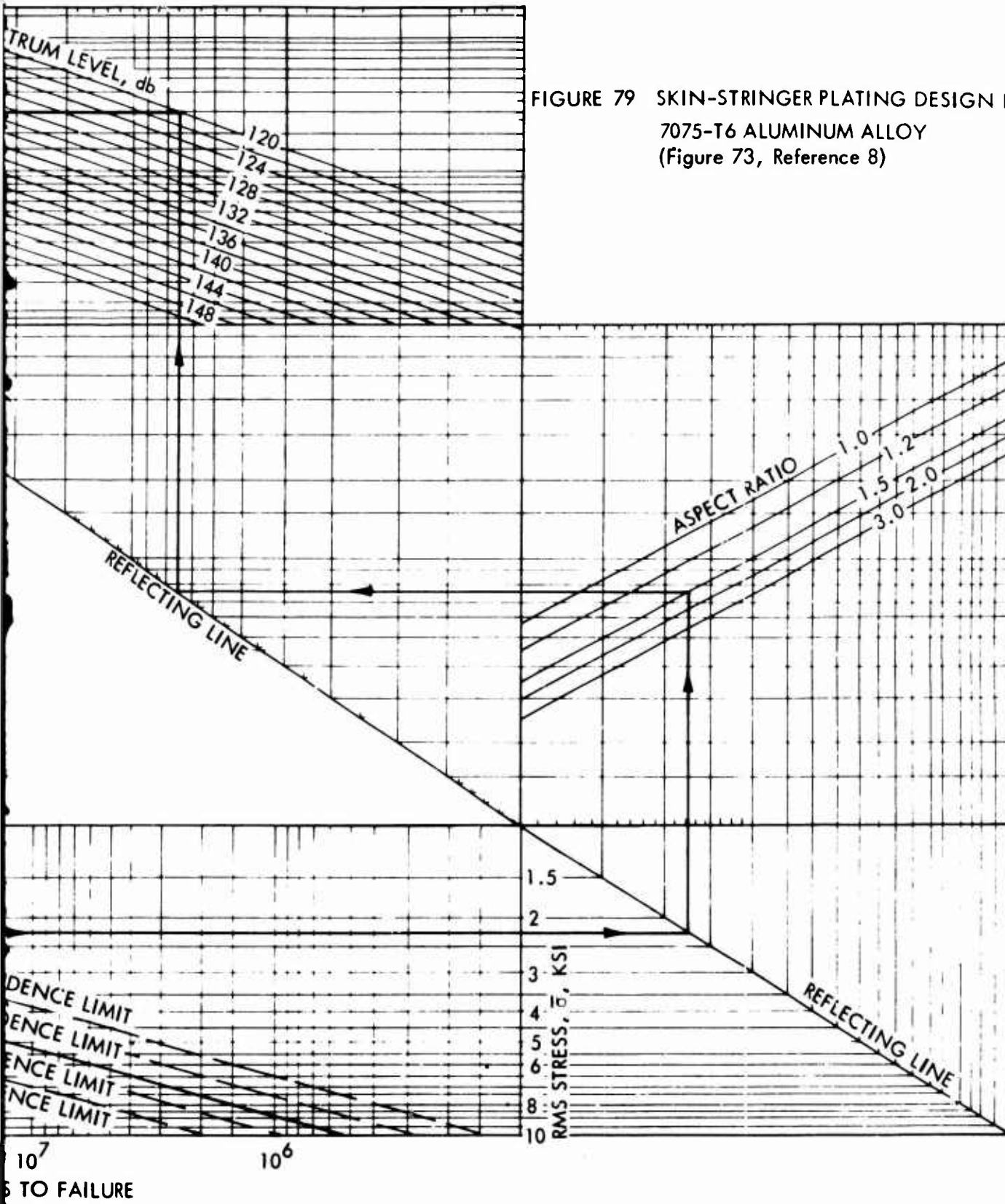
FIGURE 79 SKIN-STRINGER PLATING DESIGN NOMOGRAPH
7075-T6 ALUMINUM ALLOY
(Figure 73, Reference 8)

119

The sound pressure spectrum level, $S_p(f_1)$, for the fundamental mode is expressed in units of pressure as

$$S_p(f_1) = 2.91 \times 10^{(spl/20-9)} \text{, lbs/in}^2/\sqrt{Hz} \tag{68}$$

where spl is the spectrum level in dB

From the empirically derived expression for stress, Equation 65, the estimated stress in the stringer flange at the clip attachment is obtained.

EXAMPLE: Consider a stiffened panel with the following data -

a = 9.0 in b = 18.0 in t = 0.040

h = 1.25 in I^* = 0.01255 in.^{4} (-4 zee section, Table VI)

f_1 = 148 Hz   (from Equations 22 and 23)

S_p = 0.01158   (from Equation 68, spl = 132 dB.)

ζ_1 = 0.015   (estimated)

$(b/a) + (a/b)$ = 2.50

Then, $\overline{\sigma}_c$ = 5.16 (from Equation 67)

and $\overline{\sigma}_e$ = 4.64 ksi (from Equation 65).

From, Figure 44, the cycles to failure, N_c, estimated to be 1.22×10^6. From Figure 79, and the above data the number of cycles to failure are estimated to be 2.2×10^7 cycles.

The above procedure should be repeated until the desired fatigue life for the skin and the stringers is achieved.

C. Box Structure

1. Box Structure Skin and Rib Flange Stresses

To calculate the stresses in the skin and rib flanges for a box structure, the design procedure utilizes Timoshenko's approximate technique for computing stresses in continuous supported panels (Section II.D.4), the frequency estimate for the (1,1,1) mode (Equations 44 and 45), and the empirically determined expression for stress given by Equation 66. The method is best illustrated by an example.

EXAMPLE: Consider the data for specimen BX-1 (Table VII). From Equations 48a and 48b, the bending moment at the middle of the short side of the center bay is given by

$$M_y = ((0.0575)(100) + (0.0575)(100))/3 = 3.84$$

121

and at the middle of the long side of the center bay

$$M_x = ((0.065)(121) + (0.082)(100))/3 = 5.35$$

for a uniform pressure of unit magnitude over the surface of the structure.

To obtain stress in the skin, frame flange, and rib flange, one uses Equation 49. For the skin at the middle of the short side (frame line) of the center bay the skin stress response is

$$\overline{\sigma}_1 = (6.0)(3.84)/(0.063)^2 = 5800 \text{ psi},$$

and the frame flange stress response is

$$\overline{\sigma}_2 = (6.0)(3.84)/(0.080)^2 = 3600 \text{ psi}.$$

For the skin at the middle of the long side (rib line) of the center bay the skin stress response is

$$\overline{\sigma}_3 = (6.0)(5.35)/(0.063)^2 = 8080 \text{ psi},$$

and the rib flange stress response is

$$\overline{\sigma}_4 = (6.0)(5.35)/(0.063)^2 = 8080 \text{ psi}.$$

From Equations 44 and 45 the frequency of the fundamental, $(1,1,1)$, mode is estimated to be 79.0 Hz. For this example, the damping ratio is estimated to be 0.020 for the entire structure, and a sound pressure spectrum level of 124 dB/$\sqrt{}$Hz. is assumed. From Equation 3, one obtains the expression (ignoring the constant)

$$\overline{\sigma}_{ci} = \sqrt{(f_1/\varsigma_1)} \, S_p(f_1) \overline{\sigma}_i; \tag{69}$$

Then, for the above data

$$f_1 = 79.0, \text{ Hz.} \qquad \varsigma_1 = 0.020 \qquad S_p(f_1) = 0.00462$$

so that

$$\overline{\sigma}_{c1} = (62.8)(.00462)(5800) = 1682 \text{ psi},$$

$$\overline{\sigma}_{c2} = (62.8)(.00462)(3600) = 1045 \text{ psi},$$

$$\overline{\sigma}_{c3} = (62.8)(.00462)(8080) = 2340 \text{ psi},$$

$$\overline{\sigma}_{c4} = (62.8)(.00462)(8080) = 2340 \text{ psi}.$$

From Equation 66, the estimated overall rms stress is given by

$$\overline{\sigma}_{e1} = 0.245 (1682)^{.411} = 5.20 \text{ ksi},$$

$$\overline{\sigma}_{e2} = 0.245 (1045)^{.411} = 4.25 \text{ ksi},$$

$$\overline{\sigma}_{e3} = 0.245 (2340)^{.411} = 6.30 \text{ ksi},$$

$$\overline{\sigma}_{e4} = 0.245 (2340)^{.411} = 6.30 \text{ ksi}.$$

For the skin stresses $\overline{\sigma}_{e1}$ and $\overline{\sigma}_{e3}$ the number of cycles to failure are obtained from Figure 80 as 1.2×10^7 cycles and 5×10^6 cycles, respectively. For the frame and rib stresses the number of cycles to failure are obtained from Figure 69 as 2.3×10^7 cycles, respectively.

The above method can be repeated until the desired fatigue life is obtained.

D. Frequencies of a Three-Cell Wedge Structure

The vibration analysis of a three-cell wedge structure is presented in Section II.E. An example will be presented here for a specific data case. The results given here were obtained using the computer program given in Appendix IV (WDGVIB); however, Equations 57 and 58 can be used if desired.

EXAMPLE: With reference to Figure 9, consider the data case:

$$_1t_s = _2t_s = t_r = 0.050 \text{ in.}$$

$$a = b_1 = b_2 = b_3 = 10.0 \text{ in.}$$

$$\alpha = 11.46 \text{ degrees (0.2 radian)}$$

$$Y = 0.101 \text{ lbs/in}^2$$

$$E = 1.03 \times 10^7 \text{ psi}$$

$$\nu = 0.302$$

$$_1D_s = 114.46 \text{ in} - \text{lb.}$$

Then, the first few modal frequencies are

mode number (m, n, q)	f_{mnq}, Hz.
(1,1,1)	134.0
(1,1,3)	298.0
(1,2,1)	298.0
(1,2,3)	611.0
(1,3,1)	530.0
(1,3,3)	964.0
(2,1,1)	261.0

Typical rib mode shapes are illustrated in Figure 11 for this data.
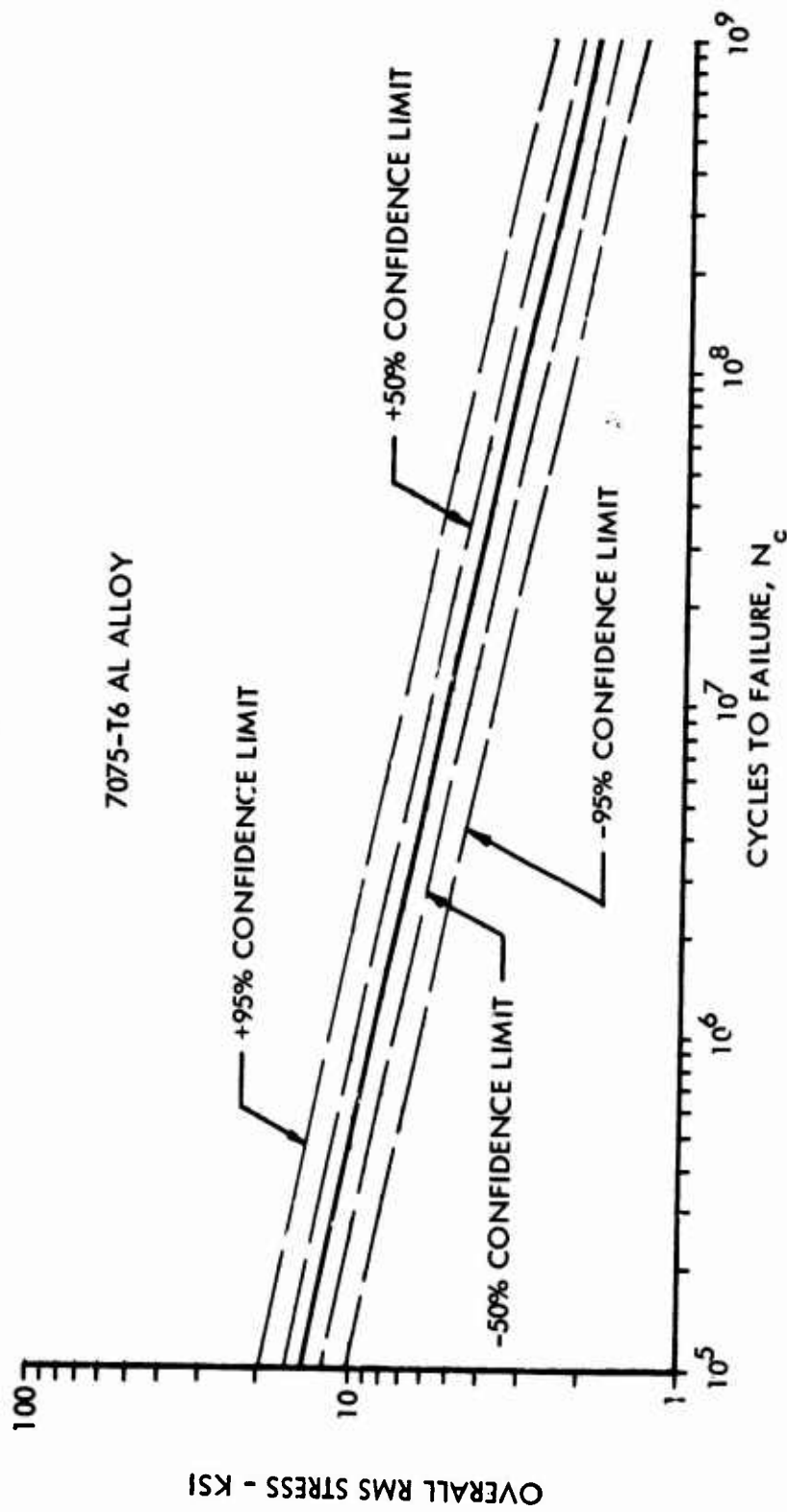
FIGURE 80 SKIN-STRINGER PLATING FATIGUE CURVE
(Figure 34, p. 91, Ref. 8)

E. Curved Panel Frequencies

1. Szechenyi's Approximate Formulae

Application of Szechenyi's approximate formulae for estimating the natural frequencies of cylindrical panels will be illustrated by an example. The data used is obtained from experimental values quoted by Petyt, Reference 13.

EXAMPLE: Using the frequency expression given by Equation 59, and Figures 13 and 14 one can compute frequencies for the various lower order panel modes of a cylindrical panel. Consider the data case (see Figure 12)

$$a = 3.0 \text{ in}, \quad b = 4.0 \text{ in}, \quad t = 0.013 \text{ in}, \quad R = 30.0 \text{ in}$$

$$E = 10^7 \text{ psi}, \quad Y = 0.096 \text{ lb/in}^3, \quad \nu = 0.33$$

The comparison between Szechenyi's approximate formula (Equation 59) and the experimental results quoted by Petyt are

Equation 59	Experiment
f_{11} = 1053., Hz.	— , Hz.
f_{12} = 968., Hz.	814., Hz.
f_{13} = 1192., Hz.	940., Hz.
f_{14} = 1730., Hz.	1735/1770, Hz.

Considering the simplicity of Szechenyi's method the results are considered to be good.

2. Plumblee's Approximate Formulae

The expressions for the frequency ratio and stress ratio for curved to flat panel response in the fundamental mode presented in Section II.F.2 can be applied directly for specific data cases. The nomogram developed by Plumblee (Figure 87, Reference 8, page 174) is presented as Figure 81. This nomogram is used in conjunction with Figure 79 for estimating curved panel fatigue life for acoustic excitation.
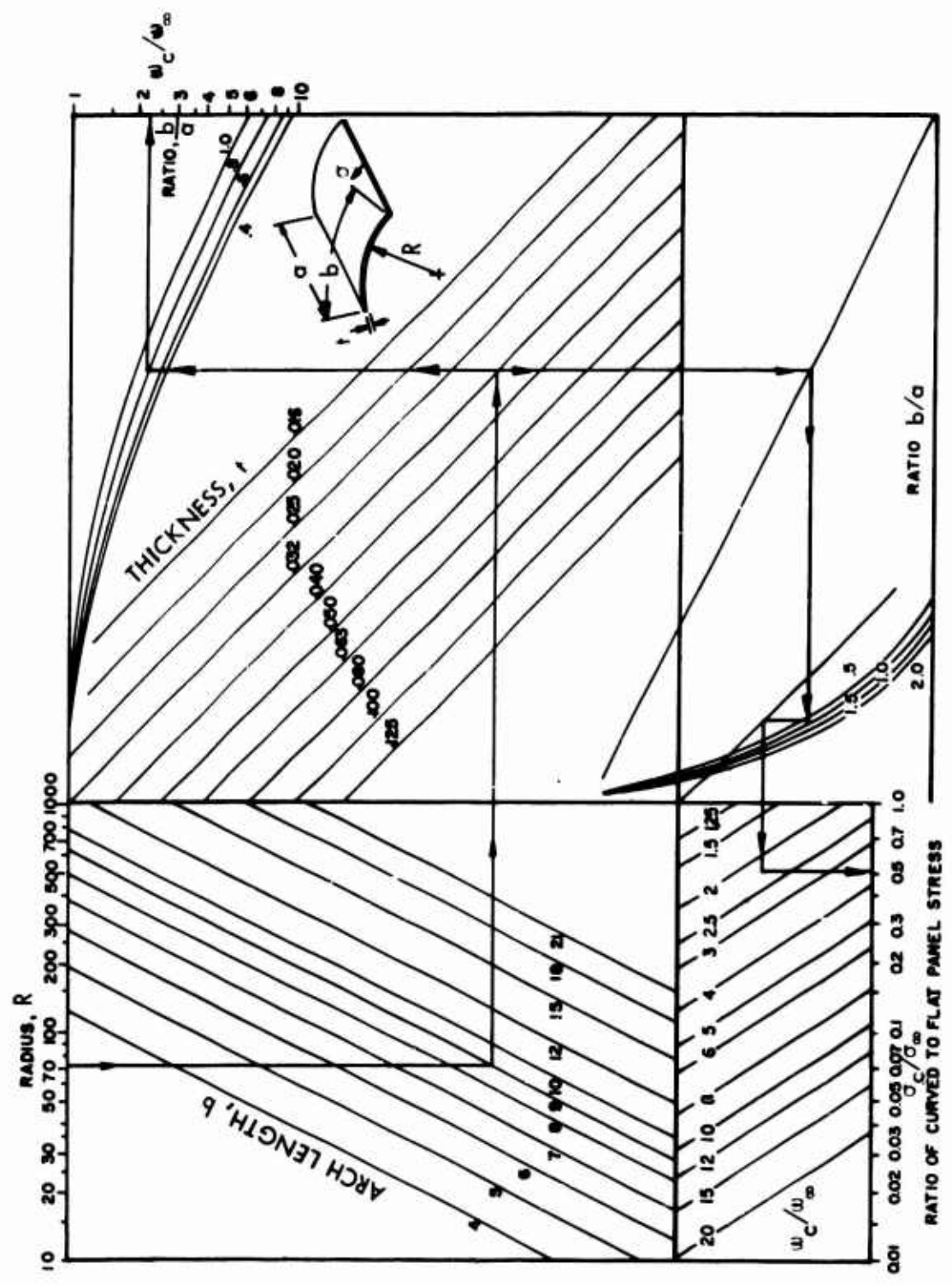
FIGURE 81 EFFECT OF CURVATURE ON STRESS RATIO FOR SKIN-STRINGER PANELS WITH RANDOM LOADING (REFERENCE 8)

126

IV - CONCLUSIONS

Methods have been developed to estimate the acoustic fatigue resistance of aircraft structural components. These methods apply to flat stiffened panels, and to box type and wedge-type structures such as flaps and trailing edges of wings and control surfaces. In the acoustic fatigue analysis the response frequencies of these structural components are estimated by the use of the Rayleigh energy method which accounts for the bending and torsional flexibilities of the supporting structure. The mean square stress response of the skin which is subjected to the random acoustic load is computed by the use of Miles equation for a single-degree-of-freedom system. The life of the structure is then estimated by using experimentally derived S-N curves and a Miner's cumulative damage calculation. Acoustic fatigue tests of twelve stiffened flat panels and six box structure designs were performed to check the theory and supply the S-N data for the analysis. The resulting S-N curves are given in two graphs, one for the stiffened plates, the other for the box structure. Computer programs are also given for estimating frequencies of the stiffened flat panels, box structures, and wedge structures. Based upon this program the following conclusions were made:

a. The results of the analytical and experimental investigations reported here indicate that the overall rms stress induced in stiffened panel skins and box structure skin and skin-rib connections by broad-band noise can be estimated with sufficient accuracy for design purposes using approximate results from thin plate theory and Miles' response theory.

b. The approach taken to establish stringer flange design data is considered to be valid within the nature of the data obtained in the experimental program. The difficulties in measuring strain at the failure point and the extreme strain gradients present at the clip attachment produce an additional scatter to the fatigue data which is inherent in the type of structure considered.

c. The confidence limits established by the limited fatigue data obtained in the experimental program are too broad. Additional testing will be required to better define the acoustic fatigue characteristics for both stringer flange failures and rib flange failures.

d. The vibration analysis for wedge structure should be reformulated to provide both frequency and stress response estimates. Even through the frequency analysis presented here yields reasonable results, the simple mode shapes used do not allow an estimate of stress to be made. Acoustic fatigue testing of wedge-type structure will be required to establish fatigue design criteria.

e. The design equations developed from the analytical and experimental programs will increase acoustic fatigue design capabilities, but these equations should be considered preliminary until more experimental data is available.

127

APPENDIX I

GENERAL EXPRESSIONS FOR STIFFENER GEOMETRIC PARAMETERS

The geometric parameters defined here are developed in terms of a centroidal (x, y, z) coordinate system. General expressions for the cross-sectional area, the area moments, torsion constant, and warping constants are presented for zee, channel, and hat cross-section shapes. The definition of these parameters is as follows:

$\bar{x}$, the location of the centroid, as indicated

e, the location of shear center, as indicated

A, the cross-sectional area

$$I_{xx} = \int_A z^2 dA \qquad I_{xz} = \int_A xz\, dA \qquad I_{zz} = \int_A x^2 dA$$

$$J = \int_A \left[(\varphi_{,x} - z)^2 + (\varphi_{,z} + x)^2 \right] dA \qquad \text{(St. Venant's Torsion Constant)}$$

$$R_{Ez} = \int_A x\varphi\, dA \qquad R_{Ex} = \int_A z\varphi\, dA \qquad \Gamma_e = \int_A \varphi^2 dA$$

where $\varphi(x, z)$ is the warping function for the cross-section with the pole taken as the shear center.

GENERAL EXPRESSIONS FOR STIFFENER GEOMETRIC PARAMETERS
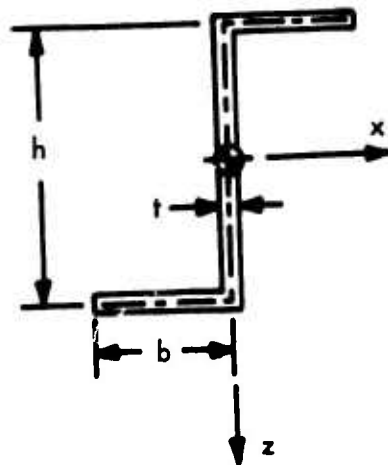
$$A = t(h + 2b)$$

$$I_{xx} = \frac{t}{12}\left[h^2(6b + h) + t^2(3h + 2b)\right]$$

$$I_{xz} = -\frac{th}{8}(2b + t)(2b - t)$$

$$I_{zz} = \frac{t}{12}\left[8b^3 + ht^2\right]$$

$$J = \frac{t^3}{3}\left[2b + h\right]$$

$$\Gamma_e = \frac{tb^3h^2(b + 2h)}{12(2b + h)}$$

FIGURE A-I-1   GEOMETRIC PROPERTIES - ZEE SECTION

GENERAL EXPRESSIONS FOR STIFFENER GEOMETRIC PARAMETERS

$$\bar{x} = b^2/(2b + h)$$

$$e = 3b^2/(6b + h)$$

$$A = t(h + 2b)$$

$$I_{xx} = \frac{t}{12}[h^2(6b + h) + t^2(3h + 2b)]$$

$$I_{xz} = 0$$

$$I_{zz} = \frac{t}{12}[12h\bar{x}^2 + 8b^3 - 24\bar{x}b(b - \bar{x}) + 12b(b - 2\bar{x})t + 6(b - \bar{x})t^2 + t^3]$$

$$J = \frac{1}{3}t^3(2b + h)$$

$$\Gamma_e = \frac{tb^3h^2(3b + 2h)}{12(6b + h)}$$

$$R_{Ez} = 0$$

$$R_{Ex} = 0$$
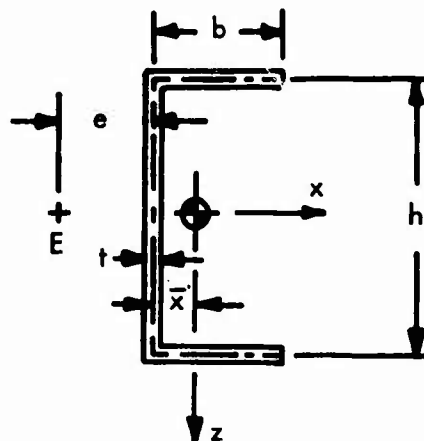
NOTE: For warping constants, the pole is taken at the shear center.

FIGURE A-I-2 GEOMETRIC PROPERTIES - CHANNEL SECTION

131

GENERAL EXPRESSIONS FOR STIFFENER GEOMETRIC PARAMETERS

$$\bar{x} = \frac{b(b + 2h_1)}{(2b + h + 2h_1)}$$

$$e = \frac{b(3bh^2 + 2h_1(3h^2 - 4h_1^2))}{[h^2(6b + h) + 2h_1(3h^2 + 6hh_1 + 4h_1^2)]}$$

$$A = t(h + 2b + 2h_1)$$

$$I_{xx} = \frac{1}{12}t(h - t)^3 + \frac{1}{6}t(b + t)(t^2 + 3h^2) + \frac{1}{48}t(2h_1 - t)[(2h_1 - t)^2 + 12(h + h_1)^2]$$

$$I_{xz} = 0$$

$$I_{zz} = \frac{1}{12}t(h - t)(t^2 + \bar{x}^2) + \frac{2}{3}t(b + t)^3 + \frac{1}{2}t\bar{x}(b + t)[\bar{x} - 2b + 2t]$$
$$+ \frac{1}{24}t(2h_1 - t)[t^2 + 24(b - \bar{x})^2]$$

$$J = \frac{1}{3}t^3[h + 2b + 2h_1]$$

$$R_{ex} = 0$$

$$R_{ez} = 0$$

$$\Gamma_e = \frac{t}{12}[2b^3h^2 + 6bh^2e(e - b) + 2b^2h_1(3h^2 - 6hh_1 + 4h_1^2)$$
$$- 4bh_1e(3h^2 - 4h_1^2) + e^2(h + 2h_1)^3]$$
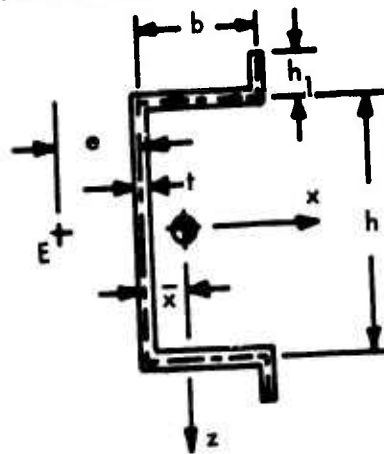
FIGURE A-I-3 GEOMETRIC PROPERTIES - HAT SECTION

132

APPENDIX II

TEST DETAILS AND INSTRUMENTATION

A. Introduction

In general, the test details and instrumentation used to conduct the experimental program are, except for the statistical analysis, identical to the procedures described by Ballentine (Appendix I, Reference 8). The procedures used for the box specimen mode studies were slightly different than that used for the stiffened panel specimens due to the box structure configuration. These differences are described in Section III. The statistical data analysis will be described here, and the reader can obtain other details as described in Reference 8.

B. Statistical Data Analysis

The data used to obtain the S-N curves presented in this report consisted of R.M.S. values for strain, zero crossings with negative slope of the strain signal, and the time that fatigue failure was first observed. All fatigue failure data reported in this report correspond to a failure initiated at or very close to the strain gage. The zero crossing count was obtained using a B & K Model 161 Probability Density Analyzer, a frequency counter, and the recorded strain signal. The average of the frequency count (zero crossings with negative slope) for three minutes of strain data was taken as the zero crossing count. The block diagram for the system is illustrated in Figure A-II-1.

The amplitude distribution plots illustrated in this report were also obtained using the B & K Model 161 Probability Density Analyzer. Six minutes of recorded strain data were used to obtain each plot. The Gaussian distribution referenced in each plot was obtained by analyzing a 1 volt rms random noise signal from a B & K Model 1024 sine-random noise generator. The block diagram for the system is illustrated in Figure A-II-2.

133
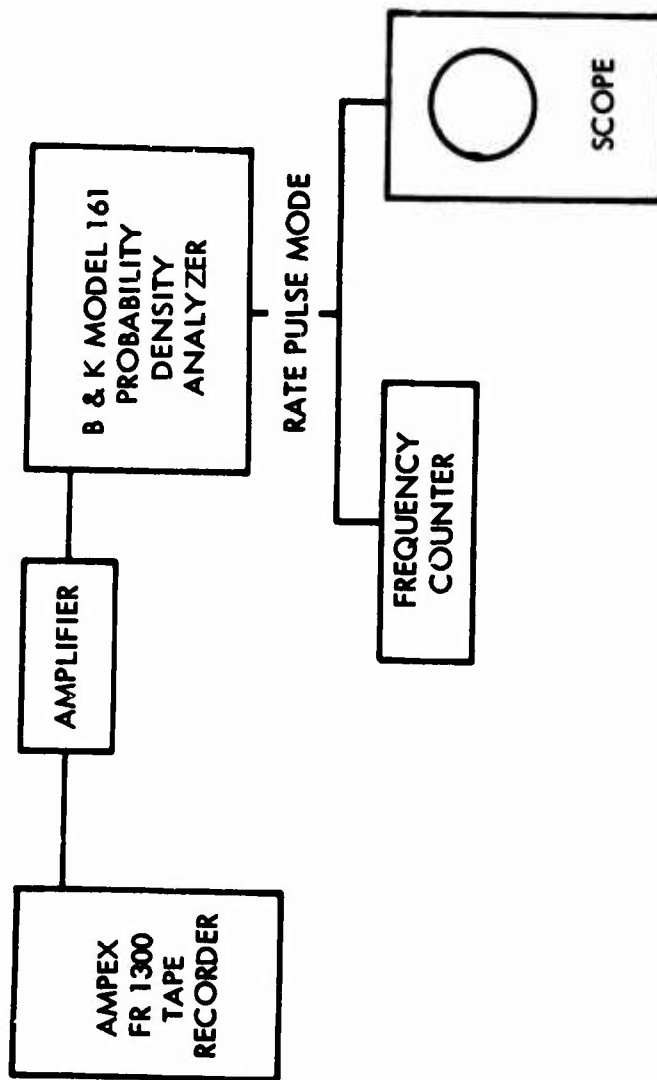
FIGURE A-II-1   BLOCK DIAGRAM FOR OBTAINING ZERO CROSSING COUNT FOR STRAIN SIGNALS
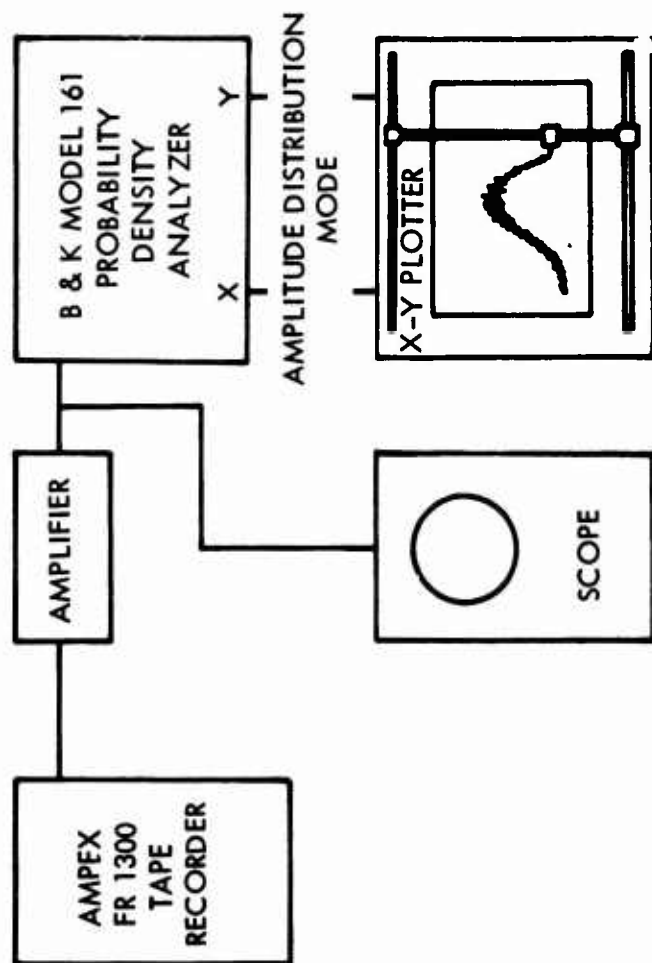
FIGURE A-II-2   BLOCK DIAGRAM FOR OBTAINING AMPLITUDE DISTRIBUTION
OF STRAIN SIGNAL

APPENDIX III

EXPERIMENTAL SPECIMEN MODE SHAPES

1. Introduction

The experimental frequencies and mode shapes described here were obtained as described in Sections III.C and III.D. The specimen plan view is illustrated (no scale). The frame and stringer attach lines are indicated. The frame lines are horizontal and the stringer attach lines are vertical. The node lines for a given bay are indicated by dashed lines. Predominant modes for each specimen are indicated by an asterisk.

FIGURE AIII-   STIFFENED PANEL MODE SHAPES
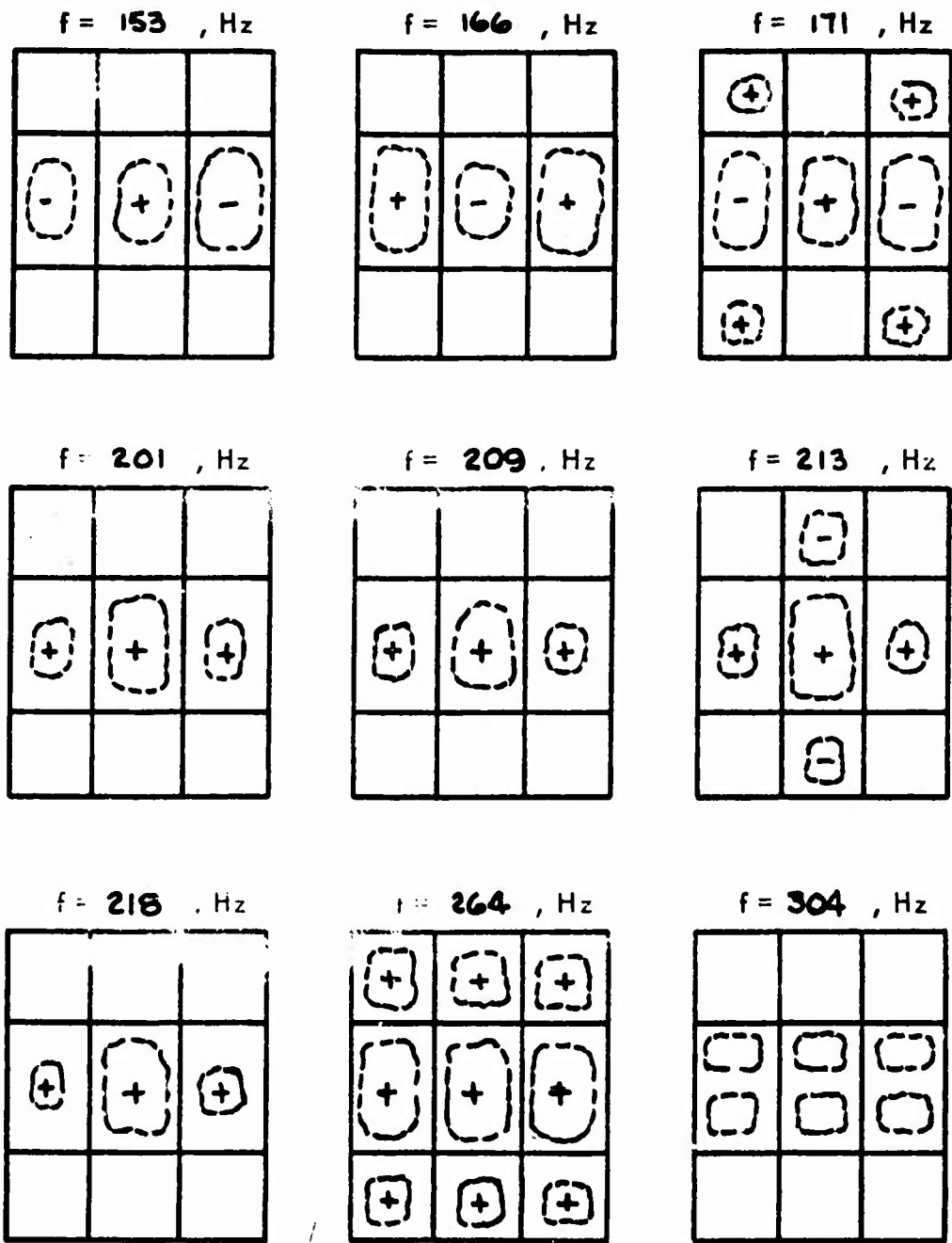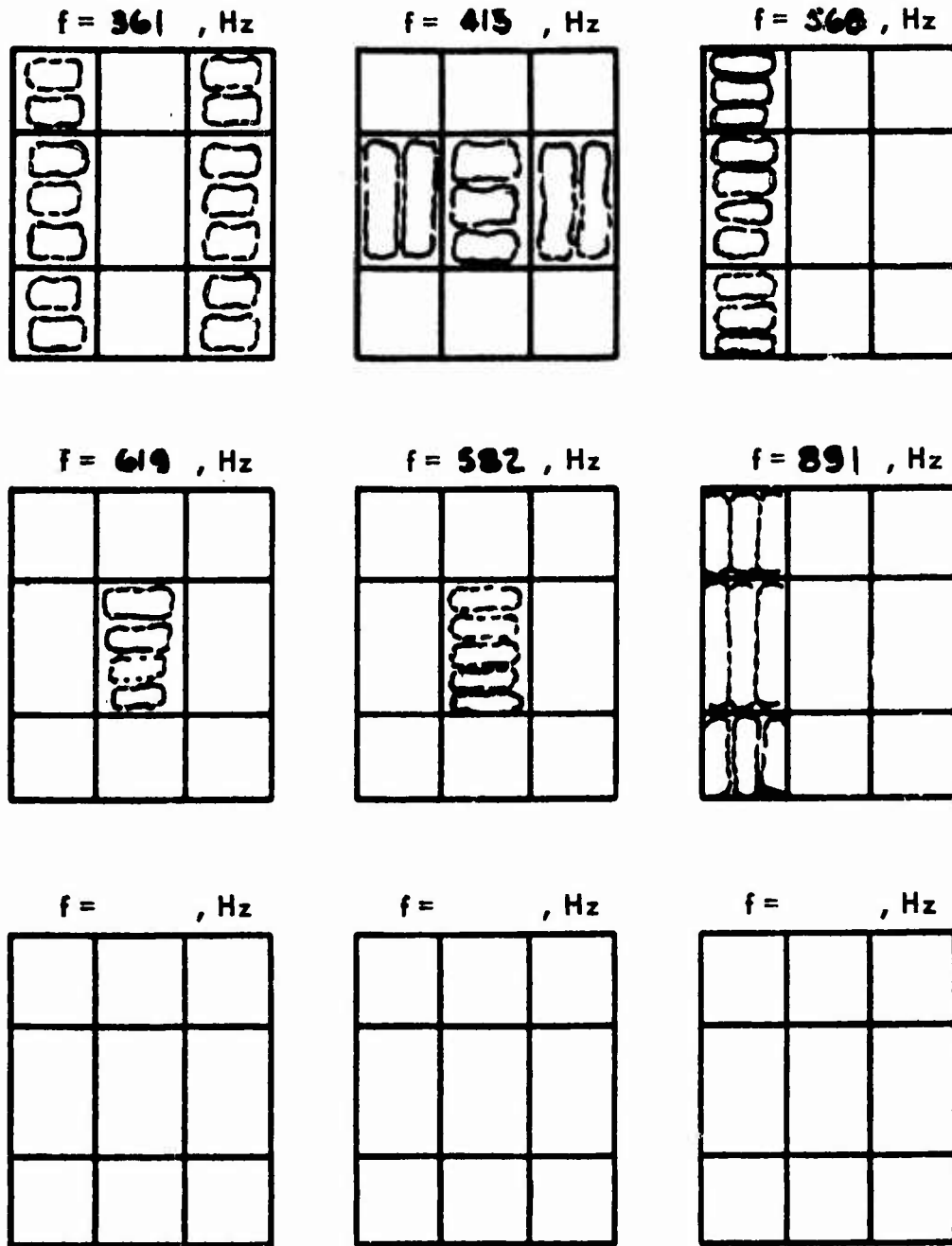
STR- 31 A

FIGURE AIII-   STIFFENED PANEL MODE SHAPES

138

FIGURE AIII-   STIFFENED PANEL MODE SHAPES

FIGURE AIII-   STIFFENED PANEL MODE SHAPES

140

STR- 32A

FIGURE AIII-   STIFFENED PANEL MODE SHAPES

FIGURE AIII-   STIFFENED PANEL MODE SHAPES

FIGURE AIII-   STIFFENED PANEL MODE SHAPES

143

FIGURE AIII-   STIFFENED PANEL MODE SHAPES

FIGURE AIII-   STIFFENED PANEL MODE SHAPES

f = 121 , Hz   f = 158 , Hz   f = 167 , Hz

f = 195 , Hz   f = 285 , Hz   f = 311 , Hz

f = 326, Hz   f = 357 , Hz   f = 448 , Hz

STR- 34 B

FIGURE AIII-   STIFFENED PANEL MODE SHAPES
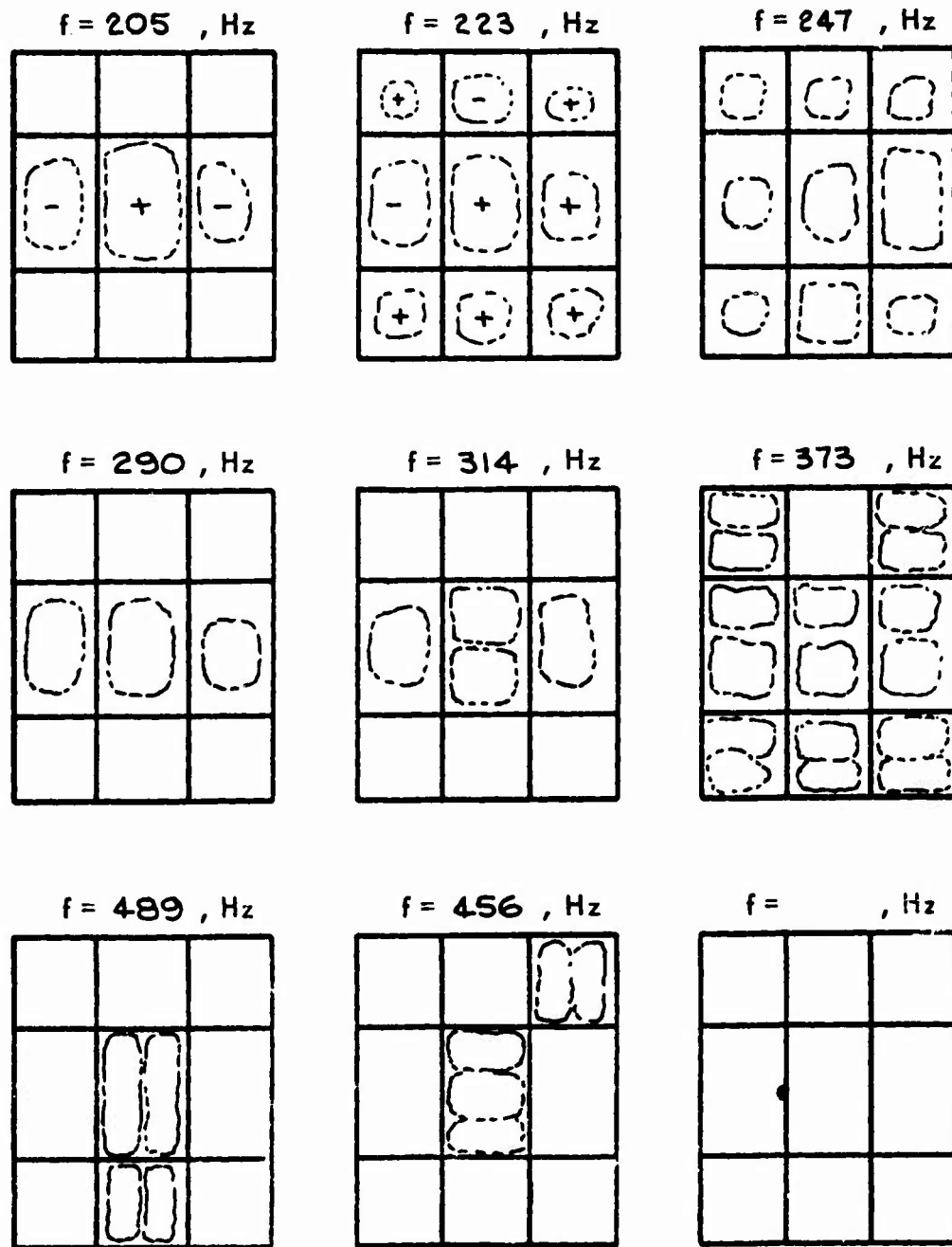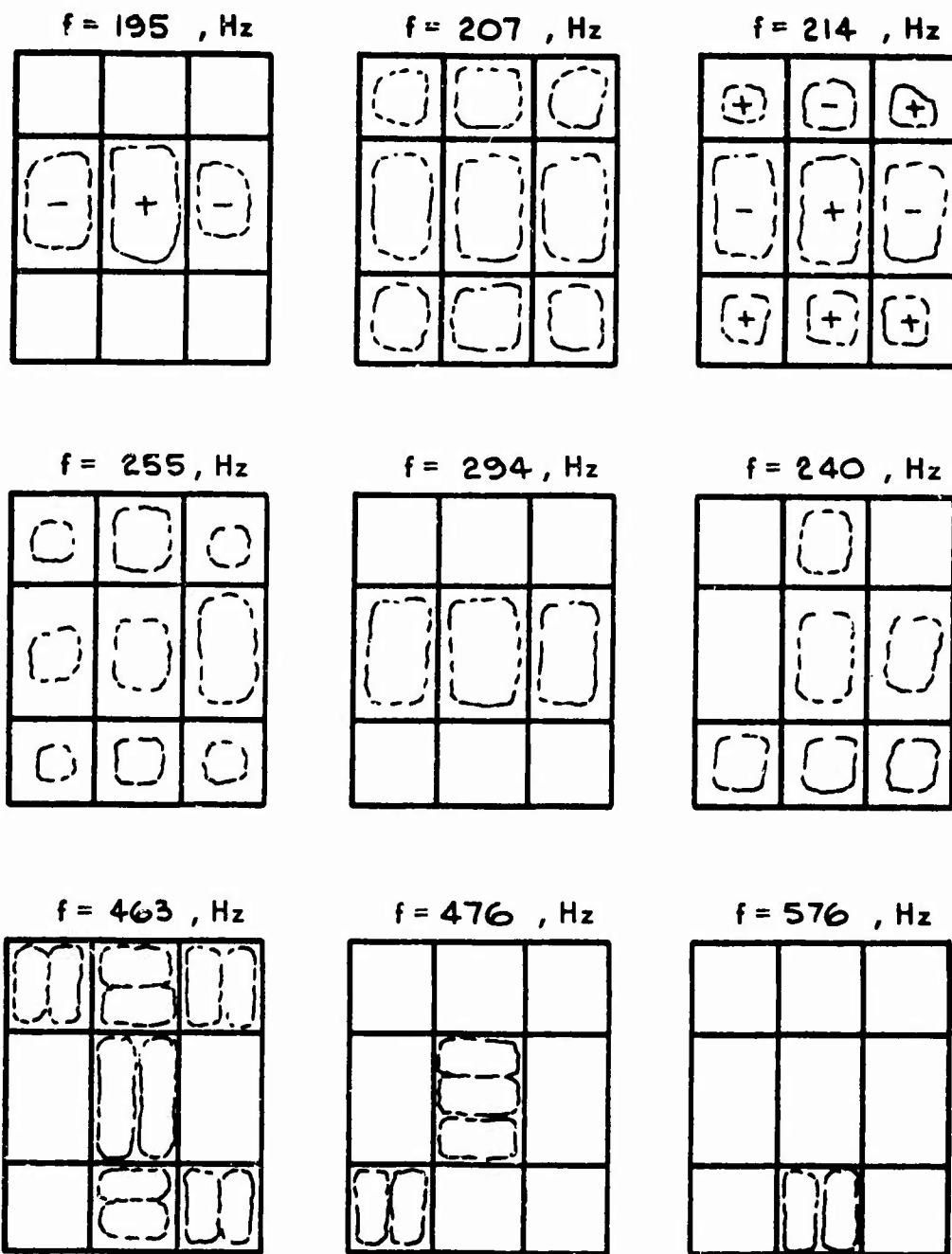
146

FIGURE AIII-   STIFFENED PANEL MODE SHAPES

f = 195 , Hz　　f = 207 , Hz　　f = 214 , Hz

f = 255 , Hz　　f = 294 , Hz　　f = 240 , Hz

f = 463 , Hz　　f = 476 , Hz　　f = 576 , Hz

STR- 35B

FIGURE AIII-　STIFFENED PANEL MODE SHAPES

f = 166 , Hz f = 212 , Hz f = 260, Hz

f = 294 , Hz f = 324 , Hz f = 367 , Hz

f = 477 , Hz f = 550 , Hz f = 599 , Hz
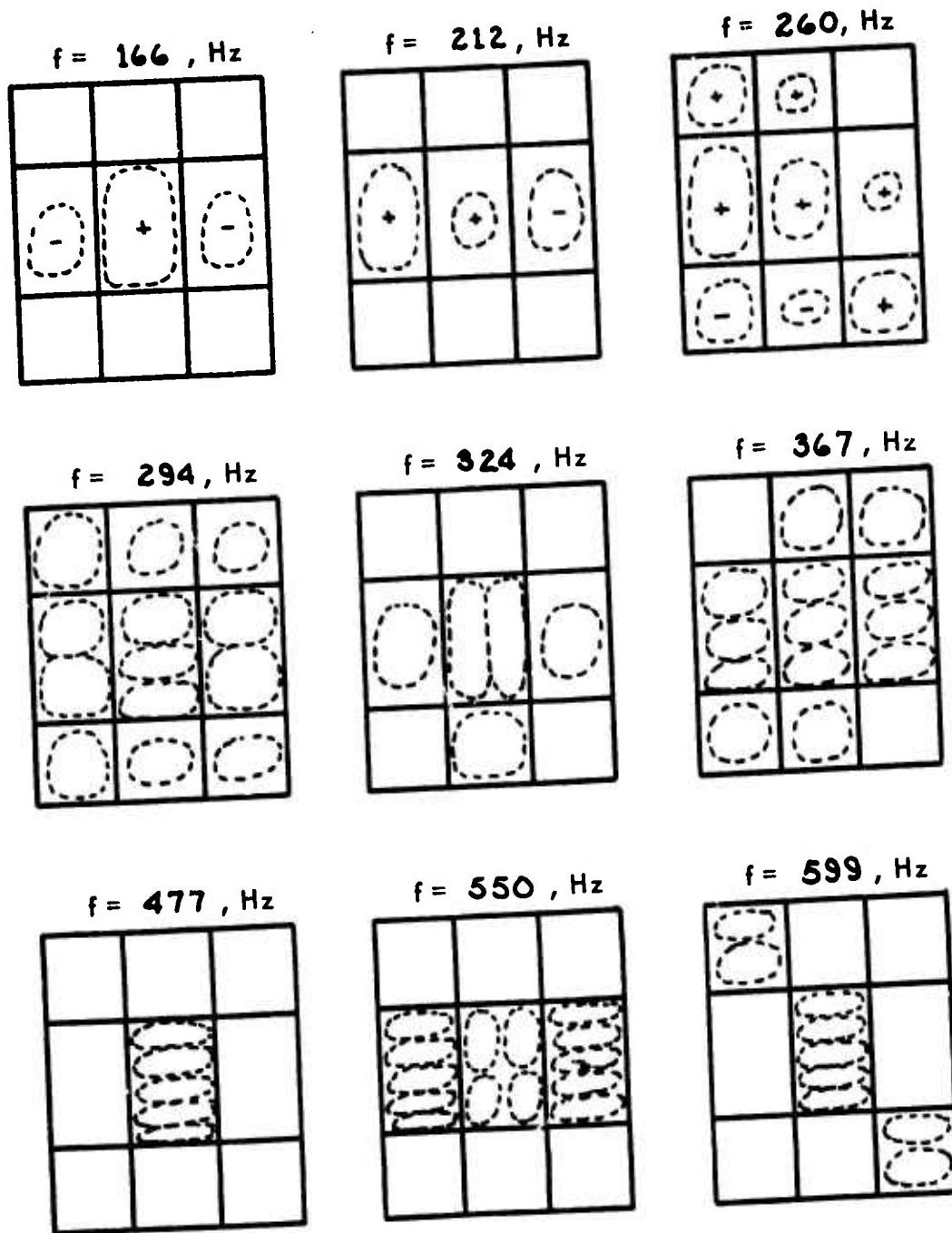
STR- 36 A

FIGURE AIII-   STIFFENED PANEL MODE SHAPES

149

FIGURE AIII-   STIFFENED PANEL MODE SHAPES

f = 75 , Hz   f = 121 , Hz   f = 178 , Hz

f = 208 , Hz   f = 229 , Hz   f = 276 , Hz

f = 320 , Hz   f = 357 , Hz   f = 562, Hz
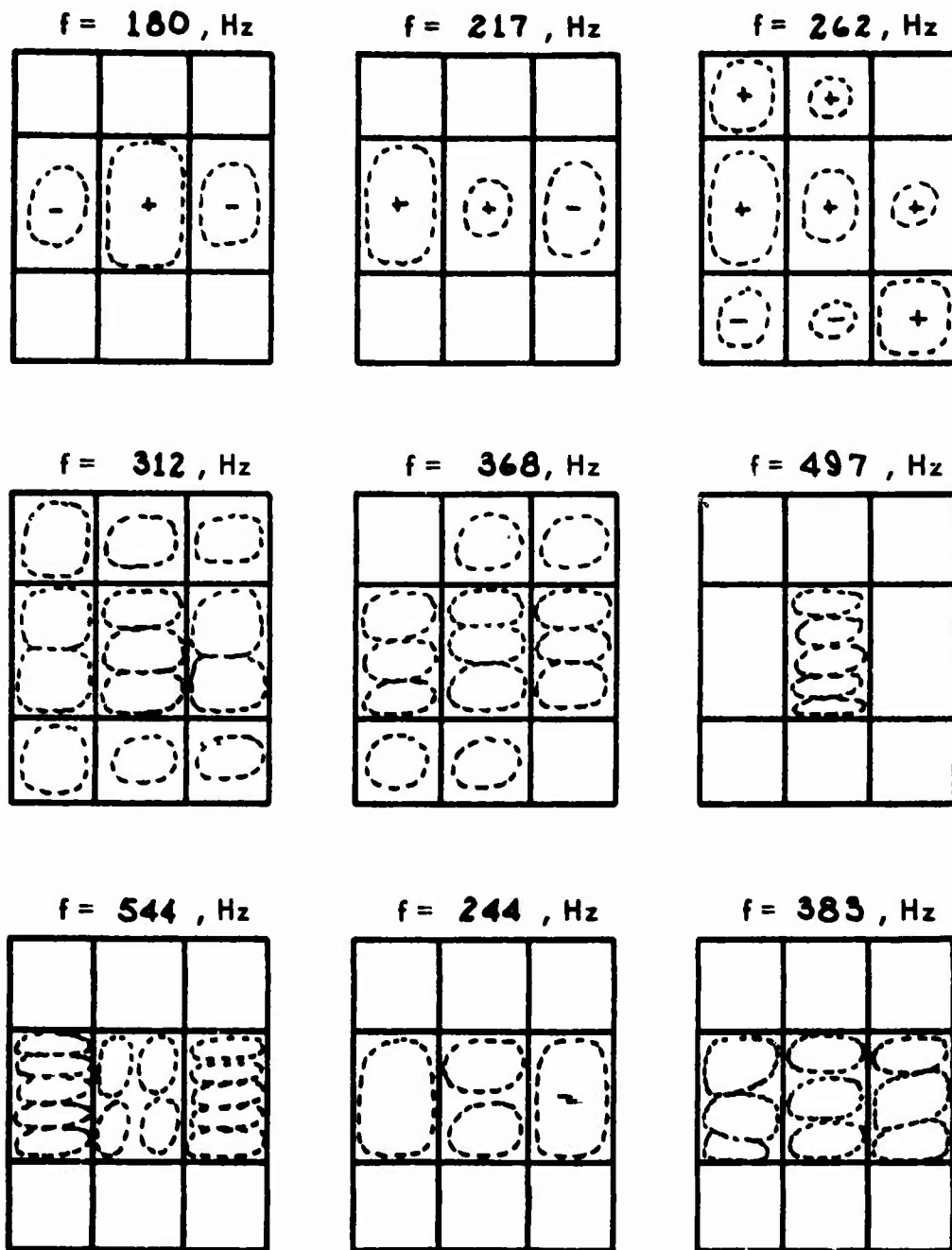
STR- 37A

FIGURE AIII-   STIFFENED PANEL MODE SHAPES

FIGURE AIII-   STIFFENED PANEL MODE SHAPES

152

FIGURE AIII-   STIFFENED PANEL MODE SHAPES

153

f = 81 , Hz f = 121 , Hz f = 178 , Hz

f = 213 , Hz f = 272 , Hz f = 306 , Hz

f = 362 , Hz f = 506 , Hz f = 553 , Hz

STR- 38 B

FIGURE AIII-   STIFFENED PANEL MODE SHAPES

154

FIGURE AIII-   STIFFENED PANEL MODE SHAPES

155

f = 169 , Hz   f = 196 , Hz   f = 224 , Hz

f = 266 , Hz   f = 313 , Hz   f = 347 , Hz

f = 580 , Hz   f =   , Hz   f =   , Hz

STR- 39 B

FIGURE AIII-   STIFFENED PANEL MODE SHAPES

STR- 40 A

FIGURE AIII-   STIFFENED PANEL MODE SHAPES

157

f = 60 , Hz   f = 71 , Hz   f = 96 , Hz

f = 137 , Hz   f = 167 , Hz   f = 192 , Hz

f = 211 , Hz   f = 241 , Hz   f =   , Hz

STR- 40 B

FIGURE AIII-   STIFFENED PANEL MODE SHAPES

158

f = 88 , Hz   f = 103 , Hz   f = 123 , Hz

f = 141 , Hz   f = 164 , Hz   f = 201 , Hz

f = 308 , Hz   f = 353 , Hz   f =   , Hz
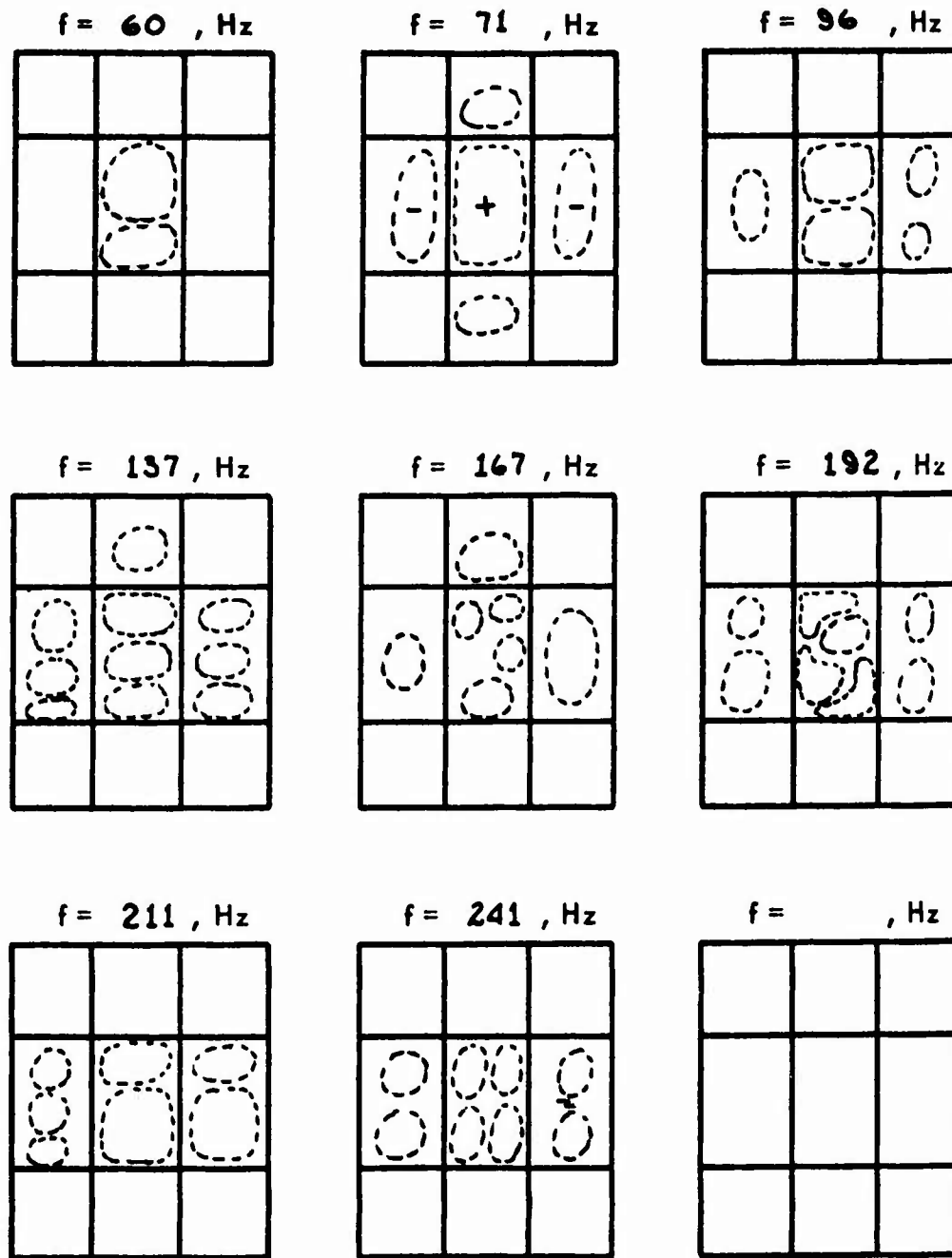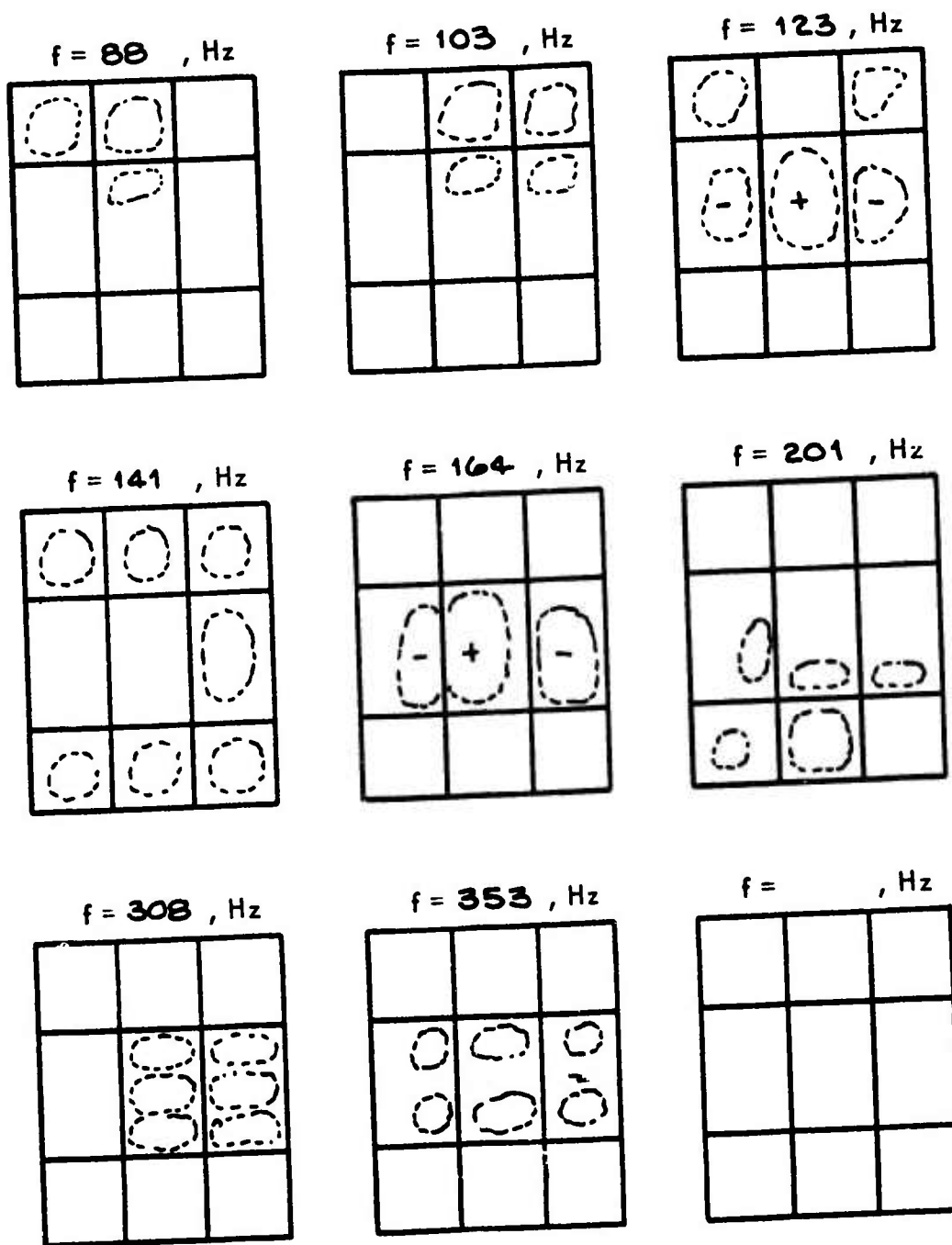
STR- 41A

FIGURE AIII-   STIFFENED PANEL MODE SHAPES

159
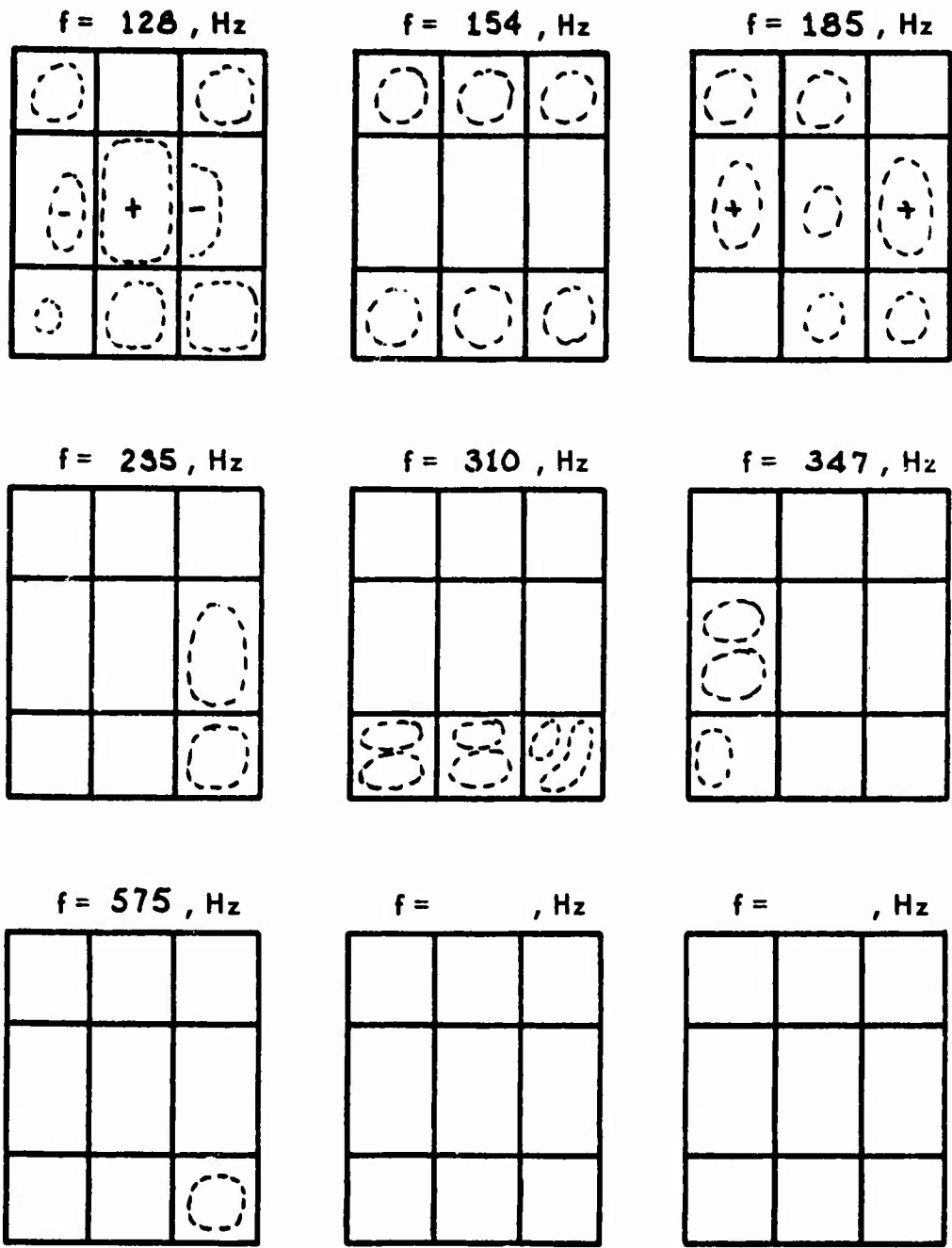
STR- 41B

FIGURE AIII-   STIFFENED PANEL MODE SHAPES

160

STR- 42A

FIGURE AIII-   STIFFENED PANEL MODE SHAPES

161

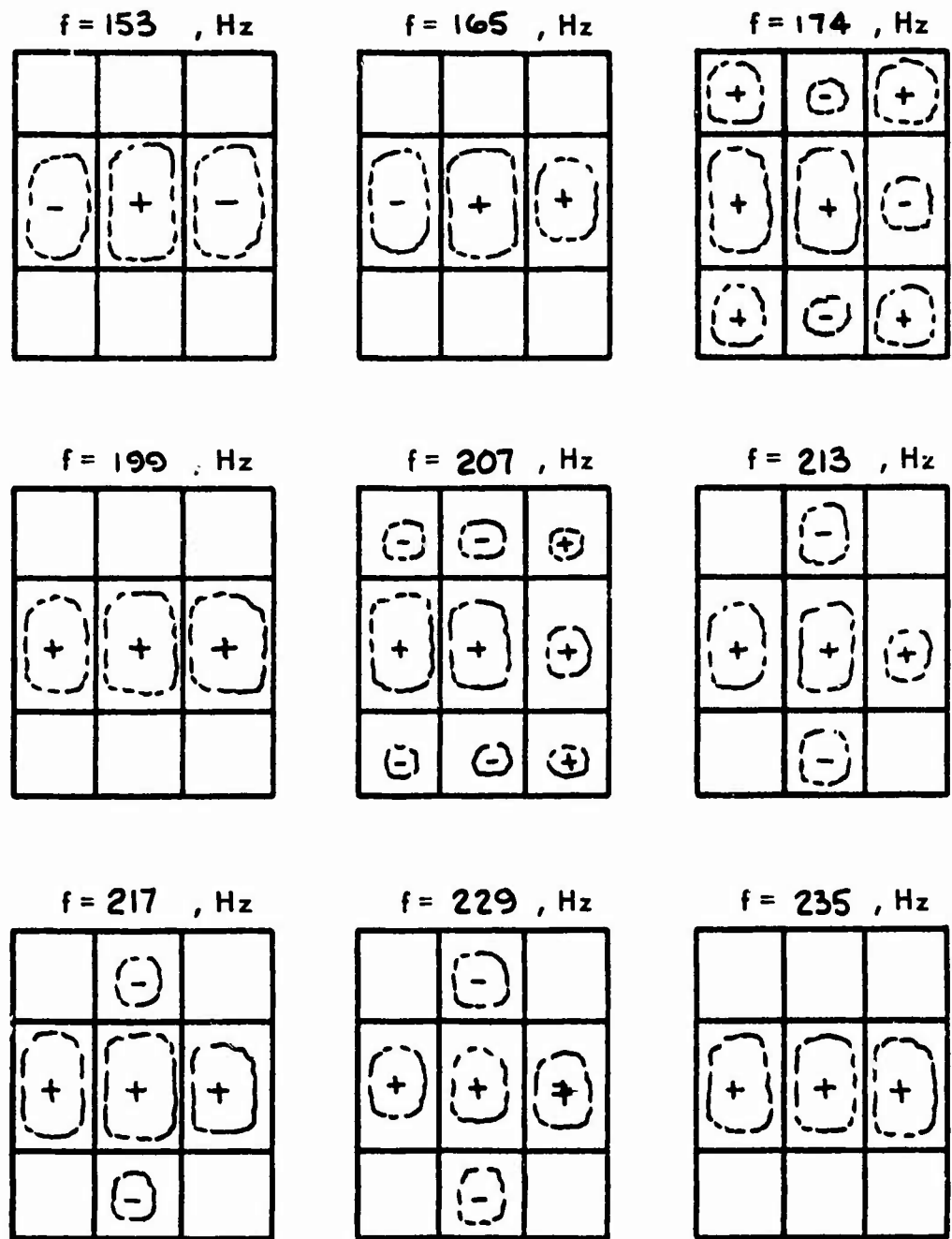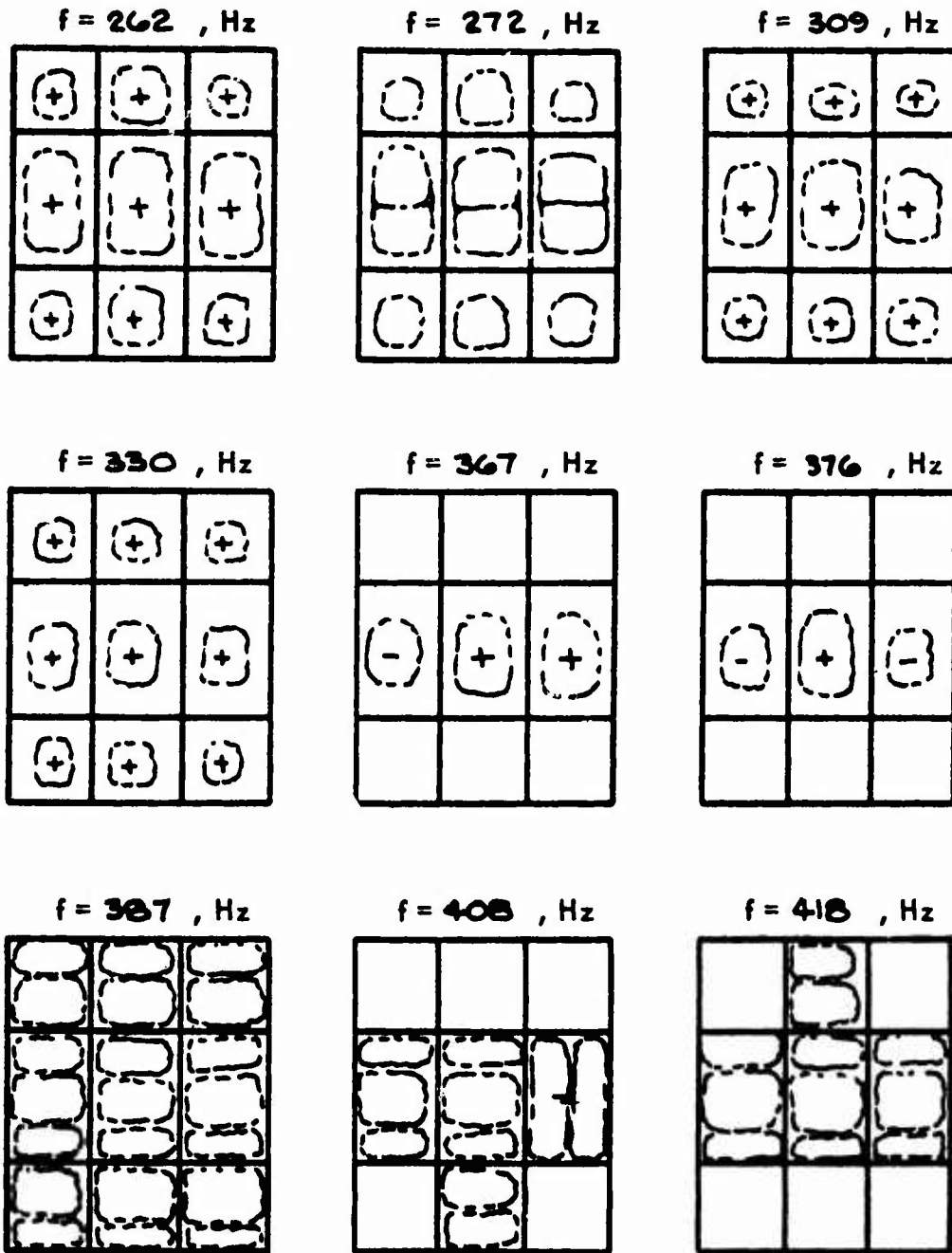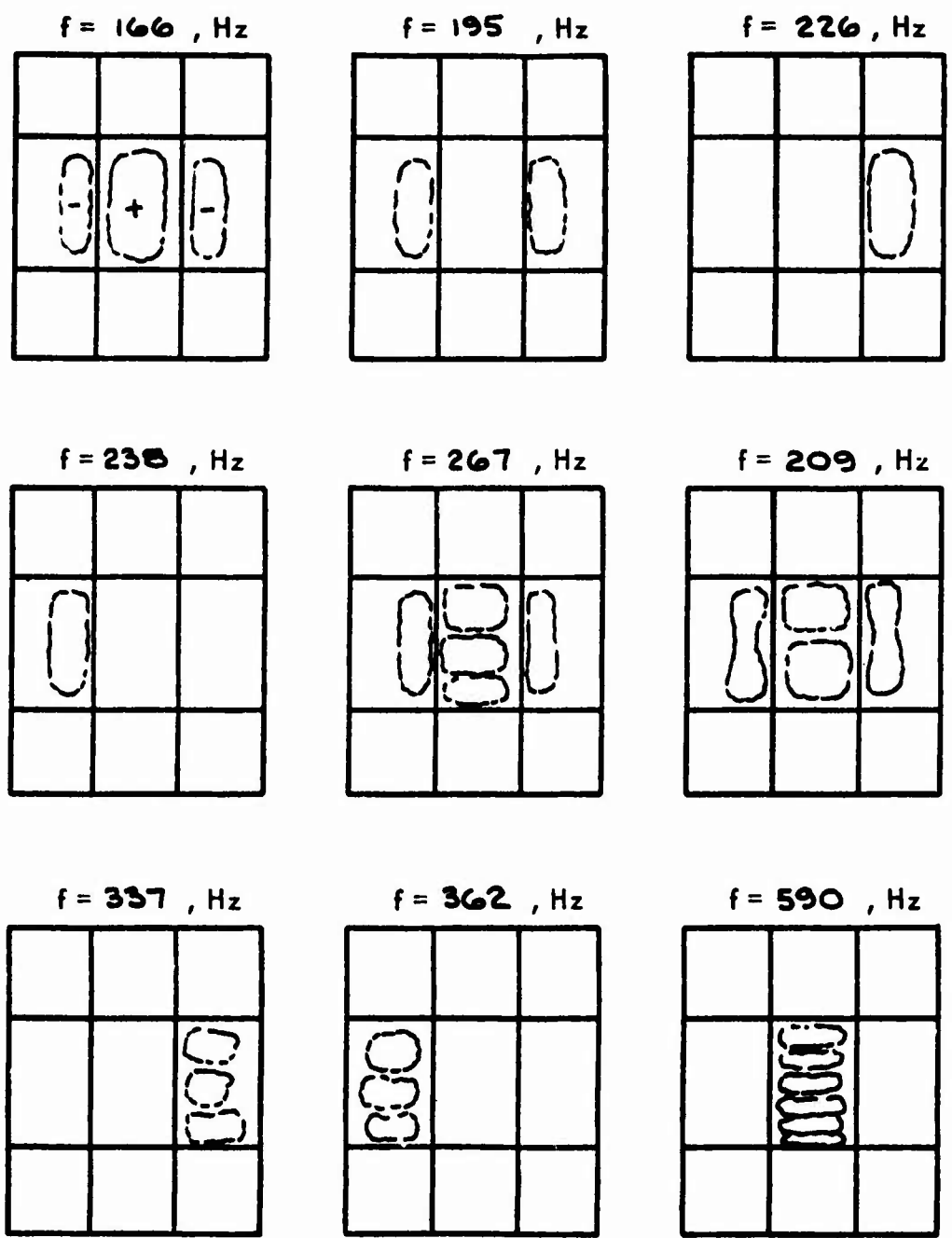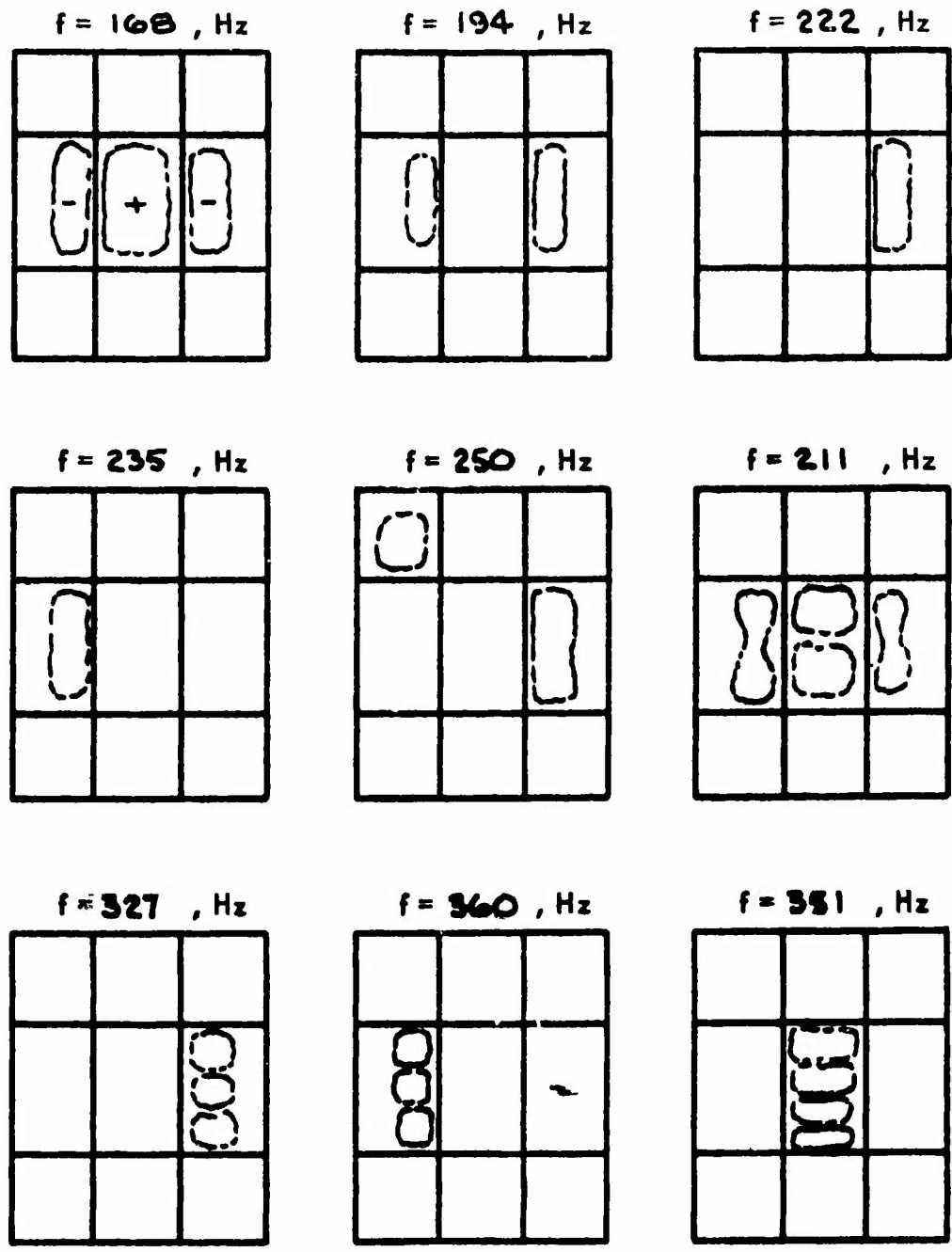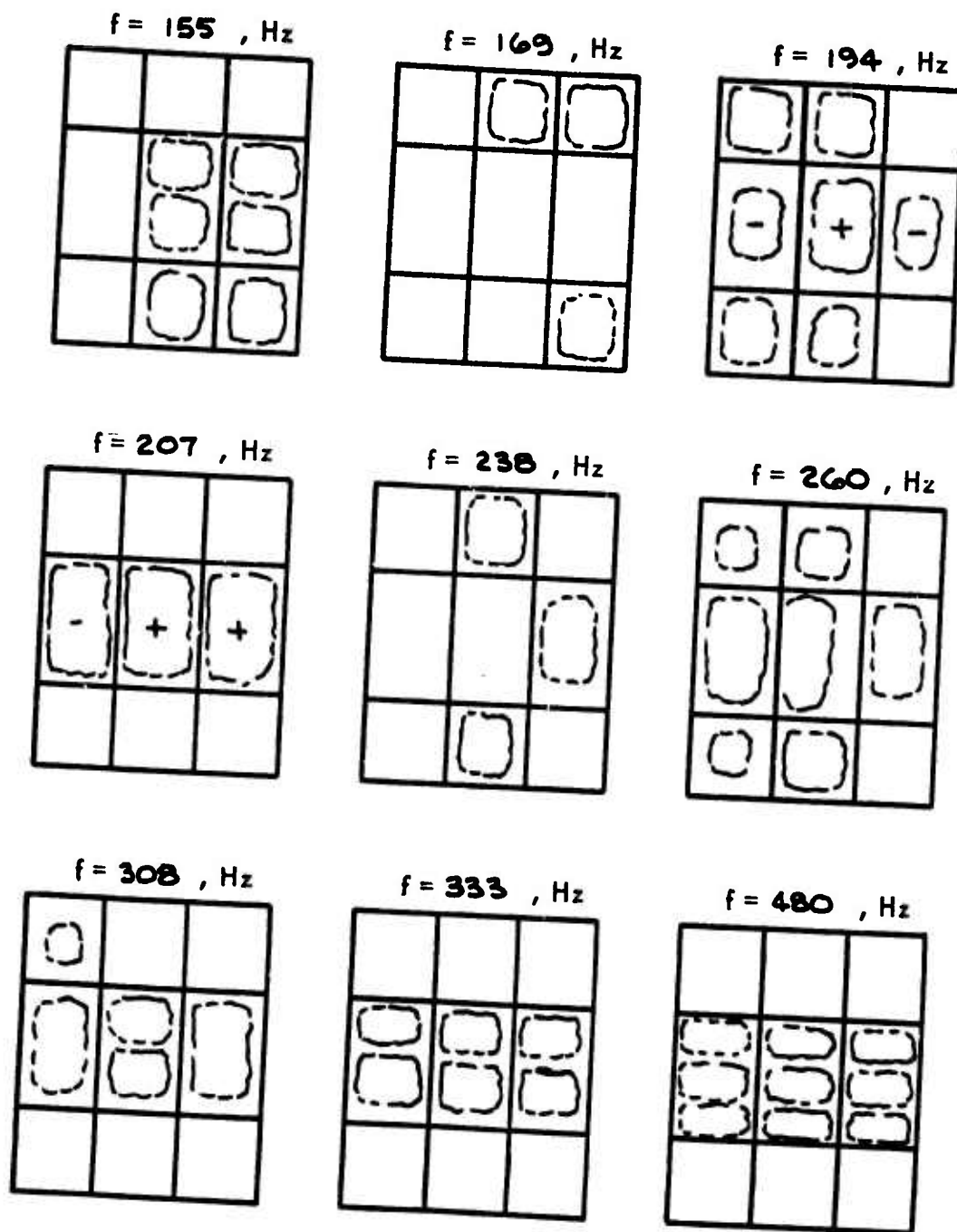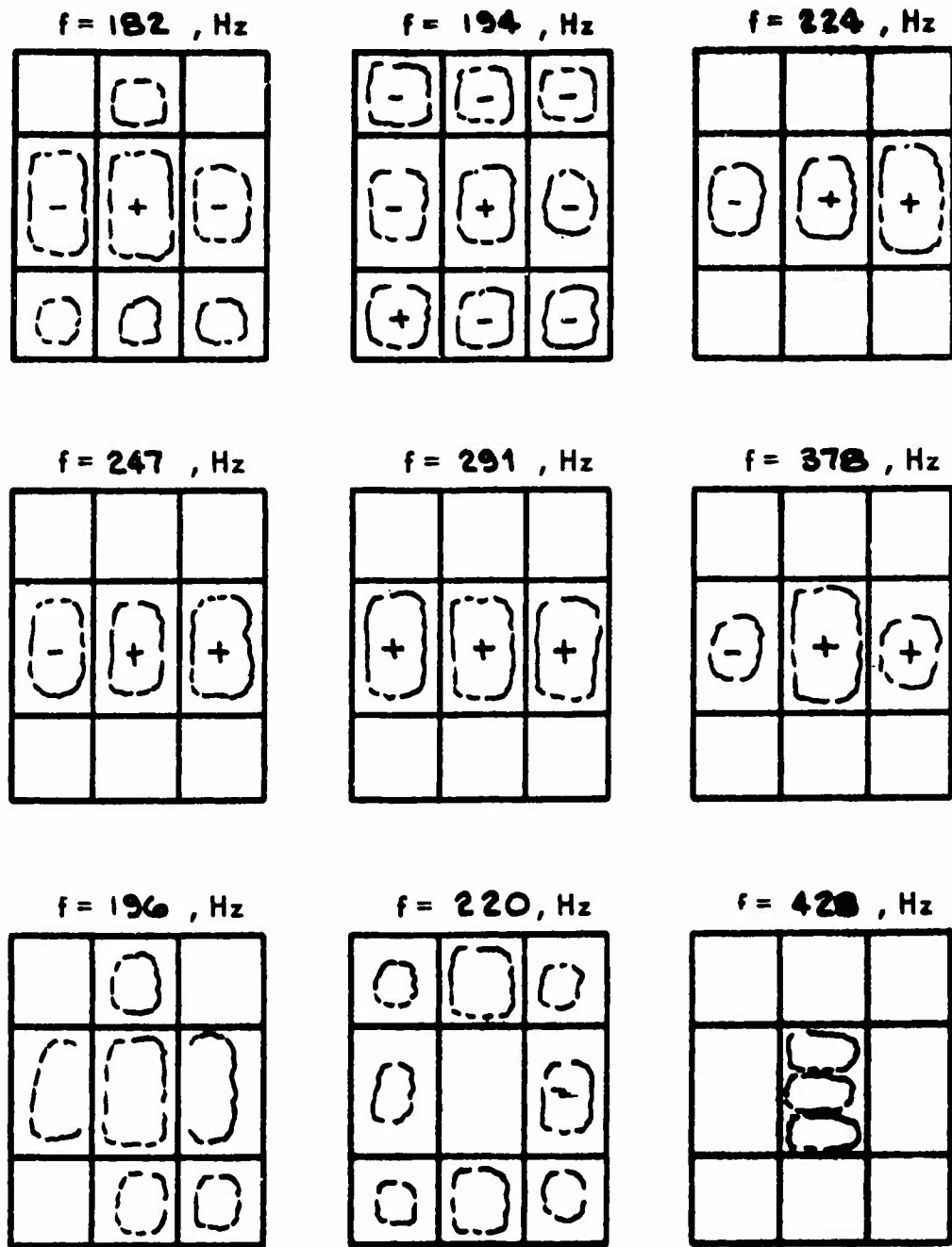f = 103 , Hz   f = 136 , Hz   f = 154 , Hz

f = 199 , Hz   f = 239 , Hz   f = 275 , Hz

f = 374 , Hz   f = 589 , Hz   f =   , Hz
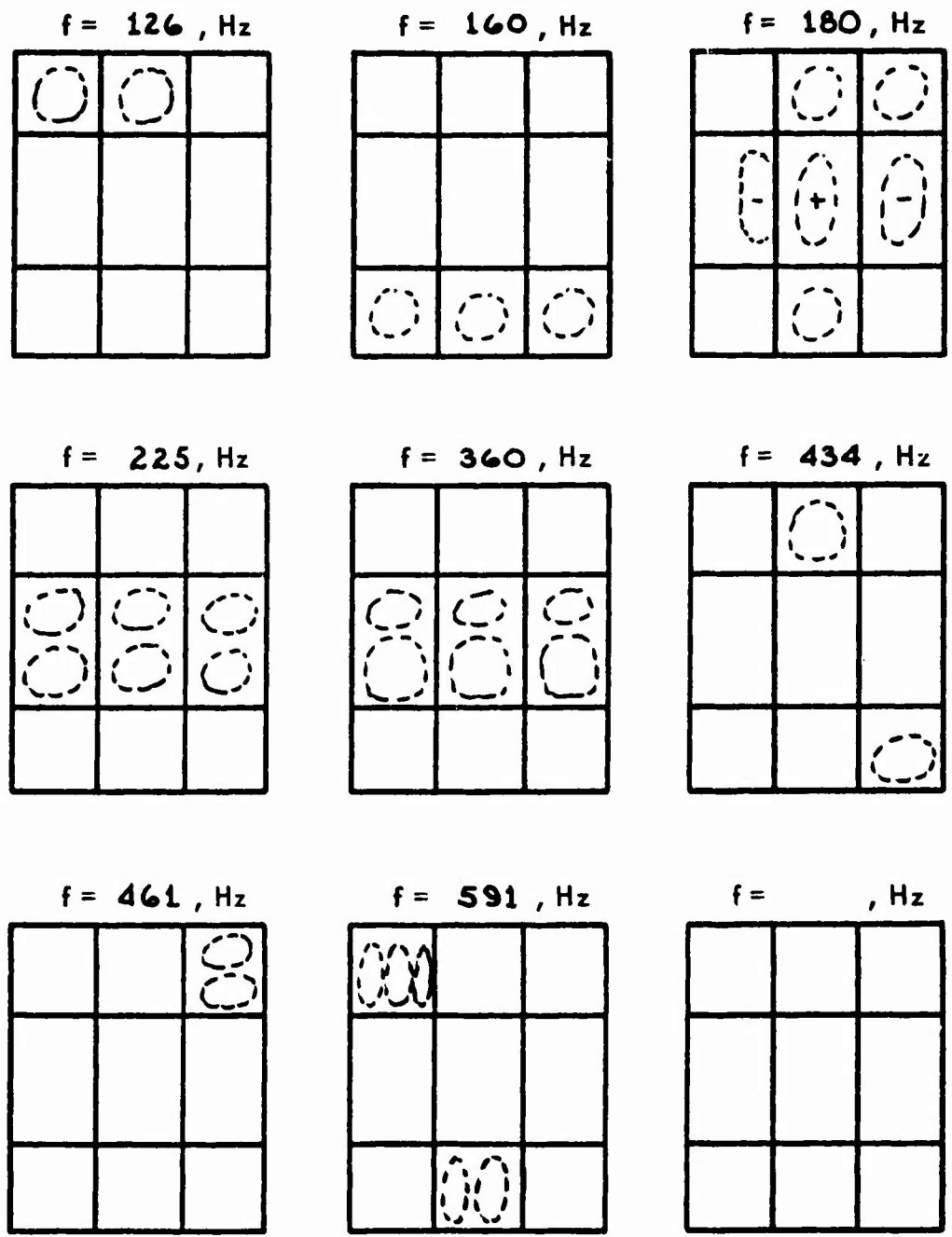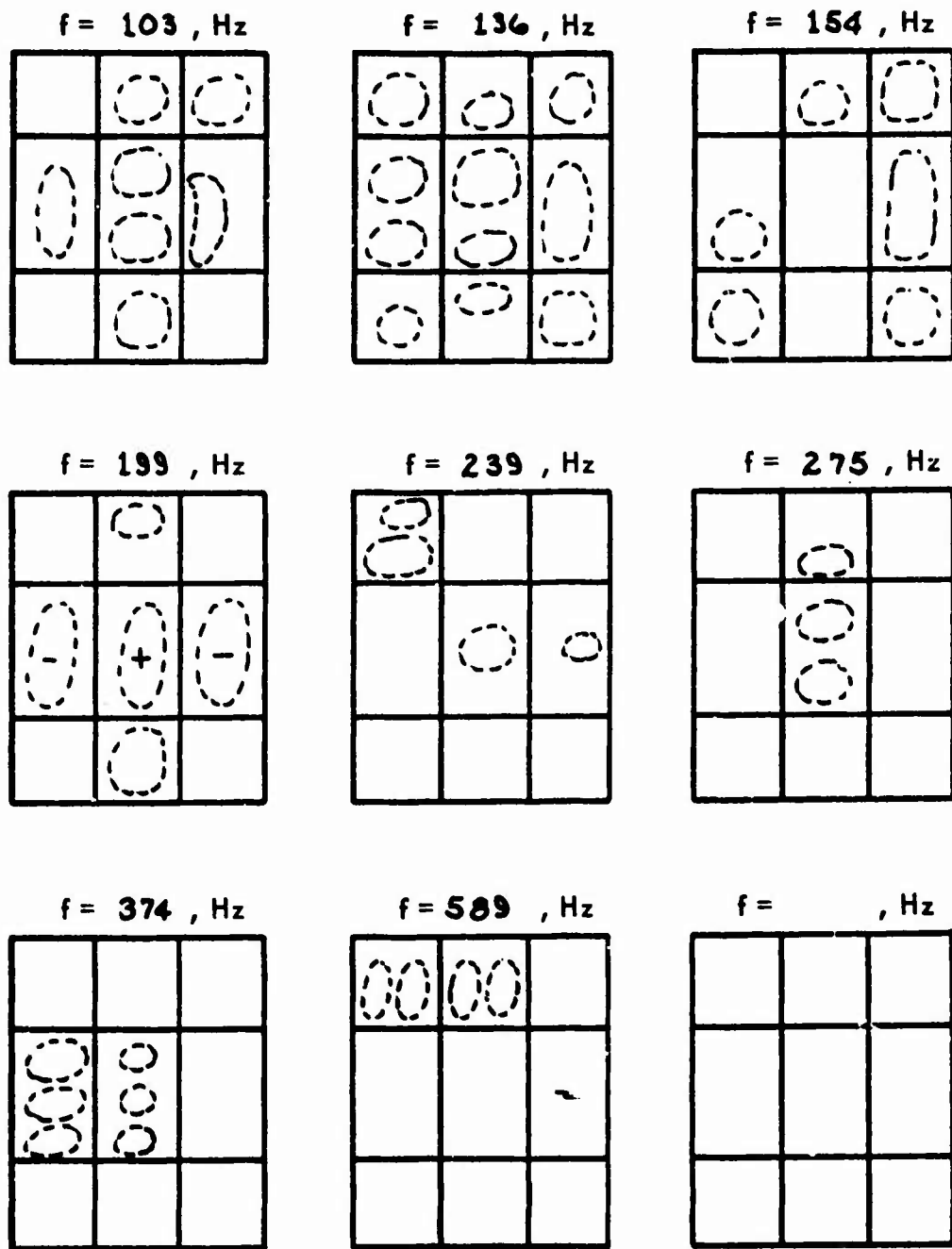
STR- 42 B

FIGURE AIII-   STIFFENED PANEL MODE SHAPES

162

APPENDIX IV

COMPUTER PROGRAMS

1. Introduction

The computer programs listed here are based upon the analysis given in Section II. All programs compute frequencies and modal amplitudes. The wedge structure vibration analysis computes the mode shapes for the ribs as a function of position along the radial axis at the center line of the rib. These computer programs have been written for the UNIVAC 418 computer; however, with very slight modifications, they can be adapted to any computer. Special functions and subprograms are listed with the main program.

2. Nine Bay Stiffened Panel Vibration Analysis (PLTVIB)

Purpose: To compute the natural frequencies and modal amplitudes for the panel bays and ribs as described in Section II.C. The program is listed in Figure A IV-1. Typical output format is listed in Figure A IV-2.

Subprograms Required: SGN (K)

Input Data Format (PLTVIB): 5 Cards per Data Case

CARD 1

COL (FORMAT)	1(I4)	5(I2)	7(I2)	9(I2)	5(I2)
NAME	NDATA	MS	MF	NS	NF

CARD 2

COL (FORMAT)	1(E10.4)	11(E10.4)	21(E10.4)	31(E10.4)
NAME	A1	A2	B1	B2

CARD 3

COL (FORMAT)	1(E10.4)	11(E10.4)	21(E10.4)	31(E10.4)
NAME	TS	GMS	ES	PRS

CARD 4/5 (Cont'd)

COL (FORMAT)	1(E10.4)	11(E10.4)	21(E10.4)	31(E10.4)
NAME	GX/GY	XJ/YJ	EX/EY	GMX/GMY

163

CARD 4/5

COL (FORMAT)	41(E10.4)	51(E10.4)	61(E10.4)
NAME	AX/AY	XI/YI	WCX/WCY

NDATA	four digit data identification number
MS,MF	initial and final values for mode number m
NS,NF	initial and final values for mode number n
A1,A2	panel bay dimensions in X-direction (see Figure 1)
B1,B2	panel bay dimensions in Y-direction (see Figure 1)
TS	skin thickness
GMS	weight density of skin material
ES	Young's modulus of skin material
PRS	Poisson's ratio of skin material
GX/GY	shear modulus of stringers parallel to X/Y axis
XJ/YJ	St. Venant's torsion constant for stringers parallel to X/Y axis
EX/EY	Young's modulus for stringers parallel to X/Y axis
GMX/GMY	weight density of material for stringers parallel to X/Y axis
AX/AY	cross section area for stringers parallel to X/Y axis
XI/YI	I_{px}/A_x and I_{py}/A_y (see Equations 8a and 8b)
WCX/WCY	warping constant for cross-section of stringers parallel to X/Y axis.

3. Nine-Cell Box Structure Vibration Analysis (BOXVIB)

Purpose: To compute the natural frequencies and modal amplitudes for the skin, rib, and frame of a nine-cell box structure as described in Section II.D. The program is listed in Figure A IV-3 and typical output is listed in Figure A IV-4.

Subprograms Required: STIFF(SK,I,J,K), MASS(SM,I,J,K), F(N,I,J), SGN(K).

Input Data Format (BOXVIB): Five Cards per Data Case

CARD 1

COL (FORMAT)	1(I4)	5(I2)
NAME	NDATA	IOUT

CARD 2

COL (FORMAT)	1(I2)	3(I2)	5(I2)	6(I2)	7(I2)	11(I2)
NAME	MS	MF	NS	NF	QS	QF

CARD 3

COL (FORMAT)	1(E11.4)	12(E11.4)	23(E11.4)	34(E11.4)	45(E11.4)
NAME	A1	A2	B1	B2	H

CARD 4

COL (FORMAT)	1(E11.4)	12(E11.4)	23(E11.4)	34(E11.4)	45(E11.4)
NAME	T1S	T2S	GMS	ES	PRS

CARD 5

COL (FORMAT)	1(E11.4)	12(E11.4)	23(E11.4)	34(E11.4)	45(E11.4)
NAME	T1R	T2R	GMR	ER	PRR

NDATA	four digit data identification number
IOUT	output option: = 0, frequencies are printed for each mode = 1, frequencies and modal amplitudes are printed for each mode
MS, MF	initial and final values for mode number m
NS, NF	initial and final values for mode number n
QS, QF	initial and final values for mode number q
A1, A2	length of panel bays parallel to x-axis (see Figure 3)
B1, B2	length of panel bays parallel to y-axis (see Figure 3)
H	height of box
T1S/T2S	upper/lower skin thickness (see Figure 3)
GMS	weight density of skin material
ES	Young's modulus for skin material
PRS	Poisson's ratio for skin material
T1R/T2R	rib/frame thickness (see Figure 3)
GMR	weight density of rib and frame material
ER	Young's modulus of rib and frame material
PRR	Poisson's ratio for rib and frame material

4. Three-Cell Wedge Structure Vibration Analysis (WDGVIB)

Purpose: To compute the natural frequencies and modal amplitudes for the ribs and skin of a three-cell wedge structure as described in Section II.E. The computer program is listed in Figure A IV-5 and typical output is listed in Figure A IV-6.

Subprograms Required: SGN(K)

Input Data Format (WDGVIB): 5 Cards per Data Case

CARD 1

COL (FORMAT)	1(I4)	5(I2)	7(I2)	9(I2)	11(I2)	13(I2)	15(I2)
NAME	NDATA	MS	MF	NS	NF	QS	QF

CARD 2

COL (FORMAT)	1(E10.4)	11(E10.4)	21(E10.4)	31(E10.4)
NAME	A1	B1	B2	ALPHA

CARD 3/4

COL (FORMAT)	1(E10.4)	11(E10.4)	21(E10.4)	31(E10.4)
NAME	T1S/T2S	GM1S/GM2S	E1S/E2S	PR1S/PR2S

CARD 5

COL (FORMAT)	1(E10.4)	11(E10.4)	21(E10.4)	31(E10.4)
NAME	T1R	GMR	ER	PRR

NDATA	four digit data identification number
MS, MF	initial and final values for mode number m
NS, NF	initial and final values for mode number n
QS, QF	initial and final values for mode number q
	NOTE: only odd values of q are considered. $QF \le 5$.
A1	radius of rib
B1/B2	rib spacing (B3 = B1: see Figure 9)
ALPHA	TOTAL wedge angle in DEGREES
T1S/T2S	thickness of upper/lower cover sheet (see Figure 9)
GM1S/GM2S	weight density of upper/lower cover sheet material
E1S/E2S	Young's modulus of upper/lower cover sheet material
PR1S/PR2S	Poisson's ratio of upper/lower cover sheet material
T1R	thickness of rib
GMR	weight density of rib material
ER	Young's modulus of rib material
PRR	Poisson's ratio of rib material

```
C         THIS PROGRAM EVALUATES THE MODAL MASS AND STIFFNESS,
C         FREQUENCY AND MODE SHAPES OF A STIFFENED PANEL
          DIMENSION A(23),F(5),XK(3),YK(3),W(3,3),SX(2,3),SY(2,3)
          IN=1
          IO=2
      200 READ(IN,100)NDATA,MS,MF,NS,NF
          READ(IN,101)A1,A2,B1,B2
          READ(IN,101)TS,GMS,ES,PRS
          READ(IN,101)GX,XJ,EX,GMX,AX,XI,WCX
          READ(IN,101)GY,YJ,EY,GMY,AY,YI,WCY
          A(1)=A1/A2
          A(2)=B1/B2
          A(3)=A2/B2
          A(4)=A2*B2
          A(5)=A(4)**3/B2
          A(6)=A(5)*B2/A2
          A(7)=A(1)**3
          A(8)=A(2)**3
          A(9)=(A2+2.*A1)*(B2+2.*B1)*GMS*TS/4.
          A(10)=9.86959*GMX*AX*XI/B2*A(3)*(1.+2.*A(7))
          A(11)=9.86959*GMY*AY*YI/A2/A(3)*(1.+2.*A(8))
          A(12)=ES*TS**3/(12.*(1.-PRS*PRS))/A(4)*24.35227
          A(13)=EX*WCX/A(5)*961.38506
          A(14)=EY*WCY/A(6)*961.38506
          A(15)=B1/A1
          A(16)=B1/A2
          A(17)=B2/A1
          A(18)=GX*XJ/(EX*WCX)
          A(19)=GY*YJ/(EY*WCY)
          A(20)=A1**2
          A(21)=A2**2
          A(22)=B1**2
          A(23)=B2**2
          DO 202 M=MS,MF
          SHM=SGN(M)
          FM=FLOAT(M)
          FM2=FM*FM
          FM4=FM2*FM2
          PIMA2=3.14159*FM/A2
          FMPISQ=(FM*3.14159)**2
          DO 201 N=NS,NF
          SGN=SGN(N)
          FN=FLOAT(N)
          FN2=FN*FN
          FN4=FN2*FN2
          PINB2=3.14159*FN/B2
          FMOFN=FM/FN
```

FIGURE A-IV-1   PROGRAM PLTVIB

167

```
F(1)=((FMOFN*A(15)+1./(A(15)*FMOFN))**2*4.*A(1)*A(2)
F(2)=((FMOFN/A(3)+A(3)/FMOFN))**2
F(3)=((FMOFN*A(16)+1./(A(16)*FMOFN))**2*2.*A(2)
F(4)=((FMOFN*A(17)+1./(A(17)*FMOFN))**2*2.*A(1)
F(5)=F(1)+F(2)+F(3)+F(4)
FNPISQ=(FN*3.14159)**2
XK(1)=A(18)*A(20)
XK(2)=A(18)*A(21)
XK(3)=1.+XK(2)/FMPISQ+2./A(1)*(1.+XK(1)/FMPISQ)
YK(1)=A(19)*A(22)
YK(2)=A(19)*A(23)
YK(3)=1.+YK(2)/FNPISQ+2./A(2)*(1.+YK(1)/FNPISQ)
SMM=(A(9)+A(10)*FN2+A(11)*FM2)/386.
SKM=A(12)*FM2*FN2*F(5)+A(13)*FM4*FN2*XK(3)+A(14)*FM2*FN4*YK(3)
FREQ=SQRT(SKM/SMM)/6.28318
W(1,1)=SNM*SNN*A(1)*A(2)
W(2,1)=SNN*A(2)
W(3,1)=W(1,1)
W(1,2)=SNM*A(1)
W(2,2)=1.
W(3,2)=W(1,2)
W(1,3)=W(1,1)
W(2,3)=W(2,1)
W(3,3)=W(1,1)
SX(1,1)=SNM*PINB2*A(1)
SX(1,2)=PINB2
SX(1,3)=SX(1,1)
SX(2,1)=SNN*SX(1,1)
SX(2,2)=SNN*PINB2
SX(2,3)=SX(2,1)
SY(1,1)=SNN*PIMA2*A(2)
SY(1,2)=PIMA2
SY(1,3)=SY(1,1)
SY(2,1)=SNM*SY(1,1)
SY(2,2)=SNM*PIMA2
SY(2,3)=SY(2,1)
WRITE(IO,215)
WRITE(IO,220)NDATA
WRITE(IO,225)M,N,FREQ
WRITE(IO,230)SMM,SKM
WRITE(IO,235)
WRITE(IO,240)((W(I,J),J=1,3),I=1,3)
WRITE(IO,245)
WRITE(IO,240)('SX(I,J),J=1,3),I=1,2)
WRITE(IO,250)
WRITE(IO,240)((SY(I,J),J=1,3),I=1,2)
201 CONTINUE
```

FIGURE A-IV-1   PROGRAM PLTVIB (Continued)

```
  202 CONTINUE
      GC TO 200
  100 FORMAT(I4,4I2)
  101 FORMAT(7E10.4)
  215 FORMAT(1H1,9X,42HDYNAMIC ANALYSIS OF A STIFFENED FLAT PANEL)
  220 FORMAT(///,23X,9HDATA CASE,I5)
  225 FORMAT(//,3X,13HMODE NUMBER (,I2,1H,,I2,1H),10X,10HFREQUENCY=,E12.
     15,4H HZ.)
  230 FORMAT(/,3X,11HMODAL MASS=,E12.5,3X,16HMODAL STIFFNESS=,E12.5)
  235 FORMAT(//,22X,16HMODAL AMPLITUDES,///,23X,14HPANEL - W(I,J),//)
  240 FORMAT(10X,E12.5,2X,E12.5,2X,E12.5)
  245 FORMAT(//,10X,39HSTIFFENERS IN THE X DIRECTION - SX(I,J),//)
  250 FORMAT(//,10X,39HSTIFFENERS IN THE Y DIRECTION - SY(I,J),//)
      STOP
      END



      FUNCTION SGN(K)
      C=1.0
      DO 5 I=1,K
      C=-C
    5 CONTINUE
      SGN=C
      RETURN
      END
```

FIGURE A-IV-1   PROGRAM PLTVIB (Concluded)

DYNAMIC ANALYSIS OF A STIFFENED FLAT PANEL

DATA CASE   37

MODE NUMBER (1, 1)   FREQUENCY= 0.23672E+03,Hz.

MODAL MASS= 0.16264E-02   MODAL STIFFNESS= 0.35979E+04

MODAL AMPLITUDES

PANEL - W(I,J)

```
 0.20370E+00   -0.61111E+00    0.20370E+00
-0.33333E+00    0.10000E+01   -0.33333E+00
 0.20370E+00   -0.61111E+00    0.20370E+00
```

STIFFENERS IN THE x DIRECTION - SX(I,J)

```
-0.10666E+00    0.17453E+00   -0.10666E+00
 0.10666E+00   -0.17453E+00    0.10666E+00
```

STIFFENERS IN THE y DIRECTION - SY(I,J)

```
-0.11636E+00    0.34907E+00   -0.11636E+00
 0.11636E+00   -0.34907E+00    0.11636E+00
```

FIGURE A-IV-2   PROGRAM PLTVIB: TYPICAL OUTPUT

170

```
      DIMENSION W1(3,3),W2(3,3),U(2,3),V(2,3)
      COMMON A(16),B(7)
      INTEGER QS,Q
      IN=1
      IO=2
100   READ(IN,105) NDATA,IOUT
      READ(IN,115) MS,M,NS,N,QS,Q
      READ(IN,110) A1,A2,B1,B2,H
      READ(IN,110) T1S,T2S,GMS,ES,PRS
      READ(IN,110) T1R,T2R,GMR,ER,PRR
105   FORMAT(I4,I2)
110   FORMAT(5E11.4)
115   FORMAT(6I2)
      A(1)= A1/A2
      A(2)= H/A1
      A(3)= H/A2
      A(4)= B1/A1
      A(5)= B1/A2
      A(6)= B1/B2
      A(7)= H/B1
      A(8)= B2/A1
      A(9)= B2/A2
      A(10)=H/B2
      A(11)=T2S/T1S
      A(12)=T2R/T1R
      A(13)=T1R/T1S
      A(14)=GMR/GMS
      A(15)=ER/ES
      A(16)=(1.0-PRS*PRS)/(1.0-PRR*PRR)
      CM=GMS*T1S*A2*B2/1544.0
      CK=2.029356*ES*T1S**3/(A2*B2*(1.0-PRS*PRS))
      CF=0.15915493*SQRT(CK/CM)
      C1=A(1)**3
      C2=A(6)**3
      C3=2.0*A(10)**3
      C4=A(9)**3
      C5=A(11)**3
      C6=A(13)**3
      B(1)=(1.0+A(11))*(1.0+2.0*C1+2.0*C2+4.0*C1*C2)
      B(2)=C3*A(14)*A(13)
      B(3)=1.0+2.0*A(1)
      B(4)=C4*(1.0+2.0*A(5))*A(12)
      B(5)=1.0+C5
      B(6)=2.0*C6*A(15)*A(16)
      DO 210 K=QS,Q
      WRITE(IO,215)
      WRITE(IO,220) NDATA
```

FIGURE A-IV-3   PROGRAM BXVIB

171

```
          IF(IOUT) 116,116,117
116   WRITE(IO,260)
117   SNQ=SGN(K)
      FQ=FLOAT(K)
      DO 205 I=MS,M
      SNM=SGN(I)
      FM=FLOAT(I)
      DO 205 J=NS,N
      SNN=SGN(J)
      FN=FLOAT(J)
      CALL STIFF(SK,I,J,K)
      CALL MASS(SM,I,J,K)
      FREQ=CF*SQRT(SK/SM)
      SMM=CM*SM
      SKM=CK*SK
      IF(IOUT) 201,201,120
120   W1(1,1)=SNM*SNN*A(1)*A(6)
      W1(1,2)= SNM*A(1)
      W1(1,3)= W1(1,1)
      W1(2,1)= SNN*A(6)
      W1(2,2)= 1.00000
      W1(2,3)= W1(2,1)
      W1(3,1)= W1(1,1)
      W1(3,2)= W1(1,2)
      W1(3,3)= W1(1,1)
      U(1,2)=-FM*A(3)/FQ
      U(1,1)= SNN*A(6)*U(1,2)
      U(1,3)= U(1,1)
      U(2,1)= SNM*U(1,1)
      U(2,2)= SNM*U(1,2)
      U(2,3)= SNM*U(1,1)
      V(1,2)=-FN*A(10)/FQ
      V(1,1)= SNM*A(1)*V(1,2)
      V(1,3)= V(1,1)
      V(2,1)= SNN*V(1,1)
      V(2,2)= SNN*V(1,2)
      V(2,3)= SNN*V(1,1)
      DO 200 I1=1,3
      DO 200 J1=1,3
      W2(I1,J1)=SNQ*W1(I1,J1)
200   CONTINUE
      GO TO 202
201   WRITE(IO,265) I,J,K,SKM,SMM,FREQ
      GO TO 205
202   WRITE(IO,225) I,J,K,FREQ
      WRITE(IO,230) SMM,SKM
      WRITE(IO,235)
```

FIGURE A-IV-3   PROGRAM BOXVIB (Continued)

172

```
      WRITE(IO,240) ((W1(I1,J1),J1=1,3),I1=1,3)
      WRITE(IO,245)
      WRITE(IO,240) ((U(I1,J1),J1=1,3),I1=1,2)
      WRITE(IO,250)
      WRITE(IO,240) ((V(I1,J1),J1=1,3),I1=1,2)
      WRITE(IO,255)
      WRITE(IO,240) ((W2(I1,J1),J1=1,3),I1=1,3)
205   CONTINUE
210   CONTINUE
215   FORMAT(1H1,7X,45HDYNAMIC ANALYSIS OF A NINE CELL-BOX STRUCTURE)
220   FORMAT(/,21X,9HDATA CASE,I5)
225   FORMAT(/,3X,13HMODE NUMBER (,I2,1H,,I2,1H,,I2,1H),7X,
     11OHFREQUENCY=,E12.5,3HHZ.)
230   FORMAT(/,3X,11HMODAL MASS=,E12.5,3X,16HMODAL STIFFNESS=,E12.5)
235   FORMAT(//,22X,16HMODAL AMPLITUDES,/,16X,19HUPPER COVER SHEET -,
     17HW1(I,J))
240   FORMAT(10X,E12.5,2X,E12.5,2X,E12.5)
245   FORMAT(/,23X,13HRIBS - U(I,J))
250   FORMAT(/,23X,13HRIBS - V(I,J))
255   FORMAT(/,17X,27HLOWER COVER SHEET - W2(I,J))
260   FORMAT(/,6X,7H(M,N,Q),3X,12HMODAL STIFF.,2X,
     11HMODAL  MASS,2X,14HFREQUENCY, HZ.,/)
265   FORMAT(6X,1H(,I1,1H,,I1,1H,,I1,1H),2X,E12.5,2X,E12.5,2X,E12.5)
      GO TO 100
      END




      SUBROUTINE STIFF(SK,I,J,K)
      COMMON A(16),B(7)
      IJ=I*I*J*J
      CIJ=FLOAT(IJ)
      F22=F(9,I,J)
      SKF=2.0*(A(1)*F(8,I,J)+A(6)*F(5,I,J)+2.0*A(1)*A(6)*F(4,I,J))/F22
      SKF=1.0+SKF
      RKF=(F(3,I,K)+2.0*A(1)*F(2,I,K))*A(10)+
     1(F(10,J,K)+2.0*A(6)*F(7,J,K))*A(3)*A(12)**3
      SK=CIJ*(B(5)*F22*SKF+B(6)*RKF)
      RETURN
      END
```

FIGURE A-IV-3   PROGRAM BOXVIB (Continued)

173

```
FUNCTION F(N,I,J)
COMMON A(16),B(7)
R1=(FLOAT(I)/FLOAT(J))*A(N)
R=R1+1.0/R1
F=R*R
RETURN
END




SUBROUTINE MASS(SM,I,J,K)
COMMON A(16),B(7)
C1=FLOAT(I)/FLOAT(J)
C2=FLOAT(J)/FLOAT(K)
RM=B(3)+B(4)*C1*C1
SM=B(1)+B(2)*RM*C2*C2
RETURN
END




FUNCTION SGN(K)
C=1.0
DO 5 I=1,K
C=-C
5      CONTINUE
SGN=C
RETURN
END
```

FIGURE A-IV-3   PROGRAM BOXVIB (Concluded)

DYNAMIC ANALYSIS OF A NINE CELL-BOX STRUCTURE

DATA CASE   1

MODE NUMBER (1, 1, 1)   FREQUENCY= 0.78729E+02HZ.

MODAL MASS= 0.14126E-01   MODAL STIFFNESS= 0.34566E+04

MODAL AMPLITUDES
UPPER COVER SHEET -W1(I,J)

0.70383E+00	-0.11375E+01	0.70383E+00
-0.61875E+00	0.10000E+01	-0.61875E+00
0.70383E+00	-0.11375E+01	0.70383E+00

RIBS - U(I,J)

0.61875E+00	-0.10000E+01	0.61875E+00
-0.61875E+00	0.10000E+01	-0.61875E+00

RIBS - V(I,J)

0.56875E+00	-0.50000E+00	0.56875E+00
-0.56875E+00	0.50000E+00	-0.56875E+00

LOWER COVER SHEET - W2(I,J)

-0.70383E+00	0.11375E+01	-0.70383E+00
0.61875E+00	-0.10000E+01	0.61875E+00
-0.70383E+00	0.11375E+01	-0.70383E+00

MODE NUMBER (1, 2, 1)   FREQUENCY= 0.14371E+03HZ.

MODAL MASS= 0.18697E-01   MODAL STIFFNESS= 0.13614E+05

MODAL AMPLITUDES
UPPER COVER SHEET -W1(I,J)

-0.70383E+00	-0.11375E+01	-0.70383E+00
0.61875E+00	0.10000E+01	0.61875E+00
-0.70383E+00	-0.11375E+01	-0.70383E+00

RIBS - U(I,J)

-0.61875E+00	-0.10000E+01	-0.61875E+00
0.61875E+00	0.10000E+01	0.61875E+00

RIBS - V(I,J)

0.11375E+01	-0.10000E+01	0.11375E+01
0.11375E+01	-0.10000E+01	0.11375E+01

LOWER COVER SHEET - W2(I,J)

0.70383E+00	0.11375E+01	0.70383E+00
-0.61875E+00	-0.10000E+01	-0.61875E+00
0.70383E+00	0.11375E+01	0.70383E+00

FIGURE A-IV-4   PROGRAM BOXVIB: TYPICAL OUTPUT

175

```
C       THIS PROGRAM EVALUATES THE MODAL MASS AND STIFFNESS,
C       FREQUENCY AND MODE SHAPES OF A WEDGE STRUCTURE
        DIMENSION A(22),F(6),W(2,3),V(20,4)
        REAL IM(10)
        INTEGER Q,QS,QF,QM1D2
        IN=1
        IO=2
        IM(1)=.24699
        IM(2)=.07888
        IM(3)=.03958
        IM(4)=.02408
        IM(5)=.01632
200     READ(IN,100)NDATA,MS,MF,NS,NF,QS,QF
        READ(IN,101)A1,B1,B2,ALPHA
        ALPHA=.0087266*ALPHA
        READ(IN,101)T1S,GM1S,E1S,PR1S
        READ(IN,101)T2S,GM2S,E2S,PR2S
        READ(IN,101)T1R,GMR,ER,PRR
        A(1)=2.*ALPHA*A1/B2
        A(2)=B1/B2
        A(3)=A1/B2
        A(4)=A1*B2
        A(5)=A1/B1
        A(6)=A(1)**3
        A(7)=E1S*T1S**3/(1.-PR1S*PR1S)/12.
        A(8)=E2S*T2S**3/(1.-PR2S*PR2S)/12.
        A(9)=ER*T1R**3/(1.-PRR*PRR)/12.
        A(10)=GM1S*T1S
        A(11)=A(10)*A(4)/1544.
        A(12)=1.+GM2S*T2S/A(10)
        A(13)=A(12)*(2.*A(2)+1.)*A(11)
        A(14)=GMR*T1R/A(10)*A(6)*A(11)
        A(15)=24.35227*A(7)/A(4)
        A(16)=(1.+A(8)/A(7))*A(15)
        A(17)=(ALPHA/1.570795)**2
        A(18)=A(9)/A(7)*A(1)*A(17)*A(15)
        A(19)=2.*A(16)/A(2)
        A(20)=2./A(17)
        A(21)=(15.+8.*PRR)
        A(22)=2.*A(20)
        DO 203 M=MS,MF
        SNM=SGN(M)
        FM=FLOAT(M)
        FM2=FM*FM
        PIMDA=3.14159*FM
        DO 202 N=NS,NF
        SNN=SGN(N)
        FN=FLOAT(N)
```

FIGURE A-IV-5   PROGRAM WDGVIB

```
      FN2=FN*FN
      FMOFN=FM/FN
      F(1)=((FMOFN/A(5)+A(5)/FMOFN)**2)*A(16)
      F(2)=((FMOFN/A(3)+A(3)/FMOFN)**2)*A(16)
      F(3)=F(1)+F(2)
      DO 201 Q=QS,QF,2
      J1U2=(Q-1)/2
      SQ=SGN(Q)
      SQM1=SGN(Q-1U2)
      FQ=FLOAT(Q)
      FQ2=FQ*FQ
      F(4)=((A(20)*FQ2-2.)**2)*IM(M)
      F(5)=9.86959*FM2+A(21)+A(22)*FQ2
      F(6)=A(18)*(F(4)+C(5))/FQ2
      SKM=FM2*FN2*(F(3)+F(6))
      SM=(1.-.303964/F2)*A(14)*FN2/FQ2+A(13)
      FREQ=SQRT(SKM/SM)/6.2831S
      W(1,1)=SM*A(2)
      W(1,2)=1.
      W(1,3)=W(1,1)
      W(2,1)=-W(1,1)
      W(2,2)=-1.
      W(2,3)=W(2,1)
      DO 204 IR=1,20
      R=FLOAT(IR)
      R=0.05*R
      CON=2.*ALPHA*SQRT*FN/FQ**W(3)
      SPRA=SIN(PIMDA*R)
      V(IR,1)=SM*CON*SPRA
      V(IR,2)=CON*SMPRA
      V(IR,3)=V(IR,1)
  204 V(IR,4)=V(IR,2)
      WRITE(10,215)
      WRITE(10,220)MONTL
      WRITE(10,225)MODE,FREQ
      WRITE(10,230)SM,SKM
      WRITE(10,235)
      WRITE(10,240)(W(1,J),J=1,3)
      WRITE(10,245)
      WRITE(10,246)(W(2,J),J=1,3)
      WRITE(10,250)
      DO 205 I=1,20
      R=FLOAT(I)
      R=.05*R
  205 WRITE(10,241)(R,(V(I,J),J=1,4))
  201 CONTINUE
  202 CONTINUE
  203 CONTINUE
```

FIGURE A-IV-5   PROGRAM WDGVIB (Continued)

177

```
      GO TO 200
100 FORMAT(I4,6I2)
101 FORMAT(4E10.4)
215 FORMAT(1H1,11X,37HDYNAMIC ANALYSIS OF A WEDGE STRUCTURE)
220 FORMAT(/22X,9HDATA CASE,I5)
225 FORMAT(/3X,13HMODE NUMBER (,I2,1H,,I2,1H,,I2,1H),5X,10HFREQUENCY=,
   1E12.5,4H HZ.)
230 FORMAT(/3X,11HMODAL MASS=,E12.5,2X,16HMODAL STIFFNESS=,E12.5)
235 FORMAT(//20X,16HMODAL AMPLITUDES,//16X,26HUPPER COVER SHEET - W(1,
   1J),/)
240 FORMAT(10X,E12.5,2X,E12.5,2X,E12.5)
241 FORMAT(F5.2,3X,4E12.5)
245 FORMAT(//16X,26HLOWER COVER SHEET - W(2,J),/)
250 FORMAT(//17X,22HSECTOR PLATES - V(I,J),/11X,6HSECTOR,6X,6HSECTOR,6
   1X,6HSECTOR,6X,6HSECTOR,/2X,3HR/A,5X,8HPLATE NO,4X,8HPLATE NO,4X,8H
   2PLATE NO,4X,8HPLATE NO,/13X,1H1,11X,1H2,11X,1H3,11X,1H4,//)
      END




      FUNCTION SGN(K)
      C=1.0
      DO 5 I=1,K
      C=-C
    5 CONTINUE
      SGN=C
      RETURN
      END
```

FIGURE A-IV-5 PROGRAM WDGVIB (Concluded)

DYNAMIC ANALYSIS OF A WEDGE STRUCTURE

DATA CASE 2000

MODE NUMBER (2, 1, 1)   FREQUENCY= 0.26011E+03,HZ.

MODAL MASS= 0.19622E-02   MODAL STIFFNESS= 0.52410E+04

MODAL AMPLITUDES

UPPER COVER SHEET - W(1,J)

-0.10000E+01   0.10000E+01   -0.10000E+01

LOWER COVER SHEET - W(2,J)

0.10000E+01   -0.10000E+01   0.10000E+01

SECTOR PLATES - V(I,J)

R/A	SECTOR PLATE NO 1	SECTOR PLATE NO 2	SECTOR PLATE NO 3	SECTOR PLATE NO 4
0.05	0.61808E-02	-0.61808E-02	0.61808E-02	-0.61808E-02
0.10	0.23513E-01	-0.23513E-01	0.23513E-01	-0.23513E-01
0.15	0.48544E-01	-0.48544E-01	0.48544E-01	-0.48544E-01
0.20	0.76090E-01	-0.76090E-01	0.76090E-01	-0.76090E-01
0.25	0.10001E+00	-0.10001E+00	0.10001E+00	-0.10001E+00
0.30	0.11413E+00	-0.11413E+00	0.11413E+00	-0.11413E+00
0.35	0.11327E+00	-0.11327E+00	0.11327E+00	-0.11327E+00
0.40	0.94052E-01	-0.94052E-01	0.94052E-01	-0.94052E-01
0.45	0.55627E-01	-0.55627E-01	0.55627E-01	-0.55627E-01
0.50	0.53703E-06	-0.53703E-06	0.53703E-06	-0.53703E-06
0.55	-0.67988E-01	0.67988E-01	-0.67988E-01	0.67988E-01
0.60	-0.14108E+00	0.14108E+00	-0.14108E+00	0.14108E+00
0.65	-0.21036E+00	0.21036E+00	-0.21036E+00	0.21036E+00
0.70	-0.26631E+00	0.26631E+00	-0.26631E+00	0.26631E+00
0.75	-0.30002E+00	0.30002E+00	-0.30002E+00	0.30002E+00
0.80	-0.30436E+00	0.30436E+00	-0.30436E+00	0.30436E+00
0.85	-0.27509E+00	0.27509E+00	-0.27509E+00	0.27509E+00
0.90	-0.21162E+00	0.21162E+00	-0.21162E+00	0.21162E+00
0.95	-0.11744E+00	0.11744E+00	-0.11744E+00	0.11744E+00
1.00	-0.21481E-05	0.21481E-05	-0.21481E-05	0.21481E-05

FIGURE A-IV-6   PROGRAM WDGVIB: TYPICAL OUTPUT

REFERENCES

1. Clarkson, B. L., "Stresses in Skin Panels Subjected to Random Acoustic Loading," The Aeronautical Journal of the Royal Aeronautical Society, Vol. 72, Nov. 1968, pp. 1000-1010.

2. Miles, John W., "On Structural Fatigue Under Random Loading," Journal of the Aeronautical Sciences, Vol. 21, 1954, pp. 753-762.

3. Zak, A. R., and French, C. E., An Experimental and Analytical Investigation of a Two Dimensionally Stiffened Panel, AFML-TR-68-390, Air Force Materials Laboratory, Wright-Patterson Air Force Base, Ohio, 1969.

4. Zak, A. R., Theoretical and Experimental Analysis of Stiffened Panels Under Dynamic Conditions, AFML-TR-70-22, Air Force Materials Laboratory, Wright-Patterson Air Force Base, Ohio, 1970.

5. Rudder, F. F., Jr., "Study of Effects of Design Details on Structural Response to Acoustic Excitation," NASA CR-1959 , 1971.

6. Vlasov, V. Z., Thin-Walled Elastic Beams, Second Ed., NSFTT 61-1140, The Israel Program for Scientific Translations, 1961 (Available from OTS, U.S. Dept. of Commerce).

7. Oden, J. T., Mechanics of Elastic Structures, McGraw-Hill Book Co., Inc., 1967.

8. Ballentine, J. R., et.al., Refinement of Sonic Fatigue Structural Design Criteria, AFFDL-TR-67-156, Air Force Flight Dynamics Laboratory, Wright-Patterson Air Force Base, Ohio, 1968.

9. Timoshenko, S., and Woinowsky-Krieger, S., Theory of Plates and Shells, Second Edition, McGraw-Hill Book Co., Inc., 1959.

10. Clarkson, B. L., and Abrahamson, A. L., "The Response of Skin/Rib Structure to Jet Noise," Proc. of a conference on Current Developments in Sonic Fatigue, Institute of Sound and Vibration Research, Univ. of Southampton, England, 6-9 July 1970, paper N.1.

11. Sen Gupta, G., and Mead, D. J., "Wave Group Theory Applied to the Analysis of Forced Vibrations of Rib-Skin Structure," Symposium on Structural Dynamics, Loughborough University of Technology, 23-25 March 1970, paper D.3.

12. Szechenyi, E., "Approximate Methods for the Determination of the Natural Frequencies of Stiffened and Curved Plates," J. Sound Vib., 14, No. 3, 8 February 1971, pp. 401-418.

13. Petyt, M., "Vibration of Curved Plates," J. Sound Vib., Vol. 15, No. 3, 8 April 1971, pp. 381-396.

14. Thomson, W. T., Vibration Theory and Applications, Prentice-Hall, Inc., Englewood Cliffs, N. J., 1965.

15. McGowan, P. R., et al., "Structural Design for Acoustic Fatigue," ASD-TDR-63-820, October 1963.

DOCUMENT CONTROL DATA - R&D

(Security classification of title, body of abstract and indexing annotation must be entered when the overall report is classified)

1 ORIGINATING ACTIVITY *(Corporate author)*	2a REPORT SECURITY CLASSIFICATION
Lockheed-Georgia Company South Cobb Drive Marietta, Georgia 30060	Unclassified
	2b GROUP

3 REPORT TITLE

ACOUSTIC FATIGUE OF AIRCRAFT STRUCTURAL COMPONENT ASSEMBLIES

4 DESCRIPTIVE NOTES *(Type of report and inclusive dates)*

Final - March 1970 to September 1971

5 AUTHOR(S) *(Last name, first name, initial)*

Rudder, Fred F. Jr.

6. REPORT DATE	7a TOTAL NO. OF PAGES	7b. NO. OF REFS
FEBRUARY 1972	180	15

8a CONTRACT OR GRANT NO. F33615-70-C-1274 b. PROJECT NO. 1471 c. Task No. 147101 d.	9a ORIGINATOR'S REPORT NUMBER(S) ER-11143 9b. OTHER REPORT NO(S) *(Any other numbers that may be assigned this report)* AFFDL-TR-71-107

10. AVAILABILITY/LIMITATION NOTICES

Distribution limited to U.S. Government agencies only; test and evaluation; statement applied July 1971. Other requests for this document must be referred to Air Force Flight Dynamics Laboratory, (FY), Wright-Patterson AFB, Ohio 45433

11. SUPPLEMENTARY NOTES	12 SPONSORING MILITARY ACTIVITY
	Air Force Flight Dynamics Laboratory Wright-Patterson AFB, Ohio 45433

13 ABSTRACT

Analytical results for estimating natural frequencies and stress response for conventional stiffened flat panels, two-sided box structure, wedge structure, and unstiffened cylindrical panels are presented. Acoustic fatigue tests of twelve stiffened flat panel and six box structure designs, two specimens for each design, were used to develop design equations for estimating acoustic fatigue resistance of skin, stringer, and rib structure. Computer programs are presented for estimating frequencies of stiffened flat panels, box structure, and wedge structure. Nomographs are presented for skin design and curved panel stress response.

The methods described in this report are intended to be used by aircraft designers to design structural areas on an aircraft subjected to high intensity acoustic loading. The methods are applicable to structural components, which are flat or curved, such as fuselage side-wall structures, and wedge-shaped or box-type structures, such as flaps, stabilizers, and rudders. The application of these methods will lead to optimization of the structure under design from a sonic fatigue viewpoint, and thus reduce the weight of the structural component, and at the same time predict the structural life. The general requirements for this type of analysis and life prediction are specified in MIL-A-8893 (USAF).

DD FORM 1JAN 64 **1473**

Security Classification

14 KEY WORDS	LINK A		LINK B		LINK C	
	ROLE	WT	ROLE	WT	ROLE	WT
Acoustic Fatigue						
Dynamic Response						
Structural Design						
Curvature effects						

INSTRUCTIONS

1. ORIGINATING ACTIVITY: Enter the name and address of the contractor, subcontractor, grantee, Department of Defense activity or other organization (*corporate author*) issuing the report.

2a. REPORT SECURITY CLASSIFICATION: Enter the overall security classification of the report. Indicate whether "Restricted Data" is included. Marking is to be in accordance with appropriate security regulations.

2b. GROUP: Automatic downgrading is specified in DoD Directive 5200.10 and Armed Forces Industrial Manual. Enter the group number. Also, when applicable, show that optional markings have been used for Group 3 and Group 4 as authorized.

3. REPORT TITLE: Enter the complete report title in all capital letters. Titles in all cases should be unclassified. If a meaningful title cannot be selected without classification, show title classification in all capitals in parenthesis immediately following the title.

4. DESCRIPTIVE NOTES: If appropriate, enter the type of report, e.g., interim, progress, summary, annual, or final. Give the inclusive dates when a specific reporting period is covered.

5. AUTHOR(S): Enter the name(s) of author(s) as shown on or in the report. Enter last name, first name, middle initial. If military, show rank and branch of service. The name of the principal author is an absolute minimum requirement.

6. REPORT DATE: Enter the date of the report as day, month, year; or month, year. If more than one date appears on the report, use date of publication.

7a. TOTAL NUMBER OF PAGES: The total page count should follow normal pagination procedures, i.e., enter the number of pages containing information.

7b. NUMBER OF REFERENCES: Enter the total number of references cited in the report.

8a. CONTRACT OR GRANT NUMBER: If appropriate, enter the applicable number of the contract or grant under which the report was written.

8b, 8c, & 8d. PROJECT NUMBER: Enter the appropriate military department identification, such as project number, subproject number, system numbers, task number, etc.

9a. ORIGINATOR'S REPORT NUMBER(S): Enter the official report number by which the document will be identified and controlled by the originating activity. This number must be unique to this report.

9b. OTHER REPORT NUMBER(S): If the report has been assigned any other report numbers (*either by the originator or by the sponsor*), also enter this number(s).

10. AVAILABILITY/LIMITATION NOTICES: Enter any limitations on further dissemination of the report, other than those imposed by security classification, using standard statements such as:

(1) "Qualified requesters may obtain copies of this report from DDC."

(2) "Foreign announcement and dissemination of this report by DDC is not authorized."

(3) "U. S. Government agencies may obtain copies of this report directly from DDC. Other qualified DDC users shall request through

_____."

(4) "U. S. military agencies may obtain copies of this report directly from DDC. Other qualified users shall request through

_____."

(5) "All distribution of this report is controlled. Qualified DDC users shall request through

_____."

If the report has been furnished to the Office of Technical Services, Department of Commerce, for sale to the public, indicate this fact and enter the price, if known.

11. SUPPLEMENTARY NOTES: Use for additional explanatory notes.

12. SPONSORING MILITARY ACTIVITY: Enter the name of the departmental project office or laboratory sponsoring (*paying for*) the research and development. Include address.

13. ABSTRACT: Enter an abstract giving a brief and factual summary of the document indicative of the report, even though it may also appear elsewhere in the body of the technical report. If additional space is required, a continuation sheet shall be attached.

It is highly desirable that the abstract of classified reports be unclassified. Each paragraph of the abstract shall end with an indication of the military security classification of the information in the paragraph, represented as *(TS)*, *(S)*, *(C)*, or *(U)*

There is no limitation on the length of the abstract. However, the suggested length is from 150 to 225 words.

14. KEY WORDS: Key words are technically meaningful terms or short phrases that characterize a report and may be used as index entries for cataloging the report. Key words must be selected so that no security classification is required. Identifiers, such as equipment model designation, trade name, military project code name, geographic location, may be used as key words but will be followed by an indication of technical context. The assignment of links, rules, and weights is optional.